REGIONAL VARIATIONS IN UPPER MANTLE STRUCTURE BENEATH NORTH AMERICA

Thesis by

Bruce Rene Julian

In Partial Fulfillment of the Requirements

For the Degree of

Doctor of Philosophy

California Institute of Technology

Pasadena, California

1970

(Submitted October 6, 1969)

ACKNOWLEDGMENTS

The individuals in the Division of Geological Sciences who have helped, in many ways, during my stay at Caltech, are unfortunately too numerous to thank individually. Nevertheless, my debt to all these individuals, particularly the staff and students of the Seismological Laboratory, is very great. Particularly, however, I would like to thank Drs. Don L. Anderson and Charles B. Archambeau, whose continuing encouragement, help, and advice in this work have been invaluable. Special thanks, too, are due to Mrs. Barbara Sloan, Mrs. Virginia Gilliam, and Mrs. Bernita Larsh who typed this thesis, and Mr. Lazlo Lenches, who worked long and hard preparing the figures and tables.

I am greatly indebted to the U.S. Geological Survey's National Center for Earthquake Research, and Mr. L. C. Pakiser in particular, for generously providing data, including record sections, from the Project Early Rise and Project Gasbuggy experiments.

During most of my tenure as a graduate student, I have been supported by a National Science Foundation Graduate Fellowship. This research was supported by the Air Force Office of Scientific Research under contracts AF-49(638)-1337 and AFOSR-F44620-69-C-0067.

ABSTRACT

Several types of seismological data, including surface wave group and phase velocities, travel times from large explosions, and teleseismic travel time anomalies, have indicated that there are significant regional variations in the upper few hundred kilometers of the mantle beneath continental areas. Body wave travel times and amplitudes from large chemical and nuclear explosions are used in this study to delineate the details of these variations beneath North America.

As a preliminary step in this study, theoretical P wave travel times, apparent velocities, and amplitudes have been calculated for a number of proposed upper mantle models, those of Gutenberg, Jeffreys, Lehman, and Lukk and Nersesov. These quantities have been calculated for both P and S waves for model CIT11GB, which is derived from surface wave dispersion data. First arrival times for all the models except that of Lukk and Nersesov are in close agreement, but the travel time curves for later arrivals are both qualitatively and quantitatively very different. For model CIT11GB, there are two large, overlapping regions of triplication of the travel time curve, produced by regions of rapid velocity increase near depths of 400 and 600 km. Throughout the distance range from 10 to 40 degrees, the later arrivals produced by these discontinuities have larger amplitudes than the first arrivals. The amplitudes of body waves,

in fact, are extremely sensitive to small variations in the velocity structure, and provide a powerful tool for studying structural details.

Most of eastern North America, including the Canadian Shield has a Pn velocity of about 8.1 km/sec, with a nearly abrupt increase in compressional velocity by ~ 0.3 km/sec near at a depth varying regionally between 60 and 90 km. Variations in the structure of this part of the mantle are significant even within the Canadian Shield. The low-velocity zone is a minor feature in eastern North America and is subject to pronounced regional variations. It is 30 to 50 km thick, and occurs somewhere in the depth range from 80 to 160 km. The velocity decrease is less than 0.2 km/sec.

Consideration of the absolute amplitudes indicates that the attenuation due to anelasticity is negligible for 2 hz waves in the upper 200 km along the southeastern and southwestern margins of the Canadian Shield. For compressional waves the average Q for this region is $\gtrsim 3000$. The amplitudes also indicate that the velocity gradient is at least 2×10^{-3} both above and below the low-velocity zone, implying that the temperature gradient is $< 4.8°C/km$ if the regions are chemically homogeneous.

In western North America, the low-velocity zone is a pronounced feature, extending to the base of the crust and having minimum velocities of 7.7 to 7.8 km/sec. Beneath the Colorado Plateau and Southern Rocky Mountains provinces, there is a rapid velocity increase of about 0.3 km/sec, similar to that observed in eastern North

America, but near a depth of 100 km.

Complicated travel time curves observed on profiles with stations in both eastern and western North America can be explained in detail by a model taking into account the lateral variations in the structure of the low-velocity zone. These variations involve primarily the velocity within the zone and the depth to the top of the zone; the depth to the bottom is, for both regions, between 140 and 160 km.

The depth to the transition zone near 400 km also varies regionally, by about 30-40 km. These differences imply variations of 250 °C in the temperature or 6 % in the iron content of the mantle, if the phase transformation of olivine to the spinel structure is assumed responsible. The structural variations at this depth are not correlated with those at shallower depths, and follow no obvious simple pattern.

The computer programs used in this study are described in the Appendices. The program TTINV (Appendix IV) fits spherically symmetric earth models to observed travel time data. The method, described in Appendix III, resembles conventional least -square fitting, using partial derivatives of the travel time with respect to the model parameters to perturb an initial model. The usual ill-conditioned nature of least-squares techniques is avoided by a technique which minimizes both the travel time residuals and the model perturbations.

Spherically symmetric earth models, however, have been found inadequate to explain most of the observed travel times in this study. TVT4, a computer program that performs ray theory calculations for a laterally inhomogeneous earth model, is described in Appendix II. Appendix I gives a derivation of seismic ray theory for an arbitrarily inhomogeneous earth model.

TABLE OF CONTENTS

Chapter I

INTRODUCTION

Evidence has accumulated recently that there are significant regional variations in the structure of the upper mantle extending to depths of at least a few hundred kilometers beneath the continents. Variations in crustal thickness and in the seismic velocities in the crust and uppermost mantle have for a long time been inferred from near earthquake studies (see Gutenberg, 1959a, ch. 3, for a summary to 1959), but uncertainties caused by inadequate station coverage and inaccuracies in earthquake location have persisted. The first convincing evidence of pronounced lateral variations in upper mantle velocities came from the Gnome nuclear explosion, detonated near Carlsbad, in southeastern New Mexico in December, 1961. The observed travel times to stations in the western United States, though scattered, were in approximate agreement with the Jeffreys-Bullen times, determined from observations of earthquakes in tectonic regions. The times to eastern stations, though, were earlier by about 5 sec in the distance range from 1000 to 2000 km (Romney _et al_, 1962).

Other evidence of velocity variations in the mantle has come from empirically determined "station corrections" to the travel times of teleseismic P and S waves. These corrections vary regionally by as much as 2½ sec for P and 7 sec for S. Arrival times of P waves are about 1½ - 2 sec later, for example, in the western United States than in the east (Cleary and Hales, 1966; Press and Biehler, 1964; Doyle and Hales, 1967; Herrin and Taggart, 1968). If these variations were due only to differences within the crust, a 1 second delay would require an increase in crustal thickness of about 25 km, or a decrease in the average crustal velocity of about 25%, either of which would be easily detectable by seismic refraction and gravity techniques. Hales et al (1968) have analyzed these station residuals in detail and concluded that they are most likely produced by variations in the low-velocity zone, between depths of about 100 and 160 km.

Still another line of evidence has come from measurements of surface wave dispersion. Toksoz and Anderson (1966) studied the propagation of Love waves over five different great circle paths, and used the observed dispersion to infer the phase velocity curves for oceanic, tectonic, and shield areas in the period range from about 100 to 300 sec. Very significant differences were found, even for the longest periods, and the greatest difference was found between the shield and tectonic regions, with the oceanic areas being intermediate. The differences in the dispersion, moreover, implied structural differences extending to depths of at least 400 km.

Similar conclusions have been reached by Brune (1965a, b) from studies of the seismic phase Sa, which represents the effect of a small number of interfering modes with approximately the same group velocity and is quite sensitive to the shear velocity in the upper few hundred km of the mantle. The apparent group velocity of this phase from an earthquake in the Hindu Kush region was found to be at least 0.1 km/sec greater in shield areas than in regions of more recent tectonic activity.

Seismic body waves have also provided evidence of significant lateral variations in upper mantle velocities. In addition to the observations from the Gnome explosion mentioned above, indicating pronounced variations between the eastern and western U. S., observations of events in Nevada have indicated variations within the western U. S. Travel times to stations northeast of Nevada, in the direction of the Canadian Shield, are smaller than those to the east and southeast (see, for example, Lehmann, 1967). A detailed interpretation of travel times and amplitudes of P waves along four profiles from nuclear explosions in Nevada has been made by Archambeau et al (in press). The regional variations were found to be most significant within the uppermost mantle and the low-velocity zone, with velocities being lowest in the Basin and Range Province and highest in the Plateau and Rocky Mountain Provinces. The existence of variations beneath the low-velocity zone could be neither proven nor disproven on the basis of the Nevada data.

Seismic body waves provide an ideal tool for studying details of the earth's structure, including regional variations. Since they have smaller wavelengths than surface waves, they are more sensitive to small structural details. Furthermore, relatively small events can generate observable body waves which penetrate to hundreds of kilometers, and ordinary short-period seismographs can record them.

Only long-period surface waves, however, generated by infrequent large earthquakes and recorded on sophisticated and uncommon instruments, can provide information about the earth's deep interior.

The use of body waves to study structural details has been greatly facilitated recently by several factors, including the availability of accurately timed and located large explosions as seismic sources, the existence of large networks of standardized seismographs and seismometer arrays, and the increased accuracy and convenience of data processing with large digital computers. As a preliminary step in a comprehensive study of variations in upper mantle structure beneath North America, theoretical behavior of body wave travel times, apparent velocities, and amplitudes have been calculated for several proposed earth models and are presented in Chapter II.

Chapter III presents in detail the analysis of a large body of high quality body wave data from explosions at the Nevada Test Site, in New Mexico, and in Lake Superior. These data provide excellent areal coverage of most of the United States and southern Canada. In contrast to previous studies, which have assumed spherically symmetrical earth models, this work presents theoretical travel times and amplitudes for models with a two-dimensional velocity variation. Regional variations in observed travel times are large enough that this extension is now necessary for interpreting profiles which traverse more than one crustal-mantle province. In addition, the problem of fitting models to observed travel time data is so tedious that an automated method for performing this inversion has proved necessary. Accordingly, a perturbation theory for body wave travel times has been developed and a computer program for fitting observed data written. This program has proved to be a very convenient tool, greatly reducing the labor involved in body wave studies. The end result of the data analysis, summarized in Chapter IV, is a detailed map of the compressional velocity variations in the upper mantle beneath North America.

Details of the methods of analysis used are presented in the appendices. Appendix I gives variational formulation of seismic ray theory for an arbitrarily inhomogeneous earth, and Appendix II describes the computer program used for seismic ray calculations in a laterally inhomogeneous earth, including instructions for use of the program. Body wave perturbation theory and the inversion of observed data are discussed in Appendix III and a computer program for inverting travel time data in a spherical earth is described in Appendix IV.

Chapter II

Theoretical Body Wave Calculations

In order to study the theoretical behavior of body wave travel times, apparent velocities and amplitudes, programs have been written for the IBM 7094 and 360/75 digital computers which calculate these parameters for both spherically symmetrical and laterally varying earth models. The calculations are based on geometrical ray theory, a derivation of which is given in Appendix I. Both geometric spreading and attenuation due to anelasticity are taken into account in calculating amplitudes. The most general computer program is described in Appendix II. As a first step in a more complete study of the problem of the velocity structure of the earth's interior, we have calculated the travel times, apparent velocities, and amplitudes for the standard earth models and some more recent models, based upon both surface wave and body wave studies.

Earth Models. The upper mantle P wave velocities for the models of Gutenberg, Jeffreys and Lehmann are given in Figure 1. The general features of these models are well known. Both the Gutenberg and Lehmann models have a low velocity zone in the upper mantle. There is a first order discontinuity at 215 km in Lehmann's model, and below it a smooth increase which joins onto Jeffreys' model near 700 km. The Gutenberg model has no strong first or second order discontinuities, but has a high velocity gradient from the low velocity zone to about 900 km. The Jeffreys' model has no low velocity zone but has a second order discontinuity near 415 km. Also shown is a recent body wave structure proposed by Lukk and Nersesov (1965) and a surface wave model, CIT11GB. This latter model has a low velocity zone and regions of extremely high velocity gradients between 100-170, 350-450, and 650-750 km. This structure is similar to the oceanic model CIT11 of Anderson and Toksöz (1963), but has been modified to have a continental type crust and upper mantle. The shear wave velocities were determined from Love wave dispersion, and the P wave velocities were derived from them using the Poisson's ratio distribution of Gutenberg's model.

Model CIT11GB. The travel time curves, geometric spreading, attenuation, and other body wave parameters for the model CIT11GB are shown in Figures 2-8. On all the travel time curves presented here, the Jeffreys-Bullen times have been indicated by dots for the sake of comparison. Multibranched travel time curves, with large amplitude later arrivals, are important features of this and similar models. For P waves (Figure 2), the low velocity zone produces a shadow zone which ends with a small reverse branch between 12.2° and 13.2°. Between 14.3° and 31.8° there is a region of triplication (B-C) produced by the discontinuity at 350-450 km, and similarly the discontinuity at 650-750 km produces an overlapping triplication (D-E) between 21.1° and 40.2°. There is also a small zone of triplication near 39°, produced by a small second order discontinuity at 850 km. The travel time curve for S waves (Figure 4) is similar, the main difference being that the first ray to penetrate below the low velocity zone emerges at a greater distance, 25.4°. Slight changes in the model either above or below the low velocity zone could change this result, however. As with P waves, there are two overlapping regions of triplication: one between 14.5° and 34.1° (B-C), produced by the 350 km discontinuity, and one between 21.1° and 41.3° (D-E), produced by the 650 km discontinuity. If first arrivals alone are considered, the travel time curve for P can be considered to be made up of three approximately straight line segments, with apparent velocities of about 8.4, 10.7, and 12.9 km/sec, intersecting at 18° and 25.7°. The first arrival curve for S waves consists of two branches, with velocities of about 5.8 and 7.0 km/sec, intersecting at 25.8°.

Geometric spreading has a very pronounced effect on the amplitude of body waves. In the distance range 0°-40°, this effect varies by a factor of about 100 for both P and S waves (Figures 3, 5). The amplitude is particularly large for the upper branches near the cusps at the beginning of regions of triplication. Slightly rounding the bottoms of the discontinuities (at 450 and 750 km) would produce large amplitudes on both branches near these cusps.

Attenuation. In addition to the geometric spreading effect, for model CIT11GB the effect upon the amplitude of attenuation due to anelasticity has been calculated. The Q vs. depth structure used was model MM8 of Anderson et al. (1965), derived from surface wave attenuation. In order to determine whether the slight attenuation in the high Q lowermantle could be detected using waves which have been attenuated strongly in the upper mantle, the calculations were done for two versions of the Q model: one with the values given by Anderson *et al*. below 600 km (Q = 4500 for P waves, Q = 2000 for S waves), and the other with infinite Q (no attenuation) in this region. For a particular frequency, the main effect of anelasticity is to decrease the amplitude with increasing distance in the region of triplications between 10° and 40°, where the rays are affected most strongly by the low Q upper mantle (Figure 6). For rays penetrating below 750 km (branches E-F, Figure 6), the attenuation depends very little on distance.

Compared to the effect of geometric spreading, the effect of attenuation on the amplitude vs. distance curves is slight, except for high frequencies which are so greatly attenuated as to be difficult to observe. The most significant effect of attenuation, in fact, is upon amplitude as a function of frequency, which is shown in Figure 7 for several points from Figure 6. Immediately apparent is the greater attenuation at high frequencies of S waves, due to both their lower Q and their greater travel time. For corresponding rays, S waves are attenuated 10 to 1000 times as much as P waves at 0.5 cps and 100 to 10^6 times as much at 1 cps. Thus attenuation is responsible for the observed low frequency character of S waves. Another way of looking at amplitude vs. frequency is by means of effective Q. From Figure 8 one can see not only that the effective Q is about 2-1/4 times greater for P waves than for S waves, but also that it varies by a factor of about 6 for both wave types. Furthermore, for the models with no attenuation in the lower mantle, the effective Q is greater by as much as 30%, which is easily detectable. The lower Q upper mantle does not completely mask our view of the Q structure of the lower mantle.

Ray Plots. An option of the travel time computer program described in Appendix II is to plot the trajectories of rays. For example, Figures 9 and 10 give the trajectories for P, S, PKP, SKS, PKIKP and SKIKS in Jeffreys' earth model. The core shadow zone for P and the strong focusing of P wave energy near 145° are shown quite dramatically. Plots of this sort have proved quite useful in recognizing potential difficulties of interpretation and in "steering" rays in the process of model modifications.

The P and S wave ray paths for model CIT11GB are shown in Figure 11 and illustrate the strong focusing effect of the discontinuities. The difficulties of interpretation between 15° and 30° can be well appreciated when these figures are compared with the corresponding figures for the much smoother models.

Jeffreys Model. Figures 12 and 13 show the travel time curve, its derivative, and the amplitude, considering the effects of geometric spreading only, for P waves from a surface focus in the model of Jeffreys (1962, p. 122). Between depths of 413 and 1047 km the model was smoothed by the addition of points spaced approximately every 32 km, with velocities determined by 4-point Lagrangian interpolation between the points given by Jeffreys. The travel time curve is quite smooth except for a small region of triplication in the vicinity of 20°. This "20° discontinuity" is produced by the moderately rapid increase of velocity between 413 and about 600 km depth (Bullen's region C). The ray tracings (Figure 14) are very helpful for understanding the relationship between the earth model and the zone of triplication.

Note that, although the travel time curve is smooth, its derivative is not, and the amplitude curve is discontinuous and very erratic. This behavior is caused by very slight irregularities produced by approximating the model with shells in which the velocity is given by $v = ar^b$. The actual behavior of body waves which have a finite wavelength is doubtless not as extremely sensitive to small irregularities as geometrical ray theory predicts. Body wave amplitude appears to be a potentially very powerful tool for studying details of earth structure.

Gutenberg Model. The reduced travel time, $\frac{dT}{d\Delta}$, and amplitude (considering geometric spreading only) of P waves for the Gutenberg earth model are shown in Figures 15 and 16. For depths less than 400 km the velocities were taken from Gutenberg (1959b), while below 400 km they were taken from the tabulation of Bullard (1957). The model has, of course, the well known Gutenberg low velocity zone, between depths of about 40 and 200 km. This region produces a shadow zone, and immediately beyond it, a region of duplication in the travel time curve, between 14.7 and 18.2 degrees. There are also four small zones of triplication, at 15.5, 16.0, 18.5, and 19.1 degrees, produced by small irregularities at depths of about 225, 250, 350, and 405 km.

These features, as well as the other irregularities in the $\frac{dT}{d\Delta}$ and amplitude curves are caused by small irregularities in the model, most of which are probably not significant. The drop in amplitude at 32° is caused by a decrease in the velocity gradient at 900 km, and is an important feature of this model. Again, the extreme sensitivity of the amplitudes to small details of earth structure is evident. Ray tracings for this model, shown in Figure 14 illustrate this sensitivity clearly.

Lehmann Model. Lehmann (1964) studied the travel times of P waves from 14 underground nuclear explosions fired at the Nevada Test Site (NTS) in 1961 and 1962, and from the Gnome underground explosion, fired in SE New Mexico in 1961. The travel times used, those published in the AFTAC shot reports, include only first arrivals, except in the case of the Hardhat event, for which some later arrivals were picked. The earth model derived by Lehmann has a low velocity channel between depths of 70 and 100 km, a discontinuous increase in velocity at 215 km, and a smooth increase from 215 to 670 km. Figures 17 and 18 show the travel time curve, its derivative, and the amplitudes (considering geometric spreading only) for this model. As for the Gutenberg earth model, there is a shadow zone, followed by a region of duplication, between 6 and 15 degrees, produced by the first order discontinuity at the bottom of the low velocity zone. Overlapping this region, there is zone of triplication, from 9 to 26 degrees, produced by the discontinuity at 215 km. The ray paths for Lehmann's model are shown in Figure 19.

Lukk and Nersesov Model. Lukk and Nersesov (1965) studied earth structure along a 3500 km profile extending from the Pamirs-Hindu Kush epicentral region northeast across central Asia to the Lena River. The average station spacing along the profile was 70 to 100 km. The earth model was based on the analysis, by several different methods, of data from 240 earthquakes with focal depths between 70 and 270 km. It has a single layer crust, 45 km thick, a low velocity zone between 110 and 150 km, and discontinuous increases of velocity at 85, 200, 400, and 700 km. In addition, the velocity increases very rapidly between 700 and 780 km, then remains constant from 780 km to 900 km. For shear waves only, there is a second low velocity channel between depths of 240 and 390 km. Figures 20 and 21 show the travel time, $\frac{dT}{d\Delta}$, and amplitude, considering only geometric spreading, of P waves from a surface focus for this model. The travel time curve is divided into two unconnected segments, A-D and E-O, because of the low velocity zone. The discontinuity at 85 km, above the low velocity zone, produces the region of triplication B-C in the first segment. The second segment has a region of duplication, E-F, between 8.1° and 14.3°, produced by the bottom of the low velocity zone, and four regions of triplication, G-H (9.4°-21.3°), I-J (22.6°-29°), K-L (22.5°-29°), and M-N (22.2°-23.3°), produced, respectively, by discontinuities at 200, 400, and 700 km and the rapid velocity increase between 700 and 780 km. In addition to having many complex later arrivals, this model is interesting because the first arrival travel times are not consistent with those for the other models suggesting that the earth is significantly different in central Asia than in tectonic areas of Europe and North America. Figure 19 illustrates the ray trajectories calculated for this model.

With the exception of the model of Lukk and Nersesov, the first arrival times are similar for all the models, although the later arrivals differ considerably. Many body wave studies are based entirely on first arrivals. Because of scatter in travel time data, it is difficult or impossible, using first arrivals alone, to distinguish between a smooth curve, such as that for Jeffreys' model (Figure 12), and one with sharp bends. If a smooth curve were fitted to the first arrivals of a travel time curve similar to Figure 2, a velocity structure would result which is similar to Jeffreys'. Only if due attention is paid to later arrivals can sharp first and second order discontinuities be detected with body waves. Otherwise relatively smooth structures with very broad transition regions result. Furthermore, all the models considered here have later arrivals whose amplitude is sometimes greater than that of the first arrival. For the surface wave model CIT11GB, the amplitude is less for the first arrival than for some of the later arrivals throughout the distance range 12° to 36° for both P and S waves. The large amplitude later arrivals help explain the scatter of data near the "20 discontinuity." For a model similar to CIT11GB later arrivals from small events could easily be mistaken for the first arrival.

Chapter III

Analysis of Body Wave Data

In order to delineate in as much detail as possible the regional variations in structure beneath North America, a large volume of body wave data from explosions has been analyzed. This includes all the data recorded during Project Early Rise from a series of forty 5 ton chemical explosions detonated on the bottom of Lake Superior as well as data from chemical explosions in Hudson Bay and nuclear explosions at the Nevada Test Site and in northwestern New Mexico.

The signals from Project Early Rise were recorded along ten profiles extending radially outward from Lake Superior, the locations of which are shown in Figure 22. Travel time and amplitude data for first arrivals, as well as record sections for the profiles have been compiled by the U. S. Geological Survey (Warren *et al*, 1967). Later arrival times have been measured from the record sections and used in the analysis. Travel times to the permanent Canadian seismograph stations observed during a similar experiment in Hudson Bay were measured from Figure 2 of Barr (1967). For events at the Nevada Test Site, a compilation was made of the best available travel time data for five profiles radiating from southern Nevada (see Figure 23). These data included recordings made by the Air Force Technical Applications Center (AFTAC) as part of the Long Range Seismic Measurements (LRSM) program. Whenever possible, travel times were read directly from the seismograms; for stations for which seismograms were not available, data published in the LRSM shot reports were used.

Also included were data from the World-Wide Standardized Seismograph Network (WWSSN) and the Seismograph Network of the Dominion Observatory of Canada. These data were measured from microfilm copies of the seismograms. In addition, travel times from a few other stations were taken from the bulletins of the International Seismological Center and the U. S. Coast and Geodetic Survey. For each station, events with the largest available signal to noise ratio were used, and particular emphasis was placed upon the measurement of later arrivals. The data for the Nevada Test Site profiles are listed in Tables 1-5. Not listed in the tables, but used in the analysis, were data from two U. S. Geological Survey profiles extending north and west from the Nevada Test Site, reported by Ryall and Stuart (1963) and Hill and Pakiser (1966), and data from a profile to the east of the nuclear explosion Greeley, measured from Figures 11 and 12 of Green and Hales (1968).

In order to study in detail the structure of the Colorado Plateau - Basin and Range boundary, the Nevada Test Site east profile was approximately reversed by a profile extending west from the Project Gasbuggy nuclear explosion in northwestern New Mexico to the edge of the Sierra Nevada in California. The mobile seismograph array described by Lehner and Press (1966) was used, along with several temporary instruments set up for this purpose and the permanent stations of the Caltech seismograph network. The observed travel times for these stations are given in Table 7 and the station locations are shown in Figure 24 and Table 6. Observations at distances less than

500 km were made by the U. S. Geological Survey (Warren, 1968).

The analysis of the data was carried out using the computer programs TVT4 and TTINV, described in Appendices II and IV. TTINV was used to find a spherically symmetric earth model which approximately fitted the observed travel times. In most cases, however, lateral variations along the profile were required to fit the data well. This fitting was performed by trial and error, using the spherically symmetric model as a starting point, and calculating the travel times with program TVT4. The models were required to be consistent with seismic refraction measurements of crustal structure, wherever such measurements exist, and the structures for different profiles were required to be the same at places where the profiles cross.

Amplitudes

The amplitudes of the observed waves furnish information on attenuation along the ray path and the geometric spreading of the rays which is complementary to the information furnished by the travel times. In order to interpret these data, however, the characteristics of the source must be known. The source parameters have been calculated for the explosions of the Early Rise experiment, but not for the nuclear explosions, since the required data are not available for most of them. The theoretical amplitude calculations here are based on first order geometric ray theory, and hence some care must be exercised in their application. In this work, only amplitudes for rays whose turning points are in regions of relatively low velocity gradients have been used. Ray theory approximations are known to be reasonably accurate for this condition (Archambeau et al, in press; Landisman et al, 1966).

The phenomena accompanying underwater explosions have been studied in considerable detail, both theoretically and experimentally, and are reasonably well understood (see, for example, Cole, 1948, and Arons and Yennie, 1948). The shots in the Early Rise experiment consisted of 10,650 lbs of du Pont Nitramon WW(EL) explosive detonated on the bottom of Lake Superior, at a depth of about 600 ft. Under these conditions, both the initial shock wave and the subsequent bubble pulses contribute significantly to the observed waves. Both signals have a duration much shorter than the period of the observed seismic waves (1/2 sec.), and for our purposes the pressure can be represented as a series of delta functions in time, each with the same specific impulse as the actual disturbance. Barnard (1967) gives data from which the shock wave impulse for Nitramon WW(EL), which consists of 74.5% ammonium nitrate, 18% aluminum, 5% dinitrotoluene, and 2.5% oil (personal communication from Dr. A. B. Andrews, du Pont Eastern Division Laboratories, Gibbstown, New Jersey), can be calculated. For a 10 lb shot the impulse is 0.407 and 0.179 psi-sec at distances of 35 and 70 ft, respectively. These values are about 1.5 times the corresponding values for pentolite (Arons, 1954). Assuming that this relation also holds with respect to pentolite at distances for which the acoustic scaling law

$$I_s = \ell W^{2/3}/R$$

applies, where I_s = impulse/unit area of wavefront, W = charge weight, and R = distance from charge, we calculate a value for the constant ℓ of 4 psi sec ft/$(lb)^{2/3}$.

The pulses emitted by the oscillating gas bubble have an impulse which is somewhat larger than that for the shock wave, and hence must be taken into consideration. The period between these "bubble pulses" is given by

$$T_B = 1.14\ \rho_o^{\frac{1}{2}}\ \frac{Y^{1/3}}{P_o^{5/6}} \tag{2}$$

where ρ_o is the density of the water, P_o is the initial hydrostatic pressure, and Y is the energy of the bubble oscillations (Cole, 1948, p. 276). Assuming that the energy Y is proportional to the heat of explosion, we can extend the observed period relation for TNT (Cole, 1948) to Nitramon WW(EL). Using the values of 1060 cal/g for TNT and 1520 cal/g for Nitramon WW(EL) (A. B. Andrews, personal communication) we get

$$T_B = 4.92\ \frac{W^{1/3}}{(d + 33)^{5/6}} \tag{3}$$

where T is in seconds, W in pounds, and d is the depth in feet. Theoretically, the period should be increased by proximity to the bottom, if it is rigid, and decreased by proximity to the free surface of the water, but observations do not confirm the bottom effect, probably because of cratering by the initial shock wave. Therefore, this period equation will be used as it stands. The impulse of the bubble pulses is given by

$$I_B = 0.21\ (rQ)^{2/3}\ (d + 33)^{-1/6}\ \frac{W^{2/3}}{R} \qquad (4)$$

where Q is the heat of explosion in cal/gm, r is the fraction of the explosion energy going into the bubble oscillations (about 40%), and d, W, and R are defined as before (Cole, 1948, p. 371). Again using observations on TNT for comparison, we calculate, for Nitramon WW(EL)

$$I_B = 15.5\ (d + 33)^{-1/6}\ \frac{W^{2/3}}{R} \qquad (5)$$

The energy of the successive bubble oscillations decreases considerably more rapidly than is predicted by simple theories, probably because of the turbulence in the water, so we will consider only the first bubble pulse. For the conditions of the Early Rise experiment (w = 10,650 lb, d = 600 ft), we get, from equations (1) and (5), for the specific impulse normalized to a distance (R = 1 cm) from the shot point (assuming an uncertainty of 50%):

$$\left.\begin{aligned} I_S &= (4.2 \pm 2.1)\ \text{dyne sec/cm}^2 \\ I_B &= (1.46 \pm 0.73)\ \text{dyne sec/cm}^2 \end{aligned}\right\} . \qquad (6)$$

From (3), we get the bubble period:

$$T_B = 0.5\ \text{sec} \qquad (7)$$

In addition to the direct wave, the reflections from the water surface and the lake bottom must be taken into consideration. On the basis of a sound velocity of 4720 ft/sec (1.44 km/sec) for water, the two way vertical travel time through the lake is 0.25 sec. The reflection from the free surface of the water is essentially perfect, but that from the lake bottom is not, only about 75% of the incident power being reflected (based on values given by Ewing, Jardetsky and Press (1957), discussed below). The total pressure signal in the lake may thus be represented as a series of delta functions in time (see Figure 25). As above, the pressure is scaled to a unit distance (1 cm) from the shot point, or from the appropriate image point for the reflections. k is the reflection coefficient, in terms of power, at the lake bottom. The second and later bubble pulses have been ignored. The part of the signal considered here is that with the largest amplitude. The amplitude measured on the seismograms is the maximum value within the first cycle or two, and hence should correspond to the same part of the signal.

The amplitude spectrum for this signal will have a maximum at 2 hz, and in fact the predominant frequency of the observed seismic waves is 2 hz, the higher frequency components having been removed, presumably by attenuation. In our amplitude calculations, we will consider only the 2 hz spectral component. The spectral density at this frequency, for the signal in Figure 25, is

$$p_o = \left(2 + \sqrt{k}\right) \left(I_B + I_S\right) + \sqrt{k} \left(1 + \sqrt{k}\right)^2 I_S \tag{8}$$

and the spectral density for the displacement is

$$A_o = p_o / \omega \alpha_o \rho_o \tag{9}$$

where ω is the angular frequency (4π radians/sec), α_o is the compressional velocity (1.44 km/sec), ρ_o is the density (1 g/cm^3), and, as before, we have normalized to a unit distance. The displacement spectral density of the emerging wave is given by

$$A = A_o r_o \sqrt{\frac{E}{I} \frac{\rho_o \alpha_o}{\rho \alpha} K} \quad \exp\left(- \frac{\omega T}{2Q}\right) \tag{10}$$

where r_o is the radius used in normalizing the amplitude (in this case, r_o = 1 cm), E/I is the geometrical spreading factor for the rays (see Appendix I), α and ρ are the compressional velocity and density, respectively, at the observation point, K is the product of the transmission coefficients (in terms of power) at the interfaces along the ray path, T is the total travel time, and Q is the effective quality factor, which gives the effect of attenuation (see Appendix I and Chapter II). Equation (10) can be used to calculate the quantity

$E/I \exp\left(-\frac{\omega T}{Q}\right)$ in terms of the observed amplitude and other quantities

$$\frac{E}{I} \exp\left(-\frac{\omega T}{Q}\right) = \frac{\rho\alpha\ A^2}{\rho_o\alpha_o\ A_o^2 r_o^2\ K} \qquad (11)$$

and this can be compared with values calculated for various earth models and effective Q values. In order to make use of this equation, we need the value of the transmission coefficient K.

The only interfaces at which the transmission coefficient is significantly different from 1 are the lake bottom and (for incidence near the critical angle) the Mohorovicic discontinuity. The coefficient at the Lake bottom can be estimated from graphs given by Ewing, Jardetsky, and Press (1957, Ch. 3). For a compressional wave in water, incident at an angle of about 10° upon a solid whose compressional velocity is 3.0 times greater, roughly appropriate for the bottom of Lake Superior, the power transmission coefficient is 0.25 and reflection coefficient k is thus 0.75. This is an upper limit on the possible value of k at the lake bottom; if the velocity increase is spread out over a transition zone, the value of k will be lower. Two factors in equation (11) depend on k: A_o (equations (8) and (9)) and k (which contains the factor (1-k). The product (1-k) A_o^2 has a maximum value of 6.13×10^8 cm^2/hz^2 for a value of k of 0.25. The actual value thus must be between this value and 3.37×10^8 cm^2/hz^2, calculated for k = 0.75. The transmission coefficient at the Moho depends strongly on the angle of incidence and hence has been calculated explicitly for appropriate values of the parameters and will be discussed separately for each profile.

Finally, assuming values of 3.0 ± 1.0 km/sec for α and 2.3 ± 0.3 g/cm^3 for ρ, we get, substituting numerical values into equation (11):

$$\log_{10}\left[\frac{E}{I}\exp\left(-\frac{\omega T}{Q}\right)\right] = (-8.0 \pm 0.5) + \log_{10}\left(\frac{A^2}{K_m}\right) \quad (12)$$

where E/I is measured in cm^{-2} and A in cm/hz. K_m is the transmission coefficient for two passages through the Mohorovicic discontinuity. The transmission coefficient at the lake bottom has been included in (12). Values of E/I can now be calculated from the amplitudes observed on the various profiles, and compared with values calculated from hypothetical models.

Manitoba and Yellowknife Profiles

The Manitoba profile extends north northwest about 1500 km from Lake Superior, crossing the Superior and Churchill provinces of the Canadian Shield. The boundary between the provinces is about 1100 km from the shot point, and runs approximately transverse to the profile. The Yellowknife profile is nearly parallel to the Manitoba profile, but lies about 500 km to the southwest, and covers the distance range from 1200 to 2300 km (see Figure 22). Except for the last three stations, which lie in the Yellowknife Province, the profile lies entirely within the Churchill Province. In the distance range from 1200 to 1500 km, covered by both profiles, the travel times are in good agreement. Because of this fact and the geological similarity of the regions traversed, the profiles have been interpreted together. Seismograms from the two profiles are shown in the form of record sections in Figures 27 and 28 and a combined plot of the travel times is given in Figure 26. The travel time curve on these figures is that calculated for model YLKNF 10, discussed below.

Crustal phases appear on the records out to about 350 km, but because of the great separation of the stations, crustal structure cannot be determined reliably. In the models, the crust is assumed to be similar to that found for the Lake Superior region by O'Brien (1968), consisting of three layers with velocities of 5.0, 6.7, and 7.2 km/sec. The Pn phase, which becomes a first arrival at about 350 km, has an apparent velocity of about 8.15 km/sec. Near 650 km, however, there is a sudden increase in the first arrival velocity to about 8.5 km/sec. Later arrivals lining up with this new phase can be traced as later arrivals back to approximately 450 km, and Pn can similarly be followed from the crossover point out to about 800 km. Beyond about 1100 km, the amplitude of the 8.5 km/sec branch diminishes rapidly, and the first arrival becomes difficult to identify. At about 1300 km, however, large arrivals appear again, and can be traced continuously to beyond 2000 km. A later arriving branch appears near 1850 km and becomes a first arrival at about 2300 km, near the end of the profile.

The model YLKNF 10 which has been fitted to these data is shown in Figure 38 and Table 8. The abrupt bend in the travel time curve near 600 km is interpreted as the result of a rapid increase in velocity from 8.11 to 8.43 km/sec at a depth of about 85 km. A region of slightly diminished velocities between depths of 96 and 160 km, beneath which the velocity again increases, produces the shadow zone and the region of duplication beginning near 1300 km. The later arrivals beginning near 1850 km are produced by an increase in the velocity from 8.55 to 9.50 between 375 and 420 km (see discussion of Model CIT11GB in Chapter II). The model has a minor low-velocity zone, with the velocity decreasing gradually, and by only 0.05 km/sec.

As discussed earlier in this chapter, the observed amplitudes furnish information on the attenuation along the ray path and the velocity gradient near the bottom of the ray. Unfortunately, absolute amplitude measurements were not made for the Manitoba profile. Such measurements are available, however, for the Yellowknife profile, and they enable us to study the average attenuation down to a depth of about 180 km, immediately below the low-velocity zone. As can be seen from Figure 28, the amplitude of the first arrival can be measured reliably only beyond about 1900 km; at smaller distances the large amplitude retrograde branch of the travel time curve interferes with the first arrivals. In the range from 1900-2200 km, the velocity amplitude is about 20 mμ/sec, corresponding (at a frequency of 2 hz) to a displacement amplitude of $\frac{-20}{4\pi} = 1.6$ mμ. For an appropriate value (about 43°) of the angle of incidence at the surface, the amplitude of the incident wave is calculated to be 1.1 mμ. Representing the signal as 2 cycles of a 2 hz wave yields an amplitude spectral density (A in equation (12)) of 5.5×10^{-6} cm/hz. The angle of incidence immediately above the Mohorovicic discontinuity is 55.6°, and the reflection coefficient (for two passages) is calculated to be $K_m = 0.91$. Substituting these values in equation (12), we get

$$\log_{10}\left[\frac{E}{I}\ \exp\left(-\frac{\omega T}{Q}\right)\right] = -18.5 \pm 0.5 \qquad (13)$$

Calculated values of the factor E/I, for models with different gradients between 170 and 210 km, lie in the range from 10^{-20} to 10^{-19}, if the model is constrained to be consistent with the observed travel times. Thus the observed and calculated values are consistent only if the attenuation is negligible. Quantitatively, from (13) we must have $Q \gtrsim \omega T$. For the waves under consideration here,

$T \cong 250$ sec, so $Q \gtrsim 3000$.

Nova Scotia and Quebec Profiles

The Nova Scotia profile extends north northeast from Chapleau, Ontario, about 400 km from the shot point, across the Superior Province of the Canadian Shield to Chibogamu, Quebec, at a distance of 1100 km. It then turns to the southeast, crossing the Grenville Province, leaves the Canadian Shield at the St. Lawrence River, and ends at Glace Bay, Nova Scotia, at a distance of 2200 km. The Quebec profile, lying entirely within the Superior Province, begins near Chibogamu, and extends northeast to Schefferville, Quebec, 1700 km from the shot point (see Figure 22). Record sections for the two segments of the Nova Scotia profile are shown in Figures 29 and 30, and that for the Quebec profile is shown in Figure 31. The travel time data are shown in Figure 28. Included for comparison on all the figures is the calculated curve for model YLKNF 10, discussed above. The records for these profiles are considerably noisier than those for the Manitoba and Yellowknife profiles, but despite this fact, the travel times for both profiles are similar. The profile begins at a greater distance, so the Pn phase is not observed, except possibly at the first few stations. Out to 1200 km, the first arrival times are virtually identical to those for the

Manitoba and Yellowknife profiles, with an apparent velocity of about 8.5 km/sec. Beyond this distance, the amplitudes are small and the travel times, though scattered, are delayed slightly and appear to have a higher velocity. Within the limitations of the data, the results for the two profiles are the same; the southwestern and southeastern margins of the Canadian Shield have similar upper mantle structures.

For this profile, unlike the Manitoba profile, absolute amplitude measurements are available for distances less than 1200 km, thus allowing us to study the velocity gradients and attenuation for waves that penetrate to a depth of about 90 km. At a distance of 800 km, the observed velocity amplitude is about 15 mμ/sec. The angle of incidence at the Moho is about 62°, which corresponds to a transmission coefficient of $K_m = 0.93$. Using arguments similar to those above, we calculate, from equation (12)

$$\log_{10}\left[\frac{E}{I}\ \exp\left(-\frac{\omega T}{Q}\right)\right] = -\ 18.75 \pm 0.5 \quad . \tag{14}$$

Calculations for models with various gradients between depths of 87 and 97 indicate that if attenuation is negligible, the velocity gradient in this region must be at least $2 \times 10^{-3}\ \sec^{-1}$ to be compatible with this value. If the attenuation is significant, the value must be larger, but this seems unlikely in view of the negligible effect of attenuation observed at greater distances on the Yellowknife profile. The effect of reflections at the "discontinuity" at 85 km has not been included. Whether this effect would be significant depends on how abrupt the velocity change actually is. In view of these two uncertainties, the calculated velocity gradient should be regarded as a minimum possible value.

Hudson Bay Experiment

Travel time data for the central Canadian Shield which can be comparedwith data from the Manitoba, Yellowknife, Nova Scotia, and Quebec profiles have been obtained by Barr (1967) from the Hudson Bay Experiment of 1965. This experiment involved the detonation of 41 separate chemical explosions along two long lines in the waters of Hudson Bay. The length of the longest line was about 700 km. Hobson et al. (1967) have made a time-term interpretation of the crustal structure under the bay, using the short range data. According to their interpretation, the crust consists of a single layer with a seismic velocity of 6.3 km/sec and a thickness varying between 26 and 41 km. The teleseismic data considered here was obtained from the records of the permanent stations of the Dominion Observatory's seismograph network, and were measured from Figure 2 of Barr (1967).

Since many different paths are represented, the observed travel times show considerable scatter (see Figures 33 and 34). Although they are qualitatively similar to the times for the Manitoba and Yellowknife profiles, they are earlier, by as much as 3 to 4 seconds, out to 2000 km, indicating that there are significant regional variations in the upper 300 km of the mantle, even within the Canadian Shield. The model HUDSBY 10 fitted to the data (Figure 38 and Table 9) has an abrupt increase in velocity from 8.23 to 8.48 at a depth of 60 km, corresponding to the similar feature at 85 km in model YLKNF 10. It appears that the low velocity zone, too, may differ from that for the Yellowknife region, being thinner and shallower (boundaries at 80 and 125 km) and having a smaller velocity decrease (.02 km/sec), but this is not certain, as the travel time curve between 1000 and 2000 km is not well defined by the data. The later arrivals associated with the zone of rapid velocity increase near 400 km are shown quite clearly. These data provide the best evidence on the structure at this depth for the Canadian Shield region; the only other data, from the Yellowknife profile, are quite sparse and come from later arrivals exclusively. The velocity increases from 8.58 to 9.40 km/sec in the depth interval from 370 to 410 km in the model HUDSBY 10.

Arkansas and Texas Profiles

The Arkansas and Texas profiles extend south-southwest from Lake Superior distances of about 1650 and 2250 km, respectively. The data from these profiles are qualitatively very similar to those for the Canadian Shield, discussed above, with apparent velocities of about 8.1 km/sec increasing to 8.5 km/sec at 700 km and a delay in the arrivals beyond about 1400 km (see Figure 35). The travel time curve shown in Figure 35 is that calculated for model ER-2, shown in Figure 38 and Table 10, which was proposed by Green and Hales (1968) on the basis of the data from these profiles. The features of this model are very similar to those of the model YLKNF 11 discussed previously, with a velocity at the top of the mantle of 8.05 km/sec, an abrupt increase to 8.33 km/sec at 89 km, and a small low velocity zone, terminated by a rapid velocity increase near 160 km.

North Carolina Profile

The observed travel times for the North Carolina profile, which extends 1700 km southeast from Lake Superior are, like those for the other profiles discussed above, similar to those observed on the Manitoba and Yellowknife profiles (see Figures 36 and 37). There is, as before, an abrupt increase in apparent velocity from 8.1 to

8.5 km/sec at about 500 km, and the times beyond 800 km are delayed slightly. The model NC 1 fitted to the data is shown in Figure 38 and Table 11, and the travel time curve calculated from it is shown in Figures 36 and 37. Because of the gap in the profile caused by Lake Michigan, and the geological heterogeneity of the path traversed, this model should be considered only a rough approximation to the actual structure.

The general features of all the models discussed so far are quite similar. The Pn velocity is approximately 8.1 km/sec, with an abrupt increase to about 8.4 km/sec at a depth of 80 or 90 km. It is interesting to note that travel times observed in the eastern coastal plain during the East Coast On-Shore Off-Shore Experiment and from the Chase III, IV, and VII explosions show an 8.5 km/sec branch, beginning with large later arrivals near 500 km, indicating that a similar abrupt velocity increase occurs in that region (see Figures 5, 8, and 9 of Willis, 1968). It is likely that this feature is responsible for reports of unusually large crustal thicknesses and high Pn velocities sometimes reported for eastern North America (e.g. Rankin _et al_, 1969). Pn is a first arrival only between approximately 300 and 600 km for models like YLKNF 10, and the 8.5 km/sec branch produces large later arrivals beginning near 400 km. The Hudson Bay data suggest that the velocity jump may occur at a shallower depth in some places, which would make the interpretation of data even more difficult. Beneath this "discontinuity," there is probably a slight velocity reversal, and a rapid velocity increase near 160 km. The details of this low velocity zone cannot be determined with certainty, but diminished amplitudes, followed by larger, delayed arrivals indicate that it probably exists. Thus, most of eastern North America, including the Canadian Shield and at least the eastern part of the Interior Lowlands provice, have similar upper mantle structures, with only slight regional variations.

NTS-North Profile

Figures 38 to 41 show the observed travel times for the profile extending north from the Nevada Test Site. In order to keep the path as homogeneous as possible, only stations in the Cordillera are included. Two studies have been made of crustal structure in regions traversed by this profile, and the models proposed for the profile are in agreement with the results of these studies. Hill and Pakiser (1966) investigated crustal structure between the Nevada Test Site and Boise, Idaho, using both chemical and nuclear explosions, and found that the crustal thickness increases abruptly, from about 31 to 42 km, going from the Basin and Range Province into the Snake River Plain. Since no similar studies have been made of the Columbia Plateau, we have assumed its crustal structure to be similar to that of the Snake River Plain. White and Savage (1965) used unreversed profiles from chemical explosions near Vancouver Island to study the structure of the crust in British Columbia. Crustal thickness was found to be greatest near the coast, and to decrease considerably toward the east, having a value of about 30 km in central British Columbia, where most of the stations for this profile are located. In both of these studies, Pn velocities of 7.8 to 7.9 km/sec were found. A recent, more detailed study by White _et al_ (1968) gives generally similar conclusions.

The observed travel time data show a clear offset at about 500 km, due to the increased crustal thickness in the Snake River Plain. Beyond about 700 km, the Pn arrival, whose amplitude decreases rapidly with distance, cannot be picked reliably. A later phase, with an apparent velocity of about 8.5 km/sec is the first observable arrival between about 900 and 2000 km. How far back this branch of the travel time curve extends is uncertain, in view of the scatter of the data points and the geographic spread of the recording stations. Therefore, two alternate models have been fitted to the data (see Figure 67 and Table 12). The preferred model, NTS N3, has the 8.5 km/sec branch beginning at a cusp near 900 km, while for the alternate model, NTS N1, it begins near 550 km. In both models, a velocity reversal in the upper mantle is required to produce the observed delay in this branch. Model NTS N1 has a velocity decrease of 0.4 km/sec at a depth of 60 km and an increase to 8.05 at 116 km, while for model NTS N3, the velocity decreases by only 0.1 km/sec, to 7.8, and the bottom of the low velocity zone is near 160 km.

Later arrivals associated with the rapid velocity increase near 400 km depth are observed between 1500 and 2100 km. Unfortunately, there are no observations between 2100 and 2700 km, so all the data on the 400 km "discontinuity" comes from later arrivals. This feature is similar in both proposed models; the velocity increases from 8.56 to 9.2 km/sec between depths of 360 and 420 km. The region immediately above the transition zone, however, is slightly different for the two models. This difference is intended to indicate the range of possibilities allowed by the data. Rays which penetrate beneath the transition zone near 650 km depth are observed as first arrivals at two stations. Because of the sparcity of relevant observations, however, the structure indicated for this zone in the two models is not reliable.

As can be seen from Figures 39-42, arrivals on the 8.5 km/sec branch, between 1000 and 2000 km, show considerable scatter. The residuals between the observed times and those calculated from the models, however, have a systematic geographical distribution, as is shown in Figure 44. Stations toward the east have positive residuals, while those toward the west have negative ones. Still further toward the west, the residuals appear to become positive again. Teleseismic P wave residuals show a similar north-south trending band of negative residuals, as is shown by the recent P-delay map of Herrin and Taggart (1968), a portion of which is reproduced as Figure 43.

Since P waves do not generally emerge vertically, and since the data of Herrin and Taggart have been averaged over all azimuths, travel time anomalies like those of Figures 43 and 44 give only a rough picture of the nature of the corresponding anomalies in seismic velocity. A more precise indication of the location of the velocity anomalies is obtained by studying the travel time residuals from a single earthquake, located in the region of interest, which can be done conveniently by plotting the observed residuals on an imaginary sphere centered at the earthquake focus, using the mapping defined by the seismic rays. Figure 45 shows such a plot, in an equal area projection, of the lower half of the focal sphere for the Puget Sound earthquake of April 29, 1965 (epicenter 47.41°N 122-29°W, depth = 59 km, magnitude M = 6.3). The anomalies are taken from the compilation of data for this earthquake by the Coast and Geodetic Survey. Positive residuals (late arrivals) have been indicated by pluses, and negative ones by circles, the absolute value being indicated by the size of the symbol. Davies and McKenzie

(   ) have used plots of this type to study earthquakes and the nuclear explosion "Longshot" in the Aleutian Islands and found a band of negative residuals which they interpreted as evidence of a slab of high velocity material dipping at an angle of about 45° northward beneath the island arc. The existence of such dipping slabs beneath island arcs has been suggested previously on the basis of studies of seismicity, earthquake focal mechanisms, and seismic wave attenuation (Isacks et al, 1968; Oliver and Isacks, 1967; Sykes, 1966).

A similar pattern may be seen in Figure 45; rays leaving the focus with a dip of about 50° to the east have negative residuals. Furthermore, as can be seen from Figure 46, which shows a map of the world in the same projection, many of the negative residuals outside this band correspond to stations located on island arc structures, such as Japan, the Aleutians, the Marianas, etc.

The analyses of travel time residuals is subject to a fundamental ambiguity with respect to the velocity distribution which produces them; the residual pattern of Figure 45 for example, could be by velocity anomalies beneath the receiving stations, rather than a slab of high velocity material in the source region. To partially overcome this ambiguity, we can study the residual pattern for another earthquake in the same general region but far enough away so that it is not located directly above the hypothetical slab.

The residuals should be approximately the same if anomalies beneath the stations are responsible, but should be different if structures near the focus are responsible. Figure 7 shows a residual plot, similar to that of Figure 45 for an earthquake on the Queen Charlotte Island fault off the coast of Vancouver Island. It is seen that the band of negative residuals which was found for the Puget Sound earthquake is absent, but that otherwise the residual pattern is similar. Travel time residuals thus furnish strong evidence of anomalously high seismic velocities, localized in a narrow zone dipping eastward about 50° from the Puget Sound region. The Cascade Range thus is probably an example of an island arc structure, although probably a nearly inactive one. Further support for this hypothesis comes from the focal mechanism of the Puget Sound earthquake considered here (Julian and McKenzie, in preparation).

Yukon Profile

The Yukon profile extends northwest from Lake Superior a distance of 3000 km, crossing from the Canadian Shield into the Interior Lowlands physiographic province, and then into the Rocky Mountains, where it ends near the Alaskan border (see Figure 22). Crustal structure determinations for areas near the profile have been made in central western Manitoba (Hall and Brisbin, 1965) and in the Albertan plains (Richards and Walker, 1959). With one notable exception in the vicinity of Lake Winnipeg (see below), the crustal structure for the model proposed here is consistent with these determinations. In the absence of any direct determinations for northern British Columbia or the Yukon, the crustal structure for these areas was assumed to be the same as that determined for southern British Columbia by White and Savage (1965, see discussion of Nevada Test Site north profile). A different crustal structure for this region would have little effect on other features of the model.

The travel times observed on this profile, as well as those for all the other profiles which include stations in both eastern and western North America, are relatively complicated, with several changes in apparent velocity, abrupt offsets of the travel time curve, etc. Kanasewich *et al.* (1968) have interpreted data from the Yukon profile in terms of a spherically symmetric earth, and obtained a rather complicated model, with two major low-velocity zones in the upper 350 km. It is apparent, however, from the differences in the observed travel times for eastern and western paths (*e.g.* the Yellowknife and NTS north profiles) that there are quite significant regional variations along profiles such as this one. The model proposed here includes these variations explicitly and is able to explain the complications in the observed travel times without resort to an extremely complicated model. Lateral changes in the structure of the low-velocity zone, in fact, are sufficient to explain most of the observations.

The observed travel times for the Yukon profile are shown in Figures 48 and 49, and record sections are given in Figures 50-52. The calculated travel time curve for model YUKON 4 (Table 13) is shown on all the figures. A cross-section of the crust and upper mantle illustrating the general features of the model is shown in Figure 53.

The travel times of the phase Pn are similar to those observed on the Manitoba and other eastern profiles out to a distance of 500 km. At this distance, however, the travel time curve is abruptly offset, and between 500 and 900 km the arrivals are early by as much as 2 seconds. A sudden change in crustal thickness is thus implied by the data. For the proposed model YUKON 4, the crust thins from 44 to 19 km and gradually thickens back to its original value in western Manitoba. Such pronounced changes in crustal thickness are indeed remarkable, but perhaps not completely unexpected; even more pronounced variations have been suggested to exist beneath Lake Superior (Smith _et al_, 1966; Berry and West, 1966). Also the crustal structure studies of Hall and Brisbin (1965), which were made about 200 km to the north of the region traversed by this profile, also indicated a rather low crustal thickness, 31 km, and that the value decreased toward the south. It is possible, of course, that errors in the travel time measurements are responsible for this apparent offset. Furthermore, the magnitude of the change depends on the average velocity in the crust, which is unknown. In any case, changes in this feature would have little effect on other parts of the model. Crustal structure in the vicinity of Lakes Winnipeg and Manitoba presents an intriguing topic for further investigation.

Beyond about 1300 km, the amplitudes of the first arrivals decrease, as did those on the various eastern profiles, due to the effect of the low-velocity zone. The branch of travel time curve corresponding to rays penetrating beneath the low-velocity zone, however, is delayed by about 3 seconds, much more than for the eastern profiles, indicating that the low-velocity zone is a more pronounced feature beneath the plains than in the east. The model YUKON 4 (Table 13 and Figure 53) has a low velocity zone between depths of 105 and 160 km in this region. Another small offset of the travel time curve apparently occurs near 1800 km, suggesting another slight change in the low-velocity zone, although the signal-to-noise ratio for these arrivals is poor.

The later arrivals near 1800 km associated with the "discontinuity" around 400 km depth are more clearly shown on this profile than on any other (Figures 48, 49, 51, and 52). This branch of the travel time curve is not smooth, however, but has peculiar changes in slope and curvature. An abrupt transition in the model to a low-velocity zone like that for NTS N3, however, explains this phenomenon quite well. Thus a model with lateral changes in the depth of the top of the low-velocity zone explains most of the peculiarities of the travel times observed along this profile, and is in agreement with structures determined independently near the ends of the profile.

Utah Profile

The Early Rise Utah profile begins about 450 km southwest of Lake Superior and extends across the Interior Lowlands, Southern Rocky Mountains, and Colorado Plateau physiographic provinces, ending in Utah on the edge of the Basin and Range province, 2250 km from the shot point. Observations during the 1964 Lake Superior experiment were made along a nearly identical profile as far as Denver, Colorado (Roller and Jackson, 1966) which included stations closer to the shot point. The crustal structure inferred from these observations is generally similar to that found in the Lake Superior region (O'Brien, 1968). Other crustal structure determinations have been made in the high plains of eastern Colorado (Jackson *et al*, 1963), the southern Rocky Mountains (Jackson and Pakiser, 1966), and the central Colorado Plateau

(Roller, 1965). The model UTAH 1 (Figure 57 and Table 15) proposed here has crustal structure consistent with these earlier studies.

The first arrivals have an apparent velocity of 8.4 km/sec out to a distance of 900 km. The velocity and travel time of this phase are consistent with those for waves refracted below the discontinuity at 90 km depth found for the Lake Superior region. The phase Pn is only observed as a first arrival at smaller distances, if at all. The observations of Roller and Jackson (1966) suggest the presence of this phase as a first arrival in the range from 300 to 400 km. At about 900 km there is a sudden offset in the first arrival curve. Arrivals beyond 900 km are delayed by about 2 sec and have an apparent velocity of 8.7 km/sec. This new phase, which can be traced as a later arrival back to 800 km, is analogous to a similar phase observed on the Yukon profile (see Figures 50 and 51), which is refracted beneath the low-velocity zone. Its travel time is smaller, however, indicating that the low-velocity zone is a less pronounced feature to the southwest of Lake Superior than to the northwest.

Beyond about 1500 km, where the profile enters the Rocky Mountains, the apparent velocity decreases and then near 1900 km increases again to near its original value. A delay, increasing with distance as the low-velocity zone becomes more pronounced, similar to that observed for the Yukon profile, is to be expected, but the value of the observed delay (5 sec), is unexplainably large. For this profile, unlike the other

Early Rise profiles, independent information on the mantle structure is available; the profile is approximately reversed by the Nevada Test Site northeast and east-northeast profiles. In addition, the Nevada Test Site east and Gasbuggy west profiles furnish structural information for the central Colorado Plateau, slightly south of the Utah profile. The models derived from these data are in substantial agreement with each other, but they cannot be reconciled with the late arrivals observed between 1700 and 2100 km on the Utah profile. The quality of the data themselves suggests that they are not reliable (see Figure 56). The amplitudes and the signal to noise ratio are both very small, and in fact the arrival times were indicated to be questionable by Warren et al, (1967). Furthermore, the travel times measured by Roller and Jackson (1966) in central Arizona, at a distance of 1800 km, during the 1964 Lake Superior experiment are smaller than those for the Utah profile, and are in agreement with the times calculated from the model UTAH 1. Thus, although the low-velocity zone does introduce a delay at the stations in the west, it is probably not as great as that indicated by the data in Figures 54, 55, and 56.

A cross-section of the crust and upper mantle along the line of the profile is shown in Figure 57. Though differing in detail, the structure of the upper mantle is seen to be similar along this profile and the Yukon profile (Figure 53). Data from the Nevada Test Site northeast, east-northeast, and east profiles, and the Gasbuggy west profile, discussed below were also used in deriving this structure.

NTS Northeast and East-northeast Profiles

Since travel time data for the Nevada Test Site east-northeast profile are less numerous than those for other profiles, and since they were mostly measured from small events, this profile and the Nevada Test Site northeast profile have been interpreted together. The observed travel times are shown in Figures 58 and 59, along with the calculated times for the proposed model NTS NE1. The model is based also on data from the Early Rise Utah profile, which approximately reverses these profiles, and is essentially the same as the model UTAH 1 (see above).

The phase Pn is observed at distances less than 500 km, but not beyond, due to the small size of the events involved. Beyond 500 km the arrivals are delayed about 4 seconds and have an apparent velocity of about 8.4 km/sec. This phase is more clearly observed on the NTS east and Gasbuggy west profiles, for which the station density is higher. It is analogous to the phase observed in eastern North America which is refracted beneath the 90 km discontinuity, and indicates that a similar feature exists at a depth of about 100 km beneath the Colorado Plateau. The phase continues to a distance of 1500 km, beyond which waves refracted beneath the low velocity zone are the first arrival. The branches of the travel time curve associated with the 400 km discontinuity are observed exceptionally clearly on this profile, as both first and later arrivals. Between about 1600 and 200 km, however, there is an offset of about 5 seconds in the travel time curve, indicating a change in the depth to the discontinuity. In the proposed model, NTS NE 1, the discontinuity is 30 km shallower to the northeast than to the southwest, the change occurring at a distance of 9.2° (1020 km) from the Nevada Test Site, approximately beneath the edge of the Rocky Mountains near the Wyoming-Montana border. This may be nothing more than a coincidence, as comparison of the NTS north and Yukon profiles indicates that the discontinuity is deep beneath the plains in Canada and shallow in the Pacific northwest, while the NTS east profile (see below) indicates that it remains deep in both the southwestern and south central United States. Waves refracted beneath the 600 km discontinuity are observed as first arrivals beyone 3400 km. Because of the gap in the station coverage between 2500 and 3400 km and the lack of later arrival data, though, the structure at this depth in the model is not reliable.

NTS East Profile

Figures 60 and 61 show the observed travel times for the profile extending east from the Nevada Test Site to the Atlantic Ocean. Included are the data measured by Ryall and Stuart (1963) along a profile to Ordway, in eastern Colorado (Figure 24). The initial law Pn velocity (7.6 km/sec) caused by the greater crustal thickness in the western Colorado Plateau is evident, as well as an increase in velocity at 400 to 500 km, as the crust becomes thinner again. Pn observations on the Gasbuggy west profile (see below) which approximately reverses this profile, are consistent with a crustal structure of this type, but a detailed interpretation has not been attempted. Beginning at about 500 km as a later arrival is a branch of the travel time curve with an apparent velocity of about 8.3 km/sec. Ryall and Stuart called this phase P_c, but gave no interpretation of it. Its travel time is consistent with that calculated for an abrupt increase in velocity of about 0.3 km/sec at a depth of 100 km, as are the times of similar phases observed on the NTS northeast, NTS east-northeast, and Gasbuggy west profiles. These observations provide strong evidence that such a discontinuity is present beneath the Colorado Plateau. The data suggest that this phase disappears at about 1000 km, although inadequate station coverage from 1000 to 1500 km makes this conclusion uncertain. For the profiles northeast of NTS, the phase continues to about 1500 km. Thus, it appears that the discontinuity may not exist beneath the Southern Rocky Mountains in Colorado (see Figure 57). Beyond 1500 km, the travel times observed for this profile are generally similar to those for the two northeasterly NTS profiles. Waves refracted beneath the 400 km discontinuity, however, are about 3 sec later, indicating that its depth does not decrease in the southern plains as it does further north.

Gasbuggy West Profile

The Project Gasbuggy nuclear explosion was detonated in northwestern New Mexico on December 10, 1967. Stations of the CIT portable seismic array (Lehner and Press, 1966) were operated along a profile extending from northwestern Arizona to the edge of the Sierra Nevada in California, extending a profile of U.S. Geological Survey stations (Figure 24). Data from the CIT stations are shown in the form of a record section in Figure 63. The dashed lines connecting the picked phases are only initial tentative correlations, and do not correspond exactly to the final interpretation, which is shown in Figure 62. Prominent features on the records are the crustal phase $\overline{P}$, with a velocity of about 6.2 km/sec, and, about 10 seconds earlier, a similar phase with a velocity of about 7 km/sec which is probably a wave guided in the lower crustal layer. The high apparent velocity of Pn between 500 and 700 km is in agreement with the hypothesis that the crust is thicker in the western Colorado Plateau than in the Basin and Range province (see discussion of NTS east profile, above). At about 700 km, near the calculated cusp for waves reflected at the 100 km discontinuity, large later arrivals are observed. The times of the first arrivals at greater distances, however, indicate that this discontinuity does not continue into the Basin and Range province.

Waves refracted from below the low-velocity zone are observed near 900 km.

Since the profile is not long enough to observe this phase as a first arrival, the velocity beneath the low-velocity zone is not well determined by these data.

NTS Southeast Profile

The data recorded to the southeast from the Nevada Test Site (Figure 64) are of poor quality, since most of the events used were small. They are generally consistent with the travel times observed on the NTS north profile; however, (Figure 4) suggesting that Basin and Range structure in Nevada and in southern Arizona and New Mexico are similar.

Washington Profile

The travel times observed along the Early Rise Washington profile are shown in Figures 65 and 66. Lewis and Meyer (1968) have interpreted these data in terms of a model with discontinuous increases of velocity at 70 and 125 km and a minor velocity decrease between 130 and 200 km. The modification of their model proposed here (Table 19 and Figure 67) explains the observed times better, and is qualitatively very similar to the other models for eastern and central North America. It has an abrupt velocity increase of about 0.25 km/sec at 60 km, and a low-velocity zone between 80 and 140 km.

Uniqueness of Proposed Models

Several factors lead to a degree of non-uniqueness in the proposed models. As has been mentioned for several of the individual profiles, data of poor quality cause uncertainties in particular features of some of the models. Later arrival data, especially, are subject to larger uncertainties than first arrivals; features such as the "sharpness" of discontinuities, which depend on later arrivals are less certain than those based on first arrivals, such as velocities above and below discontinuities. Since travel times are most sensitive to the velocity near turning points of the rays, the sampling of laterally inhomogeneous structures provided by travel time data is not the same in different regions. The structure indicated in Figure 53 for the low-velocity zone beneath the Canadian Rocky Mountains, for example, is based on data from the Yukon and NTS north profiles, for both of which rays measure only the total delay through the zone. Variations, such as a "lid" above the low-velocity zone, are possible. Those features which are less certain are mentioned in the discussions of the individual profiles and models, and are indicated by dashed lines on the cross-sections of Figures 53 and 57.

Another type of uncertainty arises because of the number of degrees of freedom involved in specifying a two-dimensional velocity structure. It is well known that the interpretation of unreversed profiles is subject to ambiguities between vertical and horizontal velocity variations. For example, the spherically symmetric model proposed by Kanasewich et al (1968), with multiple discontinuities and low-velocity zones, explains the observed travel times for the Yukon profile as well as the model YUKON 4 proposed here. The consideration of data from many profiles, including ones which cross or reverse each other, eliminates many such ambiguities, however. Data for the Canadian Shield and western North America indicate that the structure along the Yukon profile is not spherically symmetrical.

Chapter IV

Conclusions

The data analyzed in Chapter III gives a fairly detailed picture of the structure of the upper mantle in North America. Significant regional differences in mantle structure have been found; within the upper 200 km the compressional velocity varies by almost 10%. Differences of smaller magnitude persist to a depth of at least 400 km. The general features of upper mantle structure determined in Chapter III are summarized and discussed below.

Eastern North America

The structural features of the upper mantle are generally similar throughout the Canadian Shield, the eastern part of the Interior Lowland province, and the eastern United States. The velocity structures for the models derived from profiles in these regions are shown in Figure 38. The velocity at the top of the mantle is between 8.0 and 8.1 km/sec, except in the central Canadian Shield beneath Hudson Bay, where Hobson et al have reported a velocity of 8.23 km/sec. The most striking feature of the models is an abrupt, or nearly abrupt, increase in the compressional velocity by about 0.2 or 0.3 km/sec somewhere between the depths of 60 and 90 km. The shallower depths are based on data of somewhat lower quality than the deeper values, but the depth variations nevertheless appear to be real. This "discontinuity" is a very widespread feature beneath North America; it is also found beneath much of the western United States, although at a slightly greater depth (see below), and beneath the Gulf of Mexico (Hales, personal communication).

Confusion of waves reflected and refracted from this discontinuity with the phase Pn are probably responsible for unusually large crustal thicknesses and Pn velocities sometimes reported for eastern North America. It is interesting to note that Ringwood (1969) has predicted a velocity increase of about 0.3 km/sec near 70 km depth due to the transformation from a pyroxene pyrolite to a garnet pyrolite mineral assemblage. Beneath the discontinuity there is, in most areas at least, a minor low-velocity zone. The details of the velocity variation cannot be determined precisely from travel time data, and the details clearly vary regionally, but the zone occurs somewhere within the depth range from 80 to 160 km, is 30 to 50 km thick, and the velocity decrease is less than 0.2 km/sec.

Included in Figure 38 for the sake of comparison are the compressional and shear velocity distributions for model CANSD, derived by Brune and Dorman (1963) from surface wave dispersion in the Canadian Shield. It can be seen that the compressional velocity in the upper mantle for model CANSD is lower than that for the other models by up to 0.4 km/sec. Since surface wave phase velocities are about 5 times more sensitive to shear velocity than to compressional velocity, a small change in the former would compensate for this difference. It is interesting that the velocity reversal occurs at roughly the same depth in the proposed models as the shear velocity reversal for model CANSD, which has a low velocity zone for shear waves only.

Amplitudes and Velocity Gradients

The absolute amplitudes of the observed waves have been used to obtain information about the seismic attenuation and the velocity gradients near the southwestern and southeastern margins of the Canadian Shield. The minimum value of the quality factor Q for the upper 200 km (including the low velocity zone) is approximately 3000. The minimum possible velocity gradient, both above and below the low velocity zone, is about 2×10^{-3} sec^{-1}. Under the assumption of chemical uniformity for these regions, this value can be related to the temperature gradient. We have

$$\frac{dV}{dz} = \left(\frac{\partial V}{\partial P}\right)_T \frac{dP}{dz} + \left(\frac{\partial V}{\partial T}\right)_P \frac{dT}{dz}$$

where

V = compressional velocity

z = depth

P = pressure

T = temperature

Anderson and Sammis (in press) have compiled measured values of $\left(\frac{\partial V}{\partial P}\right)_T$ and $\left(\frac{\partial V}{\partial T}\right)_P$ for presumed mantle constituents. For a mixture with the composition estimated by Ringwood (1969, Figure 3) at depths between 80 and 160 km (56% olivine, 40% pyroxene, 4% garnet), the velocity derivatives are

$$\left(\frac{\partial V}{\partial P}\right)_T = 13.7 \times 10^{-3} \text{ km/sec kb}$$

and

$$\left(\frac{\partial V}{\partial T}\right)_P = -5.0 \times 10^{-4} \text{ km/sec °C.}$$

Taking the hydrostatic pressure gradient of $\frac{dP}{dz} = 0.32$ kb/km, we find that the observed minimum velocity gradient implies a maximum temperature gradient of 4.8 °C/km. This value is lower than that estimated by Ringwood (1966) (7-10°C/km) and also those calculated from other seismic models (5-11°C/km, Anderson and Sammis, in press). For the Canadian Shield, however, lower temperatures and thermal gradients are to be expected, in view of the high seismic velocities and low heat flow. Assuming a conductivity of 6×10^{-3} cal/cm sec°C, the inferred heat flow in the mantle is 0.29 $\mu cal/cm^2$ sec, compared to values observed at the surface of 0.8 $\mu cal/cm^2$ sec for the Canadian Shield, and 1.1 $\mu cal/cm^2$ sec for the rest of eastern North America (Simmons and Roy, 1969). The observed thermal gradient is also comparable to the melting point gradient of 4°C/km (as one would expect in view of the unpronounced and highly variable nature of the low-velocity zone in eastern North America). Thus the observed amplitudes can be used to infer the velocity gradient in the mantle, which is very poorly defined by the travel time data alone. Extension of the technique to other known seismic sources, particularly nuclear explosions, and the development of more accurate theories for calculating theoretical amplitudes can greatly increase our knowledge of details of the structure of the earth.

Western North America

The upper mantle structure in western North America differs from that in the east primarily in the existence of a pronounced low velocity zone, with velocities of the order of 7.7-7.8 km/sec (see Figure 67). For profiles extending east and northeast from the Nevada Test Site, evidence has been found for a "discontinuity" similar to the one found at depths varying between 60 and 90 km in eastern North America (see above). The velocity increase is about the same, $\sim$ 0.3 km/sec, but the absolute velocities are lower and the depth to the discontinuity is greater, $\sim$ 100 km. For paths to the north and southeast from NTS, in the Basin and Range Province, there is no evidence for such a feature, the low-velocity zone apparently extending to the base of the crust.

The travel time curves for profiles which include stations in both eastern and western North America are relatively complicated. Previous interpretations of these data in terms of a spherically symmetric earth have invoked very complicated models, with mulitple low-velocity zones. The lateral changes in the structure of the low-velocity zone, however, are sufficient to explain the observations without resort to such complex models. The depth to the bottom of the low-velocity zone does not vary greatly, being between 140 and 160 km for all the models considered. This depth is the same as that found under oceans by Anderson and Toksoz (1963). The velocity in the zone and the depth to the top vary greatly (Figures 53 and 57).

Data from all the long profiles show clear evidence of the existence of a rapid velocity increase near 400 km depth. There is clear evidence, moreover, that the structure of this transition region varies regionally. Previous studies have suggested such variations (Archambeau *et al*, in press) but the conclusion was uncertain because of the influence of the more pronounced structural differences at shallower depths. Most of the deviation seems to involve the depth to the discontinuity, which varies by at least 30 km, and to have no simple relation to the variations at shallower depths. In fact, no obvious pattern is evident in the measured depths (see Figure 68). The assumption that the discontinuity is caused by the transition of olivine to the spinel structure would imply temperature variations of 250°C or variations of .06 in the mole fraction of fayalite in the olivine (Anderson, 1967). Further discussion of the physical significance of these regional differences will have to await the availability of more data, so that the structural details can be further refined.

Appendix I

A Variational Formulation of Seismic Ray Theory in an Arbitrarily Heterogeneous Earth

Recently V. A. Eliseevnin (1965) has formulated the ray problem for an arbitrarily inhomogeneous medium. Starting with the eikonal equation,

$$(\bar{\nabla} u)^2 = n^2,$$

where $u(\bar{r})$ is the eikonal, or phase function, and $n(\bar{r})$ is the refractive index of the medium, he derived the following system of six simultaneous differential equations for the motion of a disturbance along a ray:

$$\begin{aligned}
\frac{dx}{dt} &= v \cos \alpha \\
\frac{dy}{dt} &= v \cos \beta \\
\frac{dz}{dt} &= v \cos \gamma \\
\frac{d\alpha}{dt} &= \frac{\partial v}{\partial x} \sin \alpha - \frac{\partial v}{\partial y} \cot \alpha \cos \beta - \frac{\partial v}{\partial z} \cot \alpha \cos \gamma \\
\frac{d\beta}{dt} &= - \frac{\partial v}{\partial x} \cos \alpha \cot \beta + \frac{\partial v}{\partial y} \sin \beta - \frac{\partial v}{\partial z} \cot \beta \cos \gamma \\
\frac{d\gamma}{dt} &= - \frac{\partial v}{\partial x} \cos \alpha \cot \gamma - \frac{\partial v}{\partial y} \cos \beta \cot \gamma + \frac{\partial v}{\partial z} \sin \gamma
\end{aligned} \qquad (1)$$

where:

x, y, z are the cartesian coordinates of a point on the ray.

α, β, γ are the direction angles of the tangent to the ray.

$v(x, y, z)$ is the wave speed.

t = time.

Only five of these equations are independent, because the last three are connected by the relation $\cos^2\alpha + \cos^2\beta + \cos^2\gamma = 1$. We shall give a different derivation, based on Fermat's principle of least time, and carry out the derivation in spherical coordinates, so that the result will be in a seismologically useful form.

Let r, θ, ϕ be the spherical coordinates, at time t, of a point on a ray. Further, letting $\hat{e}_r$, $\hat{e}_\theta$, $\hat{e}_\phi$ be the conventional unit vectors for spherical coordinates, define:

i_r = angle between ray direction and $\hat{e}_r$.

i_θ = angle between ray direction and $\hat{e}_\theta$.

i_ϕ = angle between ray direction and $\hat{e}_\phi$.

The first three differential equations follow geometrically:

$$\frac{dr}{dt} = v \cos i_r \tag{2}$$

$$\frac{d\theta}{dt} = \frac{v}{r} \cos i_\theta \tag{3}$$

$$\frac{d\phi}{dt} = \frac{v}{r \sin\theta} \cos i_\phi \tag{4}$$

To find the differential equations for $\frac{di_r}{dt}$, $\frac{di_\theta}{dt}$, and $\frac{di_\phi}{dt}$, we consider conditions for the travel time to be stationary with respect to small changes in the ray path. The travel time of a ray between two points where $\theta = \theta_1$ and $\theta = \theta_2$ is

$$T = \int_{\theta=\theta_1}^{\theta=\theta_2} \frac{ds}{v} = \int_{\theta_1}^{\theta_2} \frac{r d\theta}{v \cos i_\theta}$$

where ds is an element of length of the ray path. Consider a small change in the ray path specified by $\delta r(\theta)$, $\delta\phi(\theta)$ with $\delta r(\theta_1) = \delta r(\theta_2) = \delta\phi(\theta_1) = \delta\phi(\theta_2) = 0$, that is, with the end points of the ray fixed. The change in the travel time is

$$\delta T = \int_{\theta_1}^{\theta_2} \frac{\delta r \, d\theta}{v \cos i_\theta} + \int_{\theta_1}^{\theta_2} \delta(\frac{1}{v}) \frac{r d\theta}{\cos i_\theta} + \int_{\theta_1}^{\theta_2} \delta(\frac{1}{\cos i_\theta}) \frac{r d\theta}{v} . \quad (5)$$

Now $$\delta(\frac{1}{v}) = - \frac{1}{v^2} \left[\frac{\partial v}{\partial r} \delta r + \frac{\partial v}{\partial \phi} \delta\phi\right] \quad (6)$$

and from (2), (3) and (4) we get

$$\tan^2 i_\theta = (\frac{1}{r} \frac{dr}{d\theta})^2 + (\sin \theta \frac{d\phi}{d\theta})^2$$

which leads to

$$\tan i_\theta \sec^2 i_\theta \, \delta i_\theta = \frac{1}{r}\frac{dr}{d\theta}\left[-\frac{1}{r^2}\frac{dr}{d\theta}\,\delta r + \frac{1}{r}\frac{d}{d\theta}(\delta r)\right]$$

$$+ \sin^2\theta \frac{d\phi}{d\theta}\frac{d}{d\theta}(\delta\phi)$$

so

$$\delta\left(\frac{1}{\cos i_\theta}\right) = \tan i_\theta \sec i_\theta \, \delta i_\theta = -\frac{\cos i_\theta}{r^3}\left(\frac{dr}{d\theta}\right)^2 \delta r$$
$$+ \frac{\cos i_\theta}{r^2}\frac{dr}{d\theta}\frac{d}{d\theta}(\delta r) + \cos i_\theta \sin^2\theta \frac{d\phi}{d\theta}\frac{d}{d\theta}(\delta\phi). \qquad (7)$$

Using (7), the third term on the right side of (5) becomes

$$\int_{\theta_1}^{\theta_2} \delta\left(\frac{1}{\cos i_\theta}\right)\frac{r d\theta}{v} = -\int_{\theta_1}^{\theta_2}\frac{\cos i_\theta}{vr^2}\left(\frac{dr}{d\theta}\right)^2 \delta r \, d\theta$$
$$+ \int_{\theta_1}^{\theta_2}\frac{\cos i_\theta}{rv}\frac{dr}{d\theta}\frac{d}{d\theta}(\delta r)\, d\theta \qquad (8)$$
$$+ \int_{\theta_1}^{\theta_2}\frac{r\cos i_\theta}{v}\sin^2\theta\frac{d\phi}{d\theta}\frac{d}{d\theta}(\delta\phi)\, d\theta.$$

Integrating by parts:

$$\int_{\theta_1}^{\theta_2}\frac{\cos i_\theta}{rv}\frac{dr}{d\theta}\frac{d}{d\theta}(\delta r)\, d\theta = \left[\frac{\cos i_\theta}{rv}\frac{dr}{d\theta}\,\delta r\right]_{\theta_1}^{\theta_2}$$
$$- \int_{\theta_1}^{\theta_2}\frac{d}{d\theta}\left[\frac{\cos i_\theta}{rv}\frac{dr}{d\theta}\right]\delta r \, d\theta \qquad (9)$$

and

$$\int_{\theta_1}^{\theta_2} \frac{r \cos i_\theta}{v} \sin^2 \theta \frac{d\phi}{d\theta} \frac{d}{d\theta} (\delta\phi)\, d\theta$$

$$= \left[\frac{r \cos i_\theta}{v} \sin^2 \theta \frac{d\phi}{d\theta} \delta\phi \right]_{\theta_1}^{\theta_2} \tag{10}$$

$$- \int_{\theta_1}^{\theta_2} \frac{d}{d\theta} \left[\frac{r \cos i_\theta}{v} \sin^2 \theta \frac{d\phi}{d\theta} \right] \delta\phi\, d\theta.$$

Since δr and $\delta\phi$ vanish for $\theta = \theta_1$ and $\theta = \theta_2$, the first term on the right side of each of these equations vanishes.

Using (6), (8), (9), and (10), (5) now becomes (rearranging terms)

$$\delta T = \int_{\theta_1}^{\theta_2} \left\{ \left[\frac{1}{v \cos i_\theta} - \frac{r}{v^2 \cos i_\theta} \frac{\partial v}{\partial r} - \frac{\cos i_\theta}{vr^2} \left(\frac{dr}{d\theta}\right)^2 \right. \right.$$

$$\left. - \frac{d}{d\theta} \left(\frac{\cos i_\theta}{rv} \frac{dr}{d\theta} \right) \right] \delta r + \left[- \frac{r}{v^2 \cos i_\theta} \frac{\partial v}{\partial \phi} \right. \tag{11}$$

$$\left. \left. - \frac{d}{d\theta} \left(\frac{r \cos i_\theta}{v} \sin^2 \theta \frac{d\phi}{d\theta} \right) \right] \delta\phi \right\} d\theta.$$

Since we want $\delta T = 0$ for arbitrary δr and $\delta\phi$, the coefficients of δr and $\delta\phi$ in (11) must vanish. Noting, from (2), (3), and (4) that

$$\frac{dr}{d\theta} = \frac{r \cos i_r}{\cos i_\theta}$$

and

$$\frac{d\phi}{d\theta} = \frac{\cos i_\phi}{\sin\theta \cos i_\theta}$$

and doing some algebraic manipulation, these conditions can be written as

$$\frac{v}{r} \cos i_\theta \frac{di_r}{d\theta} = \sin i_r \left(\frac{\partial v}{\partial r} - \frac{v}{r}\right) - \cot i_r \left[\frac{-\cos i_\theta}{r} \frac{\partial v}{\partial \theta} + \frac{\cos i_\phi}{r \sin\theta} \frac{\partial v}{\partial \phi}\right] \tag{12}$$

and

$$\frac{v}{r} \cos i_\theta \frac{di_\phi}{d\theta} = -\cot i_\phi \left[\cos i_r \left(\frac{\partial v}{\partial r} - \frac{v}{r}\right) + \frac{\cos i_\theta}{r} \left(\frac{\partial v}{\partial \theta} - v \cot\theta\right)\right] + \frac{\sin i_\phi}{r \sin\theta} \frac{\partial v}{\partial \phi}. \tag{13}$$

Using (3), we see that these are the expressions for $\frac{di_r}{dt}$ and $\frac{di_\phi}{dt}$. The expression for $\frac{di_\theta}{dt}$ can be found from them using the fact that

$\cos^2 i_r + \cos^2 i_\theta + \cos^2 i_\phi = 1$. The six differential equations for the ray then are:

$$\frac{dr}{dt} = v \cos i_r \tag{14}$$

$$\frac{d\theta}{dt} = \frac{v}{r} \cos i_\theta \tag{15}$$

$$\frac{d\phi}{dt} = \frac{v}{r \sin\theta} \cos i_\phi \tag{16}$$

$$\frac{di_r}{dt} = \sin i_r \left(\frac{\partial v}{\partial r} - \frac{v}{r}\right) - \cot i_r \left[\frac{\cos i_\theta}{r} \frac{\partial v}{\partial \theta} + \frac{\cos i_\phi}{r \sin\theta} \frac{\partial v}{\partial \phi}\right] \tag{17}$$

$$\frac{di_\theta}{dt} = \frac{\sin i_\theta}{r} \frac{\partial v}{\partial \theta} - \cot i_\theta \left[\cos i_r \left(\frac{\partial v}{\partial r} - \frac{v}{r}\right) + \frac{\cos i_\phi}{r} \left(\frac{1}{\sin\theta} \frac{\partial v}{\partial \phi} + \frac{\cos i_\phi}{\cos i_\theta} v \cot\theta\right)\right] \tag{18}$$

$$\frac{di_\phi}{dt} = \frac{\sin i_\phi}{r \sin\theta} \frac{\partial v}{\partial \phi} - \cot i_\phi \left[\cos i_r \left(\frac{\partial v}{\partial r} - \frac{v}{r}\right) + \frac{\cos i_\theta}{r} \left(\frac{\partial v}{\partial \theta} - v \cot\theta\right)\right] \tag{19}$$

Instead of i_θ or i_ϕ, it is simpler to use the angle ζ between the vertical plane in the ray direction and the meridional plane. We have

$$\cos \zeta = \frac{\cos i_\theta}{\sin i_r} \qquad \sin \zeta = \frac{\cos i_\phi}{\sin i_r}$$

so

$$\sin \zeta \frac{d}{dt} = \frac{\sin i_\theta}{\sin i_r} \frac{di_\theta}{dt} + \frac{\cos i_\theta \cos i_r}{\sin^2 i_r} \frac{di_r}{dt} = \frac{1-\cos \zeta}{r \sin i_r} \frac{\partial v}{\partial \theta}$$

$$- \frac{\cos \zeta \sin \zeta}{\sin i_r} \cdot \frac{1}{r \sin \theta} \frac{\partial v}{\partial \phi} - \frac{v}{r} \sin i_r \sin^2 \zeta \cot \theta$$

and we can write the five equations for the ray as

$$\frac{dr}{dt} = v \cos i_r \tag{20}$$

$$\frac{d\theta}{dt} = \frac{v}{r} \sin i_r \cos \zeta \tag{21}$$

$$\frac{d\phi}{dt} = \frac{v}{r \sin \theta} \sin i_r \sin \zeta \tag{22}$$

$$\frac{di_r}{dt} = \sin i_r \left(\frac{\partial v}{\partial r} - \frac{v}{r}\right) - \frac{\cos i_r}{r} \left[\cos \zeta \frac{\partial v}{\partial \theta} + \frac{\sin \zeta}{\sin \theta} \frac{\partial v}{\partial \phi}\right] \tag{23}$$

$$\frac{d\zeta}{dt} = \frac{1-\cos\zeta}{r\sin i_r \sin\zeta}\frac{\partial v}{\partial\theta} - \frac{\cos\zeta}{\sin i_r}\cdot\frac{1}{r\sin\theta}\frac{\partial v}{\partial\phi} - \frac{v}{r}\sin i_r \sin\zeta \cot\theta \tag{24}$$

Amplitudes - Geometric Spreading

Two phenomena affect the amplitudes of body waves: geometric spreading of the rays and attenuation due to anelasticity. We will direct our attention to geometric spreading first, assuming the earth is non-dissipative.

Let

$I(i_{ro}, \zeta_o)$ = power/unit solid angle radiated at the focus

$E(\Theta, \Phi)$ = power/unit area of wavefront at the point of observation

where i_{ro}, ζ_o are the initial values of i_r, ζ and Θ, Φ are the values of θ, ϕ at the point of observation. In a non-dissipative earth

$$I(r_o, \zeta_o)\, d\Omega = E(\Theta,\Phi)\, dS \tag{25}$$

where $d\Omega$ and dS are the corresponding elements of solid angle at the source and surface area of wavefront at the receiver and are given by

$$d\Omega = \mathrm{Sin}\, i_{ro}\, d\, i_{ro}\, d\, \zeta_o$$

$$dS = \frac{R^2 \sin\Theta}{\cos i_r}\, d\,\Theta\, d\,\Phi \tag{26}$$

R is the earth's radius. Here i_r refers to the value at the observation point. $d\Theta$ and $d\Phi$ refer to changes with t held fixed, along a wave-front, not along the earth's surface. $d\, i_{ro}$, $d\,\zeta_o$, $d\Theta$ and $d\Phi$ are related by the Jacobian of the transformation from Θ,Φ to i_{ro}, ζ_o defined by the rays:

$$\frac{\partial(\Theta,\Phi)}{\partial(i_{ro},\zeta_o)} = \begin{vmatrix} \frac{\partial\Theta}{\partial i_{ro}} & \frac{\partial\Phi}{\partial i_{ro}} \\ \frac{\partial\Theta}{\partial \zeta_o} & \frac{\partial\Phi}{\partial \zeta_o} \end{vmatrix} \tag{27}$$

From (25), (26), and (27) we get

$$E = I \frac{\sin i_{ro} \cos i_r}{R^2 \sin\Theta \; \frac{\partial(\theta,\Phi)}{\partial(i_{ro},\zeta_o)}} \tag{28}$$

To evaluate the partial derivatives in (27) we must solve ten more differential equations, for $\frac{\partial r}{\partial i_{ro}}$, $\frac{\partial r}{\partial \zeta_o}$, ... $\frac{\partial \zeta}{\partial i_{ro}}$, $\frac{\partial \zeta}{\partial \zeta_o}$ simultaneously with (20)-(24). These equations are obtained by differentiating equations (20)-(24) with respect to i_{ro} and ζ_o and reversing the order of differentiation ($\frac{\partial}{\partial i_{ro}} [\frac{dr}{dt}] = \frac{d}{dt} [\frac{\partial r}{\partial i_{ro}}]$, etc.). The derivatives $\frac{\partial r}{\partial i_{ro}}$, $\frac{\partial r}{\partial \zeta_o}$, etc. thus obtained are those which apply when the travel time is held fixed; that is they apply to values on a particular wavefront. In their general form, these ten equations are complicated and would probably be impractical to solve even on a large computer. We will restrict ourselves to a special case.

Velocity varies in the direction of propagation, as well as with r

This actually includes two cases: one in which the velocity is constant along small circles centered at the focus, and one in which the velocity is constant along great circles perpendicular to the direction of propagation. The equations for the ray path, (20)-(24), take the same form in both cases. In the first case we take $v = v(r, \theta)$ and initial conditions $\theta = \quad = 0$. From (22) and (24) we see that $\int = 0$ and ϕ = const. for all t; the rays lie in meridional planes ϕ = const. and propagate in the θ direction. The ray path equations become

$$\frac{dr}{dt} = v \cos i_r \tag{29}$$

$$\frac{d\theta}{dt} = \frac{v}{r} \sin i_r \tag{30}$$

$$\frac{di_r}{dt} = \left(\frac{\partial v}{\partial r} - \frac{v}{r}\right) \sin i_r - \frac{1}{r}\frac{\partial v}{\partial \theta} \cos i_r \tag{31}$$

In the second case we take $v = v(r,\phi)$ and initial conditions $\theta =$ $= \pi/2$. From (21) and (24) we see that $\theta = \quad = \pi/2$ for all time; the rays stay in the equatorial plane $\theta = \pi/2$ and propagate in the ϕ direction. The ray equations are the same as (29)-(31), if θ and ϕ are interchanged.

The geometric spreading is not the same for these two cases, though. In the first case, it is evident from symmetry considerations that $\frac{\partial\Phi}{\partial i_{ro}} = \frac{\partial\theta}{\partial\zeta_o} = 0$ and $\frac{\partial\Phi}{\partial\zeta_o} = 1$. Only $\frac{\partial\theta}{\partial i_{ro}}$ needs to be evaluated in (27). To do this, it is necessary to solve only three additional equations, which are obtained from (20), (21), and (23):

$$\frac{d}{dt}\left(\frac{\partial r}{\partial i_{ro}}\right) = -v \sin i_r \frac{\partial i_r}{\partial i_{ro}} + \cos i_r \frac{Dv}{Di_{ro}} \tag{32}$$

$$\frac{d}{dt}\left(\frac{\partial\theta}{\partial i_{ro}}\right) = \frac{v}{r}\cos i_r \frac{\partial i_r}{\partial i_{ro}} - \frac{v}{r^2}\sin i_r \frac{\partial r}{\partial i_{ro}} + \frac{1}{r}\sin i_r \frac{Dv}{Di_{ro}} \tag{33}$$

$$\frac{d}{dt}\left(\frac{\partial i_r}{\partial i_{ro}}\right) = \left(\frac{\partial v}{\partial r} - \frac{v}{r}\right)\cos i_r + \frac{\sin i_r}{r}\frac{\partial v}{\partial\theta}\ \frac{\partial i_r}{\partial i_{ro}}$$

$$+ \frac{1}{r^2}\ v \sin i_r + \frac{\partial v}{\partial\theta}\cos i_r\ \frac{\partial r}{\partial i_{ro}} \tag{34}$$

$$+ \sin i_r\ \frac{D}{Di_{ro}}\left(\frac{\partial v}{\partial r}\right) - \frac{1}{r}\frac{Dv}{Di_{ro}} - \frac{\cos i_r}{r}\frac{D}{Di_{ro}}\left(\frac{\partial v}{\partial\theta}\right)$$

In the second case, $\frac{\partial\Theta}{\partial i_{ro}} = \frac{\partial\Phi}{\partial\zeta_o} = 0$, and both $\frac{\partial\Phi}{\partial i_{ro}}$ and $\frac{\partial\Theta}{\partial\zeta_o}$ must be calculated. The equations for $\frac{\partial\Phi}{\partial i_{ro}}$ are the same as equations (32)-(34), with θ and ϕ interchanged. The equations for $\frac{\partial\Theta}{\partial\zeta_o}$ are

$$\frac{d}{dt}\left(\frac{\partial\theta}{\partial\zeta_o}\right) = -\frac{v}{r}\sin i_r \frac{\partial\zeta}{\partial\zeta_o} \tag{35}$$

$$\frac{d}{dt}\left(\frac{\partial \wp}{\partial \wp_o}\right) = \frac{v}{r} \sin i_r \frac{\partial \theta}{\partial \;\;{}_o} + \frac{1}{r \sin i_r} \frac{\partial v}{\partial \phi} \frac{\partial}{\partial \;\;{}_o} \tag{36}$$

Using equation (22) with $\theta = \pi/2$, we can rewrite these as

$$\frac{d}{d\phi}\left(\frac{\partial \theta}{\partial \wp_o}\right) = - \frac{\partial \wp}{\partial \wp_o} \tag{37}$$

$$\frac{d}{d\phi}\left(\frac{\partial \theta}{\partial \wp_o}\right) = \frac{\partial \theta}{\partial \wp_o} + \frac{1}{v \sin^2 i_r} \frac{\partial v}{\partial \phi} \frac{\partial \wp}{\partial \wp_o} . \tag{38}$$

The initial conditions are $\frac{\partial \theta}{\partial \wp_o} = 0$, $\frac{\partial \wp}{\partial \wp_o} = 1$.

These equations, in either form, could be solved numerically, the ray path being known. We will give an alternate, perturbation approach. If $\frac{\partial v}{\partial \phi} = 0$, the solution is clearly

$$\frac{\partial \theta}{\partial \wp_o} = - \sin \phi \tag{39}$$

$$\frac{\partial \wp}{\partial \wp_o} = \cos \phi \tag{40}$$

so we let

$$\frac{\partial \theta}{\partial \wp_o} = - \sin \phi + q\,(\phi). \tag{41}$$

(37) gives

$$\frac{\partial \wp}{\partial \wp_o} = \cos \phi - q'\,(\phi) \tag{42}$$

(The prime indicates differentiation with respect to ϕ.) Putting these into (38) and rearranging we get

$$q''(\phi) + q(\phi) + \frac{1}{v \sin^2 i_r} \frac{\partial v}{\partial \phi} \left[\cos\phi - q'(\phi) \right] = 0 \tag{43}$$

Assuming $q'(\phi)$ is small compared to $\cos\phi$ this becomes

$$q''(\phi) + q(\phi) = - \frac{\cos\phi}{v \sin^2 i_r} \frac{\partial v}{\partial \phi} = f(\phi) \tag{44}$$

which has the solution

$$q(\phi) = \int_0^{\phi} f(\xi) \sin(\phi - \xi)\, d\xi \tag{45}$$

Finally, then

$$\frac{\partial \theta}{\partial \xi_0} \quad - \sin\phi + \int_0^{\phi} f(\xi) \sin(\phi - \xi)\, d\xi \tag{46}$$

where $f(\phi)$ is defined by (44).

From inspection (27) and (28), remembering that the roles of θ and ϕ are interchanged, we see that the power in the second case is divided by the factor

$$- \frac{1}{\sin\phi} \int_0^{\phi} f(\xi) \sin(\phi - \xi)\, d\xi \tag{47}$$

relative to the first case.

Attenuation

The effect of attenuation due to anelasticity is to reduce the power in the wave by the factor

$$\exp\left(- \omega \int \frac{dt}{Q}\right) \qquad (48)$$

where

Q = dimensionless quality factor

ω = angular frequency

and the integral with respect to time is evaluated along the ray path. For both compressional and shear waves, the power is related to the amplitude by

$$E = \frac{\rho\, v\, \omega^2 A^2}{2} \qquad (49)$$

where ρ = density

A = displacement amplitude.

In this discussion, only the amplitude of the emerging wave has been considered; to calculate the surface mation, the effect of the reflected waves must also be considered.

Appendix II

```
CCCCCCCCCCCCCCCCCCCCCCCCCCCCCCCCCCCCCCCCCCCCCCCCCCCCCCCCCCCCCCCCCCCCCCCCCC
C
C       TVT4 - SEISMIC BODY WAVE TRAVEL TIME PROGRAM
C
C
C    PURPOSE
C         THIS PROGRAM CALCULATES SEISMIC BODY WAVE TRAVEL TIMES AND AMPLITUDES
C       FOR A GIVEN LATERALLY INHOMOGENEOUS , ISOTROPIC EARTH MODEL.
C
C
C    METHOD
C         THE VELOCITY (V) IS ASSUMED TO VARY WITH RADIUS (R) AND DISTANCE
C       ALONG THE PROFILE (THETA).  THIS IS ACCOMPLISHED BY DIVIDING THE EARTH
C       INTO SEGMENTS WITH VERTICAL BOUNDARIES, IN EACH OF WHICH THE VELOCITY IS
C       A FUNCTION OF R ALONE.  THE VELOCITY IN EACH SEGMENT IS SPECIFIED IN
C       TERMS OF THE VALUES OF R AND VELOCITY, V, AT A NUMBER OF DISTINCT
C       POINTS, BETWEEN WHICH IT IS ASSUMED TO FOLLOW THE LAW V = A*R**B, WHERE
C       A AND B ARE CONSTANTS.  AMPLITUDES ARE CALCULATED TAKING INTO ACCOUNT
C       THE EFFECTS OF GEOMETRICAL SPREADING AND (IF Q VALUES ARE INCLUDED IN
C       THE MODEL) ATTENUATION DUE TO ANELASTICITY.  OPTIONS ARE AVAILABLE FOR
C       PLOTTING TRAVEL TIME, D(T)/D(DELTA), AMPLITUDE, AND EFFECTIVE Q CURVES,
C       EITHER ON THE PRINTER OR THE X-Y PLOTTER.  OBSERVED DATA MAY BE READ IN
C       AND INCLUDED ON PLOTS.  IF DESIRED, RAYS WHICH CORRESPOND TO DELTA
C       VALUES FOR DATA WILL BE CALCULATED BY AN ITERATIVE PROCEEDURE WHENEVER
C       AN OBSERVED DELTA VALUE IS CROSSED IN THE COURSE OF THE CALCULATIONS.
C       RAY TRACINGS MAY BE PRODUCED ON THE X-Y PLOTTER.
C
C
C    RESTRICTIONS
C         THE NUMBER OF SEGMENTS MUST NOT EXCEED 10.
C         THE NUMBER OF POINTS (DEPTH, VELOCITY, Q) IN EACH SEGMENT MUST NOT
C       EXCEED 100.
C         ABRUPT DISCONTINUITIES IN VELOCITY ARE NOT ALLOWED WITHIN A SEGMENT.
C
C
C    USAGE
C
C I. CARD:
C    1-80 IDENT  (20A4):  80 COLUMNS OF IDENTIFICATION.  FIRST 12 COLUMNS USED
C                         AS TITLE ON X-Y PLOTS, IF ANY.
C
C
C II. CARD:
C    1- 5 NMODEL (I5):     NUMBER OF SEGMENTS.
C   11-20 RADIUS (F10.5): RADIUS OF EARTH (KM).
C   21-   THETA  (F10.5): ARRAY CONTAINING ANGULAR COORDINATES OF SEGMENT
C                         BOUNDARIES (DEGREES). NMODEL VALUES ARE REQUIRED.
C                         MAY BE CONTINUED ONTO MORE CARDS IF NECESSARY.
C                         DUE TO AN IDIOSYNCRASY OF IBM, A BLANK CARD MUST
C                         FOLLOW IF THE FINAL VALUE FALLS IN COLUMNS 71-80.
C
C
C III.  MODELS - THE FOLLOWING GROUP OF CARDS GIVES THE STRUCTURE IN ONE SEGMENT
C          AND MUST BE REPEATED NMODEL TIMES.
C
C
C    ---------------------------------------------------------------------
C    | A. CARD
C R  |  1-80 ID      (20A4):  80 COLUMNS OF IDENTIFICATION.
C E  |
C P  |
C E  | B. CARD:
C A  | 13-24 RM      (F12.8): SCALE FACTOR FOR RR ON STRUCTURE CARDS (SEE C).
C T  |                        IF NOT GIVEN, WILL BE SET = 1.
C    |
C N  |
C M  | C. STRUCTURE CARDS - EACH CARD PAIR GIVES DEPTH, VELOCITY, Q AT ONE POINT
C O  |        OF MODEL.  STRUCTURE MUST BE READ IN FROM BOTTOM UPWARDS.
C D  |        DISCONTINUITIES ARE NOT ALLOWED.
C E  |  2-12 RR      (F11.8): RADIUS OR DEPTH, DEPENDING ON I2 (SEE BELOW).
C L  |                        SCALE FACTOR RM (SEE B) IS APPLIED TO RR.
C    | 14-24 VV      (F11.8): VELOCITY CORRESPONDING TO RR.
C T  | 25-28 I2      (I4):    .EQ. 0 - RR * RM = DEPTH.
C I  |                        .NE. 0 - RR * RM = RADIUS
C M  | 33-36 LAST    (I4):    .NE. 0 - THIS IS THE LAST STRUCTURE CARD PAIR FOR
C E  |                        THIS SEGMENT.
C S  |  1-12 QQ      (F12.8): (SECOND CARD OF PAIR)
C    |                        VALUE OF Q IN INTERVAL BETWEEN THIS CARD PAIR AND
C    |                        NEXT ONE.  (SPECIFYING A Q MODEL IN OPTIONAL.)
C    |____________________________________________________________________
```

```
C V. CARD:
C     1- 6 NUMCD  (I6):     NUMBER OF TIMES THE FOLLOWING GROUP OF CARDS IS
C                           REPEATED.
C
C
C   IIIIIIIIIIIIIIIIIIIIIIIIIIIIIIIIIIIIIIIIIIIIIIIIIIIIIIIIIIIIIIIIIIIIIIIIIIIII
C   I A. CARD:
C   I  1-10 DFOC    (F10.8): DEPTH OF FOCUS.
C R I 11-20 AI      (F10.8): INITIAL TAKE-OFF ANGLE.
C E I 21-30 AC      (F10.8): TAKE-OFF ANGLE INCREMENT.
C P I                        IF AC < 0., RAYS WILL BE CHOSEN SO THAT DELTA IS
C E I                        SPACED BY APPROXIMATELY ABS(AC).  THIS OPTION HAS
C A I                        PROVED EXTREMELY USEFUL FOR MOST CASES.
C T I 31-40 AF      (F10.8): FINAL TAKE-OFF ANGLE.
C   I                        TAKE-OFF ANGLE IS MEASURED IN DEGREES.  0. DEGREES
C N I                        IS STRAIGHT DOWN, 90. DEGREES IS HORIZONTAL, 180.
C U I                        DEGREES IS STRAIGHT UP.
C M I 41-50 DREF    (F10.8): DEPTH OF REFLECTION, IF REFLECTED RAYS ARE DESIRED
C C I                        IF DREF = 0. NO REFLECTION IS ASSUMED.
C D I 61-62 NPPLT   (I2):    NO. OF PRINTER PLOTS OF TRAVEL TIME, DT/DDELTA, OR
C   I                        AMPLITUDE CURVES.  FOR EACH PLOT, CARD GIVING SCALE
C T I                        FACTORS, ETC. MUST BE GIVEN (SEE E).
C I I 63-64 IRAYPL  (I2):    .NE. 0 - PRODUCE RAY TRACINGS ON X-Y PLOTTER.  IN
C M I                        THIS CASE, CARD GIVING SCALE INFORMATION MUST BE
C E I                        INCLUDED (SEE C).
C S I 65-66 IRAY    (I2):    .NE. 0 - PRINT TABLE GIVING TIME, DELTA AT TOP OF
C   I                        EACH LAYER DURING RAY CALCULATIONS.
C   I 67-68 IPNCH   (I2):    .NE. 0 - PUNCH BCD CARDS GIVING TRAVEL TIMES.
C   I                        AMPLITUDES, ETC. FOR CALCULATED RAYS.
C   I                        TIMES, ETC. FOR CALCULATED RAYS.
C   I 69-70 NXYPL   (I2):    NO. OF X-Y PLOTS OF TRAVEL TIME, DT/DDELTA, OR
C   I                        AMPLITUDE CURVES.  FOR EACH PLOT, A CARD GIVING
C   I                        SCALE FACTORS, ETC. MUST BE GIVEN (SEE D).
C   I 71-72 IDATA   (I2):    .GT. 0 - READ OBSERVED DATA (SEE B) AND CALCULATE
C   I                        RAYS WITH SAME DELTA VALUES.
C   I                        .LT. 0 - READ OBSERVED DATA AND INCLUDE ON PLOTS.
C   I                        BUT DO NOT CALCULATE CORRESPONDING RAYS.
C   I                        .EQ. 0 - DO NOT READ OBSERVED DATA.
C   I 73-80 FREQ    (F8.2):  FREQUENCY (HZ) USED IN AMPLITUDE CALCULATIONS.  IF
C   I                        NOT GIVEN, 1 HZ IS ASSUMED.
C   I
C   I
C   I B. OBSERVED DATA CARDS - REQUIRED ONLY IF IDATA .NE. 0 (SEE A).  RAYS WITH
C   I  SAME DELTA VALUES WILL BE CALCULATED IF IDATA .LT. 0.  OTHER VALUES ARE
C   I  OPTIONAL AND ARE USED ONLY ON PLOTS.
C   I    (NOTE: DATA READ-IN IS CONTROLLED BY SUBROUTINE DATARD.  IN ADDITION TO
C   I  THE "STANDARD FORMAT" DESCRIBED BELOW, VERSIONS OF THE SUBROUTINE FOR
C   I  OTHER FORMATS, SUCH AS THAT FOR THE EARLY RISE EXPERIMENT, EXIST.)
C   I FIRST DATA CARD:
C   I  1-80         (20A4):  80 COLUMNS OF IDENTIFICATION
C   I
C   I SUBSEQUENT DATA CARDS:
C   I  1-10         (F10.5): DELTA (DEGREES).
C   I 11-20         (F10.5): TRAVEL TIME (SECONDS)
C   I 21-30         (F10.5): RAY PARAMETER, P(= DT/DDELTA)(SEC/DEG).
C   I 31-40         (F10.5): AMPLITUDE.
C   I 41-50         (F10.5): EFFECTIVE Q.
C   I 65-66 NF      (I2):    NUMBER FROM 0 TO 14, INDICATING SYMBOL TO BE USED
C   I                        WHEN PLOTTING THIS DATA POINT (SEE WRITE UP OF
C   I                        SUBROUTINE PLOTXY).
C   I 69-70 LAST    (I2):    .NE. 0 ON LAST OBSERVED DATA CARD.  ZERO OR BLANK
C   I                        ON ALL OTHER CARDS.
C   I
C   I
C   I C. CARD GIVING SCALE INFORMATION FOR RAY PLOTS (REQUIRED ONLY IF IRAYPL
C   I  .NE. 0, SEE A).
C   I  1-10 XLNGTH (F10.5): PLOT DIMENSION IN X DIRECTION (INCHES).
C   I 11-20 YLNGTH (F10.5): PLOT DIMENSION IN Y DIRECTION (INCHES).
C   I                        (IF THESE TWO FIELDS ARE LEFT BLANK, THE STANDARD
C   I                        SMALL PAPER SIZE IS ASSUMED.)
C   I 21-30 THMAX  (F10.5): ANGULAR LENGTH OF RAY PLOTS (DEGREES).
C   I 31-40 THMARK (F10.5): SPACING OF SCALE MARKS ALONG EARTH'S SURFACE
C   I                        (DEGREES).  IF .EQ. 0., NO SCALE MARKS ARE MADE.
C   I 41-50 RA     (F10.5): RADIUS OF CIRCLE TO BE DRAWN ON RAY PLOT (KM).
C   I                        (E.G. CORE BOUNDARY, MOHO, ETC.)
C   I 51-60 RB     (F10.5): RADIUS OF SECOND CIRCLE, SIMILAR TO ABOVE.
C   I                        (IF .EQ. 0., NO CIRCLES ARE DRAWN).
C R I
C E I
C P I D. (NXYPL) CARDS - SCALING INFORMATION FOR X-Y PLOTS, IF ANY (SEE A).
C E I  1-10 XLNGTH (F10.5): PLOT DIMENSION IN X (DELTA) DIRECTION(INCHES).
C A I 11-20 YLNGTH (F10.5): PLOT DIMENSION IN Y DIRECTION (INCHES).
C T I 21-30 XF     (F10.5): X SCALE FACTOR (DEG/IN OR KM/IN - SEE IKM, BELOW).
C   I 31-40 XMIN   (F10.5): MINIMUM X VALUE (KM OR DEG).
C N I 41-50 YF     (F10.5): Y SCALE FACTOR (DATA UNITS/IN).
C U I 51-60 YMIN   (F10.5): MINIMUM Y VALUE (DATA UNITS).
C M I 61-62 IT     (I2):    INDICATES WHICH FUNCTION IS TO BE PLOTTED.
C C I                       1 - REDUCED TRAVEL TIME: 2 - DT/DDELTA:
C D I                       3 - AMPLITUDE: 4 - EFFECTIVE Q.
C   I 63-64 LAP    (I2):    .EQ. 1 INDICATES LAST PLOT ON THIS SHEET.
C T I                       .EQ. 0 WILL CAUSE NEXT PLOT TO BE ON SAME SHEET.
C I I 65-66 NX     (I2):    NO. OF X INTERVALS FOR SCALE MARKS AND LABELS.
C M I 67-68 NY     (I2):    NO. OF Y INTERVALS FOR SCALE MARKS AND LABELS.
C E I 69-70 IKM    (I2):    .EQ. 1 - X SCALE IN KM.
C S I                       .EQ. 0 - X SCALE IN DEG.
C   I 71-80 RV     (F10.5): VELOCITY TO BE USED TO REDUCE TRAVEL TIMES (KM/SEC).
C   I                       IF .EQ. 0., TRAVEL TIMES WILL NOT BE REDUCED.
C   I
C   I
C   I E. (NPPLT) CARDS - SCALING INFORMATION FOR PRINTER PLOTS, IF ANY (SEE A).
C   I FORMAT IS SAME AS FOR X-Y PLOTS (SEE D).  YLNGTH MUST BE .LE. 12.
C   I LAP, NX, NY ARE IGNORED.
C   IIIIIIIIIIIIIIIIIIIIIIIIIIIIIIIIIIIIIIIIIIIIIIIIIIIIIIIIIIIIIIIIIIIIIIIIIIII
C
C        MORE THAN ONE DECK MAY BE RUN AT ONE TIME.  SIMPLY PLACE ONE DECK,
C        BEGINNING WITH IDENT CARD, IMMEDIATELY AFTER ANOTHER.
CCCCCCCCCCCCCCCCCCCCCCCCCCCCCCCCCCCCCCCCCCCCCCCCCCCCCCCCCCCCCCCCCCCCCCCCCCCCCC
```

Appendix III

Body Wave Perturbation Theory and Inversion of Observed Data

An automated procedure for fitting earth models to observed body wave data tremendously simplifies the process of interpreting these data, and is virtually a necessity in studies involving large numbers of observations. In this appendix, we derive partial derivatives of travel time, slowness, and amplitude with respect to changes in the parameters specifying the velocity distribution in a spherical earth model. These partial derivatives enable one to calculate to first order the changes in the body wave parameters produced by a small change in the earth model. We then discuss a method for inverting the process, and finding the changes in an initial earth model which are required to fit given observed data. This method is an extension of the usual least squares method, and overcomes the unstable behavior which usually plagues least squares fitting. A program utilizing this method has been written for the IBM 360/75 digital computer, and is described in Appendix IV.

Referring to Figure 69, suppose curve A is a portion of the travel time curve for an initial earth model with velocity distribution $V(r)$ and B is the curve for a model with velocity $V(r) + \delta V(r)$, where r is the radial coordinate. Further, suppose a ray, corresponding to a particular value of the ray parameter, p, emerges at point a in the first case, and at point b in the second case. Since $p = dT/d\Delta$, we see from the figure that, to first order

$$\delta(T)_\Delta = \delta(T)_p - p\delta(\Delta)_p = \delta(T - p\Delta)_p \quad . \tag{1}$$

The subscripts indicate that p or Δ, as the case may be, is held fixed. Similarly, the perturbation to the slowness, $\frac{dT}{d\Delta} = p$ is

$$\delta(p)_\Delta = -\frac{dp}{d\Delta}\,\delta(\Delta)_p \quad . \tag{2}$$

To obtain the expression for the amplitude perturbation, consider the expression for the geometric spreading factor (see Appendix I) in the case of a spherically symmetric model:

$$\frac{E}{I} = \frac{V_o \tan i_o}{R^2 r_o \sin\Delta \cos i} \left| 1 \Big/ \frac{d\Delta}{dp} \right| \tag{3}$$

where R is the earth's radius, r_o, V_o, and i_o are the values of radius, velocity, and take-off angle at the focus, and i is the angle of incidence at the surface.

The change in the spreading factor is

$$\delta\left(\frac{E}{I}\right)_\Delta = \frac{E}{I}\left\{\frac{1}{\sin i_o \cos i_o}\left(\delta i_o\right)_\Delta + \tan i\left(\delta i\right)_\Delta\right. \tag{4}$$

$$\left. - \left|1\Big/\frac{d\Delta}{dp}\right| \delta\left|\left(\frac{d\Delta}{dp}\right)\right|_\Delta\right\}$$

Since the angle of incidence at any depth is given by

$$\frac{r}{v} \sin i = p \quad , \tag{5}$$

the changes $(\delta i)_\Delta$ and $(\delta i_o)_\Delta$ are related to the change in the slowness, p:

$$(\delta i)_\Delta = \frac{v(R)}{R} \sec i \ (\delta p)_\Delta \tag{6}$$

$$(\delta i_o)_\Delta = \frac{v_o}{r_o} \sec i_o \ (\delta p)_\Delta \quad . \tag{7}$$

By arguments similar to those used above for the travel time and slowness perturbations we get

$$\delta\left(\frac{d\Delta}{dp}\right)_{\Delta} = \delta\left(\frac{d\Delta}{dp}\right)_{p} - \frac{d}{d\Delta}\left(\frac{d\Delta}{dp}\right)\delta(\Delta)_{p}$$

$$= \delta\left(\frac{d\Delta}{dp}\right)_{p} - \left\{\frac{d^2\Delta}{dp^2}\Big/\frac{d\Delta}{dp}\right\}\delta(\Delta)_{p} \quad . \qquad (8)$$

We now show how the travel times, amplitudes, and other quantities needed in these expressions may be evaluated for a given earth model.

Calculation of Travel Times

Let the earth be divided into n spherical shells, in each of which the velocity is given by some analytic function of r, the radial coordinate, and some parameters a_i:

$$v = f(r, a_i) \text{ when } r_i \leq r \leq r_{i+1} \quad \text{for } i = 1,2,\ldots,n \qquad (9)$$

Further, let $\Theta(\rho, a, p)$ and $T(\rho, a, p)$ be the angular length and travel time of a ray which makes a single passage from its deepest point to the surface in a sphere with radius ρ and parameters a; p is the conventional ray parameter. The angular length and travel time for a ray starting and ending at the surface of the earth are then:

$$\Delta = 2\left\{\Theta(r_{j+1}, \alpha_j, p) + \sum_{i=j+1}^{n}\left[\Theta(r_{i+1}, \alpha_i, p) - \Theta(r_i, \alpha_i, p)\right]\right\} \tag{10}$$

$$T = 2\left\{\mathcal{T}(r_{j+1}, \alpha_j, p) + \sum_{i=j+1}^{n}\left[\mathcal{T}(r_{i+1}, \alpha_i, p) - \mathcal{T}(r_i, \alpha_i, p)\right]\right\} \tag{11}$$

Here j is the index of the layer in which the ray bottoms. If the ray does not begin at the surface, then, of course, the contributions of some layers are deleted from the above summation.

The values of $\frac{d\Delta}{dp}$ and $\frac{d^2\Delta}{dp^2}$, needed for the amplitude calculations, are calculated similarly:

$$\frac{d\Delta}{dp} = 2\left\{\frac{\partial\Theta(r_{j+1}, \alpha_j, p)}{\partial p} + \sum_{i=j+1}^{n}\left[\frac{\partial\Theta(r_{i+1}, \alpha_i, p)}{\partial p} - \frac{\partial\Theta(r_i, \alpha_i, p)}{\partial p}\right]\right\} \tag{12}$$

$$\frac{d^2\Delta}{dp^2} = 2\left\{\frac{\partial^2\Theta(r_{j+1}, \alpha_j, p)}{\partial p^2} + \sum_{i=j+1}^{n}\left[\frac{\partial^2\Theta(r_{i+1}, \alpha_i, p)}{\partial p^2} - \frac{\partial^2\Theta(r_i, \alpha_i, p)}{\partial p^2}\right]\right\} \tag{13}$$

The analytic function used here for the velocity distribution is the so-called "Mohorovicic law," $v = ar^b$. The expressions for $\mathcal{T}$, Θ, $\frac{\partial\Theta}{\partial p}$, and $\frac{\partial^2\Theta}{\partial p}$ are particularly simple for this case:

$$T(\rho,a,b,p) = \frac{\rho^{1-b}}{a(1-b)} \sin\left[(1-b)\Theta(\rho,a,b,p)\right] = \frac{1}{1-b}\sqrt{\left(\frac{\rho^{1-b}}{a}\right)^2 - p^2} \tag{14}$$

$$\Theta(\rho,a,b,p) = \frac{1}{1-b} \cos^{-1} \frac{ap}{\rho^{(1-b)}} \tag{15}$$

$$\frac{\partial\Theta(\rho,a,b,p)}{\partial p} = -\frac{1}{1-b}\left[\left(\frac{\rho^{1-b}}{a}\right)^2 - p^2\right]^{-\frac{1}{2}}$$

$$= -\frac{1}{(1-b)^2 T(\rho,a,b,p)} \tag{16}$$

$$\frac{\partial^2\Theta(p,a,b,p)}{\partial p^2} = -\frac{p}{1-b}\left[\left(\frac{\rho^{1-b}}{a}\right)^2 - p^2\right]^{-3/2} \tag{17}$$

The values of a_i, b_i, $i = 1,\ldots,n$ are calculated so that the velocity takes on specified values at the shell boundaries. For the velocity function $v = ar^b$, for example, we have in the ith layer:

$$v(r_i) = a_i r_i^{b_i}$$

$$v(r_{i+1}) = a_i r_{i+1}^{b_i}$$

which can be solved for a_i and b_i in terms of r_i, $v(r_i)$, r_{i+1}, and $v(r_{i+1})$:

$$a_i = \exp\left(\frac{\ln v(r_{i+1}) \ln r_i - v(r_i) \ln r_{i+1}}{\ln [r_i/r_{i+1}]}\right) \tag{18}$$

$$b_i = \frac{\ln [v(r_i)/v(r_{i+1})]}{\ln [r_i/r_{i+1}]} \tag{19}$$

Perturbation Theory

To make use of equations (1), (2), and (8) it is necessary to calculate the partial derivatives of T, Θ, and $\frac{\partial \Theta}{\partial p}$ with respect to changes in the parameters a, b, and ρ, with p held fixed. From (14), (15), and (16) we get

$$\frac{\partial T}{\partial a} = - \frac{\rho^{2(1-b)}}{a^3(1-b)} \left[\left(\frac{\rho^{1-b}}{a}\right)^2 - p^2\right]^{-\frac{1}{2}} \tag{20}$$

$$\frac{\partial T}{\partial b} = \frac{T}{1-b} - \frac{\rho^{2(1-b)} \ln \rho}{a^2(1-b)} \left[\left(\frac{\rho^{1-b}}{a}\right)^2 - p^2\right]^{-\frac{1}{2}} \tag{21}$$

$$\frac{\partial T}{\partial \rho} = \frac{1}{\rho} \left(\frac{\rho^{1-b}}{a}\right)^2 \left[\left(\frac{\rho^{1-b}}{a}\right)^2 - p^2 \right]^{-1/2} \tag{22}$$

$$\frac{\partial \Theta}{\partial a} = - \frac{p}{a(1-b)} \left[\left(\frac{\rho^{1-b}}{a}\right)^2 - p^2 \right]^{-1/2} \tag{23}$$

$$\frac{\partial \Theta}{\partial b} = \frac{\Theta}{1-b} - \frac{p \,\ell n\, \rho}{1-b} \left[\left(\frac{\rho^{1-b}}{a}\right)^2 - p^2 \right]^{-1/2} \tag{24}$$

$$\frac{\partial \Theta}{\partial \rho} = \frac{p}{\rho} \left[\left(\frac{\rho^{1-b}}{a}\right)^2 - p^2 \right]^{-1/2} \tag{25}$$

$$\frac{\partial}{\partial a} \left(\frac{\partial \Theta}{\partial p}\right) = \frac{1}{(1-b)^2 T^2(\rho,a,b,p)} \frac{\partial T(\rho,a,b,p)}{\partial a} \tag{26}$$

$$\frac{\partial}{\partial b} \left(\frac{\partial \Theta}{\partial p}\right) = - \frac{2}{(1-b)^3 T\ (\rho,a,b,p)} + \frac{1}{(1-b)^2 T^2(\rho,a,b,p)} \frac{\partial T(\rho,a,b,p)}{\partial b} \tag{27}$$

$$\frac{\partial}{\partial \rho} \left(\frac{\partial \Theta}{\partial p}\right) = \frac{1}{(1-b)^2 T^2(\rho,a,b,p)} \frac{\partial T(\rho,a,b,p)}{\partial \rho} \tag{28}$$

The partial derivatives of T-p Θ, needed for the travel time perturbations (see (1)), take on particularly simple forms:

$$\frac{\partial}{\partial a} (T - p\,\Theta) = -\frac{T}{a} \tag{29}$$

$$\frac{\partial}{\partial b} (T - p\Theta) = \frac{T - p\Theta}{1-b} - T \log \rho \tag{30}$$

and

$$\frac{\partial}{\partial \rho} (T - p\Theta) = \frac{1-b}{\rho} T \tag{31}$$

With (1), (2), (4), (8), and (10)-(13) these partial derivatives could be used to calculate the effect on the total travel time, slowness, and amplitude of changing the model slightly. However, in regions where the velocity changes rapidly, the numerical value of a may become very large, so it is preferable to calculate partial derivatives with respect to the values r_i, $v(r_i)$ specified by the user. From (18) and (19) we get, writing v_i for $v(r_i)$

$$\frac{\partial a_i}{\partial v_i} = -\frac{a_i \ln r_{i+1}}{v_i \ln [r_i/r_{i+1}]} \tag{32}$$

$$\frac{\partial a_i}{\partial r_i} = \frac{a_i b_i \ln r_{i+1}}{r_i \ln [r_i/r_{i+1}]} \tag{33}$$

$$\frac{\partial b_i}{\partial v_i} = \frac{1}{v_i \ \ln\ [r_i/r_{i+1}]} \tag{34}$$

$$\frac{\partial b_i}{\partial r_i} = -\ \frac{b_i}{r_i \ \ln\ [r_i/r_{i+1}]} \tag{35}$$

and similar expressions for $\partial a_{i-1}/\partial v_i$, $\partial a_{i-1}/\partial r_i$, $\partial b_{i-1}/\partial v_i$, and $\partial b_{i-1}/\partial r_i$. Now, using (1), (10), and (11) we get: (calling, for simplicity, $\chi(\rho,a,b,p) = \mathcal{T}(\rho,a,b,p) - p\Theta(\rho,a,b,p)$)

$$\left(\frac{\partial T}{\partial v_i}\right)_\Delta = \frac{\partial}{\partial v_i}\ (T - p\Delta)_p = \sum_{j=i-1}^{i}\left(A_j\frac{\partial a_j}{\partial v_i} + B_j\frac{\partial b_j}{\partial v_i}\right) \tag{36}$$

and

$$\left(\frac{\partial T}{\partial r_i}\right)_\Delta = \frac{\partial}{\partial r_i}\ (T - p\Delta)_p = \sum_{j=i-1}^{i}\left(A_j\ \frac{\partial a_j}{\partial r_i} + B_j\ \frac{\partial b_j}{\partial r_i}\right)$$

$$- \frac{\partial}{\partial r_i}\left(\chi(r_i,a_i,b_i,p) - \chi(r_i,a_{i-1},b_{i-1},p)\right) \tag{37}$$

where

$$A_j = \frac{\partial}{\partial a_j}\left\{\chi(r_{j+1},a_j,b_j,p) - \chi(r_j,a_j,b_j,p)\right\} \tag{38}$$

$$B_j = \frac{\partial}{\partial b_j}\left\{\chi(r_{j+1},a_j,b_j,p) - \chi(r_j,a_j,b_j,p)\right\} \tag{39}$$

Similarly, the partial derivatives for p and $\frac{d\Delta}{dp}$ are

$$\left(\frac{\partial p}{\partial v_i}\right)_\Delta = -\frac{dp}{d\Delta}\left(\frac{\partial \Delta}{\partial v_i}\right)_p \tag{40}$$

$$\left(\frac{\partial p}{\partial r_i}\right)_\Delta = -\frac{dp}{d\Delta}\left(\frac{\partial \Delta}{\partial r_i}\right)_p \tag{41}$$

$$\left(\frac{\partial}{\partial v_i}\left[\frac{d\Delta}{dp}\right]\right)_\Delta = \left(\frac{\partial}{\partial v_i}\left[\frac{\partial\Delta}{\partial p}\right]\right)_p - \left\{\frac{d^2\Delta}{dp^2}\Big/\frac{d\Delta}{dp}\right\}\left(\frac{\partial\Delta}{\partial v_i}\right)_p \tag{42}$$

$$\left(\frac{\partial}{\partial r_i}\left[\frac{d\Delta}{dp}\right]\right)_\Delta = \left(\frac{\partial}{\partial r_i}\left[\frac{\partial\Delta}{\partial p}\right]\right)_p - \left\{\frac{d^2\Delta}{dp^2}\Big/\frac{d\Delta}{dp}\right\}\left(\frac{\partial\Delta}{\partial r_i}\right)_p \tag{43}$$

which can be evaluated using

$$\left(\frac{\partial\Delta}{\partial v_i}\right)_p = \sum_{j=i-1}^{i}\left(C_j \frac{\partial a_j}{\partial v_i} + D_j \frac{\partial b_j}{\partial v_i}\right) \tag{44}$$

$$\left(\frac{\partial\Delta}{\partial r_i}\right)_p = \sum_{j=i-1}^{i}\left(C_j \frac{\partial a_j}{\partial r_i} + D_j \frac{\partial b_j}{\partial r_i}\right)$$

$$- \frac{\partial}{\partial r_i}\Big(\Theta(r_i,a_i,b_i,p) - \Theta(r_i,a_{i-1},b_{i-1},p)\Big) \tag{45}$$

$$\left(\frac{\partial}{\partial v_i}\left[\frac{\partial\Delta}{\partial p}\right]\right)_p = \sum_{j=i-1}^{i}\left(E_j \frac{\partial a_j}{\partial v_i} + F_j \frac{\partial b_j}{\partial v_i}\right) \tag{46}$$

$$\left(\frac{\partial}{\partial v_i}\left[\frac{\partial\Delta}{\partial p}\right]\right)_p = \sum_{j=i=1}^{i}\left(E_j \frac{\partial a_j}{\partial r_i} + F_j \frac{\partial b_j}{\partial r_i}\right)$$

$$- \frac{\partial}{\partial r_i}\left(\frac{\partial\Theta}{\partial p}(r_i,a_i,b_i,p) - \frac{\partial\Theta}{\partial p}(r_i,a_{i-1},b_{i-1},p)\right) \tag{47}$$

where

$$C_j = \frac{\partial}{\partial a_j} \left\{ \Theta(r_{j+1}, a_j, b_j, p) - \Theta(r_j, a_j, b_j, p) \right\} \qquad (48)$$

$$D_j = \frac{\partial}{\partial b_j} \left\{ \Theta(r_{j+1}, a_j, b_j, p) - \Theta(r_j, a_j, b_j, p) \right\} \qquad (49)$$

$$E_j = \frac{\partial}{\partial a_j} \left\{ \frac{\partial \Theta}{\partial p} (r_{j+1}, a_j, b_j, p) - \frac{\partial \Theta}{\partial p} (r_j, a_j, b_j, p) \right\} \qquad (50)$$

$$F_j = \frac{\partial}{\partial b_j} \left\{ \frac{\partial \Theta}{\partial p} (r_{j+1}, a_j, b_j, p) - \frac{\partial \Theta}{\partial p} (r_j, a_j, b_j, p) \right\} \qquad (51)$$

Equations (20)-(35) derived above provide all the quantities needed to evaluate the derivatives in (36)-(39) and (44)-(51), and these, along with the calculated values of $\frac{d\Delta}{dp}$ and $\frac{d^2\Delta}{dp^2}$ give, through (36), (37), (40)-(43) the partial derivatives with respect to the values r_i, v_i, i=1,...n+1 used to specify the model. The partial derivatives for the travel time take on a fairly simple form:

$$\left(\frac{\partial T}{\partial v_i}\right)_\Delta = G-H \tag{52}$$

$$\left(\frac{\partial T}{\partial r_i}\right)_\Delta = -\frac{b_i v_i}{r_i} G + \frac{b_{i-1} v_i}{r_i} H$$

$$+ \frac{1-b_{i-1}}{r_i} \mathcal{T}(r_i, a_{i-1}, b_{i-1}, p) - \frac{1-b_i}{r_i} \mathcal{T}(r_i, a_i, b_i, p). \tag{53}$$

where

$$G = \frac{\mathcal{T}(r_i, a_i, b_i, p)}{v_i} + \frac{\chi(r_{i+1}, a_i, b_i, p) - \chi(r_i, a_i, b_i, p)}{v_i \log (r_i v_{i+1}/r_{i+1} v_i)} \tag{54}$$

$$H = \frac{\mathcal{T}(r_i, a_{i-1}, b_{i-1}, p)}{v_i} + \frac{\chi(r_i, a_{i-1}, b_{i-1}, p) - \chi(r_{i-1}, a_{i-1}, b_{i-1}, p)}{v_i \log (r_{i-1} v_i/r_i v_{i-1})} \tag{55}$$

Inversion of Observed Data

The partial derivatives derived above enable us to calculate approximately the change in the travel time, slowness, and amplitude produced by any arbitrary change in the earth model. What is more interesting, however, is usually the inverse problem: to find the change in an initial earth model which is required to fit given observed data. The usual least squares technique for inverting data is notoriously ill-behaved, because large model perturbations can be found which, in the linearized approximation, produce only small changes in the calculated parameters. The technique presented here overcomes this difficulty by minimizing not only the residuals between the observed and calculated values, but also the perturbations to the initial model.

Consider the model to be specified by parameters a_j, $j=1,\ldots m$, which might, for example, be the velocities at the shell boundaries, or coefficients in a polynomial, etc. The theoretically calculated travel time, say, is then specified as a function (possibly multi-valued) of distance, Δ, and the parameters a_j:

$$T = T(\Delta, a_1, a_2, \ldots a_m) \tag{56}$$

and, for small perturbations δa_j in the model, the change in the travel time is given, to first order, by

$$(\delta T)_\Delta \cong \sum_{j=1}^{m} \left(\frac{\partial T}{\partial a_j} \right)_\Delta \delta a_j \; . \tag{57}$$

If we have observed travel times O_i and corresponding calculated times T_i for $i=1,\ldots n$, let us try to find changes δa_j, $j=1,\ldots m$ in the model which minimize

$$\sum_{i=1}^{n} \left[T_i + \delta T_i - O_i \right]^2 + \alpha \sum_{j=1}^{m} (\delta a_j)^2 \qquad . \tag{58}$$

This may be viewed as a problem of minimizing either of the above sums, under the condition that the other sum has a fixed value, with α playing the role of a Lagrange multiplier. The case $\alpha = 0$ corresponds to conventional least squares fitting. Putting expression

(57) for $(\delta T)_\Delta$ into (58), the quantity we want to minimize becomes

$$\sum_{i=1}^{n} \left\{ \sum_{j=1}^{m} \left(\frac{\partial T}{\partial \alpha_j}\right)_\Delta \Bigg|_{T=T_i} \delta a_j - \left(O_i - T_i\right) \right\}^2 + \alpha \sum_{j=1}^{m} \left(\delta a_j\right)^2 \tag{59}$$

which can be written in matrix form as

$$\left(\tilde{A}\bar{x}-\tilde{b}\right)^2 + \alpha\bar{x}^2 \tag{60}$$

where

$$A_{ij} = \left(\frac{\partial T}{\partial \alpha_j}\right)_\Delta \Bigg|_{T=T_i} \tag{61}$$

$$x_j = \delta a_j \tag{62}$$

$$b_i = O_i - T_i \tag{63}$$

The condition for minimizing (59) is expressed by a system of m simultaneous linear algebraic equations, which are obtained by setting the partial derivatives of (59) with respect to δa_j for $j = 1,\ldots m$ equal to zero. In matrix form, the system can be written

$$\left(\tilde{A}^T\tilde{A} + \alpha\tilde{I}\right)\bar{x} = \tilde{A}^T\bar{b} \tag{64}$$

where $\tilde{A}^T$ indicates the transpose of the matrix $\tilde{A}$, and $\tilde{I}$ is the identity matrix. Thus the problem posed here differs from the conventional least squares problem only in that the constant α is added to each diagonal coefficient of the system to be solved. The behavior of the system is much more stable, however, and the solutions obtained are much more likely to be physically reasonable. This technique would probably be of great practical value in many least square fitting applications besides the one described here.

Appendix IV

```
CCCCCCCCCCCCCCCCCCCCCCCCCCCCCCCCCCCCCCCCCCCCCCCCCCCCCCCCCCCCCCCCCCCCCCCCCCCCCCCC
C
C        TTINV - SEISMIC BODY WAVE TRAVEL TIME INVERSION PROGRAM
C
C
C    PURPOSE
C          THIS PROGRAM CALCULATES SEISMIC BODY WAVE TRAVEL TIMES AND AMPLITUDES
C       FOR A GIVEN SPHERICALLY SYMMETRICAL, ISOTROPIC EARTH MODEL AND, IF
C       DESIRED, PERTURBS THE MODEL TO FIT OBSERVED TRAVEL TIME DATA.
C
C
C    METHOD
C          THE MODEL IS SPECIFIED IN TERMS OF VALUES OF VELOCITY AND RADIUS AT A
C       NUMBER OF DEPTHS IN THE EARTH.  THE VELOCITY BETWEEN THESE POINTS IS
C       ASSUMED TO OBEY THE LAW V=A*R**B.  OBSERVED DATA (TRAVEL TIME VS.
C       DELTA) IS READ IN AND THE TRAVEL TIME CURVE FOR THE GIVEN MODEL IS
C       CALCULATED.  RAYS CORRESPONDING TO DELTA VALUES FOR OBSERVED DATA ARE
C       FOUND ITERATIVELY AND PARTIAL DERIVATIVES OF TRAVEL TIME WITH RESPECT
C       TO MODEL PARAMETERS ARE STORED.  EACH DATA POINT IS ASSUMED TO BE
C       ASSOCIATED WITH THE CLOSEST BRANCH OF THE TRAVEL TIME CURVE, IF MORE
C       THAN ONE BRANCH EXISTS FOR A GIVEN DELTA VALUE, OR THE USER MAY INDICATE
C       WHICH BRANCH A GIVEN DATA POINT IS ON BY SPECIFYING THE APPROXIMATE
C       VALUE OF THE RAY PARAMETER, P.  THE PARTIAL DERIVATIVE ARE THEN USED TO
C       PERTURB THE GIVEN MODEL BY A METHOD WHICH MINIMIZES A WEIGHTED SUM OF
C       THE SQUARES OF THE TRAVEL TIME RESIDUAL VECTOR AND THE MODEL PERTUR-
C       BATION VECTOR.  THE ENTIRE OPERATION MAY BE REPEATED AS MANY TIMES AS
C       DESIRED, AND FINALLY THE TRAVEL TIMES, ETC. FOR THE FINAL MODEL ARE
C       CALCULATED.  AT THE USERS OPTION, DATA POINTS WITH LARGE RESIDUALS MAY
C       BE DISCARDED BEFORE INVERSION.  DURING THE TRAVEL TIME CALCULATIONS,
C       THEORETICAL AMPLITUDES ARE COMPUTED, CONSIDERING THE EFFECTS OF BOTH
C       GEOMETRIC SPREADING AND ATTENUATION (IF A Q VS. DEPTH MODEL IS GIVEN).
C       OPTIONS ARE INCLUDED FOR PLOTTING THE MODELS, THE TRAVEL TIME CURVES,
C       THE DT/DDELTA CURVES, AND THE AMPLITUDE CURVES, EITHER ON THE PRINTER
C       OR THE X-Y PLOTTER.
C
C
C     RESTRICTIONS
C          THE NUMBER OF POINTS (DEPTH, VELOCITY, Q) IN THE MODEL MUST NOT
C        EXCEED 100.
C          THE NUMBER OF DATA POINTS MUST NOT EXCEED 200.
C          THE NUMBER OF PARAMETERS TO BE PERTURBED MUST NOT EXCEED 50.
C          ABRUPT DISCONTINUITIES ARE NOT ALLOWED.
C
C
C     USAGE
C
C I. CARD:
C    1-80 IDENT  (20A4):  80 COLUMNS OF IDENTIFICATION.  FIRST 12 COLUMNS USED
C                         AS TITLE ON X-Y PLOTS, IF ANY.
C
C
C II. CARD:
C    1-12 RADIUS (F12.8): RADIUS OF EARTH (KM).
C   13-24 RM     (F12.8): SCALE FACTOR FOR RR ON STRUCTURE CARDS (SEE III).
C                         IF NOT GIVEN, WILL BE SET = 1.
C   25-28 MODPLT (I4):     .GT. 0 - PLOT MODEL ON PRINTER.
C                          .LT. 0 - PLOT MODEL ON X-Y PLOTTER.
C                          .EQ. 0 - DO NOT PLOT MODEL.
C                          IF PLOTS ARE REQUESTED (MODPLT .NE. 0), THE STRUCTURE
C                          CARDS MUST BE FOLLOWED BY CARDS GIVING SIZE AND SCALE
C                          FOR THE PLOTS (SEE IV).
```

```
C
C
C III. STRUCTURE CARDS - EACH CARD PAIR GIVES DEPTH, VELOCITY, Q AT ONE POINT
C          OF MODEL.  STRUCTURE MUST BE READ IN FROM BOTTOM UPWARDS.
C          DISCONTINUITIES ARE NOT ALLOWED.
C     2-12 RR      (F11.8): RADIUS OR DEPTH, DEPENDING ON I2 (SEE BELOW).
C                           SCALE FACTOR RM (SEE II) IS APPLIED TO RR.
C    14-24 VV      (F11.8): VELOCITY CORRESPONDING TO RR.
C                           AN ASTERICK (*) PRECEEDING RR AND/OR VV (COLS. 1 & 13)
C                           INDICATES WHICH PARAMETERS MAY BE PERTURBED.
C    25-28 I2      (I4):    .EQ. 0 - RR * RM = DEPTH.
C                           .NE. 0 - RR * RM = RADIUS.
C
C    33-36 LAST    (I4):    .NE. 0 - THIS IS THE LAST STRUCTURE CARD PAIR.
C     1-12 QQ      (F12.8): (SECOND CARD OF PAIR)
C                           VALUE OF Q IN INTERVAL BETWEEN THIS CARD PAIR AND NEXT
C                           ONE.  (SPECIFYING A Q MODEL IS OPTIONAL.)
C
C
C IV. ABS(MODPLT) CARDS - PARAMETERS FOR PLOTS(S) OF MODEL, IF ANY (SEE II).
C     1-10 XL      (F10.5): X LENGTH OF PAPER IN INCHES.
C    11-20 YL      (F10.5): Y LENGTH OF PAPER IN INCHES.
C                           FOR PRINTER PLOT (MODPLT .GT. 0), YL MUST BE .LE. 12.
C                           FOR X-Y PLOT (MODLPT .LT. 0), SPECIAL PAPER MUST BE
C                           USED IF YL IS .GT. 10.
C    21-30 XF      (F10.5): X (DEPTH) SCALE FACTOR (DATA UNITS / INCH).
C    31-40 XMIN    (F10.5): MINIMUM X (DEPTH) VALUE.
C    41-50 YF      (F10.5): Y (VELOCITY) SCALE FACTOR (SCALE UNITS / INCH).
C    51-60 YMIN    (F10.5): MINIMUM Y (VELOCITY) VALUE.
C    63-64 LAB     (I2):    FLAG USED ONLY WITH X-Y PLOTS.
C                           .NE. 0 - THIS IS LAST PLOT ON SHEET.
C                           .EQ. 0 - THIS IS NOT LAST PLOT ON SHEET.
C                           .EQ. -1 - SUPRESS PRINTING OF JOB AND SEQUENCE NUMBERS
C    65-66 NX      (I2):    NUMBER OF INTERVALS ALONG X AXIS FOR X-Y PLOTS.
C    67-68 NY      (I2):    NUMBER OF INTERVALS ALONG Y AXIS FOR X-Y PLOTS.
C                           (SEE WRITE-UP OF SUBROUTINE LABEL.)
C                           .EQ. 0 - SUPRESS SCALE MARKS AND LABELS ON X-Y PLOTS.
C
C
C V. CARD:
C     1- 6 NUMCD   (I6):    NUMBER OF TIMES THE FOLLOWING GROUP OF CARDS IS
C                           REPEATED.
C
C
C   IIIIIIIIIIIIIIIIIIIIIIIIIIIIIIIIIIIIIIIIIIIIIIIIIIIIIIIIIIIIIIIIIIIIIIIIIIIII
C   I VI. CARD:
C   I  1-10 DFOC      (F10.8): DEPTH OF FOCUS.
C R I 11-20 AI        (F10.8): INITIAL TAKE-OFF ANGLE.
C E I 21-30 AC        (F10.8): TAKE-OFF ANGLE INCREMENT.
C P I                            IF AC < 0., RAYS WILL BE CHOSEN SO THAT DELTA IS
C E I                            SPACED BY APPROXIMATELY ABS(AC).  THIS OPTION HAS
C A I                            PROVED EXTREMELY USEFUL FOR MOST CASES.
C T I 31-40 AF        (F10.8): FINAL TAKE-OFF ANGLE.
C   I                            TAKE-OFF ANGLE IS MEASURED IN DEGREES.  0. DEGREES
C N I                            IS STRAIGHT DOWN, 90. DEGREES IS HORIZONTAL, 180.
C U I                            DEGREES IS STRAIGHT UP.
C M I 41-50 DREF      (F10.8): DEPTH OF REFLECTION, IF REFLECTED RAYS ARE DESIRED
C C I                            IF DREF = 0. NO REFLECTION IS ASSUMED.
C D I 61-62 NPPLT     (I2):    NO. OF PRINTER PLOTS OF TRAVEL TIME, DT/DDELTA, OR
C   I                            AMPLITUDE CURVES.  FOR EACH PLOT, CARD GIVING SCALE
C T I                            FACTORS, ETC. MUST BE GIVEN (SEE IX).
C I I 65-66 IRAY      (I2):    .NE. 0 - PRINT TABLE GIVING TIME, DELTA AT TOP OF
C M I                            EACH LAYER DURING RAY CALCULATIONS.
C E I 67-68 IPNCH     (I2):    .NE. 0 - PUNCH BCD CARDS GIVING TRAVEL TIMES,
C S I                            AMPLITUDES, ETC. FOR CALCULATED RAYS.
C   I                            TIMES, ETC. FOR CALCULATED RAYS.
C   I 69-70 NXYPL     (I2):    NO. OF X-Y PLOTS OF TRAVEL TIME, DT/DDELTA, OR
C   I                            AMPLITUDE CURVES.  FOR EACH PLOT, A CARD GIVING
C   I                            SCALE FACTORS, ETC. MUST BE GIVEN (SEE VIII).
C   I 71-72 INVRT     (I2):    .GT. 0 - READ OBSERVED DATA (SEE VII) AND PERTURB
C   I                            MODEL ITERATIVELY (INVRT) TIMES TO FIT DATA.
C   I                            .LT. 0 - READ OBSERVED DATA AND INCLUDE ON PLOTS,
C   I                            BUT DO NOT PERTURB MODEL.
C   I                            .EQ. 0 - DO NOT READ OBSERVED DATA.
C   I 73-80 FREQ      (F8.2):  FREQUENCY (HZ) USED IN AMPLITUDE CALCULATIONS.  IF
C   I                            NOT GIVEN, 1 HZ IS ASSUMED.
C   I
```

```
C   I
C   I VII. OBSERVED DATA CARDS - REQUIRED ONLY IF INVRT .NE. 0 (SEE VI).
C   I  ONLY DELTA AND TRAVEL TIME ARE USED FOR INVERSION.  RAY PARAMETER, IF
C   I  GIVEN, WILL BE USED TO ASSIGN DATA POINT TO CORRECT BRANCH OF TRAVEL
C   I  TIME CURVE.  OTHER VALUES ARE OPTIONAL AND ARE USED ONLY ON PLOTS.
C   I  OPTIONAL AND ARE USED ONLY ON PLOTS.
C   I  1-10          (F10.5): DELTA (DEGREES).
C   I 11-20          (F10.5): TRAVEL TIME (SECONDS)
C   I 21-30          (F10.5): RAY PARAMETER, P.
C   I 21-30          (F10.5): RAY PARAMETER, P(= DT/DDELTA)(SEC/DEG).
C   I 31-40          (F10.5): AMPLITUDE.
C   I 41-50          (F10.5): EFFECTIVE Q.
C   I 65-66 NF       (I2):    NUMBER FROM 0 TO 14, INDICATING SYMBOL TO BE USED
C   I                         WHEN PLOTTING THIS DATA POINT (SEE WRITE UP OF
C   I                         SUBROUTINE PLOTXY).
C   I 69-70 LAST     (I2):    .NE. 0 ON LAST OBSERVED DATA CARD.  ZERO OR BLANK
C   I                         ON ALL OTHER CARDS.
C R I
C E I
C P I VIII. (NXYPL) CARDS - SCALING INFORMATION FOR X-Y PLOTS, IF ANY.
C E I  1-10 XLNGTH (F10.5): PLOT DIMENSION IN X (DELTA) DIRECTION(INCHES).
C A I 11-20 YLNGTH (F10.5): PLOT DIMENSION IN Y DIRECTION (INCHES).
C T I 21-30 XF     (F10.5): X SCALE FACTOR (DEG/IN OR KM/IN - SEE IKM, BELOW).
C   I 31-40 XMIN   (F10.5): MINIMUM X VALUE (KM OR DEG).
C N I 41-50 YF     (F10.5): Y SCALE FACTOR (DATA UNITS/IN).
C U I 51-60 YMIN   (F10.5): MINIMUM Y VALUE (DATA UNITS).
C M I 61-62 IT     (I2):    INDICATES WHICH FUNCTION IS TO BE PLOTTED.
C C I                       1 - REDUCED TRAVEL TIME; 2 - DT/DDELTA;
C D I                       3 - AMPLITUDE; 4 - EFFECTIVE Q.
C   I 63-64 LAP    (I2):    .EQ. 1 INDICATES LAST PLOT ON THIS SHEET.
C T I                       .EQ. 0 WILL CAUSE NEXT PLOT TO BE ON SAME SHEET.
C I I 65-66 NX     (I2):    NO. OF X INTERVALS FOR SCALE MARKS AND LABELS.
C M I 67-68 NY     (I2):    NO. OF Y INTERVALS FOR SCALE MARKS AND LABELS.
C E I 69-70 IKM    (I2):    .EQ. 1 - X SCALE IN KM.
C S I                       .EQ. 0 - X SCALE IN DEG.
C   I 71-80 RV     (F10.5): VELOCITY TO BE USED TO REDUCE TRAVEL TIMES (KM/SEC).
C   I                       IF .EQ. 0., TRAVEL TIMES WILL NOT BE REDUCED.
C   I
C   I
C   I IX. (NPPLT) CARDS - SCALING INFORMATION FOR PRINTER PLOTS, IF ANY (SEEVI).
C   I FORMAT IS SAME AS FOR X-Y PLOTS (SEE VIII). YLNGTH MUST BE .LE. 12.
C   I LAP, NX, NY ARE IGNORED.
C   I
C   I
C   I X. CARD - PARAMETERS FOR INVERSION (IF INVRT .GT. 0, SEE VI).
C   I  1-10 ALPHA  (F10.5): CONSTRAINT PARAMETER: THE LARGER ALPHA IS, THE
C   I                       SMALLER THE MODEL PERTURBATION WILL BE.  A
C   I                       REASONABLE ESTIMATE OF THE VALUE IS THE RATIO OF THE
C   I                       EXPECTED TRAVEL TIME ERROR (SEC) TO THE EXPECTED
C   I                       MODEL PERTURBATIONS (KM/SEC).
C   I 11-15 MAX    (I5):    NUMBER OF ITERATIONS ALLOWED FOR SUBROUTINE EQSOV
C   I                       TO SOLVE LINEAR SYSTEM.  5 IS USUALLY SUFFICIENT.
C   I 16-25 EPS    (F10.5): RELATIVE ACCURACY REQUIRED IN SOLUTION OF SYSTEM.
C   I                       MUST BE .GE. .00001
C   I 26-35 TJ     (F10.5): DATA POINTS WILL BE DISCARDED IF THEY HAVE RESIDUALS
C   I                       GREATER THAN TWICE THE RMS DEVIATION BETWEEN THE
C   I                       OBSERVED AND CALCULATED TRAVEL TIMES AND IF THE
C   I                       DEVIATION EXCEEDS TJ.  IF TJ .EQ. 0, NO POINTS WILL
C   I                       BE DISCARDED.
C   I NOTE:  IF MORE THAN ONE ITERATION IS PERFORMED FOR INVERSION (INVRT .GT. 1
C   I - SEE VI), CARD X MUST BE REPEATED FOR EACH ITERATION.  ALSO, THE PLOTS
C   I (VIII & IX), IF ANY, WILL BE REPEATED FOR EACH ITERATION.  THUS VIII, IX,
C   I AND X MUST BE REPEATED FOR EACH ITERATION.
C   IIIIIIIIIIIIIIIIIIIIIIIIIIIIIIIIIIIIIIIIIIIIIIIIIIIIIIIIIIIIIIIIIIIIIIIIIII
C
C       MORE THAN ONE DECK MAY BE RUN AT ONE TIME.  SIMPLY PLACE NEXT DECK,
C       BEGINNING WITH IDENT CARD, IMMEDIATELY AFTER PREVIOUS ONE.
CCCCCCCCCCCCCCCCCCCCCCCCCCCCCCCCCCCCCCCCCCCCCCCCCCCCCCCCCCCCCCCCCCCCCCCCCCCCCC
```

REFERENCES

Anderson, Don L., Phase Changes in the Upper Mantle, Science, 157, 1165-1173, 1967.

Anderson, D. L., and M. N. Toksoz, Surface Waves on a Spherical Earth. 1. Upper Mantle Structure from Love Waves, J. Geophys. Res., 68, 3483-3500, 1963.

Anderson, D. L., and Ben-Menahem, and C. B. Archambeau, Attenuation of Seismic Energy in the Upper Mantle, J. Geophys. Res., 70, 1441-1448, 1965.

Anderson, Don L., and Charles G. Sammis, The Low-Velocity Zone, Phys. Earth and Planetary Interiors, in press.

Archambeau, C. B. and E. A. Flinn, Perturbation Theory for the Inversion of Body Wave Travel Time Data, Seismic Data Lab. Report no. 142, 1966.

Archambeau, C. B., E. A. Flinn, and D. G. Lambert, Fine Structure of the Upper Mantle, in press, J. Geophys. Res.

Arons, A. B., Underwater Explosion Shock Wave Parameters at Large Distances from the Charge, J. Acoustic. Soc. Am., 26, 343-346, 1954.

Arons, A. B., and D. R. Yennie, Energy Partition in Underwater Explosion Phenomena, Rev. Mod. Phys., 20, 519-536, 1948.

Barnard, Philip, Signal Strength of Marine Seismograph Explosives, Geophysics, 32, 827-832, 1967.

Barr, K. G., Upper Mantle Structure in Canada from Seismic Observations using Chemical Explosions, Canadian J. Earth. Sciences, 4, 961-975, 1967.

Berry, M. J., and G. F. West, A Time-Term Interpretation of the First-Arrival Data of the 1963 Lake Superior Experiment, in AGU Monograph 10, 166-180, 1966.

Brune, James N., The Sa Phase from the Hindu Kush Earthquake of July 6, 1962, Pure and Applied Geophysics, 62, 81-95, 1965a.

Brune, James N. Regional Variations in the Structure of the Upper Mantle and the Propagation of the Sa Phase, AFOSR Contract Report, 1965b.

Brune, James, and James Dorman, Seismic Waves and Earth Structure in the Canadian Shield, Bull. Seismol. Soc. Am., 53, 167-210, 1963.

Bullard, E. C., The Density within the Earth, Verhandelingen van het Koninklijk Nederlandsch Geologish-Mijnbouwkundig Genootschap, Geologische Serie, Deel XVIII, 23-41, 1957.

Bullen, K. E., An Introduction to the Theory of Seismology, 3rd Edition, Cambridge University Press, Cambridge, 1963.

Clark, S. P. and A. E. Ringwood, Density Distribution and Constitution of the Mantle, Rev. Geophys., 2, 35-88, 1964.

Coast and Geodetic Survey, The Puget Sound, Washington, Earthquake of April 29, 1965.

Cleary, J. R. and A. L. Hales, An Analysis of the Travel Times of P Waves to North American Stations, in the Distance Range 32° to 100°, Bull. Seismol. Soc. Am., 56, 467-489, 1966.

Cole, Robert H., Underwater Explosions, Princeton University Press, Princeton, 1948.

Davies, D., and D. P. McKenzie, Seismic Travel-Time Residuals and Plates, Geophys. J., Roy. Astr. Soc., in press, 1969.

Dorman, LeRoy M., Anelasticity and the Spectra of Body Waves, J. Geophys. Res., 73, 3877-3883, 1968.

Doyle, H. A., and A. L. Hales, An Analysis of the Travel Times of S Waves to North American Stations, in the Distance Range 28° to 82°, Bull. Seismol. Soc. Am., 57, 761, 1967.

Eliseevnin, V. A., Analysis of Rays Propagating in an Inhomogeneous Medium, Soviet Physics Acoustics, 10, 242-245, 1965.

Ewing, W. Maurice, Wenceslas S. Jardetzky, and Frank Press, Elastic Waves in Layered Media, McGraw-Hill, New York, 1957.

Green, R. W. E., and A. L. Hales, The Travel Times of P Waves to 30° in the Central United States and Upper Mantle Structure, Bull. Seismol. Soc. Am., 58, 267-289, 1968.

Gutenberg, Beno, Physics of the Earth's Interior, Academic Press, New York, 1959a.

Gutenberg, B., Wave Velocities Below the Mohorovicic Discontinuity, Geophys. J. Royal Astr. Soc., 2, 348-352, 1959b.

Hales, A. L., J. R. Cleary, H. A. Doyle, R. Green, and J. Roberts, P-Wave Station Anomalies and the Structure of the Upper Mantle, J. Geophys. Res., 73, 3885-3896, 1968.

Hall, D. H., and W. C. Brisbin, Crustal Structure from Converted Head Waves in Central Western Manitoba, Geophysics, 30, 1053 - 1067, 1965.

Herrin, Eugene, and James Taggart, Regional Variations in P Travel Times, Bull. Seismol. Soc. Am., 58, 1325-1337, 1968.

Hill, D. P. and L. C. Pakiser, Crustal Structure between the Nevada Test Site and Boise, Idaho from Seismic Refraction Measurements, in AGU Monograph 10, 391-419, 1966.

Hobson, G. D., A. Overton, D. N. Clay, and W. Thatcher, Crustal Structure under Hudson Bay, Canadian J. Earth Sciences, 4, 929-947, 1967.

Isacks, Bryan, Jack Oliver, and Lynn R. Sykes, Seismology and the New Global Tectonics, J. Geophys. Res., 73, 5855-5899, 1968.

Iyer, H. M., L. C. Pakiser, D. J. Stuart, D. H. Warren, Project EARLY RISE: A Seismic Probing of the Upper Mantle, J. Geophys. Res., 73, 4409-4441, 1969.

Jackson, W. H., and L. C. Pakiser, Seismic Study of Crustal Structure in the Southern Rocky Mountains, U. S. Geological Survey Prof. Paper 525-D, pages D85-D92, 1965.

Jackson, W. H., S. W. Stewart, and L. C. Pakiser, Crustal Structure in Eastern Colorado from Seismic Refraction Measurements, J. Geophys. Res., 68, 5767-5776, 1963.

Jeffreys, H., The Earth, 4th Edition, Cambridge University Press, Cambridge, 1962.

Johnson, L. R., Array Measurements of P Velocities in the Upper Mantle, J. Geophys. Res., 6309-6325, 1967.

Kanasewich, E. R., T.Alpaslan, and C. D. Hemmings, Seismic Studies of the Upper Mantle in Western Canada, paper presented at AGU Western National Meeting, San Francisco, December, 1968.

King, Phillip B., The Evolution of North America, Princeton University Press, Princeton, 1950.

Landisman, Mark, Yasuo Sato and Tatsuo Usami, Propagation of Disturbances in a Gutenberg-Bullen A' spherical earth model: Travel Times and Amplitudes of S Waves, in AGU Monograph 10 , 482-494, 1966.

Lehmann, I., On the Travel Times of P as Determined from Nuclear Explosions, Bull. Seism. Soc. Am., 54, 123-139, 1964.

Lehmann, I., On the travel times of P as Obtained from the Nuclear Explosions Bilby and Shoal, Phys. Earth and Planet. Interiors, 1, 14-23, 1967.

Lehner, F. E., and Frank Press, A Mobile Seismograph Array, Bull. Seismol. Soc. Am., 56, 889-897, 1966.

Lewis, Brian T. R., and Robert P. Meyer, A Seismic Investigation of the Upper Mantle to the West of Lake Superior, Bull. Seismol. Soc. Am., 58, 565-596, 1968.

Lukk, A. A., and I. L. Nersesov, Structure of the Upper Mantle as Shown by Observations of Earthquakes of Intermediate Focal Depth, Doklady Akad. Nauk SSSR, Earth Sciences Sections, 162, 14-16, 1965.

Molnar, Peter, and Jack Oliver, Lateral Variations of Attenuation in the Upper Mantle and Discontinuities in the Lithosphere, J. Geophys. Res., 74, 2648-2682, 1969.

O'Brien, P.N.S., Lake Superior Crustal Structure - A reinterpretation of the 1963 Seismic Experiment, J. Geophys. Res., 73, 2669-2689, 1968.

Oliver, Jack, and Bryan Isacks, Deep Earthquake Zones, Anomalous Structures in the Upper Mantle, and the Lithosphere, J. Geophys. Res., 72, 4259-4275, 1967.

Press, Frank, and Shawn Biehler, Inferences on Crustal Velocities and densities from P Wave Delays and Gravity Anomalies, J. Geophys. Res., 69, 2979-2995, 1964.

Rankin, Douglas S., Ravi Ravindra, and David Zwicker, Preliminary Interpretation of the first Refraction Arrivals in Gaspe from Shots in Labrador and Quebec, Canadian J. Earth Sciences, 6, 771-774, 1969.

Reagar, B. D., D. W. Gordon, and J. N. Jordan, Seismic Analysis of a Nuclear Explosion: Gasbuggy, ARPA Report, 1968.

Richards, T. C., and D. J. Walker, Measurement of the Thickness of the Earth's Crust in the Albertan Plains of Western Canada, Geophysics, 262-284, 1959.

Ringwood, A. E., Mineralogy of the Mantle, in Advances in Earth Science, P. M. Hurley Ed., MIT Press, Cambridge, 357-399, 1966.

Ringwood, A. E., Composition and Evolution of the Upper Mantle, in AGU Monograph 13, 1-17, 1969.

Roller, John C., Crustal Structure in the Eastern Colorado Plateaus Province from Seismic Refraction Measurements, Bull. Seismol. Soc. Am., 55, 107-119, 1965.

Roller, J. C., and W. H. Jackson, Seismic Wave Propagation in the Upper Mantle: Lake Superior, Wisconsin to Central Arizona, J. Geophys. Res., 71, 5933-5941, 1966.

Romney, Carl, Bilby G. Brooks, Robert H. Mansfield, Dean S. Carder, James N. Jordan, and David W. Gordon, Travel Times and Amplitudes of Principal Body Phases Recorded from Gnome, Bull. Seismol. Soc. Am., 52, 1057-1074, 1962.

Ryall, Alan, and David J. Stuart, Travel Times and Amplitudes from Nuclear Explosions, Nevada Test Site to Ordway, Colorado, J. Geophys. Res., 68, 5821-5835, 1963.

Simmons, Gene, and Robert F. Roy, Heat Flow in North America, in AGU Monograph 13, 78-81, 1969.

Smith, T. Jefferson, John S. Steinhart, and L. T. Aldrich, Crustal Structure Under Lake Superior, AGU Monograph 10, 181-197, 1966.

Stewart, S. W., and L. C. Pakiser, Crustal Structure in Eastern New Mexico Interpreted from the Gnome Explosion, Bull. Seismol. Soc. Am., 52, 1017-1030, 1962.

Steinhart, J. S., and R. P. Meyer, Explosion Studies of Continental Structure, Carnegie Inst. Wash. Publ. 622, 1961.

Stockwell, C. H., A Tectonic Map of the Canadian Shield, in The Tectonics of the Canadian Shield, John S. Stevenson, editor, Royal Society of Canada Special Publication No. 4, 1962.

Sykes, Lynn R., Seismicity and Deep Structure of Island Arcs, J. Geophys. Res., 71, 2981-3006, 1966.

Toksoz, M. Nafi, and Don L. Anderson, Phase Velocities of Long-Period Surface Waves and Structures of the Upper Mantle, J. Geophys. Res., 71, 1649-1658, 1966.

Warren, David H., A Seismic Refraction Survey of Crustal Structure in Central Arizona, Geol. Soc. America Bull., 80, 257-282, 1969.

Warren, D., and Wayne H. Jackson, Surface Seismic Measurements of the Project Gasbuggy Explosion at Intermediate Distance Ranges, U. S. Geological Survey Open File Report, 1968.

Warren, D. H., J. H. Healy, J. C. Hoffman, Reinis Kempe, Srinevasreddy Raula, Project Early Rise: Travel Times and Amplitudes, National Center for Earthquake Research Technical Letter No. 6, 1967.

White, W. R. H., Bone, M. N., and W. G. Milne, Seismic Refraction Surveys in British Columbia, 1941-1966: A Preliminary Interpretation, in AGU Monograph 12, 81-93, 1968.

White, W. R. H., and J. C. Savage, A Seismic Refraction and Gravity Study of the Earth's Crust in British Columbia, Bull. Seismol. Soc. Am., 55, 463-486, 1965.

Willden, Ronald, Seismic-Refraction Measurements of Crustal Structure between American Falls Reservoir, Idaho, and Flaming Gorge Reservoir, Utah, in U. S. Geological Survey Prof. Paper 525-C, p. C44-C50, 1965.

Willis, David E., An Investigation of Seismic Wave Propagation in the Eastern United States, AFOSR Report 8071-16-T, 1968.

Wold, Richard J., and Ned A. Ostenso, Aeromagnetic Gravity and Sub-Bottom Profiling Studies in Western Lake Superior, in AGU Monograph 10, 66-94, 1966.

List of Tables

Table 19. Velocity structure for model WASH 1.

Explanation of Abbreviations used in Tables 1-5, 7

Source Abbreviations

Nuclear event names longer than six letters have been abbreviated as follows:

ARDVRK - Aardvark

ARMDLO - Armadillo

CHRTRS - Chartreuse

CLRWTR - Clearwater

COMODR - Commodore

DORMSE - Dormouse

DORMS' - Dormouse Prime

FLTLES - Faultless

GASBGY - Gasbuggy

HALFBK - Half Beak

HRDHAT - Hardhat

HAYMKR - Haymaker

MERMAC - Merrimac

MISISP - Mississippi

Receiver Abbreviations

Three letter codes are the standard abbreviations established by the U.S. Coast and Geodetic Survey. Four and five letter codes are those used by the Air Force Technical Applications Center (AFTAC) for stations of the Long Range Seismic Measurements (LRSM) network. Codes such as USGS 1 (Table 7) refer to data obtained by U.S. Geological

Survey recording units (see Warren 1968).

Table 1

NTS-N NEVADA TEST SITE NORTH PROFILE

SOURCE	RCVR	DELTA DEG	DELTA KM	AZIMUTH S-->R DEG	AZIMUTH R-->S DEG	CORRECTED TIME SEC	FLIP CORR SEC	ELEV CORR SRCE SEC	ELEV CORR RCVR SEC
BOXCAR	ATNV	2.236	248.4	347.6	167.2	38.31	0.0	-0.25	-0.44
HRDHAT	ATNV	2.383	264.8	340.7	160.1	39.96	0.0	-0.40	-0.44
BILBY	EUR	2.420	268.7	0.9	181.0	40.64	0.0	-0.17	-0.49
ARDVRK	ATNV	2.549	283.1	341.5	160.8	42.30	0.0	-0.25	-0.44
AUK	UVN	3.756	417.4	334.0	152.7	58.81	0.0	-0.26	-0.43
BILBY	WINV	4.427	491.9	345.8	164.9	68.39	0.0	-0.17	-0.34
GREELY	MOID	5.765	640.4	1.0	181.1	91.59	0.0	-0.23	-0.18
GREELY	MOID	5.765	640.4	1.0	181.1	97.69	0.0	-0.23	-0.18
GREELY	MOID	5.765	640.4	1.0	181.1	89.99	0.0	-0.23	-0.18
GREELY	MOID	5.765	640.4	1.0	181.1	88.19	0.0	-0.23	-0.18
HRDHAT	VTOR	6.179	686.6	343.7	162.2	94.08	0.0	-0.40	-0.32
ARDVRK	VTOR	6.345	705.0	343.9	162.4	96.33	0.0	-0.25	-0.32
HALFBK	BMO	7.556	839.6	354.5	173.9	121.66	0.0	-0.37	-0.27
HALFBK	BMO	7.556	839.6	354.5	173.9	114.06	0.0	-0.37	-0.27
HALFBK	BMO	7.556	839.6	354.5	173.9	126.26	0.0	-0.37	-0.27
BILBY	BMO	7.834	870.4	353.3	172.4	120.27	0.0	-0.17	-0.27
BILBY	BMO	7.834	870.4	353.3	172.4	117.77	0.0	-0.17	-0.27
BILBY	BMO	7.834	870.4	353.3	172.4	124.47	0.0	-0.17	-0.27
HAYMKR	PKCR	8.547	949.7	346.2	164.3	129.51	0.0	-0.25	-0.23
HRDHAT	PTOR	8.636	959.6	346.7	164.8	130.31	0.0	-0.40	-0.09
YUBA	PTOR	8.643	960.4	347.4	165.6	137.47	0.0	-0.64	-0.09
ARDVRK	PTOR	8.803	978.2	346.8	164.9	133.66	0.0	-0.25	-0.09
ARDVRK	TRWA	9.782	1087.1	341.3	158.4	146.04	0.0	-0.25	-0.11
FLTLES	CCWA	9.795	1088.7	340.3	157.0	145.69	0.0	-0.28	-0.23
FLTLES	CCWA	9.795	1088.7	340.3	157.0	148.19	0.0	-0.28	-0.23
FLTLES	CCWA	9.795	1088.7	340.3	157.0	154.79	0.0	-0.28	-0.23
GREELY	LON	10.257	1140.0	338.6	155.0	151.68	0.0	-0.23	-0.19
HAYMKR	ELWA	10.472	1163.8	342.0	158.8	155.23	0.0	-0.25	-0.22
CUP	LON	10.508	1167.9	337.7	153.8	156.08	0.0	-0.24	-0.19
CUP	SPC	10.619	1180.0	355.2	174.3	157.40	0.0	-0.24	-0.16
FLTLES	PNT	10.874	1208.5	348.1	165.7	161.00	0.0	-0.28	-0.12
BOXCAR	CCWA	11.007	1223.2	343.4	160.3	162.12	0.0	-0.25	-0.23
CUP	TUM	11.096	1233.3	334.8	150.2	168.05	0.0	-0.24	-0.01
FLTLES	VIC	11.169	1241.7	334.5	149.5	163.58	0.0	-0.28	-0.04
CLRWTR	TKWA	11.846	1316.4	349.1	166.8	174.25	0.0	-0.54	-0.11
BILBY	TKWA	12.013	1334.9	348.6	166.1	174.82	0.0	-0.17	-0.11
BILBY	TKWA	12.013	1334.9	348.6	166.1	184.02	0.0	-0.17	-0.11
HALFBK	PNT	12.153	1350.6	349.6	167.3	177.40	0.0	-0.37	-0.12
HALFBK	PNT	12.153	1350.6	349.6	167.3	177.40	0.0	-0.37	-0.12
GREELY	VIC	12.324	1369.9	337.6	152.8	191.12	0.0	-0.23	-0.04
GREELY	VIC	12.324	1369.9	337.6	152.8	183.42	0.0	-0.23	-0.04
GREELY	VIC	12.324	1369.9	337.6	152.8	179.42	0.0	-0.23	-0.04
CUP	PNT	12.356	1373.1	349.0	166.5	181.44	0.0	-0.24	-0.12
MISISP	MUWA	12.522	1391.7	341.9	157.9	183.29	0.0	-0.25	-0.16
FLTLES	MCC	13.520	1502.6	353.7	172.0	196.99	0.0	-0.28	-0.14
MISISP	CKBC	14.193	1577.4	346.2	162.5	203.03	0.0	-0.25	-0.12
FLTLES	PHC	14.447	1606.4	330.2	142.3	214.81	0.0	-0.28	-0.01
FLTLES	PHC	14.447	1606.4	330.2	142.3	207.81	0.0	-0.28	-0.01
GREELY	MCC	14.828	1647.9	354.7	173.2	214.23	0.0	-0.23	-0.14
MISISP	HMBC	15.015	1668.7	346.8	163.0	214.70	0.0	-0.25	-0.25
GREELY	PHC	15.546	1728.3	333.0	145.3	240.36	0.0	-0.23	-0.01
GREELY	PHC	15.546	1728.3	333.0	145.3	232.26	0.0	-0.23	-0.01
GREELY	PHC	15.546	1728.3	333.0	145.3	226.66	0.0	-0.23	-0.01
GREELY	PHC	15.546	1728.3	333.0	145.3	221.96	0.0	-0.23	-0.01
HALFBK	JPAT	15.632	1737.2	356.0	174.7	242.17	0.0	-0.37	-0.25
HALFBK	JPAT	15.632	1737.2	356.0	174.7	234.87	0.0	-0.37	-0.25
HALFBK	JPAT	15.632	1737.2	356.0	174.7	226.57	0.0	-0.37	-0.25
HALFBK	JPAT	15.632	1737.2	356.0	174.7	225.17	0.0	-0.37	-0.25
HALFBK	JPAT	15.632	1737.2	356.0	174.7	222.87	0.0	-0.37	-0.25
CUP	PHC	15.816	1758.4	332.5	144.6	229.46	0.0	-0.24	-0.01
FLTLES	PGBC	15.961	1774.1	346.3	161.7	232.42	0.0	-0.28	-0.20
FLTLES	PGBC	15.961	1774.1	346.3	161.7	228.02	0.0	-0.28	-0.20
FLTLES	FSJ	16.723	1859.0	343.5	157.6	237.75	0.0	-0.28	-0.17
GREELY	PGBC	17.224	1914.3	347.7	163.3	258.46	0.0	-0.23	-0.20
GREELY	PGBC	17.224	1914.3	347.7	163.3	255.96	0.0	-0.23	-0.20
GREELY	PGBC	17.224	1914.3	347.7	163.3	246.36	0.0	-0.23	-0.20
GREELY	PGBC	17.224	1914.3	347.7	163.3	243.06	0.0	-0.23	-0.20
HALFBK	PGBC	17.229	1914.9	347.5	163.0	246.62	0.0	-0.37	-0.20
HALFBK	PGBC	17.229	1914.9	347.5	163.0	243.12	0.0	-0.37	-0.20
GREELY	FSJ	17.962	1996.6	345.0	159.3	255.39	0.0	-0.23	-0.17
GREELY	FSJ	17.962	1996.6	345.0	159.3	252.69	0.0	-0.23	-0.17
HALFBK	SIBC	18.967	2108.5	340.5	152.7	275.20	0.0	-0.37	-0.13
HALFBK	SIBC	18.967	2108.5	340.5	152.7	271.10	0.0	-0.37	-0.13
HALFBK	SIBC	18.967	2108.5	340.5	152.7	267.40	0.0	-0.37	-0.13
HALFBK	SIBC	18.967	2108.5	340.5	152.7	264.50	0.0	-0.37	-0.13
FLTLES	WH2YK	25.016	2781.7	338.0	143.4	333.23	0.0	-0.28	-0.19
FLTLES	WH2YK	25.016	2781.7	338.0	143.4	325.83	0.0	-0.28	-0.19
BOXCAR	WH2YK	26.192	2912.3	339.3	145.0	355.26	0.0	-0.25	-0.19
BOXCAR	WH2YK	26.192	2912.3	339.3	145.0	342.56	0.0	-0.25	-0.19
GREELY	WH2YK	26.200	2913.1	339.2	144.9	338.28	0.0	-0.23	-0.19
GREELY	WH2YK	26.200	2913.1	339.2	144.9	336.28	0.0	-0.23	-0.19
GREELY	COL	33.257	3698.6	336.1	130.7	403.93	0.0	-0.23	-0.04
GREELY	COL	33.257	3698.6	336.1	130.7	399.53	0.0	-0.23	-0.04
FORE	COL	33.524	3728.3	336.0	130.3	401.81	0.0	-0.25	-0.04
CUP	BRW	40.137	4464.0	340.9	126.0	457.26	0.0	-0.24	-0.00

Table 2

NTS-NE NEVADA TEST SITE NORTHEAST PROFILE

SOURCE	RCVR	DELTA DEG	DELTA KM	AZIMUTH S-->R DEG	AZIMUTH R-->S DEG	CORRECTED TIME SEC	ELIP CORR SEC	ELEV CORR SRCE SEC	ELEV CORR RCVR SEC
BILBY	CUNV	1.675	186.1	15.4	195.7	29.36	0.0	-0.17	-0.37
FORE	EKNV	2.083	231.3	7.1	187.3	35.21	0.0	-0.25	-0.44
BOXCAR	EYNV	2.295	255.0	22.7	203.5	38.70	0.0	-0.25	-0.45
STONES	WWUT	2.412	268.2	51.8	233.2	39.71	0.0	-0.28	-0.41
FORE	DUG	3.960	440.3	38.7	220.7	61.02	0.0	-0.25	-0.33
BILBY	SLC	4.927	547.8	40.1	222.7	77.21	0.0	-0.17	-0.32
CUP	PI2WY	7.500	834.0	39.6	223.8	114.67	0.0	-0.24	-0.49
CUP	PI2WY	7.500	834.0	39.6	223.8	111.77	0.0	-0.24	-0.49
FLTLES	LAO	10.897	1211.9	39.2	226.0	158.22	0.0	-0.28	-0.20
CUP	HYMA	11.075	1231.4	34.5	220.5	160.44	0.0	-0.24	-0.22
BILBY	FRMA	11.525	1281.5	35.5	221.8	165.62	0.0	-0.17	-0.11
BILBY	FRMA	11.525	1281.5	35.5	221.8	167.42	0.0	-0.17	-0.11
BILBY	FRMA	11.525	1281.5	35.5	221.8	183.32	0.0	-0.17	-0.11
GREELY	LAO	12.047	1339.5	35.7	222.6	172.87	0.0	-0.23	-0.20
CUP	ANMA	12.112	1346.7	34.5	221.2	174.26	0.0	-0.24	-0.20
CHRTRS	RGSD	12.411	1380.5	46.8	235.2	179.34	0.0	-0.45	-0.21
CHRTRS	RGSD	12.411	1380.5	46.8	235.2	177.54	0.0	-0.45	-0.21
CHRTRS	RGSD	12.411	1380.5	46.8	235.2	192.94	0.0	-0.45	-0.21
HALFBK	RGSD	12.419	1381.5	46.6	235.0	193.61	0.0	-0.37	-0.21
HALFBK	RGSD	12.419	1381.5	46.6	235.0	179.21	0.0	-0.37	-0.21
HALFBK	RGSD	12.419	1381.5	46.6	235.0	177.91	0.0	-0.37	-0.21
HALFBK	RGSD	12.419	1381.5	46.6	235.0	180.91	0.0	-0.37	-0.21
BILBY	GIMA	13.371	1486.9	37.1	225.1	190.12	0.0	-0.17	-0.11
BILBY	GIMA	13.371	1486.9	37.1	225.1	201.52	0.0	-0.17	-0.11
CUP	TSND	13.522	1503.7	38.8	227.1	201.28	0.0	-0.24	-0.18
CUP	TSND	13.522	1503.7	38.8	227.1	205.88	0.0	-0.24	-0.18
CUP	TSND	13.522	1503.7	38.8	227.1	192.08	0.0	-0.24	-0.18
BILBY	RYND	15.338	1705.8	39.5	229.4	224.62	0.0	-0.17	-0.11
BILBY	RYND	15.338	1705.8	39.5	229.4	218.82	0.0	-0.17	-0.11
BILBY	HHND	17.320	1926.4	41.3	233.2	243.92	0.0	-0.17	-0.11
BILBY	HHND	17.320	1926.4	41.3	233.2	247.02	0.0	-0.17	-0.11
FLTLES	FFC	18.792	2089.4	26.2	216.7	259.33	0.0	-0.28	-0.08
BILBY	EBMT	19.363	2153.8	43.2	237.3	273.62	0.0	-0.17	-0.11
BILBY	EBMT	19.363	2153.8	43.2	237.3	269.72	0.0	-0.17	-0.11
BILBY	EBMT	19.363	2153.8	43.2	237.3	266.22	0.0	-0.17	-0.11
FLTLES	RKON	20.039	2229.3	45.2	241.3	288.41	0.0	-0.28	-0.11
FLTLES	RKON	20.039	2229.3	45.2	241.3	277.71	0.0	-0.28	-0.11
FLTLES	RKON	20.039	2229.3	45.2	241.3	275.91	0.0	-0.28	-0.11
FLTLES	RKON	20.039	2229.3	45.2	241.3	273.51	0.0	-0.28	-0.11
COMODR	FFC	20.099	2234.6	24.2	214.5	275.06	0.0	-0.17	-0.08
GREELY	RKON	21.101	2347.3	42.9	238.9	285.25	0.0	-0.23	-0.11
GREELY	RKON	21.101	2347.3	42.9	238.9	295.35	0.0	-0.23	-0.11
GREELY	RKON	21.101	2347.3	42.9	238.9	288.05	0.0	-0.23	-0.11
FLTLES	FCC	24.664	2742.9	28.1	225.0	322.34	0.0	-0.28	-0.01
FLTLES	GWC	30.593	3403.9	44.4	253.2	378.91	0.0	-0.28	-0.00
FLTLES	GWC	30.593	3403.9	44.4	253.2	375.16	0.0	-0.28	-0.00
COMODR	GWC	31.601	3515.8	42.6	251.1	382.93	0.0	-0.17	-0.00
GREELY	GWC	31.662	3522.6	42.9	251.7	383.97	0.0	-0.23	-0.00
FLTLES	SCH	36.692	4083.1	47.4	264.7	430.11	0.0	-0.28	-0.11
FLTLES	SCH	36.692	4083.1	47.4	264.7	427.11	0.0	-0.28	-0.11
FLTLES	SV3QB	36.711	4085.1	47.4	264.8	444.79	0.0	-0.28	-0.13
FLTLES	SV3QB	36.711	4085.1	47.4	264.8	431.19	0.0	-0.28	-0.13
FLTLES	SV3QB	36.711	4085.1	47.4	264.8	427.19	0.0	-0.28	-0.13
HALFBK	SV3QB	37.661	4190.7	46.1	263.3	459.00	0.0	-0.37	-0.13
HALFBK	SV3QB	37.661	4190.7	46.1	263.3	450.30	0.0	-0.37	-0.13
HALFBK	SV3QB	37.661	4190.7	46.1	263.3	443.20	0.0	-0.37	-0.13
HALFBK	SV3QB	37.661	4190.7	46.1	263.3	435.50	0.0	-0.37	-0.13
GREELY	SV3QB	37.733	4198.7	46.1	263.3	438.24	0.0	-0.23	-0.13
GREELY	SV3QB	37.733	4198.7	46.1	263.3	435.94	0.0	-0.23	-0.13

Table 3

NTS-ENE NEVADA TEST SITE EAST-NORTHEAST PROFILE

SOURCE	RCVR	DELTA DEG	DELTA KM	AZIMUTH S-->R DEG	AZIMUTH R-->S DEG	CORRECTED TIME SEC	ELIP CORR SEC	ELEV CORR SRCE SEC	ELEV CORR RCVR SEC
HRDHAT	FMUT	3.624	403.2	55.7	238.1	56.38	0.0	-0.40	-0.42
CUP	FLA	4.981	554.2	60.6	244.1	78.09	0.0	-0.24	-0.38
CUP	HCU	5.053	562.3	60.8	244.3	79.19	0.0	-0.24	-0.48
FLTLES	UBO	5.412	602.3	69.8	254.0	85.56	0.0	-0.28	-0.36
HRDHAT	VNUT	6.022	670.0	55.2	239.2	92.78	0.0	-0.40	-0.42
BOXCAR	UBO	6.169	686.3	58.6	242.9	95.49	0.0	-0.25	-0.36
BILBY	FGU	6.450	717.5	51.3	235.4	99.09	0.0	-0.17	-0.44
GREELY	GOL	8.979	999.3	71.2	258.1	132.74	0.0	-0.23	-0.53
YORK	PMWY	9.237	1027.9	60.6	247.4	135.12	0.0	-0.33	-0.55
MISISP	PMWY	9.240	1028.2	60.7	247.4	135.30	0.0	-0.25	-0.55
ARDVRK	PMWY	9.263	1030.7	60.3	247.0	135.89	0.0	-0.25	-0.55
HYRAX	PMWY	9.267	1031.2	60.1	246.9	145.33	0.0	-0.32	-0.55
HAYMKR	PMWY	9.278	1032.4	60.1	246.9	136.79	0.0	-0.25	-0.55
GREELY	FKCC	9.646	1073.7	72.7	260.1	141.96	0.0	-0.23	-0.40
SEDAN	CYWY	9.647	1073.4	60.6	247.7	139.62	0.0	-0.35	-0.43
YORK	HKWY	10.122	1126.3	59.7	247.1	148.83	0.0	-0.33	-0.33
MISISP	HKWY	10.125	1126.6	59.7	247.2	148.12	0.0	-0.25	-0.33
HYRAX	HKWY	10.153	1129.7	59.2	246.6	151.95	0.0	-0.32	-0.33
HAYMKR	HSNB	11.576	1288.0	58.3	246.8	168.88	0.0	-0.25	-0.27
CUP	RCD	11.951	1329.5	50.7	239.1	172.34	0.0	-0.24	-0.22
HALFBK	WNSD	13.640	1517.9	59.3	249.7	202.35	0.0	-0.37	-0.18
HALFBK	WNSD	13.640	1517.9	59.3	249.7	195.15	0.0	-0.37	-0.18
MISISP	AYSD	14.401	1602.5	58.5	249.5	214.41	0.0	-0.25	-0.14
HYRAX	AYSD	14.431	1605.8	58.1	249.1	214.65	0.0	-0.32	-0.14
HYRAX	AYSD	14.431	1605.8	58.1	249.1	214.65	0.0	-0.32	-0.14
ARDVRK	MCSD	15.281	1700.4	58.9	250.7	216.77	0.0	-0.25	-0.08
HAYMKR	MCSD	15.296	1702.2	58.8	250.6	218.76	0.0	-0.25	-0.08
HRDHAT	SEMN	17.682	1967.7	59.4	253.5	247.75	0.0	-0.40	-0.05
YORK	SEMN	17.721	1972.0	59.1	253.2	248.41	0.0	-0.33	-0.05
MISISP	SEMN	17.723	1972.3	59.2	253.2	246.30	0.0	-0.25	-0.05
STONES	SEMN	17.740	1974.1	58.9	252.9	248.07	0.0	-0.28	-0.05
ARDVRK	SEMN	17.748	1975.0	59.0	253.0	248.59	0.0	-0.25	-0.05
MERMAC	SEMN	17.755	1975.8	58.9	253.0	248.39	0.0	-0.26	-0.05
HAYMKR	SEMN	17.763	1976.7	58.9	252.9	248.49	0.0	-0.25	-0.05
ARMDLC	SEMN	17.765	1976.9	58.9	252.9	250.64	0.0	-0.31	-0.05
YUBA	SEMN	17.803	1981.2	59.4	253.6	250.11	0.0	-0.64	-0.05
YORK	HTMN	19.069	2122.0	58.9	254.3	266.01	0.0	-0.33	-0.06
HNDCAR	WFMN	19.164	2132.8	62.4	257.9	265.82	0.0	-0.29	-0.09
AUK	WFMN	19.168	2133.2	62.2	257.6	267.76	0.0	-0.26	-0.09
AUK	WFMN	19.168	2133.2	62.2	257.6	274.06	0.0	-0.26	-0.09
AUK	WFMN	19.168	2133.2	62.2	257.6	266.06	0.0	-0.26	-0.09
AUK	WFMN	19.168	2133.2	62.2	257.6	276.76	0.0	-0.26	-0.09
PAR	WFMN	19.182	2134.8	62.4	257.9	286.82	0.0	-0.29	-0.09
PAR	WFMN	19.182	2134.8	62.4	257.9	266.42	0.0	-0.29	-0.09
ARDVRK	CNWS	20.364	2266.2	58.8	255.4	278.58	0.0	-0.25	-0.07
HAYMKR	CNWS	20.380	2267.9	58.8	255.3	279.28	0.0	-0.25	-0.07
HRDHAT	NGWS	22.486	2502.4	59.0	257.7	300.61	0.0	-0.40	-0.09
MISISP	ARWS	22.523	2506.5	58.9	257.6	301.27	0.0	-0.25	-0.08
STONES	NGWS	22.545	2509.0	58.6	257.2	304.03	0.0	-0.28	-0.09
ARDVRK	NGWS	22.552	2509.8	58.6	257.3	301.66	0.0	-0.25	-0.09
MERMAC	ARWS	22.555	2510.1	58.7	257.4	302.66	0.0	-0.26	-0.08
HAYMKR	ARWS	22.563	2511.0	58.7	257.4	302.06	0.0	-0.25	-0.08
YUBA	NGWS	22.607	2515.8	59.0	257.8	304.78	0.0	-0.64	-0.09
FLTLES	OTT	30.589	3404.7	64.1	271.8	374.60	0.0	-0.28	-0.02
MISISP	BUQB	31.282	3481.7	61.1	268.6	381.01	0.0	-0.25	-0.04
GREELY	OTT	31.327	3486.8	62.1	269.6	381.45	0.0	-0.23	-0.02
FLTLES	MNT	32.056	3568.0	63.7	273.0	387.30	0.0	-0.28	-0.03
GREELY	MNT	32.800	3650.7	61.9	270.9	393.94	0.0	-0.23	-0.03
GREELY	SFA	34.720	3864.2	58.9	270.5	410.92	0.0	-0.23	-0.05
ARDVRK	BGME	35.798	3984.4	62.9	274.5	421.41	0.0	-0.25	-0.04
FLTLES	HNME	35.937	4000.0	62.0	275.6	438.87	0.0	-0.28	-0.05
FLTLES	HNME	35.937	4000.0	62.0	275.6	425.87	0.0	-0.28	-0.05
FLTLES	HNME	35.937	4000.0	62.0	275.6	423.27	0.0	-0.28	-0.05
FLTLES	HNME	35.937	4000.0	62.0	275.6	421.47	0.0	-0.28	-0.05
BILBY	HNME	36.562	4069.4	60.2	273.2	247.48	0.0	-0.17	-0.05
FLTLES	SIC	36.591	4072.3	55.2	271.1	426.16	0.0	-0.28	-0.06
HALFBK	HNME	36.628	4076.8	60.4	273.7	437.38	0.0	-0.37	-0.05
HALFBK	HNME	36.628	4076.8	60.4	273.7	427.88	0.0	-0.37	-0.05
HALFBK	HNME	36.628	4076.8	60.4	273.7	439.88	0.0	-0.37	-0.05
BOXCAR	HNME	36.747	4090.0	60.4	273.8	436.20	0.0	-0.25	-0.05
BOXCAR	HNME	36.747	4090.0	60.4	273.8	429.00	0.0	-0.25	-0.05
GREELY	SIC	37.488	4172.1	53.7	269.4	433.90	0.0	-0.23	-0.06
FLTLES	HAL	39.207	4364.0	63.8	280.2	450.01	0.0	-0.28	-0.01
GREELY	HAL	39.945	4446.1	62.3	278.4	456.15	0.0	-0.23	-0.01
FLTLES	STJ	46.026	5122.8	57.3	283.2	564.91	0.0	-0.28	-0.01
GREELY	STJ	46.883	5218.0	56.2	281.8	511.65	0.0	-0.23	-0.01

Table 4

NTS-E NEVADA TEST SITE EAST PROFILE

SOURCE	RCVR	DELTA DEG	DELTA KM	AZIMUTH S-->R DEG	AZIMUTH R-->S DEG	CORRECTED TIME SEC	ELIP CORR SEC	ELEV CORR SRCE SEC	ELEV CORR RCVR SEC
BILBY	KNUT	2.556	284.5	89.9	271.8	41.94	0.0	-0.17	-0.39
GREELY	KNUT	2.874	319.9	94.5	276.6	46.38	0.0	-0.23	-0.39
BILBY	GCA	3.545	394.7	90.1	272.7	56.33	0.0	-0.17	-0.30
BILBY	BXUT	5.275	587.2	82.6	266.6	79.35	0.0	-0.17	-0.38
CLRWTR	BXUT	5.424	603.7	84.1	268.2	81.58	0.0	-0.54	-0.38
BILBY	DRCO	6.583	732.8	84.0	269.0	97.43	0.0	-0.17	-0.50
CLRWTR	DRCO	6.736	749.8	85.2	270.3	99.56	0.0	-0.54	-0.50
BILBY	TDNM	7.907	880.2	90.0	275.9	116.18	0.0	-0.17	-0.66
BILBY	TDNM	7.907	880.2	90.0	275.9	121.48	0.0	-0.17	-0.66
CLRWTR	TDNM	8.074	898.8	90.8	276.8	118.51	0.0	-0.54	-0.66
BILBY	RTNM	9.349	1040.7	88.5	275.5	144.09	0.0	-0.17	-0.44
BILBY	RTNM	9.349	1040.7	88.5	275.5	136.09	0.0	-0.17	-0.44
CLRWTR	RTNM	9.512	1058.9	89.2	276.4	138.03	0.0	-0.54	-0.44
BILBY	AZTX	11.496	1279.6	93.9	282.2	172.61	0.0	-0.17	-0.22
BILBY	AZTX	11.496	1279.6	93.9	282.2	169.71	0.0	-0.17	-0.22
BILBY	SKTX	12.823	1427.3	94.2	283.4	194.28	0.0	-0.17	-0.15
BILBY	SKTX	12.823	1427.3	94.2	283.4	187.38	0.0	-0.17	-0.15
HAYMKR	HBCK	13.973	1555.3	92.5	282.6	203.34	0.0	-0.25	-0.11
HRDHAT	HBCK	14.001	1558.6	93.3	283.4	214.69	0.0	-0.40	-0.11
BILBY	WMO	14.326	1594.7	94.2	284.4	205.92	0.0	-0.17	-0.11
BILBY	WMO	14.326	1594.7	94.2	284.4	217.82	0.0	-0.17	-0.11
GREELY	WMO	14.653	1631.0	94.8	285.3	210.05	0.0	-0.23	-0.11
GREELY	WMO	14.653	1631.0	94.8	285.3	235.35	0.0	-0.23	-0.11
FLTLES	WMO	14.673	1633.2	100.0	290.6	217.11	0.0	-0.28	-0.11
FLTLES	WMO	14.673	1633.2	100.0	290.6	209.41	0.0	-0.28	-0.11
ARDVRK	TOOK	16.039	1785.3	93.9	285.3	227.99	0.0	-0.25	-0.06
BILBY	GVTX	16.137	1796.1	99.3	290.2	236.10	0.0	-0.17	-0.03
BILBY	GVTX	16.137	1796.1	99.3	290.2	232.80	0.0	-0.17	-0.03
BILBY	GVTX	16.137	1796.1	99.3	290.2	229.70	0.0	-0.17	-0.03
FORE	TUL	16.325	1817.2	88.2	280.3	232.39	0.0	-0.25	-0.06
FORE	DAL	16.348	1819.5	99.4	290.5	233.01	0.0	-0.25	-0.04
BILBY	DUOK	16.398	1825.2	94.7	286.2	236.59	0.0	-0.17	-0.04
BILBY	DUOK	16.398	1825.2	94.7	286.2	231.59	0.0	-0.17	-0.04
HAYMKR	AKOK	16.446	1830.6	93.3	285.1	233.20	0.0	-0.25	-0.04
FLTLES	GLTX	16.849	1875.1	103.6	295.1	239.98	0.0	-0.28	-0.04
FLTLES	GLTX	16.849	1875.1	103.6	295.1	237.28	0.0	-0.28	-0.04
MISISP	CTOK	17.175	1911.8	92.6	284.9	242.08	0.0	-0.25	-0.07
GREELY	KCMO	17.177	1912.0	76.5	270.0	245.01	0.0	-0.23	-0.06
GREELY	KCMO	17.177	1912.0	76.5	270.0	241.31	0.0	-0.23	-0.06
GREELY	KCMO	17.177	1912.0	76.5	270.0	255.71	0.0	-0.23	-0.06
AUK	FAY	17.550	1953.6	86.6	279.7	246.95	0.0	-0.26	-0.09
ARDVRK	MPAR	18.712	2082.9	90.7	284.2	261.07	0.0	-0.25	-0.08
HAYMKR	PVAR	19.019	2117.1	89.3	283.2	264.60	0.0	-0.25	-0.05
ARDVRK	CWAR	19.522	2173.1	88.4	282.7	271.11	0.0	-0.25	-0.03
BUFF	ENMO	20.308	2260.6	82.8	278.2	299.72	0.0	-0.23	-0.05
BUFF	ENMO	20.308	2260.6	82.8	278.2	279.12	0.0	-0.23	-0.05
BUFF	ENMO	20.308	2260.6	82.8	278.2	281.32	0.0	-0.23	-0.05
BILBY	LVLA	20.455	2276.8	96.7	290.5	290.43	0.0	-0.17	-0.00
BILBY	LVLA	20.455	2276.8	96.7	290.5	282.63	0.0	-0.17	-0.00
BILBY	LVLA	20.455	2276.8	96.7	290.5	280.53	0.0	-0.17	-0.00

NTS-E NEVADA TEST SITE EAST PROFILE

SOURCE	RCVR	DELTA DEG	DELTA KM	AZIMUTH S-->R DEG	AZIMUTH R-->S DEG	CORRECTED TIME SEC	ELIP CORR SEC	ELEV CORR SRCE SEC	ELEV CORR RCVR SEC
GREELY	JELA	20.809	2316.0	98.0	292.0	305.56	0.0	-0.23	-0.01
GREELY	JELA	20.809	2316.0	98.0	292.0	290.86	0.0	-0.23	-0.01
GREELY	JELA	20.809	2316.0	98.0	292.0	285.46	0.0	-0.23	-0.01
GREELY	CGM	21.356	2377.3	81.7	278.2	281.04	0.0	-0.23	-0.03
GREELY	OXF	22.020	2451.1	89.1	285.1	297.84	0.0	-0.23	-0.02
ARDVRK	JSTN	22.100	2460.1	85.3	281.8	300.91	0.0	-0.25	-0.03
HAYMKR	JSTN	22.106	2460.8	85.3	281.7	298.91	0.0	-0.25	-0.03
MISISP	CVTN	23.065	2567.5	84.7	281.9	308.41	0.0	-0.25	-0.04
BILBY	EUAL	23.437	2608.7	92.1	288.4	311.42	0.0	-0.17	-0.01
BILBY	EUAL	23.437	2608.7	92.1	288.4	317.82	0.0	-0.17	-0.01
GREELY	EU2AL	23.737	2642.1	92.3	288.9	348.36	0.0	-0.23	-0.01
GREELY	EU2AL	23.737	2642.1	92.3	288.9	342.16	0.0	-0.23	-0.01
GREELY	EU2AL	23.737	2642.1	92.3	288.9	333.86	0.0	-0.23	-0.01
GREELY	EU2AL	23.737	2642.1	92.3	288.9	314.56	0.0	-0.23	-0.01
ARDVRK	MMTN	24.528	2730.4	84.3	282.5	321.26	0.0	-0.25	-0.09
BILBY	CPO	24.530	2730.6	84.2	282.5	321.30	0.0	-0.17	-0.13
BILBY	CPO	24.530	2730.6	84.2	282.5	327.50	0.0	-0.17	-0.13
BILBY	CPO	24.530	2730.6	84.2	282.5	322.70	0.0	-0.17	-0.13
HRDHAT	MMTN	24.535	2731.2	84.6	282.9	338.52	0.0	-0.40	-0.09
HALFBK	CPO	24.726	2752.4	84.6	283.1	337.70	0.0	-0.37	-0.13
HALFBK	CPO	24.726	2752.4	84.6	283.1	326.20	0.0	-0.37	-0.13
HALFBK	CPO	24.726	2752.4	84.6	283.1	323.10	0.0	-0.37	-0.13
DUMONT	AX2AL	24.858	2767.0	91.0	288.4	329.16	0.0	-0.19	-0.05
DUMONT	AX2AL	24.858	2767.0	91.0	288.4	326.56	0.0	-0.19	-0.05
DUMONT	AX2AL	24.858	2767.0	91.0	288.4	324.86	0.0	-0.19	-0.05
FLTLES	AX2AL	25.053	2788.5	94.2	292.0	339.37	0.0	-0.28	-0.05
FLTLES	AX2AL	25.053	2788.5	94.2	292.0	326.47	0.0	-0.28	-0.05
STONES	WTTN	25.056	2789.1	82.6	281.5	326.92	0.0	-0.28	-0.10
GREELY	AX2AL	25.142	2798.5	91.2	288.9	337.82	0.0	-0.23	-0.05
GREELY	AX2AL	25.142	2798.5	91.2	288.9	327.72	0.0	-0.23	-0.05
GREELY	AX2AL	25.142	2798.5	91.2	288.9	329.92	0.0	-0.23	-0.05
CUP	ATL	26.078	2902.9	88.6	287.2	335.50	0.0	-0.24	-0.06
GREELY	ATL	26.367	2934.9	88.7	287.6	338.31	0.0	-0.23	-0.06
MISISP	GDVA	27.035	3009.4	79.0	280.0	344.17	0.0	-0.25	-0.08
CUP	BLWV	27.482	3059.2	77.9	279.4	371.93	0.0	-0.24	-0.14
CUP	BLWV	27.482	3059.2	77.9	279.4	353.33	0.0	-0.24	-0.14
CUP	BLWV	27.482	3059.2	77.9	279.4	348.23	0.0	-0.24	-0.14
BILBY	BLWV	27.484	3059.4	77.8	279.3	348.09	0.0	-0.17	-0.14
GREELY	BLA	28.539	3176.8	79.1	281.3	358.12	0.0	-0.23	-0.14
FLTLES	AENC	28.919	3219.0	85.0	287.2	384.38	0.0	-0.28	-0.04
FLTLES	AENC	28.919	3219.0	85.0	287.2	406.38	0.0	-0.28	-0.04
FLTLES	AENC	28.919	3219.0	85.0	287.2	359.38	0.0	-0.28	-0.04
GREELY	AENC	29.214	3252.0	82.5	284.5	379.03	0.0	-0.23	-0.04
GREELY	AENC	29.214	3252.0	82.5	284.5	362.93	0.0	-0.23	-0.04
DUMONT	BEFL	29.538	3287.5	96.0	294.9	367.50	0.0	-0.19	-0.00
HALFBK	BEFL	29.751	3311.2	96.2	295.3	415.32	0.0	-0.37	-0.00
HALFBK	BEFL	29.751	3311.2	96.2	295.3	391.12	0.0	-0.37	-0.00
HALFBK	BEFL	29.751	3311.2	96.2	295.3	369.22	0.0	-0.37	-0.00
GREELY	BEFL	29.836	3320.6	96.1	295.3	423.26	0.0	-0.23	-0.00
GREELY	BEFL	29.836	3320.6	96.1	295.3	402.16	0.0	-0.23	-0.00
GREELY	BEFL	29.836	3320.6	96.1	295.3	386.06	0.0	-0.23	-0.00
GREELY	BEFL	29.836	3320.6	96.1	295.3	375.96	0.0	-0.23	-0.00
FLTLES	BEFL	29.856	3322.6	98.5	298.0	430.22	0.0	-0.28	-0.00
FLTLES	BEFL	29.856	3322.6	98.5	298.0	382.22	0.0	-0.28	-0.00
FLTLES	BEFL	29.856	3322.6	98.5	298.0	369.62	0.0	-0.28	-0.00
BILBY	ORFL	30.359	3378.9	96.1	295.4	374.83	0.0	-0.17	-0.00

Table 5

NTS-SE NEVADA TEST SITE SOUTHEAST PROFILE

SOURCE	RCVR	DELTA DEG	DELTA KM	AZIMUTH S-->R DEG	AZIMUTH R-->S DEG	CORRECTED TIME SEC	ELIP CORR SEC	ELEV CORR SRCE SEC	ELEV CORR RCVR SEC
FORE	BCN	1.511	167.9	139.6	320.3	27.68	0.0	-0.25	-0.17
BOXCAR	KGAZ	2.635	293.0	128.0	309.5	43.71	0.0	-0.25	-0.24
BOXCAR	KGAZ	2.635	293.0	128.0	309.5	44.61	0.0	-0.25	-0.24
CUP	SGAZ	2.702	300.5	122.9	304.6	44.09	0.0	-0.24	-0.38
CUP	JRAZ	4.021	447.3	123.9	306.3	68.87	0.0	-0.24	-0.29
CUP	JRAZ	4.021	447.3	123.9	306.3	62.97	0.0	-0.24	-0.29
CUP	LGAZ	4.565	507.8	125.4	308.0	78.97	0.0	-0.24	-0.40
CUP	LGAZ	4.565	507.8	125.4	308.0	74.27	0.0	-0.24	-0.40
CUP	LGAZ	4.565	507.8	125.4	308.0	70.57	0.0	-0.24	-0.40
BILBY	TFC	4.767	530.3	124.3	307.1	73.60	0.0	-0.17	-0.33
HALFBK	TFC	5.094	566.6	125.1	308.0	78.39	0.0	-0.37	-0.33
HALFBK	TFC	5.094	566.6	125.1	308.0	83.39	0.0	-0.37	-0.33
HALFBK	TFC	5.094	566.6	125.1	308.0	85.69	0.0	-0.37	-0.33
HALFBK	TFC	5.094	566.6	125.1	308.0	81.19	0.0	-0.37	-0.33
BOXCAR	TFO	5.186	576.8	124.0	307.1	79.71	0.0	-0.25	-0.33
BOXCAR	TFO	5.186	576.8	124.0	307.1	80.21	0.0	-0.25	-0.33
BOXCAR	TFO	5.186	576.8	124.0	307.1	86.51	0.0	-0.25	-0.33
CUP	GEAZ	5.619	625.0	125.1	308.3	90.63	0.0	-0.24	-0.33
CUP	GEAZ	5.619	625.0	125.1	308.3	94.23	0.0	-0.24	-0.33
CUP	GEAZ	5.619	625.0	125.1	308.3	85.33	0.0	-0.24	-0.33
FLTLES	TFC	5.905	656.5	136.0	318.9	89.49	0.0	-0.28	-0.33
DORMSE	SVAZ	6.303	701.3	114.9	299.0	95.85	0.0	-0.27	-0.48
HRDHAT	SVAZ	6.397	711.8	116.4	300.4	98.02	0.0	-0.40	-0.48
CUP	TUC	6.484	720.8	136.5	319.5	96.64	0.0	-0.24	-0.22
HALFBK	TUC	6.746	750.0	136.1	319.2	100.51	0.0	-0.37	-0.22
ARMDLC	MLNM	6.916	769.4	119.4	303.5	106.82	0.0	-0.31	-0.37
DORMSE	MLNM	6.918	769.7	119.4	303.6	105.46	0.0	-0.27	-0.37
HRDHAT	MLNM	7.025	781.5	120.6	304.8	114.13	0.0	-0.40	-0.37
HRDHAT	MLNM	7.025	781.5	120.6	304.8	105.03	0.0	-0.40	-0.37
FLTLES	TUC	7.709	856.9	143.2	326.4	114.31	0.0	-0.28	-0.22
DORMS'	TCNM	8.002	890.3	116.2	301.1	124.06	0.0	-0.30	-0.34
DORMSE	TCNM	8.014	891.7	116.2	301.1	122.29	0.0	-0.27	-0.34
CCMODR	TCNM	8.069	897.7	116.6	301.6	123.69	0.0	-0.17	-0.34
HRDHAT	TCNM	8.112	902.5	117.3	302.2	122.66	0.0	-0.40	-0.34
HRDHAT	TCNM	8.112	902.5	117.3	302.2	119.66	0.0	-0.40	-0.34
DORMS'	LCNM	9.032	1004.9	118.0	303.4	139.54	0.0	-0.30	-0.35
BILBY	LCNM	9.039	1005.6	118.1	303.5	133.98	0.0	-0.17	-0.35
DORMSE	LCNM	9.045	1006.2	118.0	303.4	135.27	0.0	-0.27	-0.35
CUP	LCNM	9.095	1011.8	118.5	303.9	135.81	0.0	-0.24	-0.35
HRDHAT	LCNM	9.147	1017.6	118.9	304.3	136.65	0.0	-0.40	-0.35
BOXCAR	LCNM	9.455	1051.9	118.1	303.7	141.29	0.0	-0.25	-0.35
BOXCAR	LCNM	9.455	1051.9	118.1	303.7	140.19	0.0	-0.25	-0.35
BOXCAR	LCNM	9.455	1051.9	118.1	303.7	151.59	0.0	-0.25	-0.35
CUP	EPT	9.524	1059.4	121.4	306.8	146.30	0.0	-0.24	-0.27
DORMSE	EPTX	9.751	1084.8	118.5	304.2	146.97	0.0	-0.27	-0.36
HRDHAT	EPTX	9.855	1096.3	119.4	305.1	147.04	0.0	-0.40	-0.36
FLTLES	LCNM	10.000	1112.2	125.5	311.1	149.67	0.0	-0.28	-0.35
FLTLES	LCNM	10.000	1112.2	125.5	311.1	162.27	0.0	-0.28	-0.35
DORMS'	EFTX	10.757	1196.6	119.7	305.8	161.28	0.0	-0.30	-0.32
DORMSE	EFTX	10.769	1198.0	119.7	305.8	161.21	0.0	-0.27	-0.32
HRDHAT	EFTX	10.876	1209.8	120.5	306.6	161.68	0.0	-0.40	-0.32
HRDHAT	EFTX	10.876	1209.8	120.5	306.6	159.48	0.0	-0.40	-0.32
HRDHAT	GNNM	11.192	1245.4	112.6	299.6	166.47	0.0	-0.40	-0.23
HRDHAT	GNNM	11.192	1245.4	112.6	299.6	163.77	0.0	-0.40	-0.23
DORMSE	BMTX	11.808	1313.6	117.5	304.3	175.99	0.0	-0.27	-0.24
HRDHAT	BMTX	11.908	1324.8	118.2	305.1	175.76	0.0	-0.40	-0.24
CUP	FOTX	12.696	1412.6	115.4	302.9	187.07	0.0	-0.24	-0.20
CUP	FOTX	12.696	1412.6	115.4	302.9	196.27	0.0	-0.24	-0.20
CCMODR	SA4TX	13.182	1466.9	109.3	297.6	211.05	0.0	-0.17	-0.18
CCMODR	SA4TX	13.182	1466.9	109.3	297.6	202.25	0.0	-0.17	-0.18
CCMODR	SA4TX	13.182	1466.9	109.3	297.6	197.15	0.0	-0.17	-0.18
CCMODR	SA4TX	13.182	1466.9	109.3	297.6	191.15	0.0	-0.17	-0.18
STONES	SSTX	13.376	1488.0	117.5	305.1	195.56	0.0	-0.28	-0.16
HRDHAT	SSTX	13.505	1502.4	118.1	305.7	199.34	0.0	-0.40	-0.16
HRDHAT	SSTX	13.505	1502.4	118.1	305.7	196.84	0.0	-0.40	-0.16
CCMODR	ST2TX	15.160	1686.9	109.7	299.0	119.80	0.0	-0.17	-0.13
CCMODR	ST2TX	15.160	1686.9	109.7	299.0	217.80	0.0	-0.17	-0.13
CCMODR	ST2TX	15.160	1686.9	109.7	299.0	216.20	0.0	-0.17	-0.13
CCMODR	GR2TX	15.188	1690.0	109.7	299.0	233.91	0.0	-0.17	-0.12
CCMODR	GR2TX	15.188	1690.0	109.7	299.0	229.41	0.0	-0.17	-0.12
CCMODR	GR2TX	15.188	1690.0	109.7	299.0	222.01	0.0	-0.17	-0.12
CCMODR	GR2TX	15.188	1690.0	109.7	299.0	218.31	0.0	-0.17	-0.12
CCMODR	GR2TX	15.188	1690.0	109.7	299.0	216.71	0.0	-0.17	-0.12
CCMODR	GR1TX	15.215	1693.0	109.7	299.0	219.01	0.0	-0.17	-0.12
CCMODR	GR1TX	15.215	1693.0	109.7	299.0	217.11	0.0	-0.17	-0.12
CCMODR	ST1TX	15.249	1696.8	109.7	299.1	222.11	0.0	-0.17	-0.12
CCMODR	ST1TX	15.249	1696.8	109.7	299.1	217.31	0.0	-0.17	-0.12
GREELY	JCT	15.368	1710.0	111.4	300.7	221.83	0.0	-0.23	-0.13
ARDVRK	LPTX	15.784	1756.0	115.1	304.1	225.89	0.0	-0.25	-0.06
HRDHAT	LPTX	15.876	1766.3	115.6	304.6	226.54	0.0	-0.40	-0.06
ARDVRK	SJTX	17.668	1965.5	117.1	306.6	251.82	0.0	-0.25	-0.03
HRDHAT	SJTX	17.765	1976.2	117.5	307.1	252.28	0.0	-0.40	-0.03
FLTLES	SJTX	18.558	2064.2	120.9	310.8	274.60	0.0	-0.28	-0.03
FLTLES	SJTX	18.558	2064.2	120.9	310.8	267.10	0.0	-0.28	-0.03
FLTLES	SJTX	18.558	2064.2	120.9	310.8	261.60	0.0	-0.28	-0.03

Table 6

Temporary Station Locations

Gasbuggy West Profile

Site No.	Latitude	Longitude	Elev. (km)
T1	36° 43.1' N	113° 04.2' W	1.500
T2	36° 43.2'	113° 20.1'	1.347
T3	36° 41.5'	113° 36.3'	1.539
T5	36° 37.5'	114° 14.2'	0.725
1	36° 37.63'	114° 51.67'	0.975
2	36° 37' 48"	115° 18' 17"	1.579
3	36° 35.26'	115° 47.86'	1.067
4	36° 35.65'	116° 4.35'	1.024
5	36° 38.65'	116° 20.82'	0.927
6	36° 34.37'	116° 39.75'	1.006
7	36° 35.31'	117° 6.60'	1.676
8	36° 32.44'	117° 31.86'	2.012

Table 7.

GASBUGGY WEST PROFILE

SOURCE	RCVR	DELTA DEG	DELTA KM	AZIMUTH S-->R DEG	AZIMUTH R-->S DEG	CORRECTED TIME SEC	ELIP CORR SEC	ELEV CORR SRCE SEC	ELEV CORR RCVR SEC
GASBGY	USGS 1	0.768	85.4	277.5	96.9	14.74	0.0	-0.19	-0.36
GASBGY	USGS 2	1.256	139.8	276.6	95.7	23.25	0.0	-0.19	-0.33
GASBGY	USGS 3	1.521	169.3	279.5	98.3	27.83	0.0	-0.19	-0.35
GASBGY	USGS 3	1.521	169.3	279.5	98.3	29.52	0.0	-0.19	-0.35
GASBGY	USGS 4	1.932	215.0	277.9	96.5	35.28	0.0	-0.19	-0.33
GASBGY	USGS 5	2.749	306.0	269.5	87.4	50.17	0.0	-0.19	-0.44
GASBGY	USGS 5	2.749	306.0	269.5	87.4	46.47	0.0	-0.19	-0.44
GASBGY	USGS 6	3.153	351.0	268.8	86.5	57.31	0.0	-0.19	-0.40
GASBGY	USGS 6	3.153	351.0	268.8	86.5	52.71	0.0	-0.19	-0.40
GASBGY	GCA	3.530	393.0	276.1	93.5	57.92	0.0	-0.19	-0.29
GASBGY	USGS 7	4.516	502.7	276.0	92.6	77.50	0.0	-0.19	-0.37
GASBGY	USGS 7	4.516	502.7	276.0	92.6	71.44	0.0	-0.19	-0.37
GASBGY	USGS 7	4.516	502.7	276.0	92.6	80.20	0.0	-0.19	-0.37
GASBGY	USGS 7	4.516	502.7	276.0	92.6	70.94	0.0	-0.19	-0.37
GASBGY	KNUT	4.520	503.1	276.0	92.7	86.43	0.0	-0.19	-0.38
GASBGY	KNUT	4.520	503.1	276.0	92.7	71.23	0.0	-0.19	-0.38
GASBGY	KNUT	4.520	503.1	276.0	92.7	80.73	0.0	-0.19	-0.38
GASBGY	T1	4.711	524.4	272.2	88.7	73.99	0.0	-0.19	-0.32
GASBGY	T2	4.923	548.1	272.3	88.7	76.92	0.0	-0.19	-0.29
GASBGY	T5	5.651	629.1	271.6	87.4	86.55	0.0	-0.19	-0.16
GASBGY	CQNV	5.918	658.8	284.1	99.7	97.62	0.0	-0.19	-0.39
GASBGY	CQNV	5.918	658.8	284.1	99.7	88.42	0.0	-0.19	-0.39
GASBGY	CQNV	5.918	658.8	284.1	99.7	90.82	0.0	-0.19	-0.39
GASBGY	CQNV	5.918	658.8	284.1	99.7	112.02	0.0	-0.19	-0.39
GASBGY	1	6.153	684.9	271.8	87.2	94.40	0.0	-0.19	-0.21
GASBGY	1	6.153	684.9	271.8	87.2	92.90	0.0	-0.19	-0.21
GASBGY	1	6.153	684.9	271.8	87.2	111.60	0.0	-0.19	-0.21
GASBGY	1	6.153	684.9	271.8	87.2	102.20	0.0	-0.19	-0.21
GASBGY	BCN	6.195	689.6	265.8	81.3	106.64	0.0	-0.19	-0.17
GASBGY	BCN	6.195	689.6	265.8	81.3	94.04	0.0	-0.19	-0.17
GASBGY	BCN	6.195	689.6	265.8	81.3	114.44	0.0	-0.19	-0.17
GASBGY	LVN	6.423	715.0	267.3	82.6	107.58	0.0	-0.19	-0.13
GASBGY	2	6.509	724.6	272.0	87.2	107.37	0.0	-0.19	-0.34
GASBGY	2	6.509	724.6	272.0	87.2	98.97	0.0	-0.19	-0.34
GASBGY	2	6.509	724.6	272.0	87.2	98.27	0.0	-0.19	-0.34
GASBGY	3	6.908	768.9	271.8	86.7	123.38	0.0	-0.19	-0.23
GASBGY	3	6.908	768.9	271.8	86.7	113.48	0.0	-0.19	-0.23
GASBGY	3	6.908	768.9	271.8	86.7	104.68	0.0	-0.19	-0.23
GASBGY	3	6.908	768.9	271.8	86.7	103.78	0.0	-0.19	-0.23
GASBGY	4	7.128	793.5	272.0	86.7	116.99	0.0	-0.19	-0.22
GASBGY	4	7.128	793.5	272.0	86.7	107.79	0.0	-0.19	-0.22
GASBGY	4	7.128	793.5	272.0	86.7	106.09	0.0	-0.19	-0.22
GASBGY	GLA	7.231	804.4	242.3	57.9	108.27	0.0	-0.19	-0.14
GASBGY	GLA	7.231	804.4	242.3	57.9	117.77	0.0	-0.19	-0.14
GASBGY	5	7.346	817.7	272.5	87.0	130.71	0.0	-0.19	-0.20
GASBGY	5	7.346	817.7	272.5	87.0	114.21	0.0	-0.19	-0.20
GASBGY	5	7.346	817.7	272.5	87.0	111.41	0.0	-0.19	-0.20
GASBGY	5	7.346	817.7	272.5	87.0	120.51	0.0	-0.19	-0.20
GASBGY	5	7.346	817.7	272.5	87.0	109.51	0.0	-0.19	-0.20
GASBGY	5	7.346	817.7	272.5	87.0	115.41	0.0	-0.19	-0.20

GASBUGGY WEST PROFILE

SOURCE	RCVR	DELTA DEG	DELTA KM	AZIMUTH S-->R DEG	AZIMUTH R-->S DEG	CORRECTED TIME SEC	ELIP CORR SEC	ELEV CORR SRCE SEC	ELEV CORR RCVR SEC
GASBGY	WZNV	7.480	832.6	283.4	97.8	137.76	0.0	-0.19	-0.45
GASBGY	WZNV	7.480	832.6	283.4	97.8	111.36	0.0	-0.19	-0.45
GASBGY	6	7.603	846.4	272.0	86.4	134.49	0.0	-0.19	-0.22
GASBGY	6	7.603	846.4	272.0	86.4	124.59	0.0	-0.19	-0.22
GASBGY	6	7.603	846.4	272.0	86.4	119.49	0.0	-0.19	-0.22
GASBGY	6	7.603	846.4	272.0	86.4	118.59	0.0	-0.19	-0.22
GASBGY	GSC	7.900	879.3	262.9	77.2	126.30	0.0	-0.19	-0.21
GASBGY	GSC	7.900	879.3	262.9	77.2	120.10	0.0	-0.19	-0.21
GASBGY	GSC	7.900	879.3	262.9	77.2	117.30	0.0	-0.19	-0.21
GASBGY	7	7.962	886.3	272.3	86.4	130.57	0.0	-0.19	-0.04
GASBGY	7	7.962	886.3	272.3	86.4	124.57	0.0	-0.19	-0.04
GASBGY	7	7.962	886.3	272.3	86.4	122.97	0.0	-0.19	-0.04
GASBGY	7	7.962	886.3	272.3	86.4	121.97	0.0	-0.19	-0.04
GASBGY	7	7.962	886.3	272.3	86.4	119.57	0.0	-0.19	-0.04
GASBGY	7	7.962	886.3	272.3	86.4	118.97	0.0	-0.19	-0.04
GASBGY	8	8.303	924.3	272.1	86.0	143.07	0.0	-0.19	-0.44
GASBGY	8	8.303	924.3	272.1	86.0	128.47	0.0	-0.19	-0.44
GASBGY	8	8.303	924.3	272.1	86.0	125.37	0.0	-0.19	-0.44
GASBGY	8	8.303	924.3	272.1	86.0	123.87	0.0	-0.19	-0.44
GASBGY	CLC	8.437	939.2	267.3	81.1	146.54	0.0	-0.19	-0.17
GASBGY	CLC	8.437	939.2	267.3	81.1	130.44	0.0	-0.19	-0.17
GASBGY	CLC	8.437	939.2	267.3	81.1	124.74	0.0	-0.19	-0.17
GASBGY	PLM	8.584	955.3	250.2	64.6	147.84	0.0	-0.19	-0.37
GASBGY	PLM	8.584	955.3	250.2	64.6	126.84	0.0	-0.19	-0.37
GASBGY	PLM	8.584	955.3	250.2	64.6	157.94	0.0	-0.19	-0.37
GASBGY	RVR	8.728	971.4	255.2	69.3	144.05	0.0	-0.19	-0.06
GASBGY	RVR	8.728	971.4	255.2	69.3	129.65	0.0	-0.19	-0.06
GASBGY	CWC	8.751	974.1	271.7	85.2	130.16	0.0	-0.19	-0.35
GASBGY	CWC	8.751	974.1	271.7	85.2	147.76	0.0	-0.19	-0.35
GASBGY	CWC	8.751	974.1	271.7	85.2	140.16	0.0	-0.19	-0.35
GASBGY	CWC	8.751	974.1	271.7	85.2	132.96	0.0	-0.19	-0.35
GASBGY	CWC	8.751	974.1	271.7	85.2	131.76	0.0	-0.19	-0.35
GASBGY	BAR	8.754	974.0	245.7	60.3	140.70	0.0	-0.19	-0.11
GASBGY	BAR	8.754	974.0	245.7	60.3	129.00	0.0	-0.19	-0.11
GASBGY	MNNV	8.864	986.6	284.7	98.0	160.68	0.0	-0.19	-0.33
GASBGY	MNNV	8.864	986.6	284.7	98.0	131.38	0.0	-0.19	-0.33
GASBGY	MNNV	8.864	986.6	284.7	98.0	129.28	0.0	-0.19	-0.33
GASBGY	ISA	9.172	1021.0	266.9	80.3	140.84	0.0	-0.19	-0.16
GASBGY	ISA	9.172	1021.0	266.9	80.3	137.84	0.0	-0.19	-0.16
GASBGY	ISA	9.172	1021.0	266.9	80.3	135.04	0.0	-0.19	-0.16
GASBGY	MWC	9.185	1022.3	257.8	71.5	172.43	0.0	-0.19	-0.37
GASBGY	MWC	9.185	1022.3	257.8	71.5	135.53	0.0	-0.19	-0.37
GASBGY	PAS	9.298	1034.9	257.5	71.2	172.05	0.0	-0.19	-0.06
GASBGY	PAS	9.298	1034.9	257.5	71.2	138.05	0.0	-0.19	-0.06
GASBGY	WDY	9.460	1053.0	267.6	80.7	141.60	0.0	-0.19	-0.11
GASBGY	WDY	9.460	1053.0	267.6	80.7	139.40	0.0	-0.19	-0.11
GASBGY	FTC	9.665	1075.8	262.7	75.9	142.80	0.0	-0.19	-0.21
GASBGY	JAS	10.615	1181.6	280.8	92.8	155.81	0.0	-0.19	-0.10
GASBGY	JAS	10.615	1181.6	280.8	92.8	158.11	0.0	-0.19	-0.10
GASBGY	JAS	10.615	1181.6	280.8	92.8	156.91	0.0	-0.19	-0.10
GASBGY	JAS	10.615	1181.6	280.8	92.8	156.11	0.0	-0.19	-0.10
GASBGY	SYP	10.617	1181.8	262.1	74.7	156.73	0.0	-0.19	-0.28
GASBGY	PRI	10.860	1208.9	271.2	83.2	162.75	0.0	-0.19	-0.26
GASBGY	PRI	10.860	1208.9	271.2	83.2	165.15	0.0	-0.19	-0.26
GASBGY	PRI	10.860	1208.9	271.2	83.2	162.45	0.0	-0.19	-0.26
GASBGY	SLD	11.233	1250.4	276.2	87.8	167.01	0.0	-0.19	-0.10
GASBGY	MHC	11.561	1287.0	277.6	88.9	168.63	0.0	-0.19	-0.28

Table 8

MODEL YLKNF 10

I	DEPTH(I)	RAD(I)	VEL(I)
1	600.00	5771.00	9.600
2	420.00	5951.00	9.500
3	375.00	5996.00	8.500
4	220.00	6151.00	8.604
5	155.00	6216.00	8.470
6	150.00	6221.00	8.400
7	145.00	6226.00	8.350
8	132.00	6239.00	8.330
9	120.00	6251.00	8.350
10	108.00	6263.00	8.464
11	86.00	6285.00	8.420
12	85.00	6286.00	8.110
13	46.00	6325.00	8.[illegible]63
14	42.00	6329.00	7.200
15	21.00	6350.00	7.200
16	17.00	6354.00	6.7[illegible]0
17	9.00	6362.00	6.700
18	6.00	6365.00	5.000
19	0.50	6370.50	5.000
20	0.00	6371.00	1.400

Table 9

MODEL HUDSBY 10

I	DEPTH(I)	RAD(I)	VEL(I)
1	600.00	5771.00	9.600
2	510.00	5861.00	9.550
3	440.00	5931.00	9.440
4	410.00	5961.00	9.400
5	400.00	5971.00	8.850
6	370.00	6001.00	8.580
7	300.00	6071.00	8.580
8	125.00	6246.00	8.440
9	124.00	6247.00	8.365
10	90.00	6281.00	8.365
11	80.00	6291.00	8.385
12	61.00	6310.00	8.380
13	60.00	6311.00	8.230
14	38.00	6333.00	8.230
15	34.00	6337.00	6.300
16	0.0	6371.00	6.300

Table 10

MODEL ER 2 GREEN & HALES (1968)

I	DEPTH(I)	RAD(I)	VEL(I)
1	260.00	6111.00	8.400
2	161.00	6210.00	8.380
3	157.00	6214.00	8.250
4	136.00	6235.00	8.250
5	132.00	6239.00	8.380
6	91.00	6280.00	8.330
7	87.00	6284.00	8.070
8	52.00	6319.00	8.020
9	48.00	6323.00	7.150
10	22.00	6349.00	6.850
11	18.00	6353.00	6.350
12	0.0	6371.00	6.300

Table 11

MODEL NC 1

I	DEPTH(I)	RAD(I)	VEL(I)
1	375.00	5996.00	8.500
2	160.00	6211.00	8.400
3	132.00	6239.00	8.400
4	130.00	6241.00	8.270
5	100.00	6271.00	8.270
6	95.00	6276.00	8.360
7	65.00	6306.00	8.250
8	60.00	6311.00	8.030
9	44.00	6327.00	8.000
10	42.00	6329.00	7.150
11	22.00	6349.00	6.850
12	18.00	6353.00	6.350
13	0.0	6371.00	6.300

Table 12

NEVADA TEST SITE NORTH PROFILE

MODEL NTS N1

BASIN AND RANGE MODEL

I	DEPTH(I)	RAD(I)	VEL(I)
1	800.00	5571.00	11.087
2	650.00	5721.00	11.033
3	600.00	5771.00	9.411
4	552.50	5818.50	9.522
5	505.00	5866.00	9.522
6	465.00	5906.00	9.510
7	420.00	5951.00	9.517
8	392.50	5978.50	9.033
9	360.00	6011.00	8.559
10	300.00	6071.00	8.498
11	250.00	6121.00	8.390
12	200.00	6171.00	8.280
13	155.00	6216.00	8.200
14	108.00	6263.00	8.050
15	104.00	6267.00	7.500
16	70.00	6301.00	7.500
17	60.00	6311.00	7.900
18	34.00	6337.00	7.900
19	31.00	6340.00	6.700
20	19.00	6352.00	6.700
21	15.00	6356.00	6.000
22	0.0	6371.00	6.000

BOUNDARY AT THETA = 4.40 DEG.

SNAKE RIVER PLAIN - COLUMBIA PLATEAU MODEL

I	DEPTH(I)	RAD(I)	VEL(I)
1	800.00	5571.00	11.087
2	650.00	5721.00	11.033
3	600.00	5771.00	9.411
4	552.50	5818.50	9.522
5	505.00	5866.00	9.522
6	465.00	5906.00	9.510
7	420.00	5951.00	9.517
8	392.50	5978.50	9.033
9	360.00	6011.00	8.559
10	300.00	6071.00	8.498
11	250.00	6121.00	8.390
12	200.00	6171.00	8.280
13	155.00	6216.00	8.200
14	108.00	6263.00	8.050
15	104.00	6267.00	7.500
16	70.00	6301.00	7.500
17	60.00	6311.00	7.900
18	50.00	6321.00	7.900
19	45.00	6326.00	6.700
20	10.00	6361.00	6.700
21	6.00	6365.00	5.200
22	0.0	6371.00	5.200

BOUNDARY AT THETA = 9.00 DEG.

BRITISH COLUMBIA MODEL

I	DEPTH(I)	RAD(I)	VEL(I)
1	800.00	5571.00	11.087
2	650.00	5721.00	11.033
3	600.00	5771.00	9.411
4	552.50	5818.50	9.522
5	505.00	5866.00	9.522
6	465.00	5906.00	9.510
7	420.00	5951.00	9.517
8	392.50	5978.50	9.033
9	360.00	6011.00	8.559
10	300.00	6071.00	8.498
11	250.00	6121.00	8.390
12	200.00	6171.00	8.280
13	155.00	6216.00	8.200
14	118.00	6253.00	8.050
15	114.00	6257.00	7.500
16	70.00	6301.00	7.500
17	60.00	6311.00	7.900
18	32.00	6339.00	7.900
19	28.00	6343.00	6.800
20	22.00	6349.00	6.800
21	18.00	6353.00	5.900
22	0.0	6371.00	5.900

END OF MODEL AT THETA = 50.00 DEG

MODEL NTS N3

I	DEPTH(I)	RAD(I)	VEL(I)
1	800.00	5571.00	11.087
2	647.00	5724.00	11.033
3	597.00	5774.00	9.411
4	552.50	5818.50	9.522
5	505.00	5866.00	9.522
6	465.00	5906.00	9.510
7	417.50	5953.50	9.517
8	390.00	5981.00	9.033
9	357.50	6013.50	8.559
10	300.00	6071.00	8.450
11	250.00	6121.00	8.360
12	200.00	6171.00	8.270
13	160.00	6211.00	8.200
14	140.00	6231.00	7.800
15	100.00	6271.00	7.800
16	60.00	6311.00	7.900
17	34.00	6337.00	7.900
18	31.00	6340.00	6.700
19	19.00	6352.00	6.700
20	15.00	6356.00	6.000
21	0.0	6371.00	6.000

I	DEPTH(I)	RAD(I)	VEL(I)
1	800.00	5571.00	11.087
2	647.00	5724.00	11.033
3	597.00	5774.00	9.411
4	552.50	5818.50	9.522
5	505.00	5866.00	9.522
6	465.00	5906.00	9.510
7	417.50	5953.50	9.517
8	390.00	5981.00	9.033
9	357.50	6013.50	8.559
10	300.00	6071.00	8.450
11	250.00	6121.00	8.360
12	200.00	6171.00	8.270
13	160.00	6211.00	8.200
14	140.00	6231.00	7.800
15	100.00	6271.00	7.800
16	60.00	6311.00	7.900
17	50.00	6321.00	7.900
18	45.00	6326.00	6.700
19	10.00	6361.00	6.700
20	6.00	6365.00	5.200
21	0.0	6371.00	5.200

BOUNDARY AT THETA = 8.00 DEG.

BRITISH COLUMBIA MODEL

I	DEPTH(I)	RAD(I)	VEL(I)
1	800.00	5571.00	11.087
2	647.00	5724.00	11.033
3	597.00	5774.00	9.411
4	552.50	5818.50	9.522
5	505.00	5866.00	9.522
6	465.00	5906.00	9.510
7	417.50	5953.50	9.517
8	390.00	5981.00	9.033
9	357.50	6013.50	8.559
10	300.00	6071.00	8.450
11	250.00	6121.00	8.360
12	200.00	6171.00	8.270
13	160.00	6211.00	8.200
14	140.00	6231.00	7.800
15	100.00	6271.00	7.800
16	60.00	6311.00	7.900
17	32.00	6339.00	7.900
18	28.00	6343.00	6.800
19	22.00	6349.00	6.800
20	18.00	6353.00	5.900
21	0.0	6371.00	5.900

Table 13

YUKON 4 EARLY RISE YUKON PROFILE

NMODEL = 7

CANADIAN SHIELD MODEL

I	DEPTH(I)	RAD(I)	VEL(I)
1	710.00	5661.00	11.033
2	665.00	5706.00	9.930
3	555.00	5816.00	9.805
4	505.00	5866.00	9.740
5	470.00	5901.00	9.690
6	445.00	5926.00	9.650
7	390.00	5981.00	8.600
8	170.00	6201.00	8.530
9	160.00	6211.00	8.410
10	150.00	6221.00	8.380
11	110.00	6261.00	8.380
12	96.00	6275.00	8.430
13	87.00	6284.00	8.430
14	85.00	6286.00	8.160
15	46.00	6325.00	8.129
16	42.00	6329.00	7.200
17	21.00	6350.00	7.200
18	17.00	6354.00	6.700
19	9.00	6362.00	6.700
20	6.00	6365.00	5.000
21	0.40	6370.60	5.000
22	0.0	6371.00	1.400

BOUNDARY AT THETA = 2.50 DEG.

TRANSITION MODEL 1

I	DEPTH(I)	RAD(I)	VEL(I)
1	710.00	5661.00	11.033
2	665.00	5706.00	9.930
3	555.00	5816.00	9.805
4	505.00	5866.00	9.740
5	470.00	5901.00	9.690
6	445.00	5926.00	9.650
7	390.00	5981.00	8.600
8	160.00	6211.00	8.550
9	158.00	6213.00	8.100
10	132.00	6239.00	8.100
11	130.00	6241.00	8.440
12	87.00	6284.00	8.430
13	85.00	6286.00	8.160
14	46.00	6325.00	8.129
15	42.00	6329.00	7.200
16	21.00	6350.00	7.200
17	17.00	6354.00	6.700
18	9.00	6362.00	6.700
19	6.00	6365.00	5.000
20	0.40	6370.60	5.000
21	0.0	6371.00	1.400

BOUNDARY AT THETA = 4.80 DEG.

TRANSITION MODEL 2

I	DEPTH(I)	RAD(I)	VEL(I)
1	710.00	5661.00	11.033
2	665.00	5706.00	9.930
3	555.00	5816.00	9.805
4	505.00	5866.00	9.740
5	470.00	5901.00	9.690
6	445.00	5926.00	9.650
7	390.00	5981.00	8.600
8	160.00	6211.00	8.550
9	158.00	6213.00	8.070
10	106.00	6265.00	8.070
11	104.00	6267.00	8.440
12	87.00	6284.00	8.430
13	85.00	6286.00	8.160
14	22.00	6349.00	8.110
15	18.00	6353.00	6.650
16	11.00	6360.00	6.650
17	9.00	6362.00	6.150
18	0.0	6371.00	6.150

BOUNDARY AT THETA = 6.00 DEG.

SOUTHWESTERN MANITOBA MODEL

I	DEPTH(I)	RAD(I)	VEL(I)
1	1000.00	5371.00	11.140
2	800.00	5571.00	11.087
3	710.00	5661.00	11.033
4	665.00	5706.00	9.930
5	555.00	5816.00	9.805
6	505.00	5866.00	9.740
7	470.00	5901.00	9.690
8	445.00	5926.00	9.650
9	390.00	5981.00	8.600
10	160.00	6211.00	8.550
11	158.00	6213.00	8.070
12	106.00	6265.00	8.070
13	104.00	6267.00	8.440
14	87.00	6284.00	8.430
15	85.00	6286.00	8.160
16	27.00	6344.00	8.114
17	23.00	6348.00	6.650
18	11.00	6360.00	6.650
19	9.00	6362.00	6.150
20	0.0	6371.00	6.150

BOUNDARY AT THETA = 7.70 DEG.

SASKATCHEWAN-ALBERTA PLAINS MODEL

I	DEPTH(I)	RAD(I)	VEL(I)
1	1000.00	5371.00	11.140
2	800.00	5571.00	11.087
3	710.00	5661.00	11.033
4	665.00	5706.00	9.930
5	555.00	5816.00	9.805
6	505.00	5866.00	9.740
7	470.00	5901.00	9.690
8	445.00	5926.00	9.650
9	390.00	5981.00	8.600
10	160.00	6211.00	8.550
11	158.00	6213.00	8.070
12	106.00	6265.00	8.070
13	104.00	6267.00	8.440
14	87.00	6284.00	8.430
15	85.00	6286.00	8.160
16	44.00	6327.00	8.127
17	42.00	6329.00	7.200
18	32.00	6339.00	7.200
19	28.00	6343.00	6.000
20	0.0	6371.00	6.000

BOUNDARY AT THETA = 14.20 DEG.

TRANSITION MODEL

I	DEPTH(I)	RAD(I)	VEL(I)
1	1000.00	5371.00	11.140
2	800.00	5571.00	11.087
3	710.00	5661.00	11.033
4	665.00	5706.00	9.930
5	555.00	5816.00	9.805
6	505.00	5866.00	9.740
7	470.00	5901.00	9.690
8	445.00	5926.00	9.650
9	390.00	5981.00	8.600
10	160.00	6211.00	8.550
11	140.00	6231.00	7.800
12	100.00	6271.00	7.800
13	85.00	6286.00	8.160
14	44.00	6327.00	8.127
15	42.00	6329.00	7.200
16	32.00	6339.00	7.200
17	28.00	6343.00	6.000
18	0.0	6371.00	6.000

BOUNDARY AT THETA = 18.00 DEG.

BRITISH COLUMBIA MODEL

I	DEPTH(I)	RAD(I)	VEL(I)
1	465.00	5906.00	9.510
2	417.50	5953.50	9.517
3	390.00	5981.00	9.033
4	357.50	6013.50	8.559
5	300.00	6071.00	8.450
6	250.00	6121.00	8.360
7	200.00	6171.00	8.270
8	160.00	6211.00	8.200
9	140.00	6231.00	7.800
10	100.00	6271.00	7.800
11	60.00	6311.00	7.900
12	32.00	6339.00	7.900
13	28.00	6343.00	6.800
14	22.00	6349.00	6.800
15	18.00	6353.00	5.900
16	0.0	6371.00	5.900

END OF MODEL AT THETA = 50.00 DEG.

Table 14

MODEL UTAH 1

NMODEL = 6

CANADIAN SHIELD MODEL

I	DEPTH(I)	RAD(I)	VEL(I)
1	1000.00	5371.00	11.140
2	710.00	5661.00	11.033
3	665.00	5706.00	9.930
4	555.00	5816.00	9.805
5	505.00	5866.00	9.740
6	470.00	5901.00	9.690
7	445.00	5926.00	9.650
8	390.00	5981.00	8.600
9	170.00	6201.00	8.530
10	160.00	6211.00	8.410
11	150.00	6221.00	8.380
12	110.00	6261.00	8.380
13	96.00	6275.00	8.430
14	87.00	6284.00	8.430
15	85.00	6286.00	8.160
16	46.00	6325.00	8.129
17	42.00	6329.00	7.200
18	21.00	6350.00	7.200
19	17.00	6354.00	6.700
20	9.00	6362.00	6.700
21	6.00	6365.00	5.000
22	0.40	6370.60	5.000
23	0.0	6371.00	1.400

BOUNDARY AT THETA = 1.00 DEG.

PLAINS MODEL I

I	DEPTH(I)	RAD(I)	VEL(I)
1	1000.00	5371.00	11.140
2	800.00	5571.00	11.087
3	710.00	5661.00	11.033
4	665.00	5706.00	9.930
5	555.00	5816.00	9.805
6	505.00	5866.00	9.740
7	470.00	5901.00	9.690
8	445.00	5926.00	9.650
9	390.00	5981.00	8.600
10	145.00	6226.00	8.450
11	143.00	6228.00	8.300
12	95.00	6276.00	8.300
13	90.00	6281.00	8.350
14	77.00	6294.00	8.330
15	75.00	6296.00	8.152
16	52.00	6319.00	8.130
17	48.00	6323.00	7.200
18	17.00	6354.00	7.200
19	13.00	6358.00	5.500
20	0.0	6371.00	5.500

BOUNDARY AT THETA = 8.00 DEG.

PLAINS MODEL II

I	DEPTH(I)	RAD(I)	VEL(I)
1	1000.00	5371.00	11.140
2	800.00	5571.00	11.087
3	710.00	5661.00	11.033
4	665.00	5706.00	9.930
5	555.00	5816.00	9.805
6	505.00	5866.00	9.740
7	470.00	5901.00	9.690
8	445.00	5926.00	9.650
9	390.00	5981.00	8.600
10	145.00	6226.00	8.450
11	143.00	6228.00	8.300
12	95.00	6276.00	8.300
13	90.00	6281.00	8.350
14	77.00	6294.00	8.330
15	75.00	6296.00	8.152
16	47.00	6324.00	8.129
17	45.00	6326.00	6.700
18	29.00	6342.00	6.700
19	26.00	6345.00	6.100
20	14.00	6357.00	6.100
21	11.00	6360.00	5.430
22	0.0	6371.00	5.430

BOUNDARY AT THETA = 12.00 DEG.

WESTERN PLAINS MODEL

I	DEPTH(I)	RAD(I)	VEL(I)
1	1000.00	5371.00	11.140
2	800.00	5571.00	11.087
3	710.00	5661.00	11.033
4	665.00	5706.00	9.930
5	555.00	5816.00	9.805
6	505.00	5866.00	9.740
7	470.00	5901.00	9.690
8	445.00	5926.00	9.650
9	390.00	5981.00	8.600
10	150.00	6221.00	8.250
11	140.00	6231.00	7.800
12	122.00	6249.00	7.800
13	120.00	6251.00	8.350
14	77.00	6294.00	8.330
15	75.00	6296.00	8.152
16	47.00	6324.00	8.129
17	45.00	6326.00	6.700
18	29.00	6342.00	6.700
19	26.00	6345.00	6.100
20	14.00	6357.00	6.100
21	11.00	6360.00	5.430
22	0.0	6371.00	5.430

BOUNDARY AT THETA = 14.00 DEG.

ROCKY MOUNTAINS MODEL

I	DEPTH(I)	RAD(I)	VEL(I)
1	1000.00	5371.00	11.140
2	800.00	5571.00	11.087
3	710.00	5661.00	11.033
4	665.00	5706.00	9.930
5	555.00	5816.00	9.805
6	505.00	5866.00	9.740
7	470.00	5901.00	9.690
8	445.00	5926.00	9.650
9	390.00	5981.00	8.600
10	200.00	6171.00	8.200
11	160.00	6211.00	8.200
12	150.00	6221.00	7.800
13	100.00	6271.00	7.800
14	90.00	6281.00	7.800
15	56.00	6315.00	7.900
16	52.00	6319.00	6.800
17	36.00	6335.00	6.800
18	32.00	6339.00	6.100
19	4.00	6367.00	6.100
20	1.00	6370.00	5.000
21	0.0	6371.00	5.000

BOUNDARY AT THETA = 16.00 DEG.

COLORADO PLATEAU MODEL

I	DEPTH(I)	RAD(I)	VEL(I)
1	1000.00	5371.00	11.140
2	800.00	5571.00	11.087
3	647.00	5724.00	11.033
4	597.00	5774.00	9.411
5	552.50	5818.50	9.522
6	505.00	5866.00	9.522
7	465.00	5906.00	9.510
8	417.50	5953.50	9.517
9	390.00	5981.00	9.033
10	357.50	6013.50	8.559
11	200.00	6171.00	8.200
12	160.00	6211.00	8.200
13	150.00	6221.00	7.800
14	112.00	6259.00	7.800
15	110.00	6261.00	8.100
16	102.00	6269.00	8.100
17	100.00	6271.00	7.900
18	41.00	6330.00	7.900
19	39.00	6332.00	6.800
20	21.00	6350.00	6.800
21	19.00	6352.00	6.200
22	0.0	6371.00	6.200

END OF MODEL AT THETA = 50.00 DEG.

Table 15

MODEL NTS NE1

NMODEL = 5

BASIN AND RANGE MODEL

I	DEPTH(I)	RAD(I)	VEL(I)
1	1000.00	5371.00	11.140
2	800.00	5571.00	11.087
3	647.00	5724.00	11.033
4	597.00	5774.00	9.411
5	552.50	5818.50	9.522
6	505.00	5866.00	9.522
7	465.00	5906.00	9.510
8	430.00	5941.00	9.450
9	390.00	5981.00	8.500
10	150.00	6221.00	8.200
11	140.00	6231.00	7.800
12	122.00	6249.00	7.800
13	120.00	6251.00	8.200
14	102.00	6269.00	8.200
15	100.00	6271.00	7.900
16	30.00	6341.00	7.900
17	28.00	6343.00	6.700
18	22.00	6349.00	6.700
19	18.00	6353.00	6.000
20	0.0	6371.00	6.000

BOUNDARY AT THETA = 3.00 DEG.

NORTHERN COLORADO PLATEAU - ROCKY MOUNTAINS MODEL

I	DEPTH(I)	RAD(I)	VEL(I)
1	1000.00	5371.00	11.140
2	800.00	5571.00	11.087
3	647.00	5724.00	11.033
4	597.00	5774.00	9.411
5	552.50	5818.50	9.522
6	505.00	5866.00	9.522
7	465.00	5906.00	9.510
8	430.00	5941.00	9.450
9	390.00	5981.00	8.500
10	150.00	6221.00	8.200
11	140.00	6231.00	7.800
12	122.00	6249.00	7.800
13	120.00	6251.00	8.200
14	102.00	6269.00	8.200
15	100.00	6271.00	7.900
16	56.00	6315.00	7.900
17	52.00	6319.00	6.800
18	36.00	6335.00	6.800
19	32.00	6339.00	6.100
20	4.00	6367.00	6.100
21	1.00	6370.00	5.000
22	0.0	6371.00	5.000

BOUNDARY AT THETA = 9.20 DEG.

WESTERN PLAINS MODEL

I	DEPTH(I)	RAD(I)	VEL(I)
1	1000.00	5371.00	11.140
2	800.00	5571.00	11.087
3	647.00	5724.00	11.033
4	597.00	5774.00	9.411
5	552.50	5818.50	9.522
6	505.00	5866.00	9.522
7	465.00	5906.00	9.510
8	400.00	5971.00	9.450
9	360.00	6011.00	8.650
10	150.00	6221.00	8.250
11	140.00	6231.00	7.800
12	122.00	6249.00	7.800
13	120.00	6251.00	8.300
14	102.00	6269.00	8.300
15	100.00	6271.00	8.000
16	47.00	6324.00	8.000
17	45.00	6326.00	6.700
18	29.00	6342.00	6.700
19	26.00	6345.00	6.100
20	14.00	6357.00	6.100
21	11.00	6360.00	5.430
22	0.0	6371.00	5.430

BOUNDARY AT THETA = 13.00 DEG.

PLAINS MODEL

I	DEPTH(I)	RAD(I)	VEL(I)
1	1000.00	5371.00	11.140
2	800.00	5571.00	11.087
3	647.00	5724.00	11.033
4	597.00	5774.00	9.411
5	552.50	5818.50	9.522
6	505.00	5866.00	9.522
7	465.00	5906.00	9.510
8	400.00	5971.00	9.450
9	360.00	6011.00	8.650
10	145.00	6226.00	8.500
11	143.00	6228.00	8.300
12	95.00	6276.00	8.300
13	90.00	6281.00	8.350
14	77.00	6294.00	8.330
15	75.00	6296.00	8.155
16	52.00	6319.00	8.132
17	48.00	6323.00	7.200
18	17.00	6354.00	7.200
19	13.00	6358.00	5.500
20	0.0	6371.00	5.500

BOUNDARY AT THETA = 19.00 DEG.

CANADIAN SHIELD MODEL

I	DEPTH(I)	RAD(I)	VEL(I)
1	1000.00	5371.00	11.140
2	800.00	5571.00	11.087
3	647.00	5724.00	11.033
4	597.00	5774.00	9.411
5	552.50	5818.50	9.522
6	505.00	5866.00	9.522
7	465.00	5906.00	9.510
8	400.00	5971.00	9.450
9	360.00	6011.00	8.650
10	170.00	6201.00	8.530
11	160.00	6211.00	8.430
12	87.00	6284.00	8.430
13	85.00	6286.00	8.165
14	46.00	6325.00	8.126
15	42.00	6329.00	7.200
16	21.00	6350.00	7.200
17	17.00	6354.00	6.700
18	9.00	6362.00	6.700
19	6.00	6365.00	5.000
20	0.40	6370.60	5.000
21	0.0	6371.00	1.400

END OF MODEL AT THETA = 50.00 DEG.

Table 16

MODEL NTS E1

NMODEL = 5

BASIN AND RANGE MODEL

I	DEPTH(I)	RAD(I)	VEL(I)
1	1000.00	5371.00	11.140
2	800.00	5571.00	11.087
3	650.00	5721.00	11.033
4	605.00	5766.00	9.522
5	465.00	5906.00	9.510
6	420.00	5951.00	9.400
7	380.00	5991.00	8.500
8	160.00	6211.00	8.200
9	140.00	6231.00	7.800
10	120.00	6251.00	7.800
11	115.00	6256.00	8.200
12	102.00	6269.00	8.200
13	100.00	6271.00	7.900
14	30.00	6341.00	7.900
15	28.00	6343.00	6.700
16	22.00	6349.00	6.700
17	18.00	6353.00	6.000
18	0.0	6371.00	6.000

BOUNDARY AT THETA = 3.00 DEG.

WESTERN COLORADO PLATEAU MODEL

I	DEPTH(I)	RAD(I)	VEL(I)
1	1000.00	5371.00	11.140
2	800.00	5571.00	11.087
3	650.00	5721.00	11.033
4	605.00	5766.00	9.522
5	465.00	5906.00	9.510
6	420.00	5951.00	9.400
7	380.00	5991.00	8.500
8	160.00	6211.00	8.200
9	140.00	6231.00	7.800
10	120.00	6251.00	7.800
11	115.00	6256.00	8.200
12	102.00	6269.00	8.200
13	100.00	6271.00	7.900
14	49.00	6322.00	7.900
15	47.00	6324.00	6.800
16	26.00	6345.00	6.800
17	24.00	6347.00	6.200
18	0.0	6371.00	6.200

BOUNDARY AT THETA = 4.00 DEG.

COLORADO PLATEAU - ROCKY MTNS. MODEL

I	DEPTH(I)	RAD(I)	VEL(I)
1	1000.00	5371.00	11.140
2	800.00	5571.00	11.087
3	650.00	5721.00	11.033
4	605.00	5766.00	9.522
5	465.00	5906.00	9.510
6	420.00	5951.00	9.400
7	380.00	5991.00	8.500
8	160.00	6211.00	8.200
9	140.00	6231.00	7.800
10	120.00	6251.00	7.800
11	115.00	6256.00	8.200
12	102.00	6269.00	8.200
13	100.00	6271.00	7.900
14	41.00	6330.00	7.900
15	39.00	6332.00	6.800
16	26.00	6345.00	6.800
17	24.00	6347.00	6.200
18	0.0	6371.00	6.200

BOUNDARY AT THETA = 9.00 DEG.

WESTERN PLAINS MODEL

I	DEPTH(I)	RAD(I)	VEL(I)
1	1000.00	5371.00	11.140
2	800.00	5571.00	11.087
3	650.00	5721.00	11.033
4	605.00	5766.00	9.522
5	465.00	5906.00	9.510
6	420.00	5951.00	9.400
7	380.00	5991.00	8.500
8	160.00	6211.00	8.200
9	140.00	6231.00	7.800
10	120.00	6251.00	7.800
11	118.00	6253.00	8.200
12	102.00	6269.00	8.200
13	100.00	6271.00	8.000
14	47.00	6324.00	8.000
15	45.00	6326.00	6.700
16	29.00	6342.00	6.700
17	26.00	6345.00	6.100
18	14.00	6357.00	6.100
19	11.00	6360.00	5.430
20	0.0	6371.00	5.430

BOUNDARY AT THETA = 13.50 DEG.

GREAT PLAINS MODEL

I	DEPTH(I)	RAD(I)	VEL(I)
1	1000.00	5371.00	11.140
2	800.00	5571.00	11.087
3	650.00	5721.00	11.033
4	605.00	5766.00	9.522
5	465.00	5906.00	9.510
6	420.00	5951.00	9.400
7	380.00	5991.00	8.500
8	160.00	6211.00	8.550
9	158.00	6213.00	8.070
10	106.00	6265.00	8.070
11	104.00	6267.00	8.440
12	87.00	6284.00	8.430
13	85.00	6286.00	8.160
14	44.00	6327.00	8.127
15	42.00	6329.00	7.200
16	32.00	6339.00	7.200
17	28.00	6343.00	6.000
18	0.0	6371.00	6.000

END OF MODEL AT THETA = 50.00 DEG.

Table 17

MODEL NTS SE1

I	DEPTH(I)	RAD(I)	VEL(I)
1	800.00	5571.00	11.087
2	647.00	5724.00	11.033
3	597.00	5774.00	9.411
4	552.50	5818.50	9.522
5	505.00	5866.00	9.522
6	465.00	5906.00	9.510
7	417.50	5953.50	9.517
8	390.00	5981.00	9.033
9	357.50	6013.50	8.559
10	300.00	6071.00	8.450
11	250.00	6121.00	8.360
12	200.00	6171.00	8.270
13	160.00	6211.00	8.200
14	140.00	6231.00	7.800
15	60.00	6311.00	7.800
16	50.00	6321.00	7.900
17	34.00	6337.00	7.900
18	31.00	6340.00	6.700
19	19.00	6352.00	6.700
20	15.00	6356.00	6.000
21	0.0	6371.00	6.000

Table 18

MODEL GBGY W1

NMODEL = 3

EASTERN AND CENTRAL COLORADO PLATEAU MODEL

I	DEPTH(I)	RAD(I)	VEL(I)	ETA(I)
1	390.00	5981.00	9.033	662.13
2	357.50	6013.50	8.559	702.59
3	300.00	6071.00	8.450	718.46
4	250.00	6121.00	8.360	732.18
5	200.00	6171.00	8.270	746.19
6	155.00	6216.00	8.200	758.05
7	150.00	6221.00	7.800	797.56
8	122.00	6249.00	7.800	801.15
9	120.00	6251.00	8.100	771.73
10	102.00	6269.00	8.100	773.95
11	100.00	6271.00	7.955	788.31
12	45.00	6326.00	7.950	795.72
13	44.00	6327.00	7.000	903.86
14	30.00	6341.00	7.000	905.86
15	29.00	6342.00	6.200	1022.90
16	3.00	6368.00	6.200	1027.10
17	1.00	6370.00	4.000	1592.50
18	0.0	6371.00	4.000	1592.75

BOUNDARY AT THETA = 2.00 DEG.

WESTERN COLORADO PLATEAU MODEL

I	DEPTH(I)	RAD(I)	VEL(I)	ETA(I)
1	390.00	5981.00	9.033	662.13
2	357.50	6013.50	8.559	702.59
3	300.00	6071.00	8.450	718.46
4	250.00	6121.00	8.360	732.18
5	200.00	6171.00	8.270	746.19
6	155.00	6216.00	8.200	758.05
7	150.00	6221.00	7.800	797.56
8	122.00	6249.00	7.800	801.15
9	120.00	6251.00	8.100	771.73
10	102.00	6269.00	8.100	773.95
11	100.00	6271.00	7.960	787.81
12	53.00	6318.00	7.950	794.72
13	52.00	6319.00	7.000	902.71
14	30.00	6341.00	7.000	905.86
15	29.00	6342.00	6.200	1022.90
16	0.0	6371.00	6.200	1027.58

BOUNDARY AT THETA = 5.00 DEG.

BASIN AND RANGE MODEL

I	DEPTH(I)	RAD(I)	VEL(I)	ETA(I)
1	390.00	5981.00	9.033	662.13
2	357.50	6013.50	8.559	702.59
3	300.00	6071.00	8.450	718.46
4	250.00	6121.00	8.360	732.18
5	200.00	6171.00	8.270	746.19
6	155.00	6216.00	8.200	758.05
7	150.00	6221.00	7.800	797.56
8	100.00	6271.00	7.800	803.97
9	80.00	6291.00	7.905	795.83
10	31.00	6340.00	7.900	802.53
11	30.00	6341.00	6.700	946.42
12	19.00	6352.00	6.700	948.06
13	15.00	6356.00	6.000	1059.33
14	2.00	6369.00	6.000	1061.50
15	0.0	6371.00	5.000	1274.20

END OF MODEL AT THETA = 50.00 DEG.

Table 19

MODEL WASH 1

I	DEPTH(I)	RAD(I)	VEL(I)
1	600.00	5771.00	9.400
2	430.00	5941.00	9.404
3	390.00	5981.00	8.659
4	145.00	6226.00	8.353
5	141.00	6230.00	8.250
6	90.00	6281.00	8.250
7	80.00	6291.00	8.310
8	65.00	6306.00	8.270
9	63.00	6308.00	8.120
10	38.00	6333.00	8.080
11	34.00	6337.00	7.100
12	31.00	6340.00	7.100
13	27.00	6344.00	6.900
14	20.00	6351.00	6.700
15	10.00	6361.00	6.500
16	0.0	6371.00	6.100

FIGURE CAPTIONS

Figure 1. Upper mantle P wave velocity distribution for the models of Jeffreys, Gutenberg, Lehmann, and Lukk and Nersesov, and both P and S wave velocity for model CIT11GB.

Figure 2. Reduced P wave travel times for model CIT11GB. Surface focus. Dots indicate Jeffreys-Bullen times. Letters are for correlation with Figures 3, 6, 8.

Figure 3. Slope of travel time curve, $\frac{dT}{d\Delta}$, and amplitude, considering geometric spreading only, for P waves in model CIT11GB. Surface focus. Letters are for correlation with Figures 2, 6, 8.

Figure 4. Reduced S wave travel times for model CIT11GB. Surface focus. Dots indicate Jeffreys-Bullen times. Letters are for correlation with Figures 5, 6, 8.

Figure 5. $\frac{dT}{d\Delta}$ and amplitude, considering geometric spreading only, for S waves in model CIT11GB. Surface focus. Letters are for correlation with Figures 4, 6, 8.

Figure 6. Amplitude, considering attenuation only, of P and S waves in model CIT11GB, Q model MM8. Surface focus. Letters are for correlation with Figures 2, 3, 4, 5, 8. Numbered points correspond to lines in Figure 7. Note break in abscissa between 40 and 95 degrees.

Figure 33. P wave travel times to Canadian stations observed during the Hudson Bay Seismic Experiment (from Barr, 1967). Calculated travel time curve is for model HUDSBY 10.

Figure 34. P wave travel times to Canadian stations observed during the Hudson Bay Seismic Experiment (from Barr, 1967). Calculated travel time curve is for model HUDSBY 10.

Figure 35. Combined plot of observed P wave travel times for Early Rise Texas and Arkansas profiles, with calculated travel time curve for model ER2 of Green and Hales (1968).

Figure 36. Observed P wave travel times for Early Rise North Carolina profile, with calculated travel time curve for model NC2.

Figure 37. Record section for Early Rise North Carolina profile, with calculated travel time curve for model ER2.

Figure 38. Proposed earth models for eastern North America.

Figure 39. Observed P wave travel times for Nevada Test Site north profile, with calculated travel time curve for model NTS N1.

Figure 40. Observed P wave travel times for Nevada Test Site north profile, with calculated travel time curve for model NTS N1.

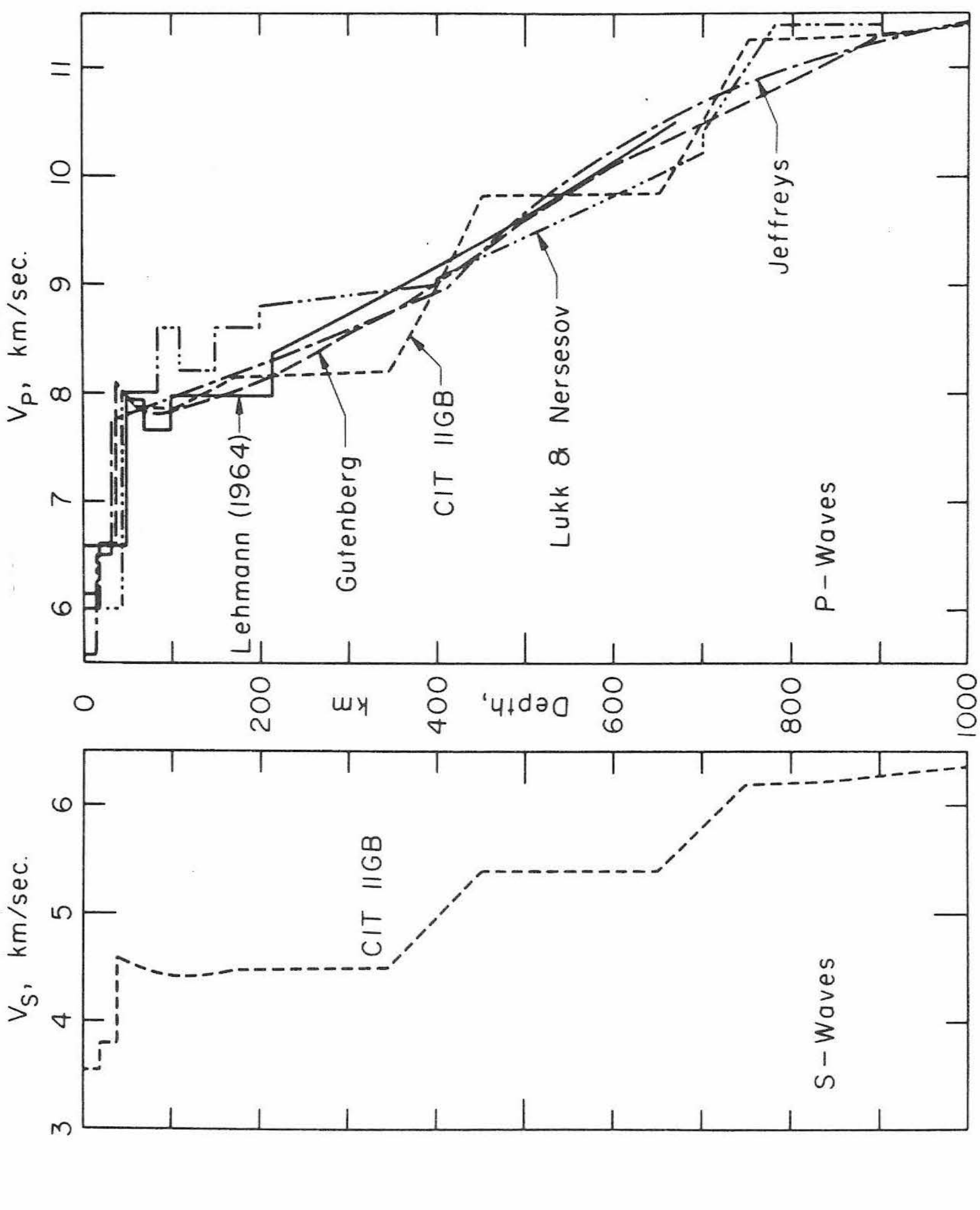

V_P, km/sec.
Lehmann (1964)
Gutenberg
CIT 11GB
Lukk & Nersesov
Jeffreys
P-Waves
Depth, km
V_S, km/sec.
CIT 11GB
S-Waves

Figure 1

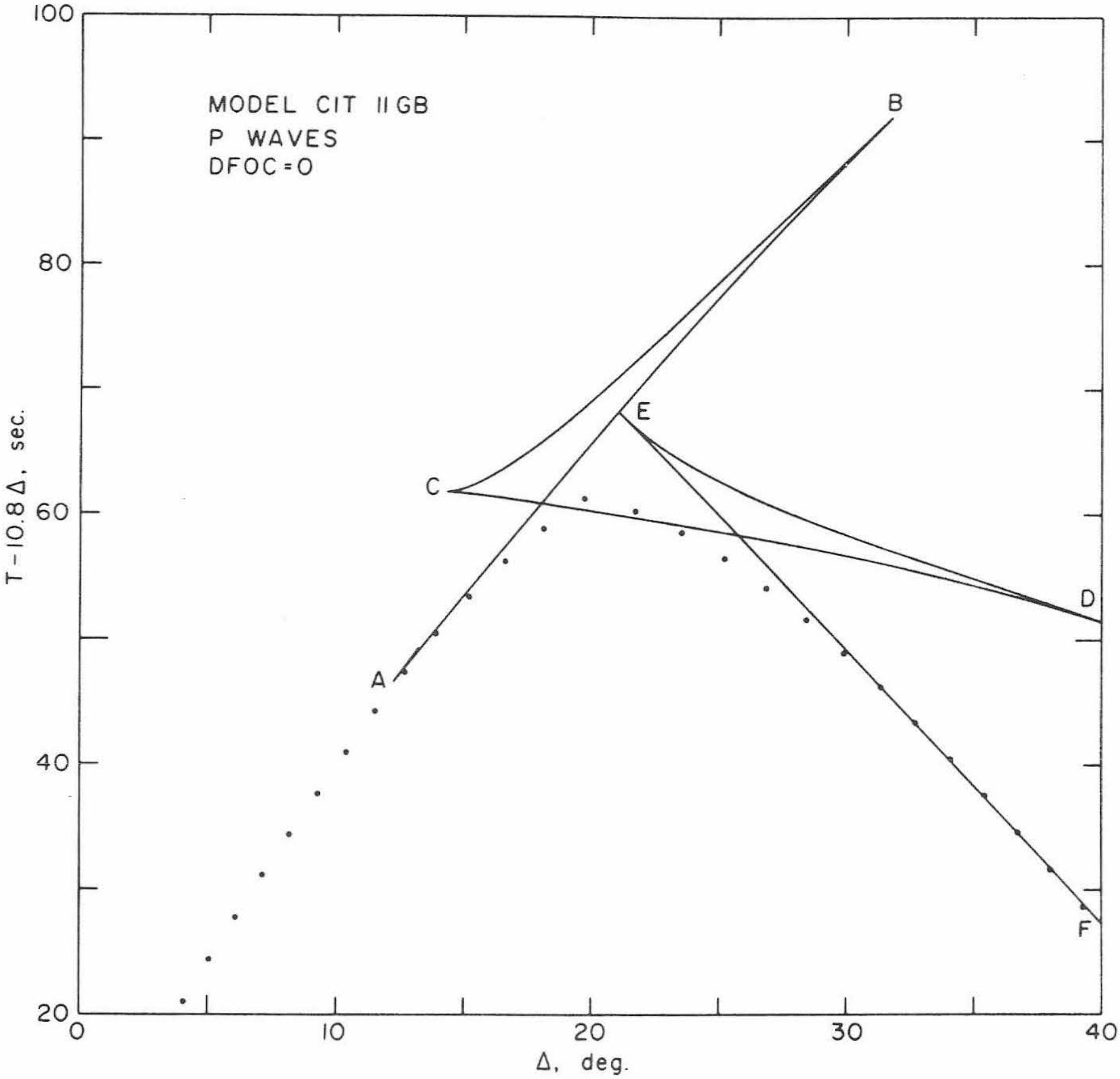
MODEL CIT 11GB
P WAVES
DFOC=0
A
B
C
D
E
F
T - 10.8 Δ, sec.
Δ, deg.
20
40
60
80
100
0
10
20
30
40

Figure 2

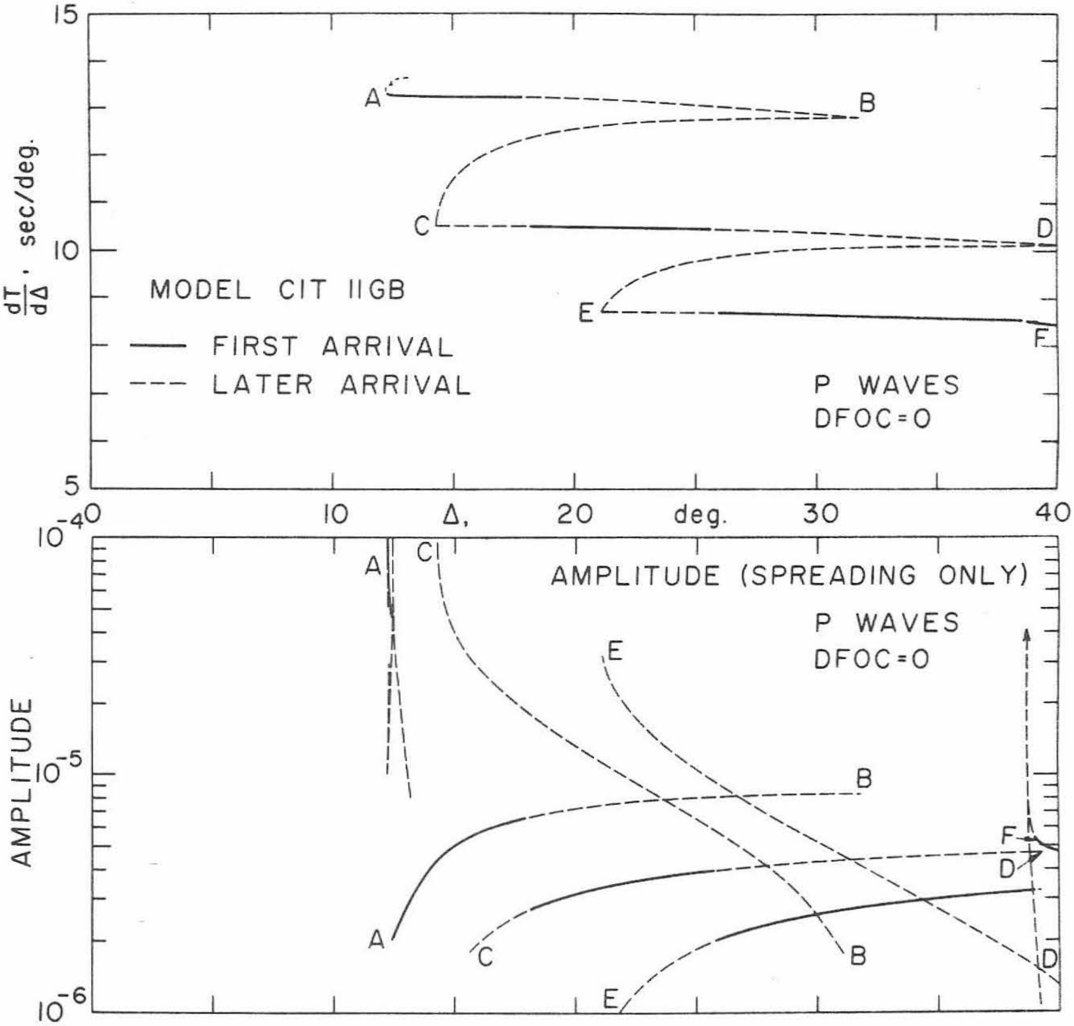
15
10
5
dT/dΔ, sec/deg.
A
B
C
D
E
F
MODEL CIT IIGB
FIRST ARRIVAL
LATER ARRIVAL
P WAVES
DFOC=0
0
10
Δ,
20
deg.
30
40
10^{-4}
10^{-5}
10^{-6}
AMPLITUDE
AMPLITUDE (SPREADING ONLY)
P WAVES
DFOC=0
A
C
E
B
F
D
A
C
E
B
D

Figure 3

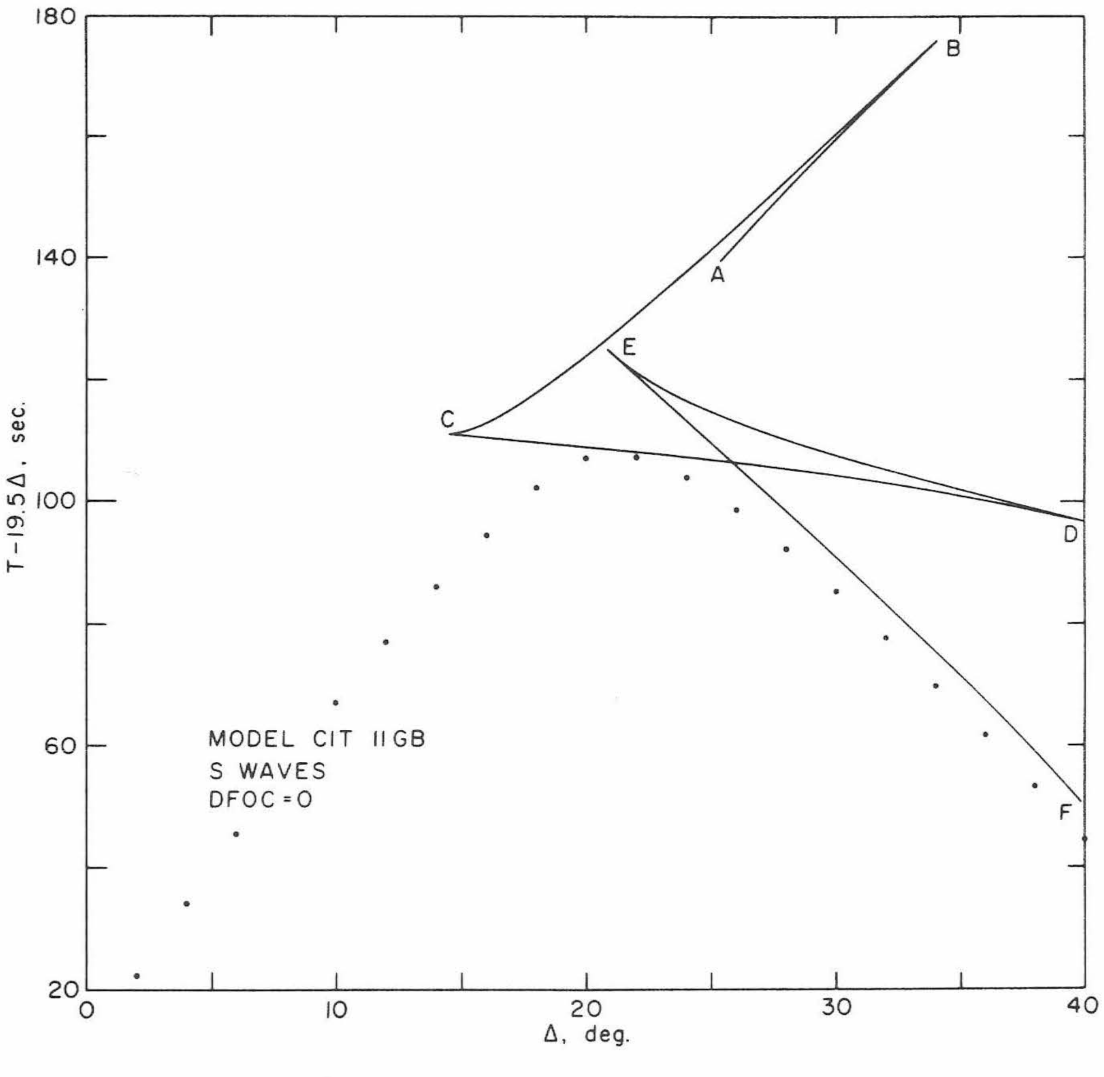
180
140
100
60
20
0
10
20
30
40
Δ, deg.
T - 19.5 Δ, sec.
A
B
C
D
E
F
MODEL CIT 11GB
S WAVES
DFOC = 0

Figure 4

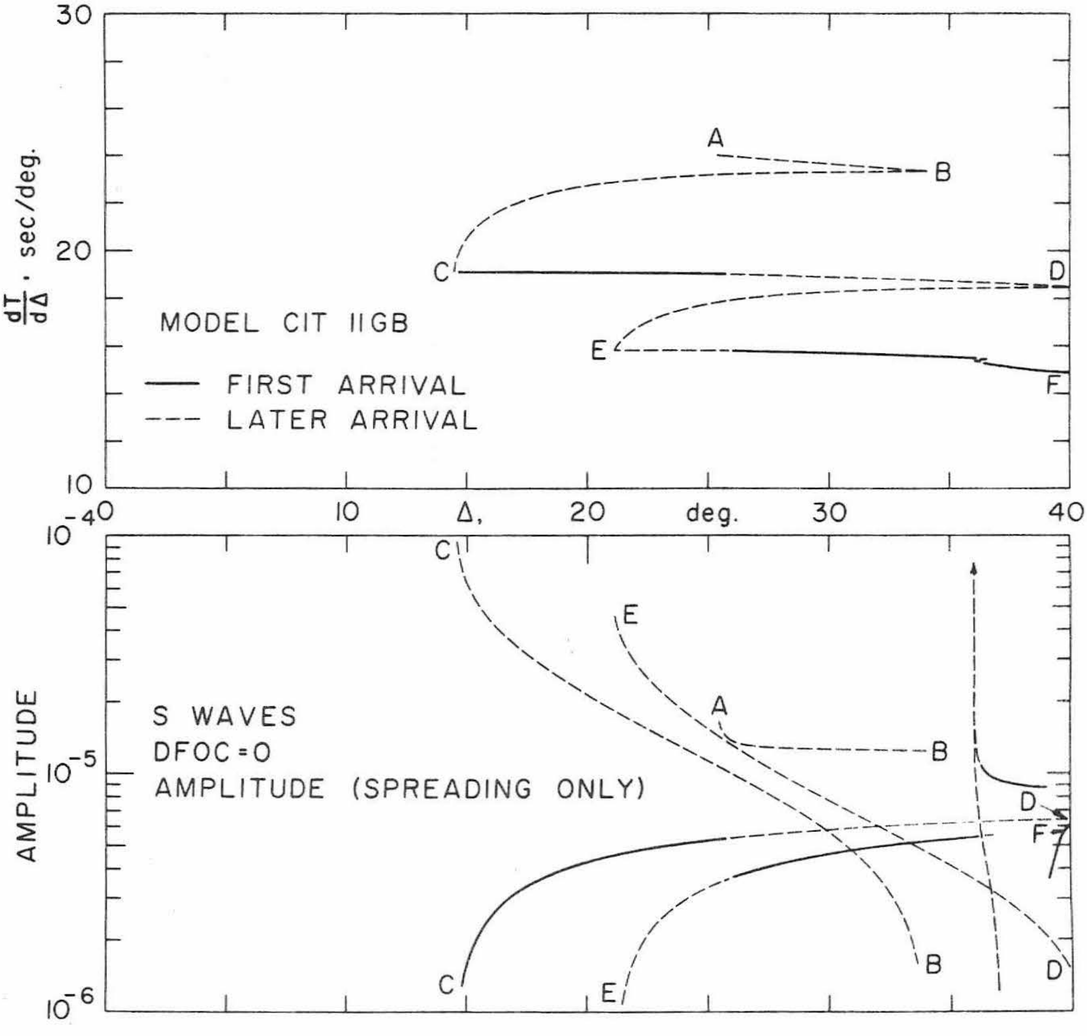

30
20
10
dT/dΔ, sec/deg.
A
B
C
D
E
F
MODEL CIT 11GB
FIRST ARRIVAL
LATER ARRIVAL
0
10
Δ,
20
deg.
30
40
10^{-4}
10^{-5}
10^{-6}
AMPLITUDE
S WAVES
DFOC=0
AMPLITUDE (SPREADING ONLY)

Figure 5

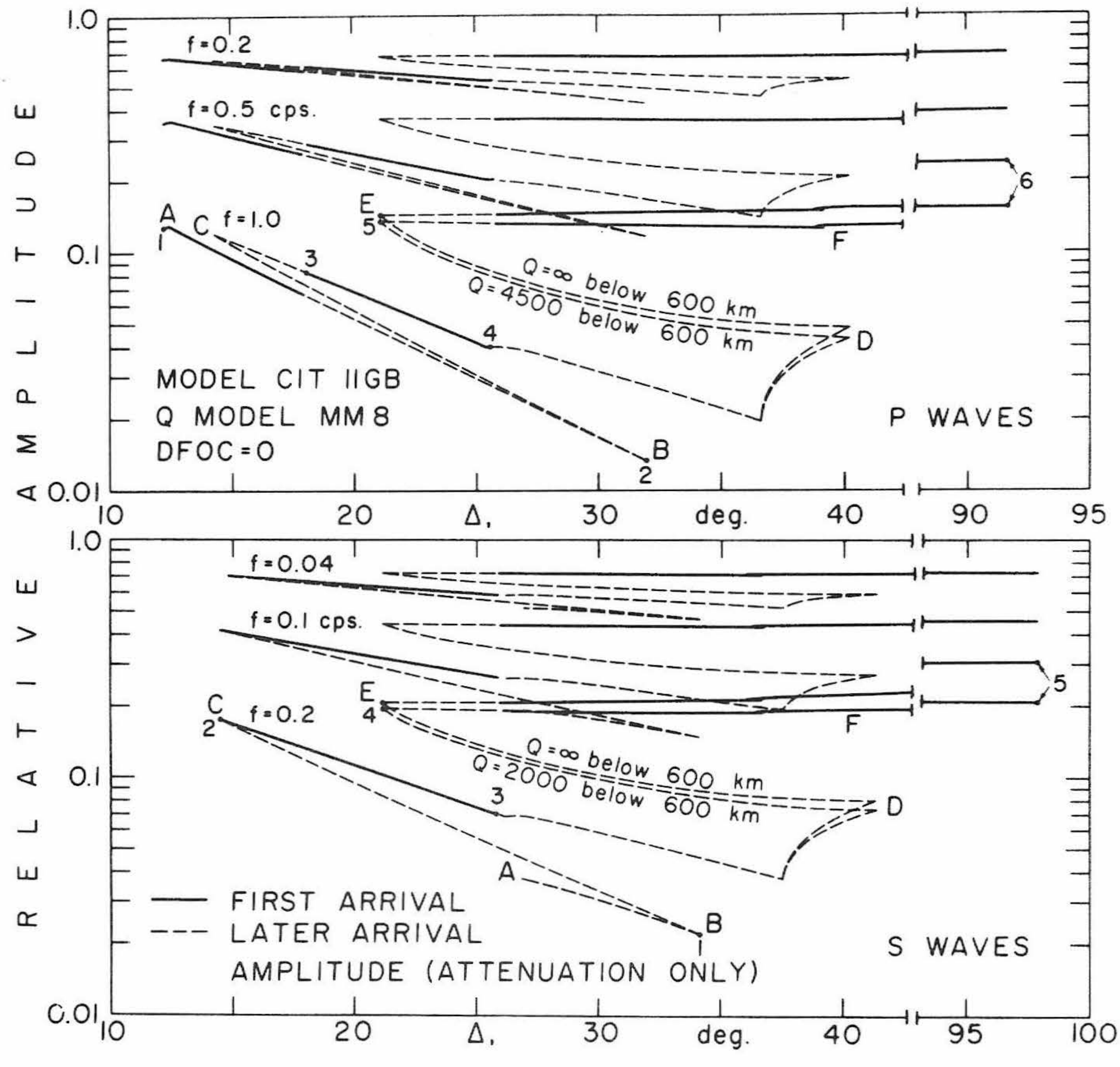
RELATIVE AMPLITUDE
1.0
0.1
0.01
f=0.2
f=0.5 cps.
f=1.0
A
1
C
3
4
2
B
E
5
F
D
6
Q=∞ below 600 km
Q=4500 below 600 km
MODEL CIT 11GB
Q MODEL MM8
DFOC=0
P WAVES
10
20
Δ,
30
deg.
40
90
95
f=0.04
f=0.1 cps.
f=0.2
C
2
E
4
F
3
D
A
B
1
5
Q=∞ below 600 km
Q=2000 below 600 km
FIRST ARRIVAL
LATER ARRIVAL
AMPLITUDE (ATTENUATION ONLY)
S WAVES
100

Figure 6

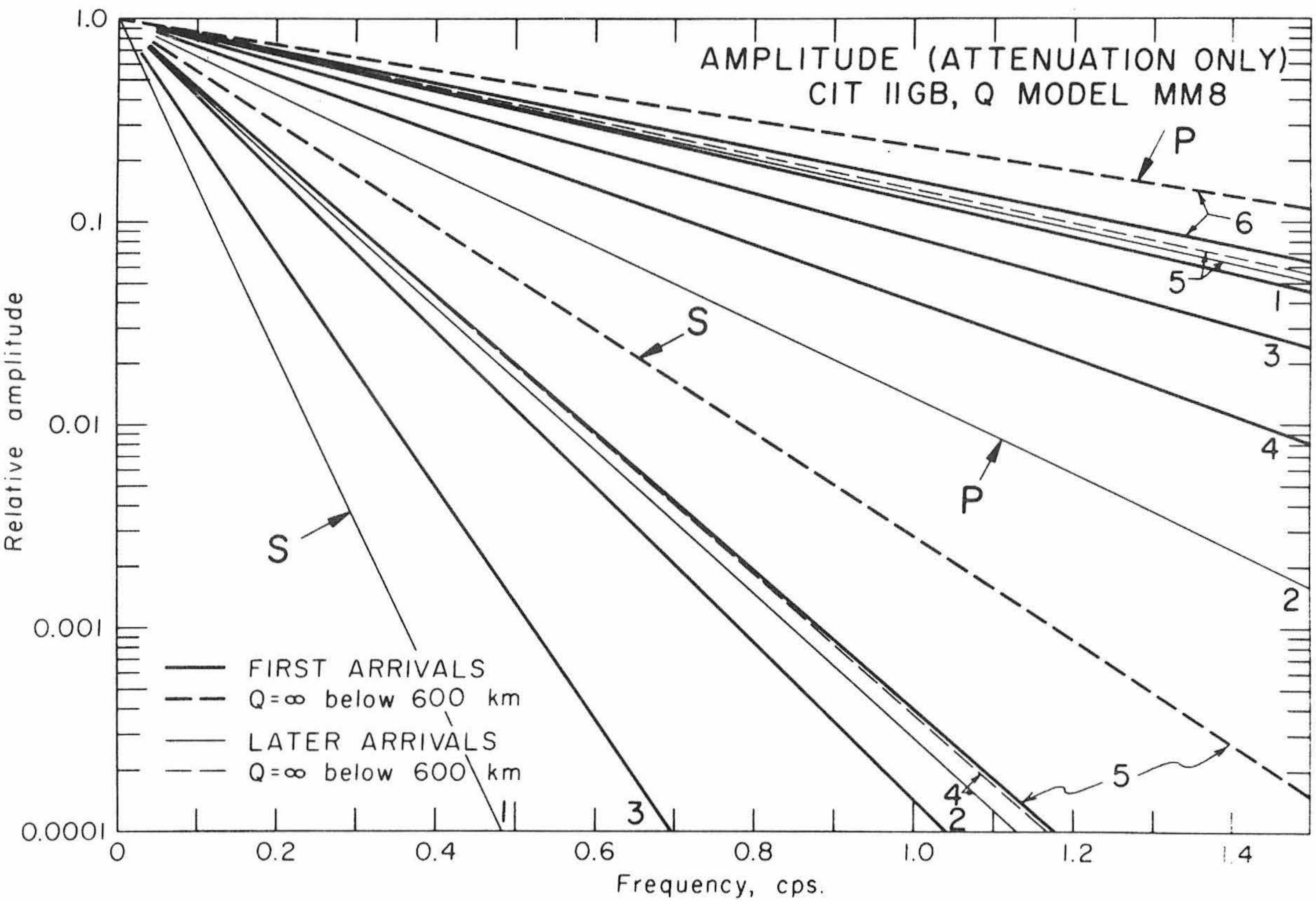
AMPLITUDE (ATTENUATION ONLY)
CIT 11GB, Q MODEL MM8
FIRST ARRIVALS
Q=∞ below 600 km
LATER ARRIVALS
Q=∞ below 600 km
Relative amplitude
Frequency, cps.
1.0
0.1
0.01
0.001
0.0001
0
0.2
0.4
0.6
0.8
1.0
1.2
1.4
P
S
1
2
3
4
5
6

Figure 7

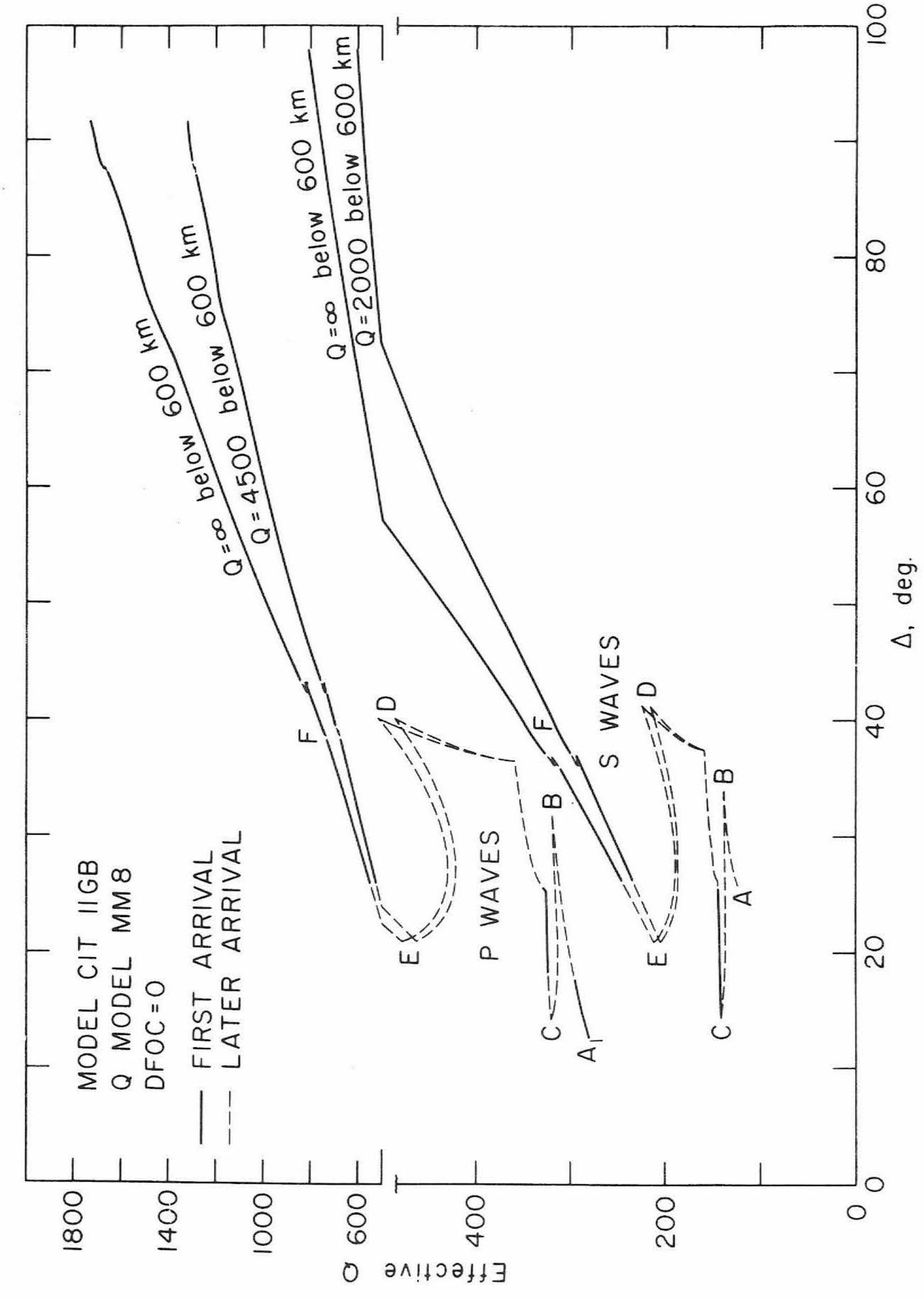
MODEL CIT 11GB
Q MODEL MM8
DFOC=0
FIRST ARRIVAL
LATER ARRIVAL
P WAVES
S WAVES
Q=∞ below 600 km
Q=4500 below 600 km
Q=∞ below 600 km
Q=2000 below 600 km
A
B
C
D
E
F
Effective Q
Δ, deg.
0
200
400
600
1000
1400
1800
0
20
40
60
80
100

Figure 8

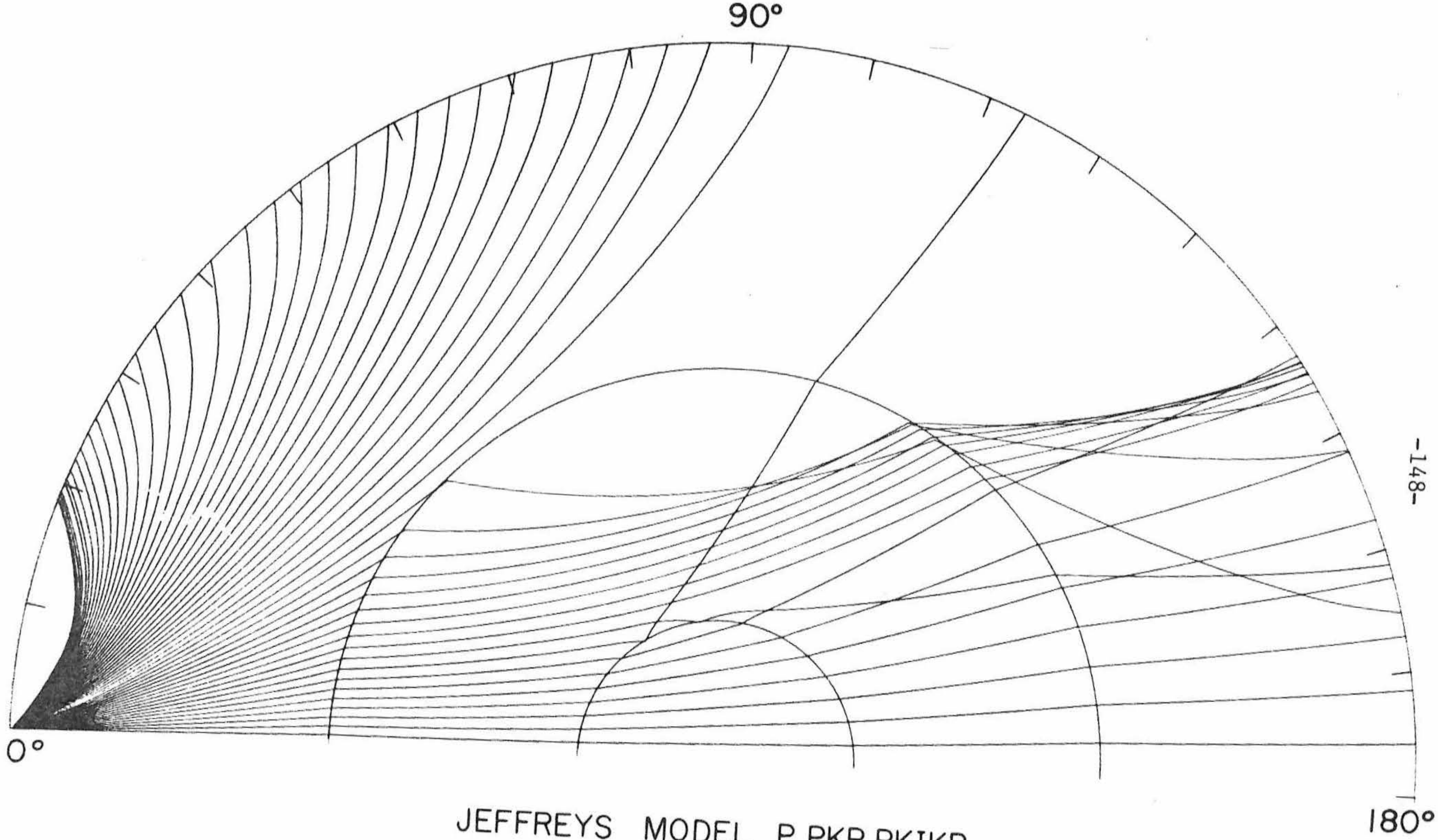

JEFFREYS MODEL P, PKP, PKIKP
DFOC = 35 Km
TOA = 1,1,51

Figure 9

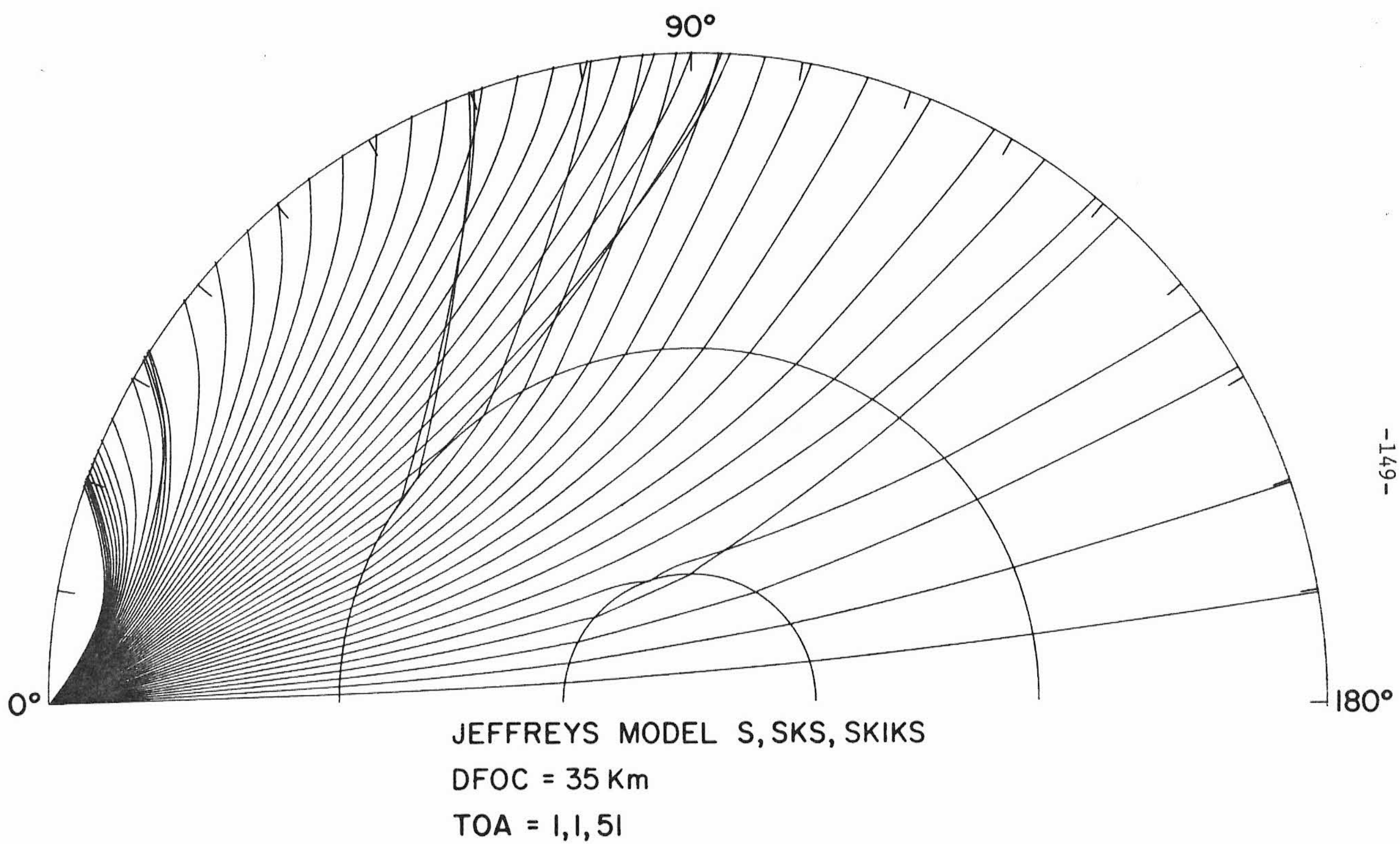

Figure 10

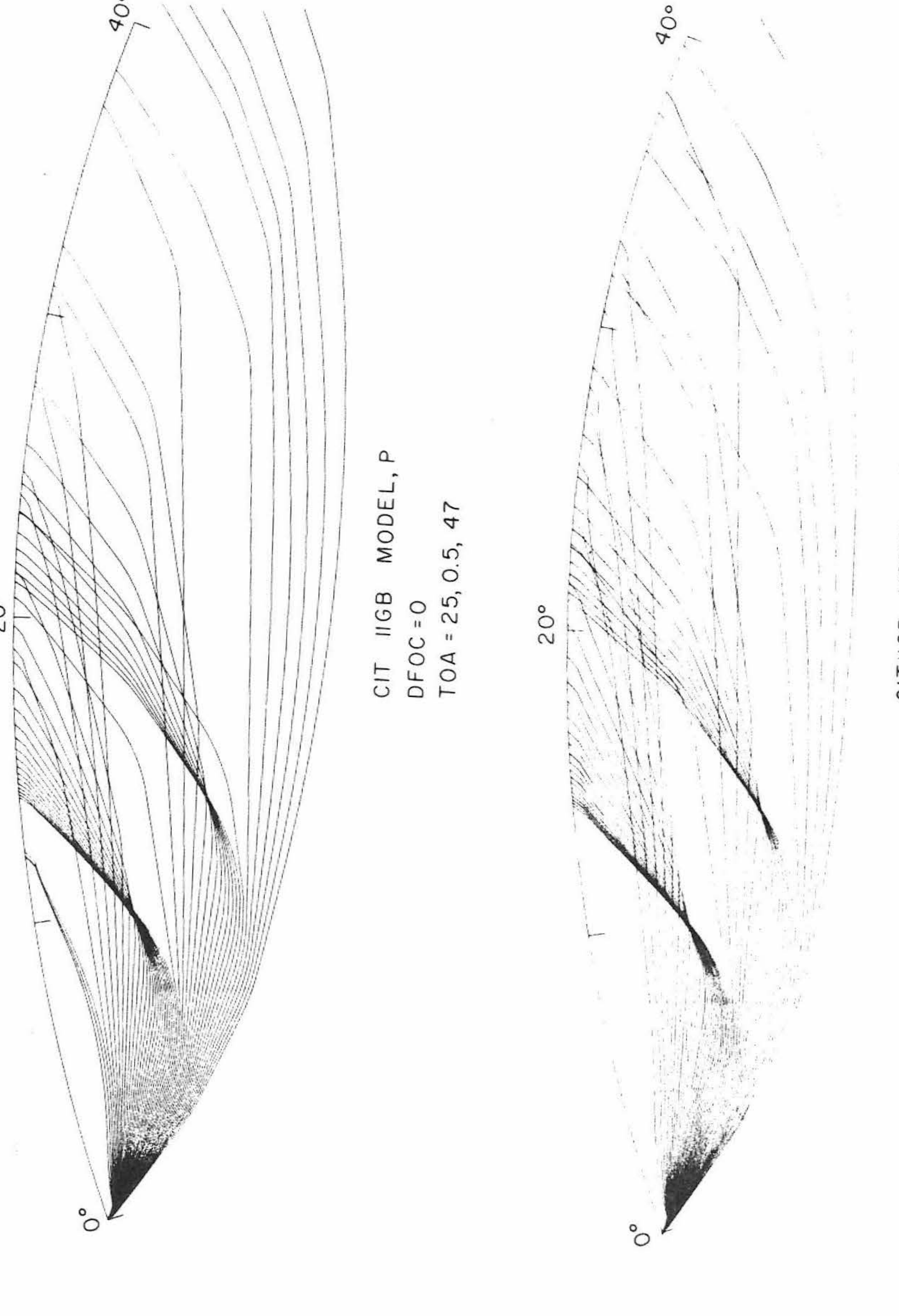
0°
20°
40°
CIT IIGB MODEL, P
DFOC = O
TOA = 25, 0.5, 47
0°
20°
40°
CITIIGB MODEL, S
DFOC = O
TOA = 28, 0.5, 50

Figure 11

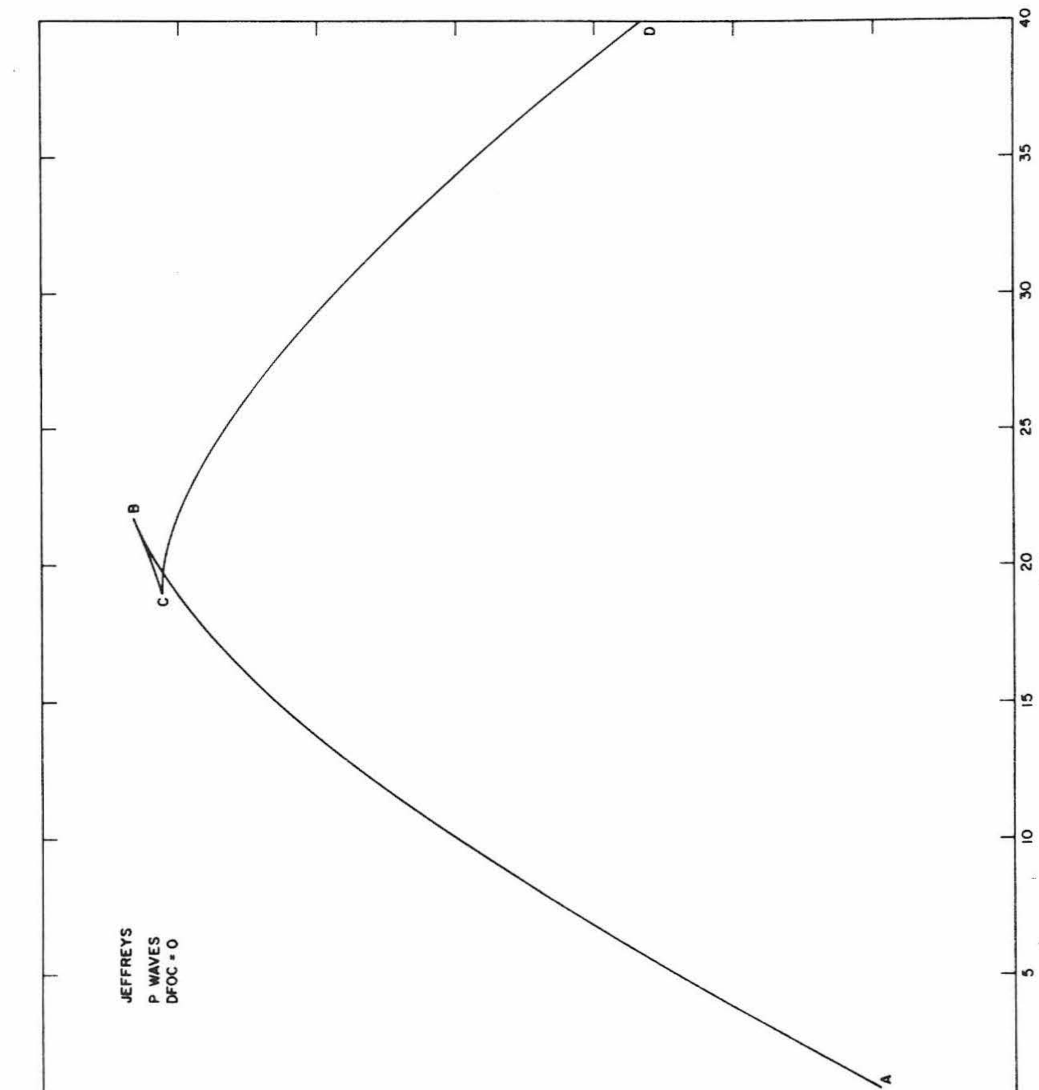
JEFFREYS
P WAVES
DFOC = 0
A
B
C
D
T-10.8 Δ, sec.
Δ, deg.
0
5
10
15
20
25
30
35
40
50
60
70

Figure 12

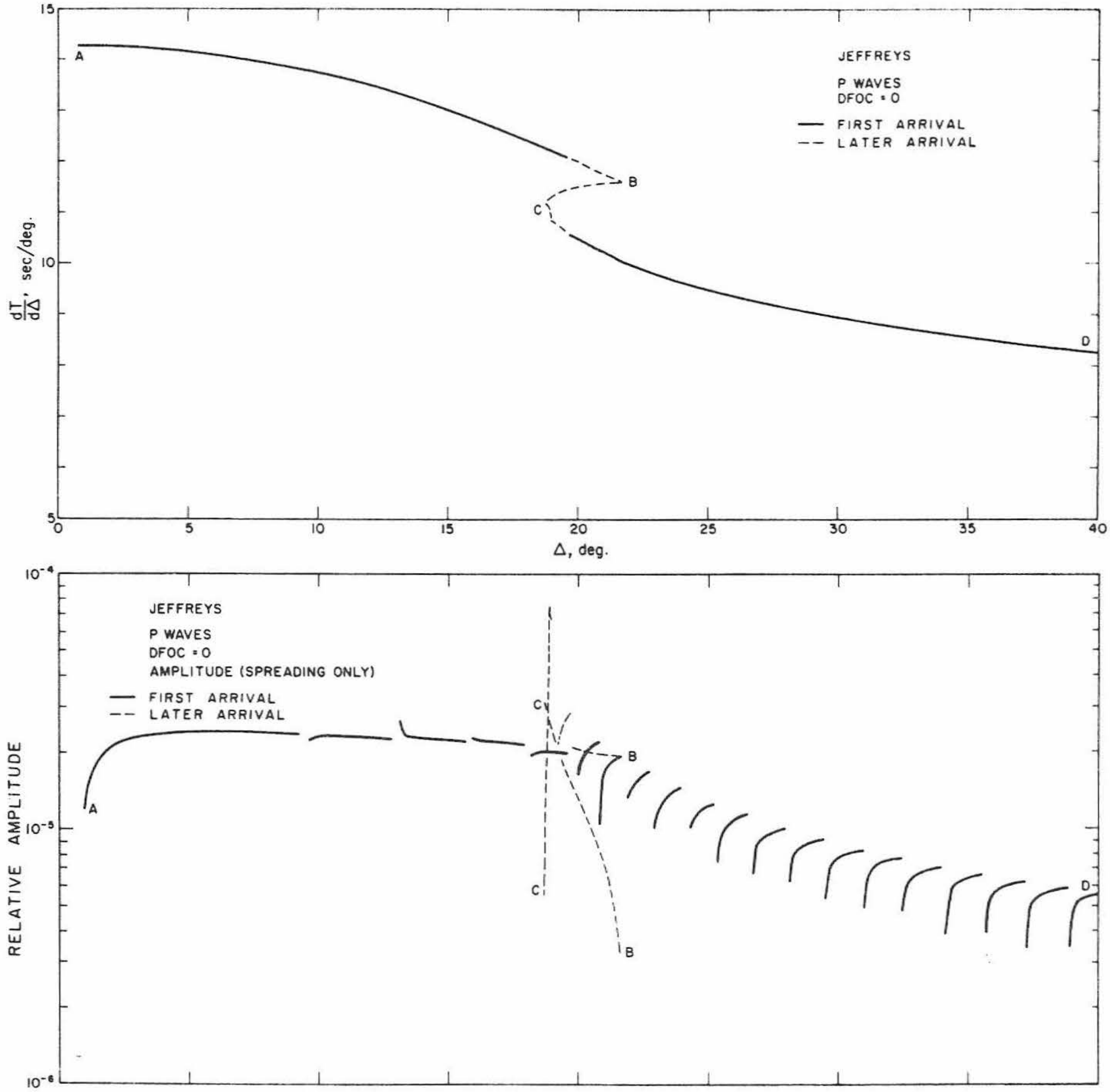
JEFFREYS
P WAVES
DFOC = 0
FIRST ARRIVAL
LATER ARRIVAL
A
B
C
D
$\frac{dT}{d\Delta}$, sec/deg.
15
10
5
0
5
10
15
20
25
30
35
40
Δ, deg.
JEFFREYS
P WAVES
DFOC = 0
AMPLITUDE (SPREADING ONLY)
FIRST ARRIVAL
LATER ARRIVAL
RELATIVE AMPLITUDE
10^{-4}
10^{-5}
10^{-6}

Figure 13

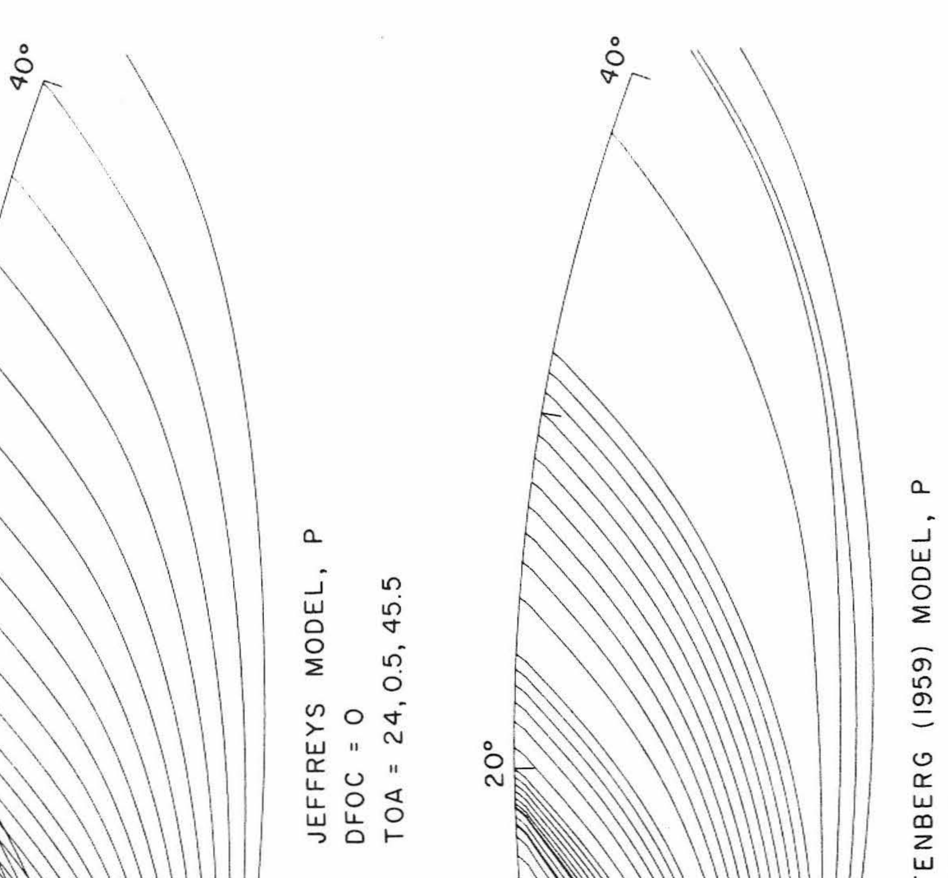
0°
20°
40°
JEFFREYS MODEL, P
DFOC = 0
TOA = 24, 0.5, 45.5
0°
20°
40°
GUTENBERG (1959) MODEL, P
DFOC = 0
TOA = 26, 0.5, 49

Figure 14

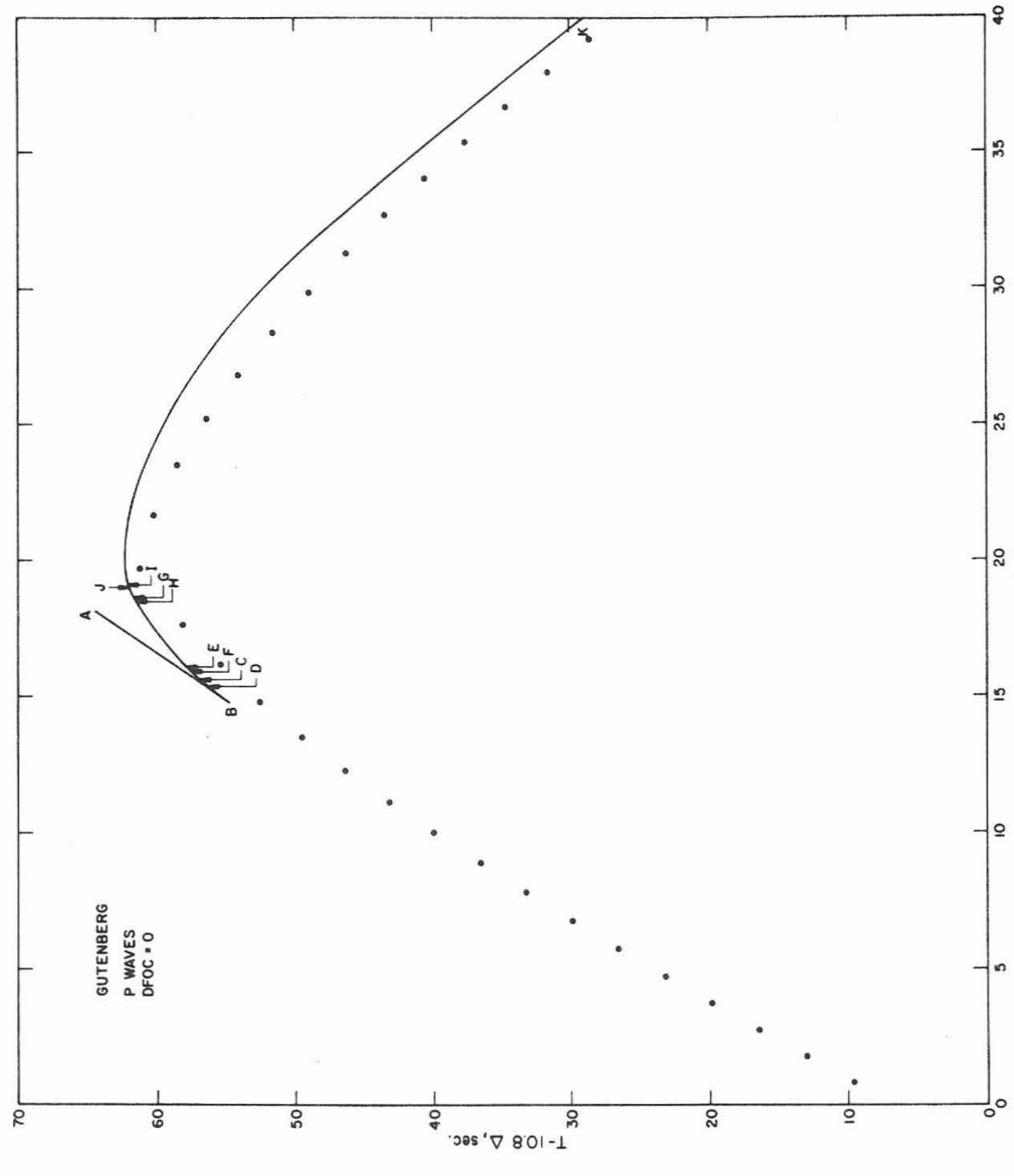
GUTENBERG
P WAVES
DFOC = 0
T-10.8 Δ, sec.
Δ, deg.
A
B
C
D
E
F
G
H
I
J
K
0
10
20
30
40
50
60
70
5
15
25
35

Figure 15

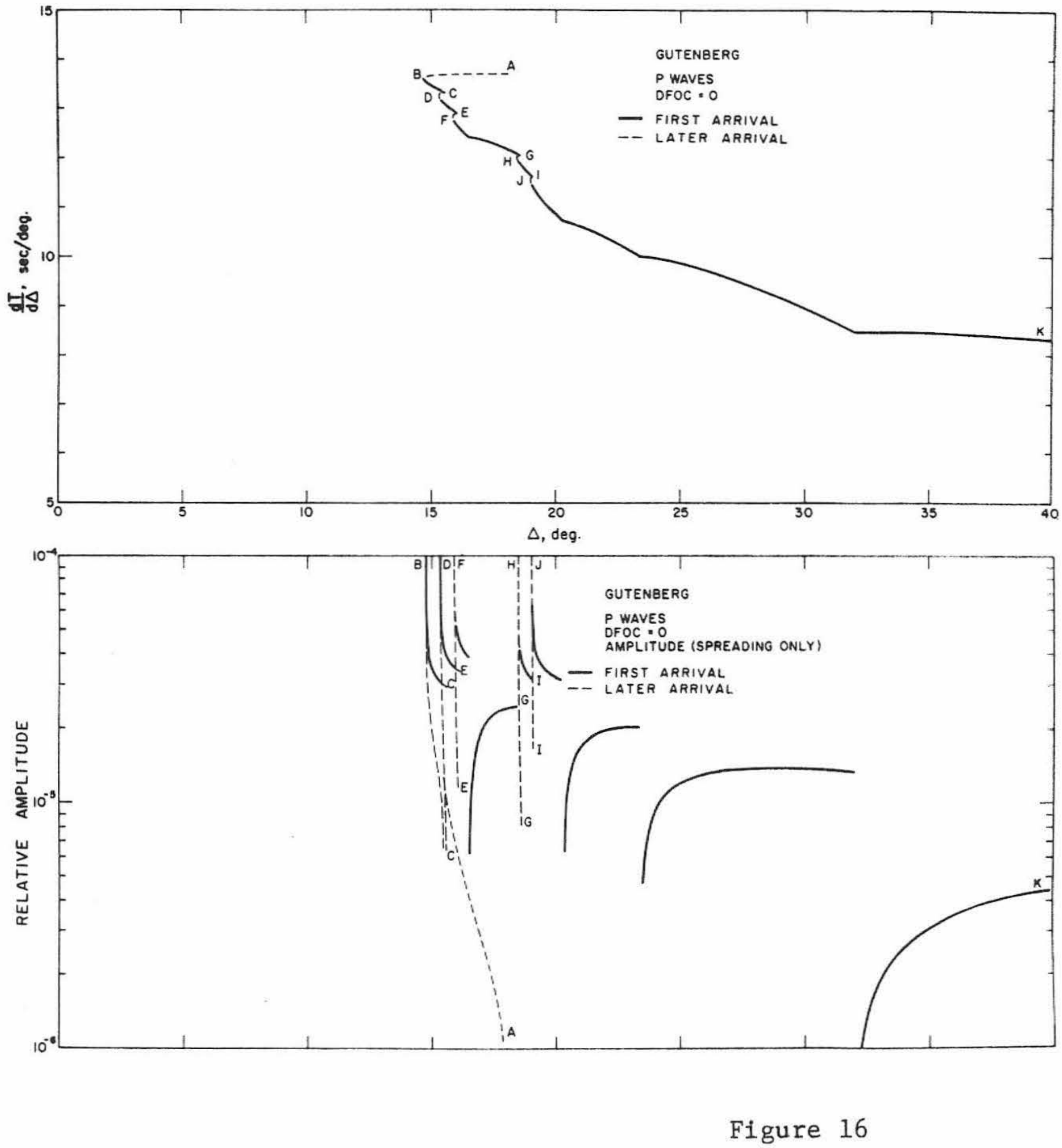
GUTENBERG
P WAVES
DFOC = 0
FIRST ARRIVAL
LATER ARRIVAL
dT/dΔ, sec/deg.
Δ, deg.
A
B
C
D
E
F
G
H
I
J
K
GUTENBERG
P WAVES
DFOC = 0
AMPLITUDE (SPREADING ONLY)
FIRST ARRIVAL
LATER ARRIVAL
RELATIVE AMPLITUDE

Figure 16

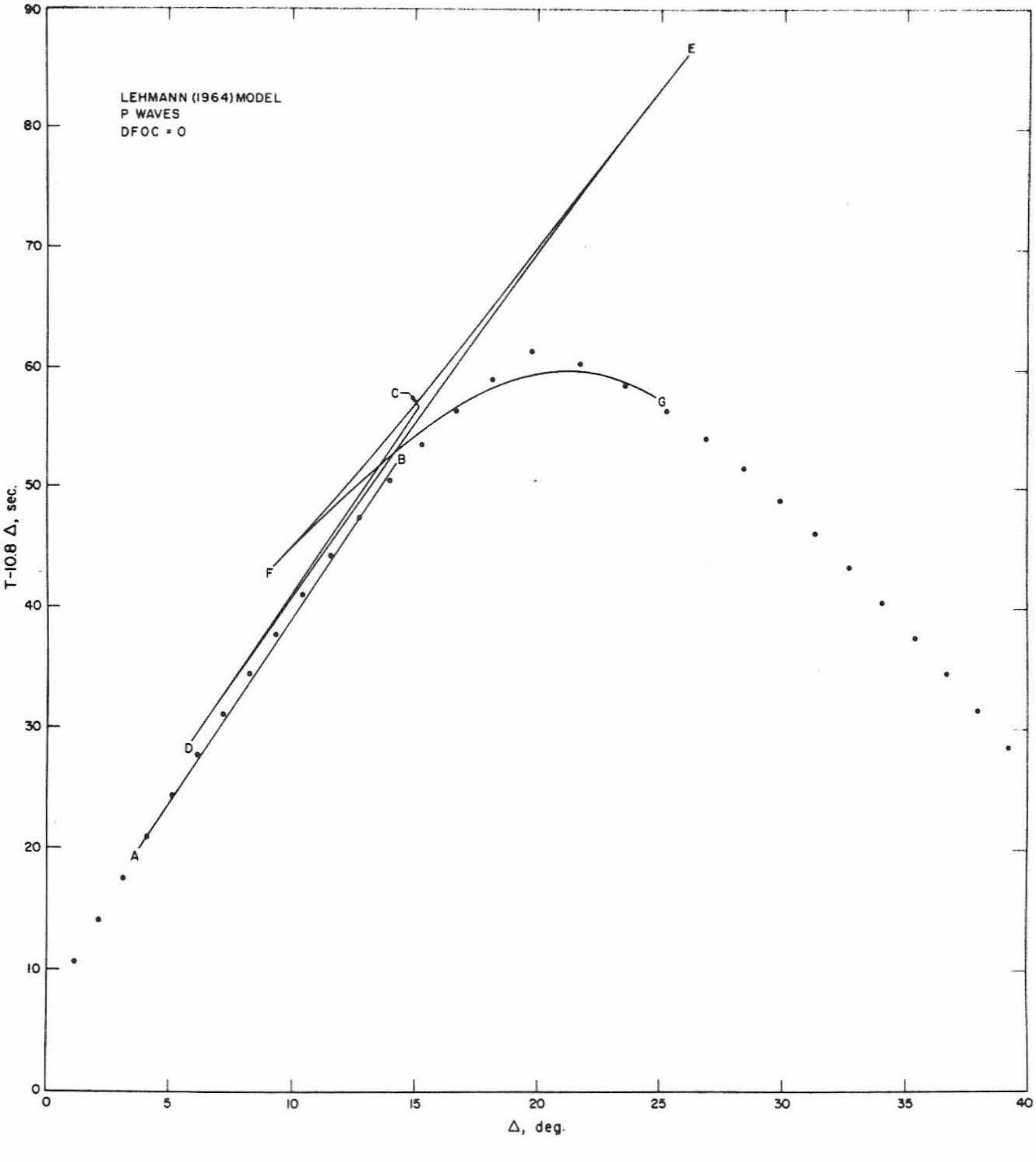
LEHMANN (1964) MODEL
P WAVES
DFOC = 0
T-10.8 Δ, sec.
Δ, deg.
A
B
C
D
E
F
G
0
10
20
30
40
50
60
70
80
90
5
15
25
35

Figure 17

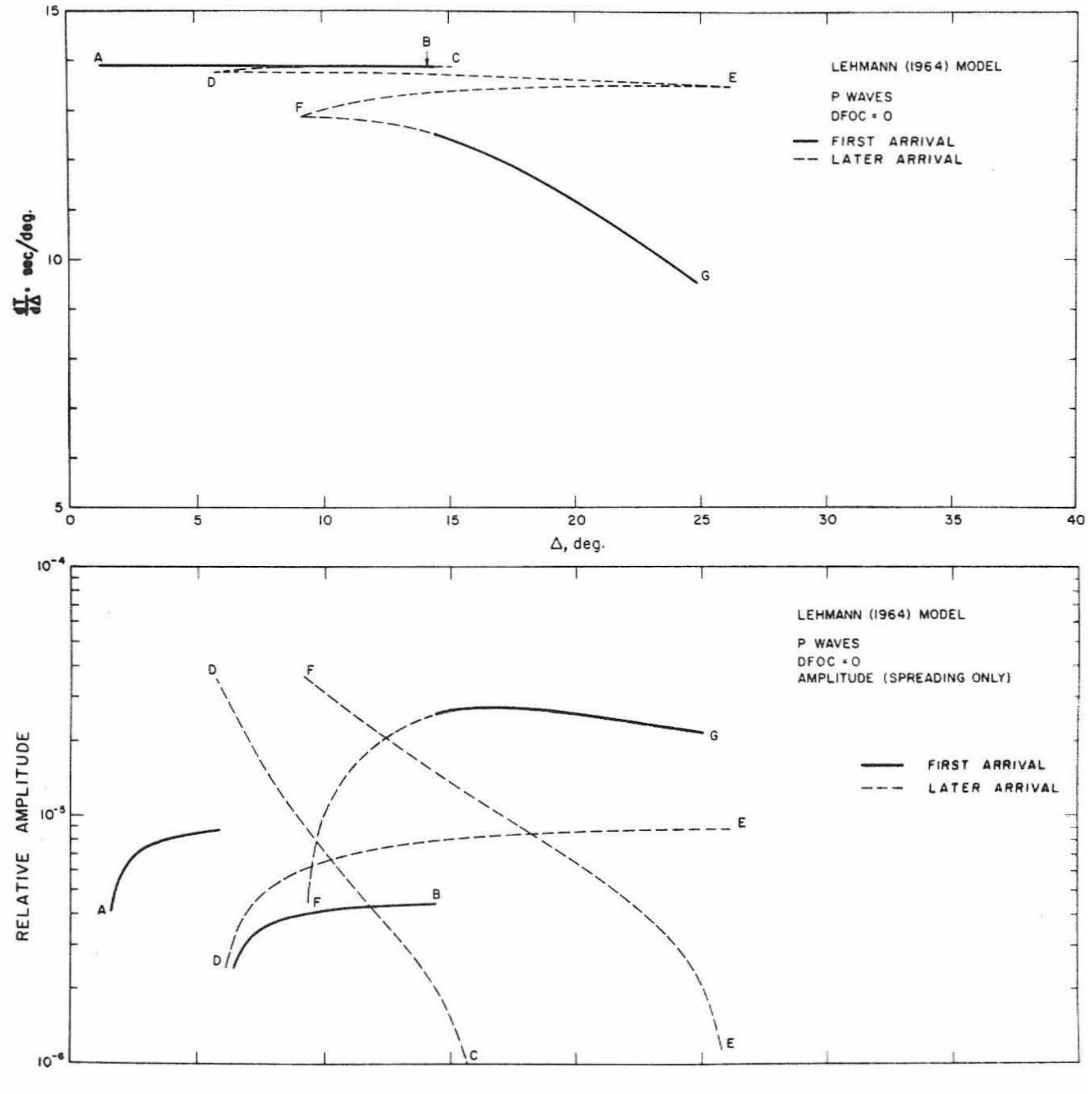

LEHMANN (1964) MODEL
P WAVES
DFOC = 0
FIRST ARRIVAL
LATER ARRIVAL
dT/dΔ, sec/deg.
Δ, deg.
A
B
C
D
E
F
G
LEHMANN (1964) MODEL
P WAVES
DFOC = 0
AMPLITUDE (SPREADING ONLY)
RELATIVE AMPLITUDE
FIRST ARRIVAL
LATER ARRIVAL

Figure 18

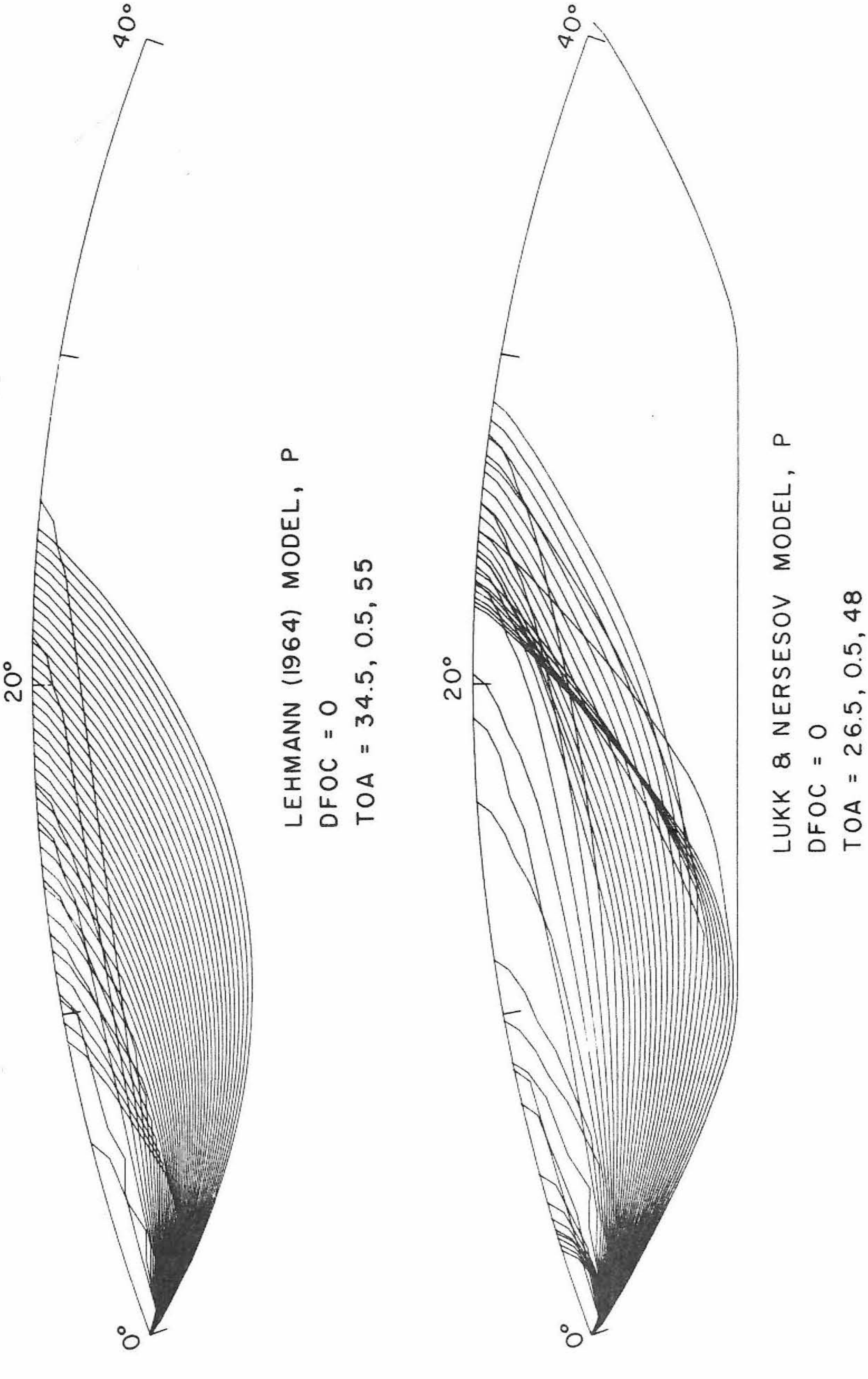
0°
20°
40°
LEHMANN (1964) MODEL, P
DFOC = 0
TOA = 34.5, 0.5, 55
0°
20°
40°
LUKK & NERSESOV MODEL, P
DFOC = 0
TOA = 26.5, 0.5, 48

Figure 19

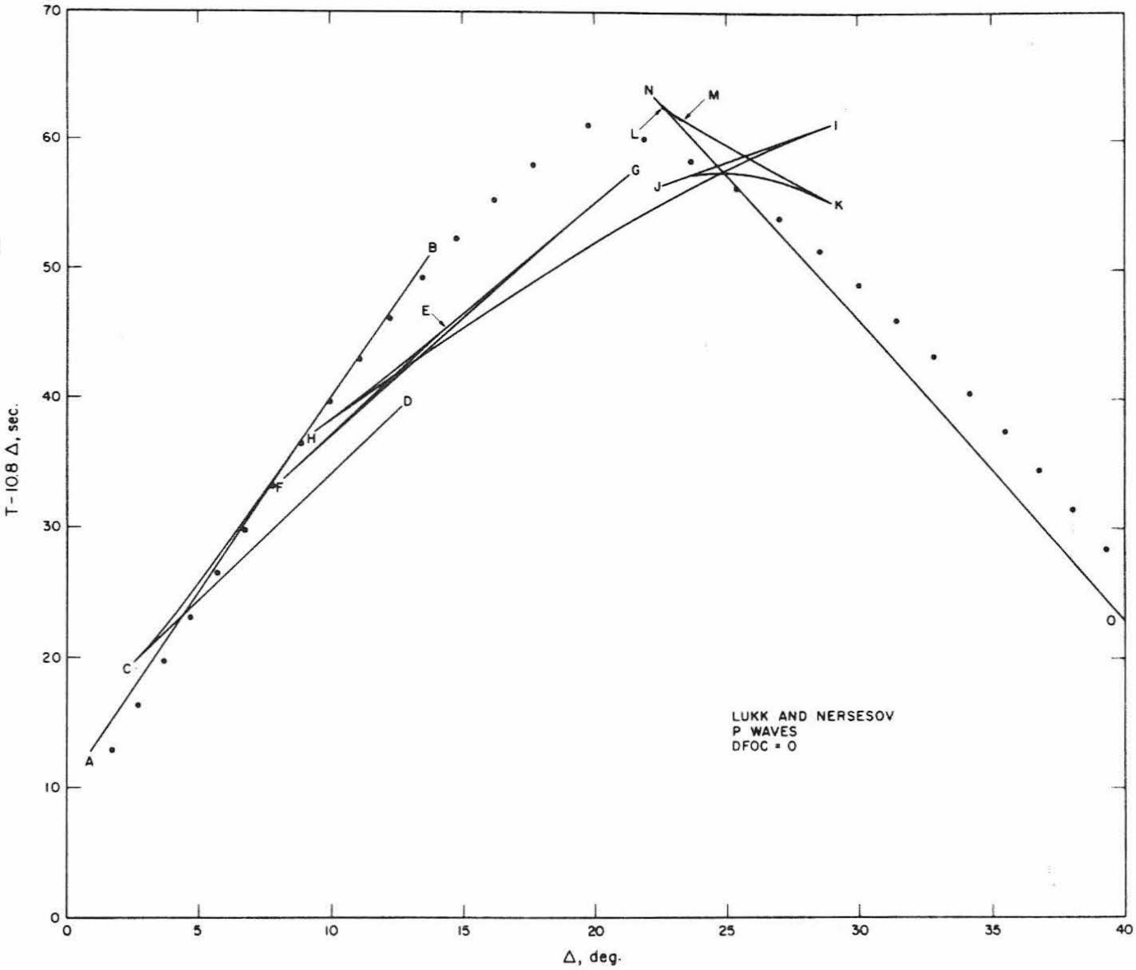

LUKK AND NERSESOV
P WAVES
DFOC = 0
T-10.8 Δ, sec.
Δ, deg.
A
B
C
D
E
F
G
H
I
J
K
L
M
N
O
0
5
10
15
20
25
30
35
40
0
10
20
30
40
50
60
70

Figure 20

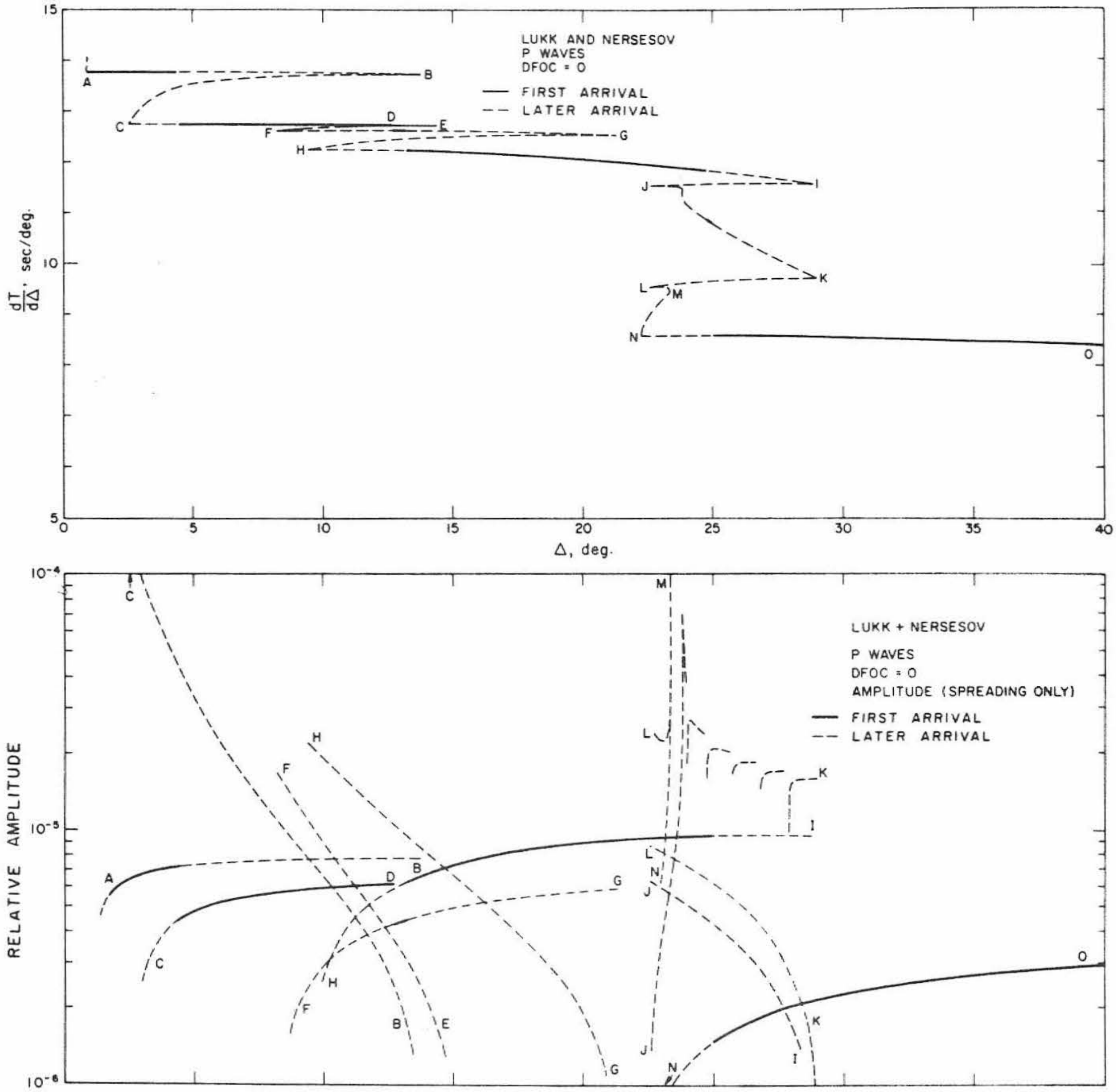
LUKK AND NERSESOV
P WAVES
DFOC = 0
FIRST ARRIVAL
LATER ARRIVAL
$\frac{dT}{d\Delta}$, sec/deg.
Δ, deg.
LUKK + NERSESOV
P WAVES
DFOC = 0
AMPLITUDE (SPREADING ONLY)
FIRST ARRIVAL
LATER ARRIVAL
RELATIVE AMPLITUDE

Figure 21

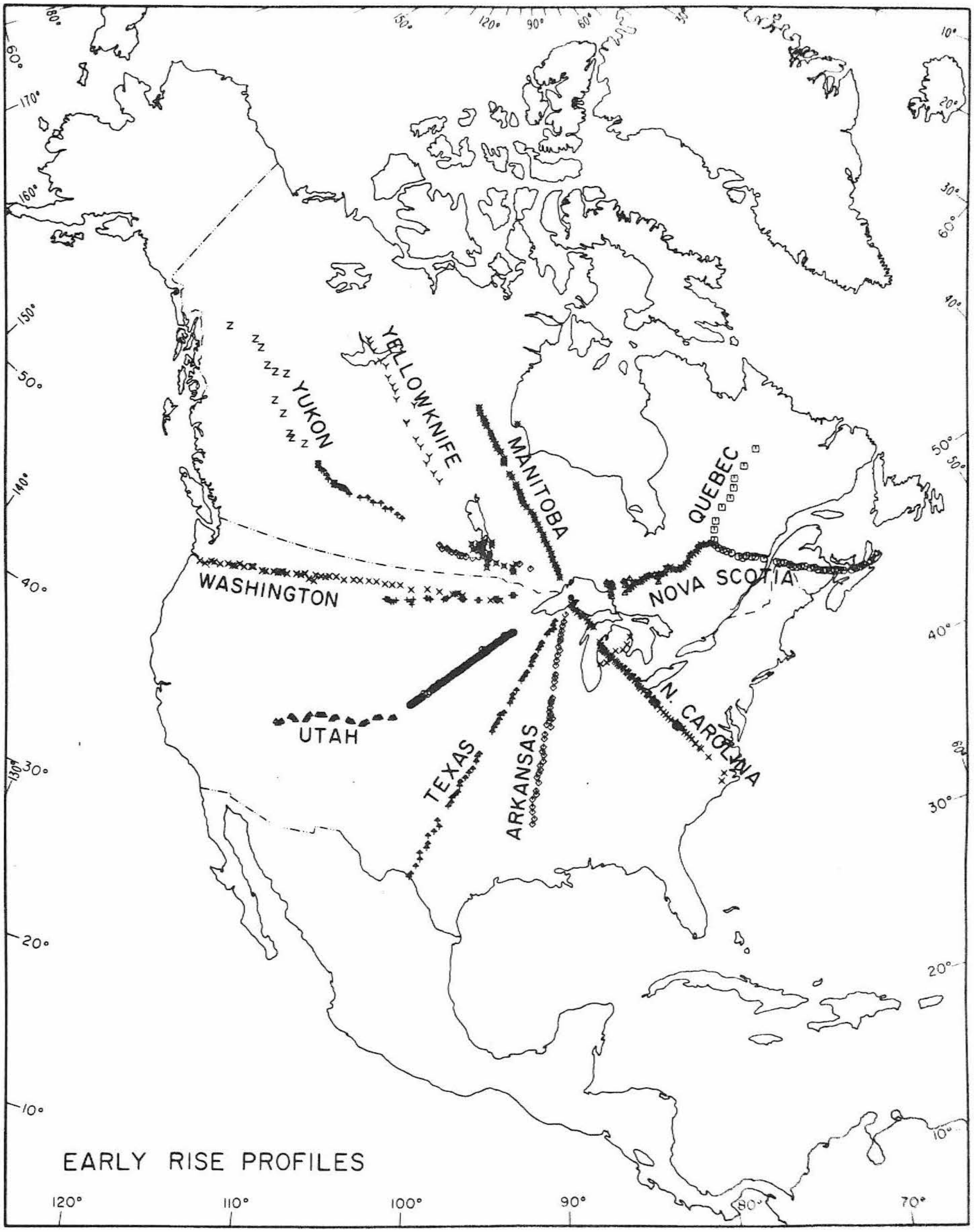
EARLY RISE PROFILES
YUKON
YELLOWKNIFE
MANITOBA
QUEBEC
WASHINGTON
NOVA SCOTIA
UTAH
TEXAS
ARKANSAS
N. CAROLINA
120°
110°
100°
90°
80°
70°
10°
20°
30°
40°
50°
60°

Figure 22

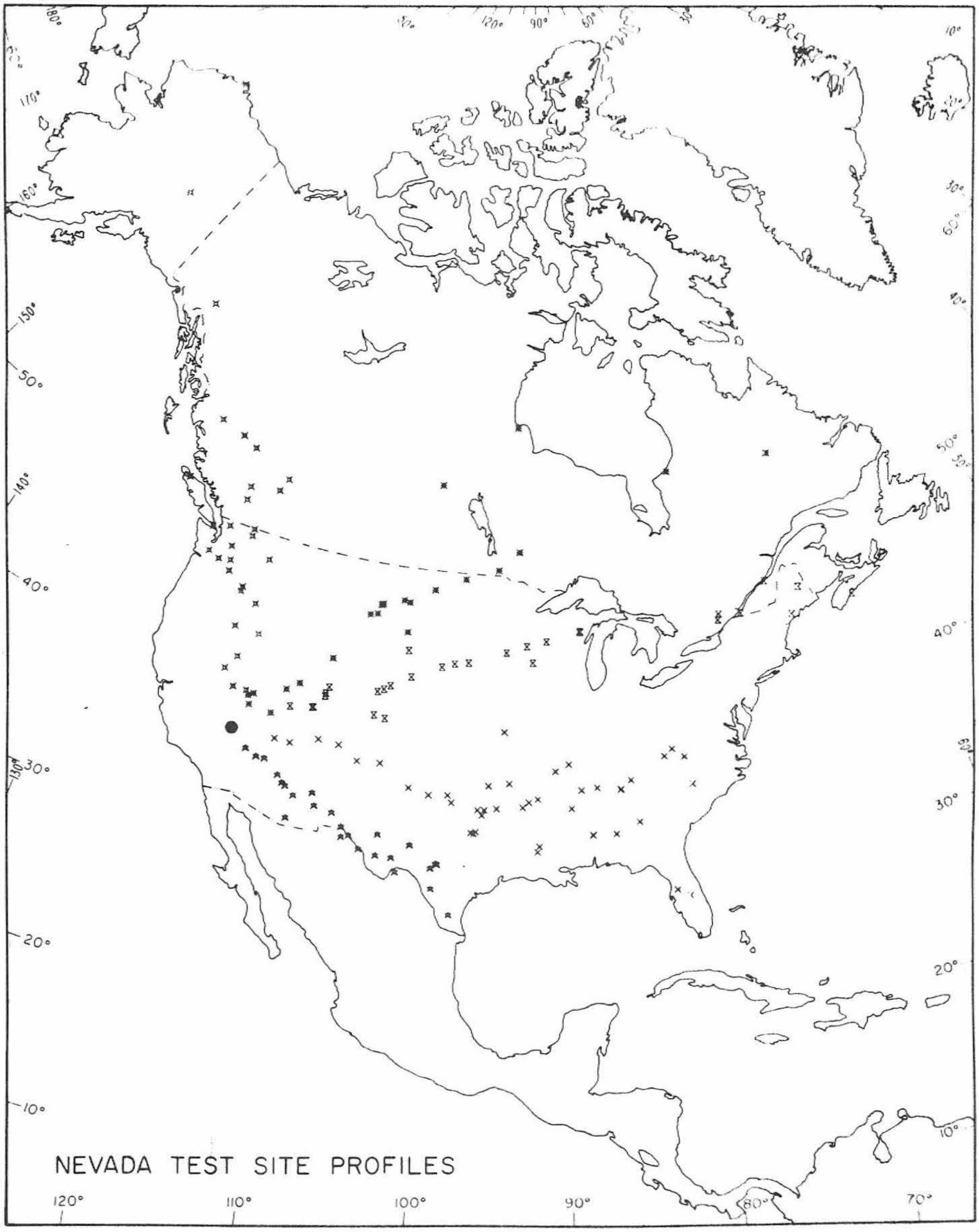

Figure 23

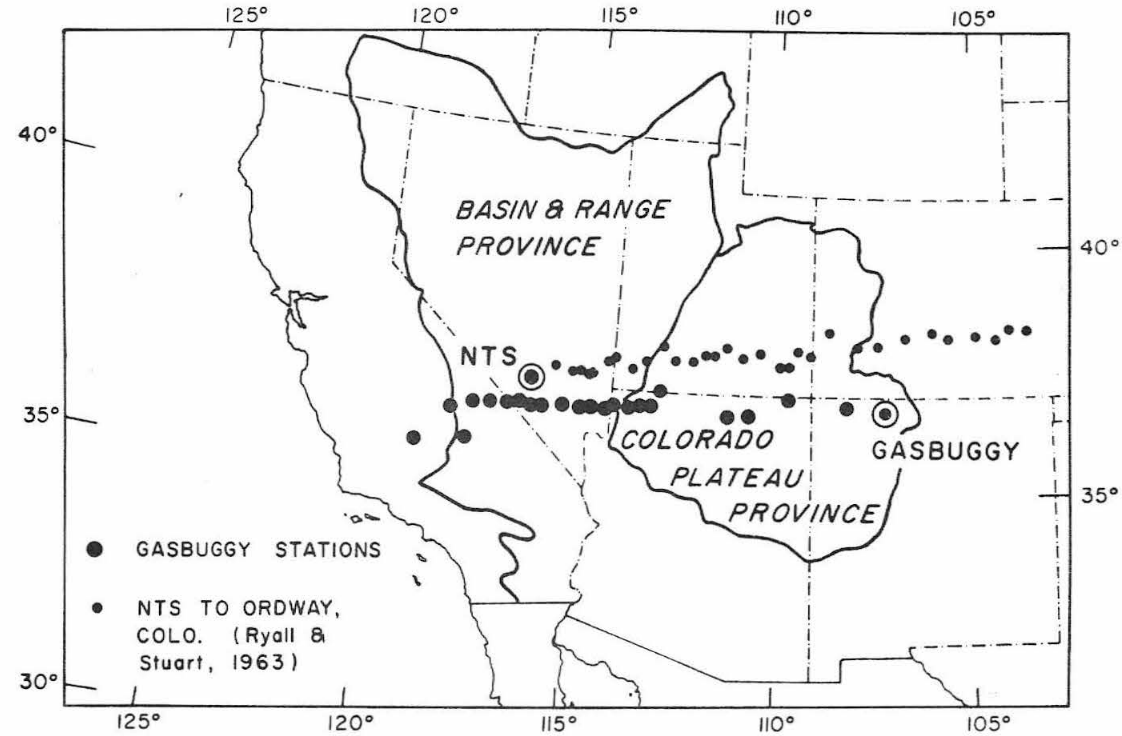

125°
120°
115°
110°
105°
40°
35°
30°
BASIN & RANGE PROVINCE
NTS
COLORADO PLATEAU PROVINCE
GASBUGGY
GASBUGGY STATIONS
NTS TO ORDWAY, COLO. (Ryall & Stuart, 1963)

Figure 24

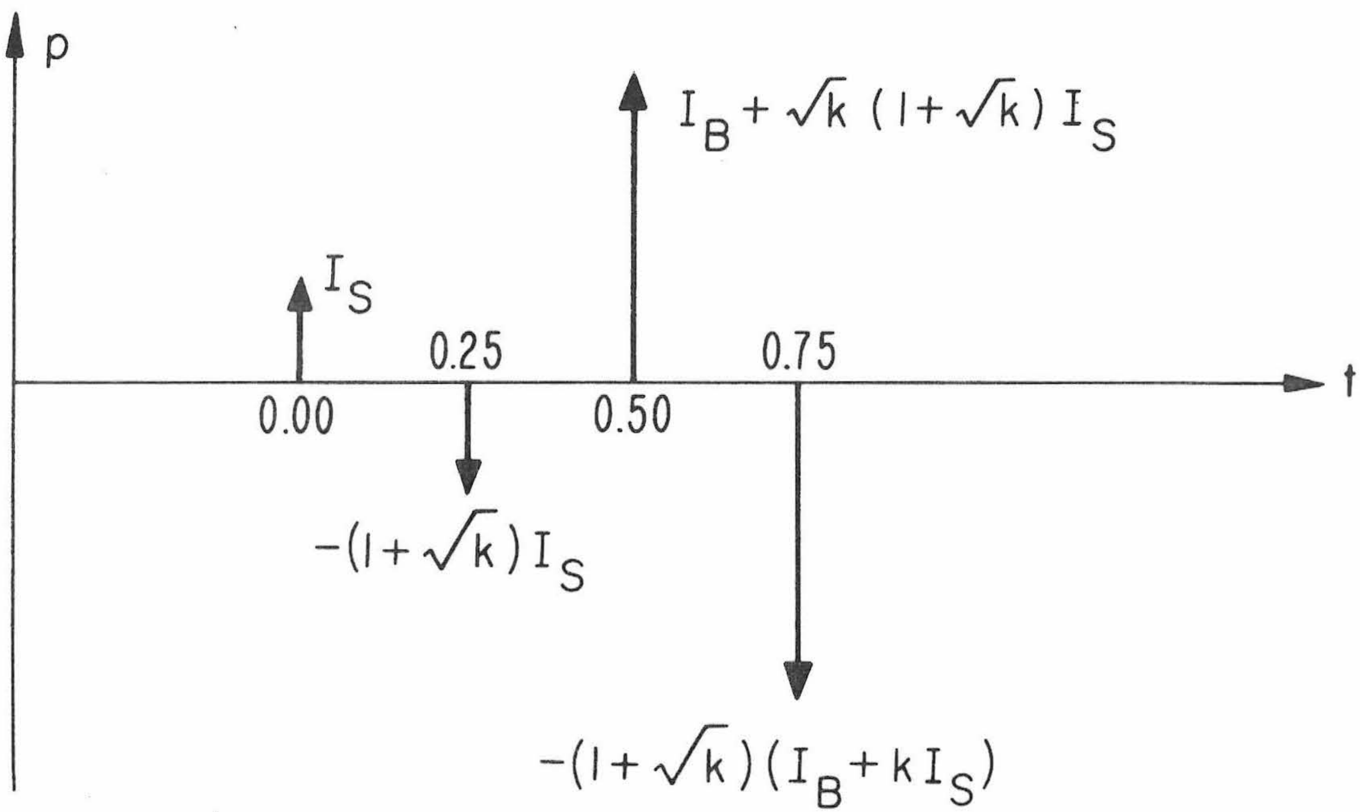
p
t
I_S
0.00
0.25
0.50
0.75
$I_B + \sqrt{k}\,(1+\sqrt{k})\,I_S$
$-(1+\sqrt{k})\,I_S$
$-(1+\sqrt{k})(I_B + k I_S)$

Figure 25

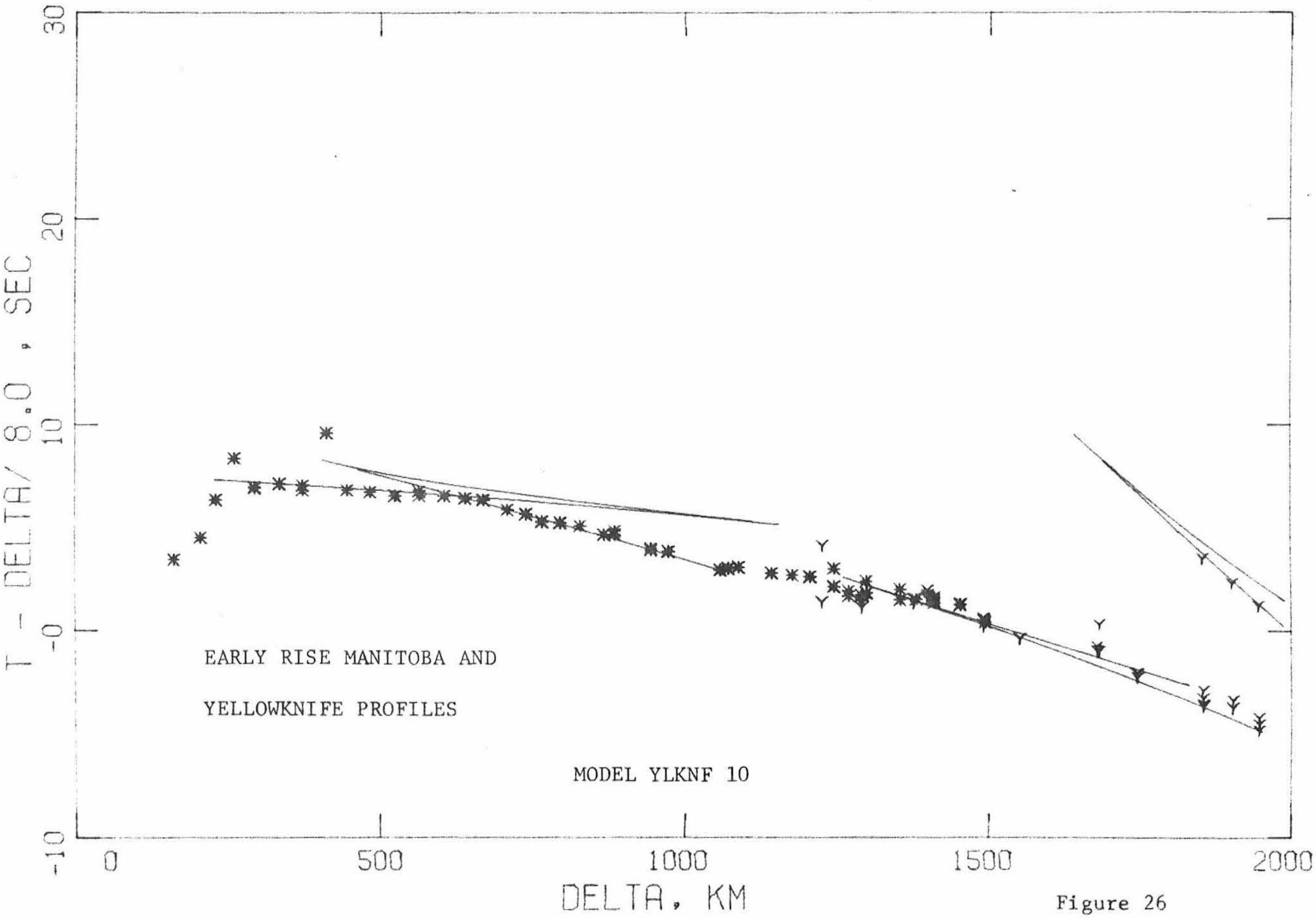
30
20
10
-0
-10
T - DELTA/ 8.0 , SEC
0
500
1000
1500
2000
DELTA, KM
EARLY RISE MANITOBA AND
YELLOWKNIFE PROFILES
MODEL YLKNF 10

Figure 26

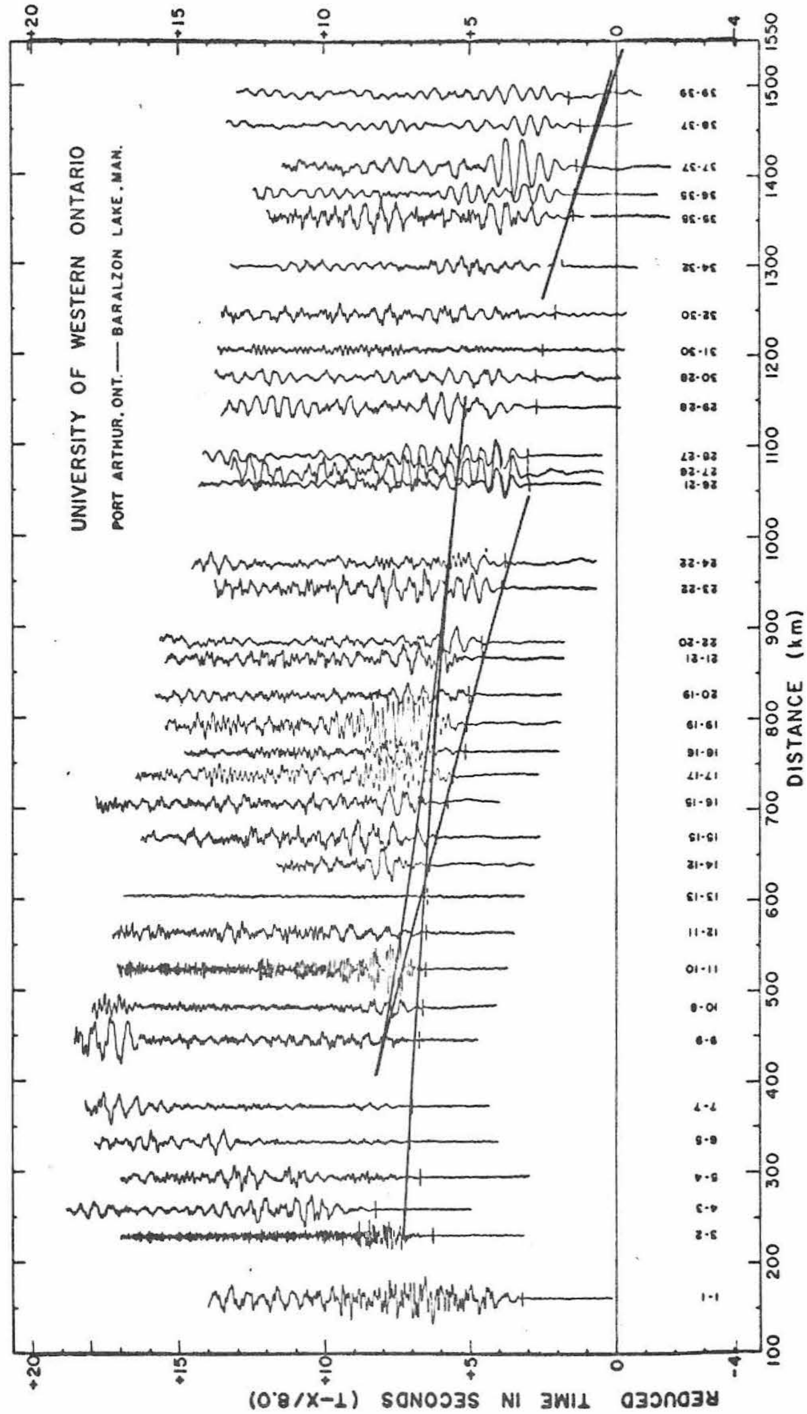
UNIVERSITY OF WESTERN ONTARIO
PORT ARTHUR, ONT. — BARALZON LAKE, MAN.
DISTANCE (km)
REDUCED TIME IN SECONDS (T-X/8.0)

Figure 27

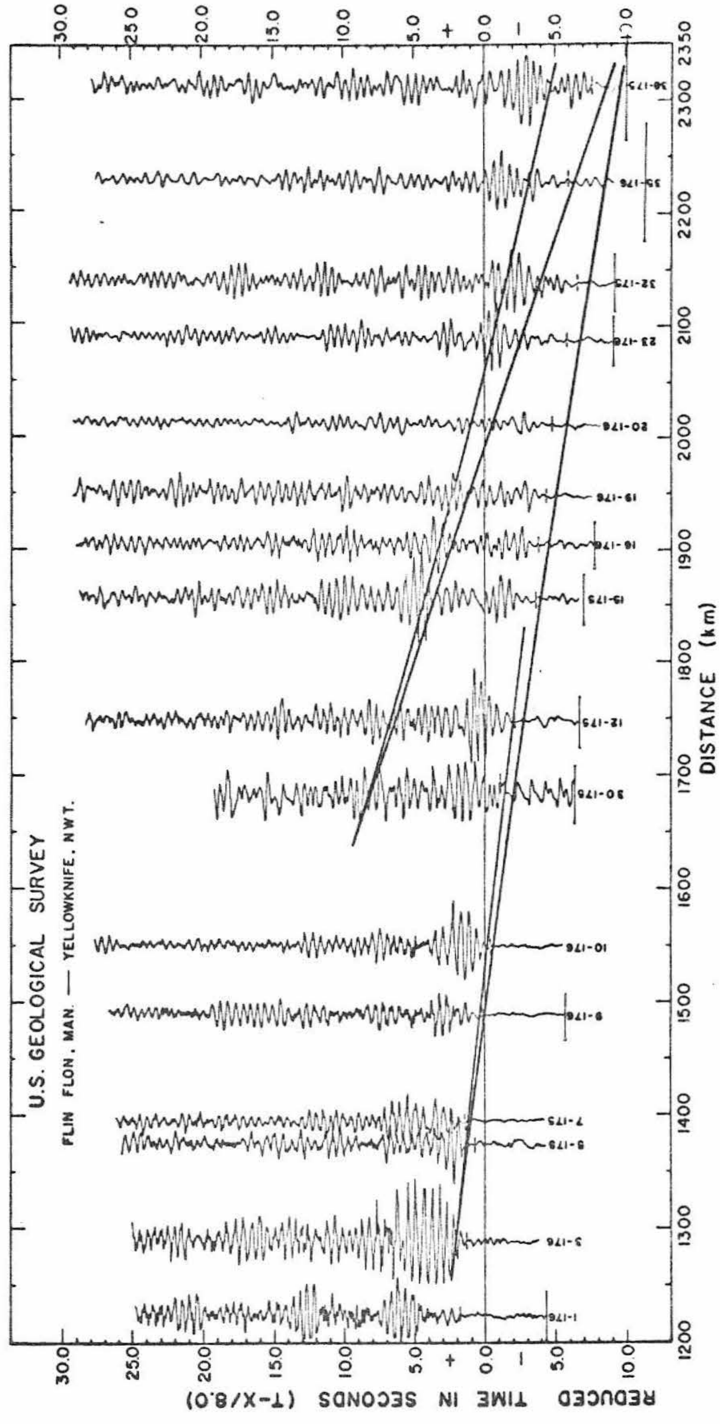
U.S. GEOLOGICAL SURVEY
FLIN FLON, MAN. — YELLOWKNIFE, NWT.
DISTANCE (km)
REDUCED TIME IN SECONDS (T-X/8.0)

Figure 28

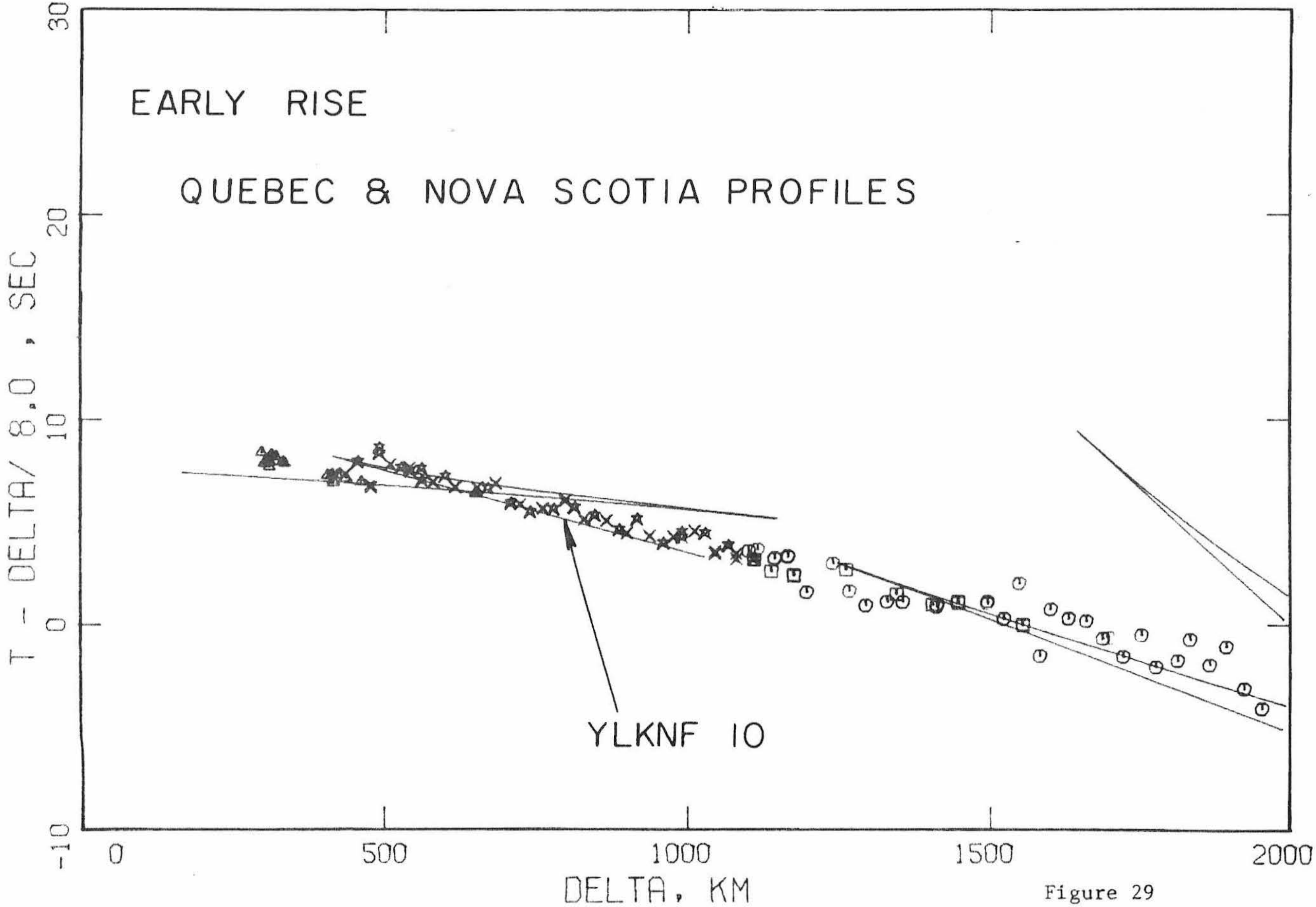
EARLY RISE
QUEBEC & NOVA SCOTIA PROFILES
YLKNF 10
T - DELTA/ 8.0 , SEC
DELTA, KM
30
20
10
0
-10
0
500
1000
1500
2000

Figure 29

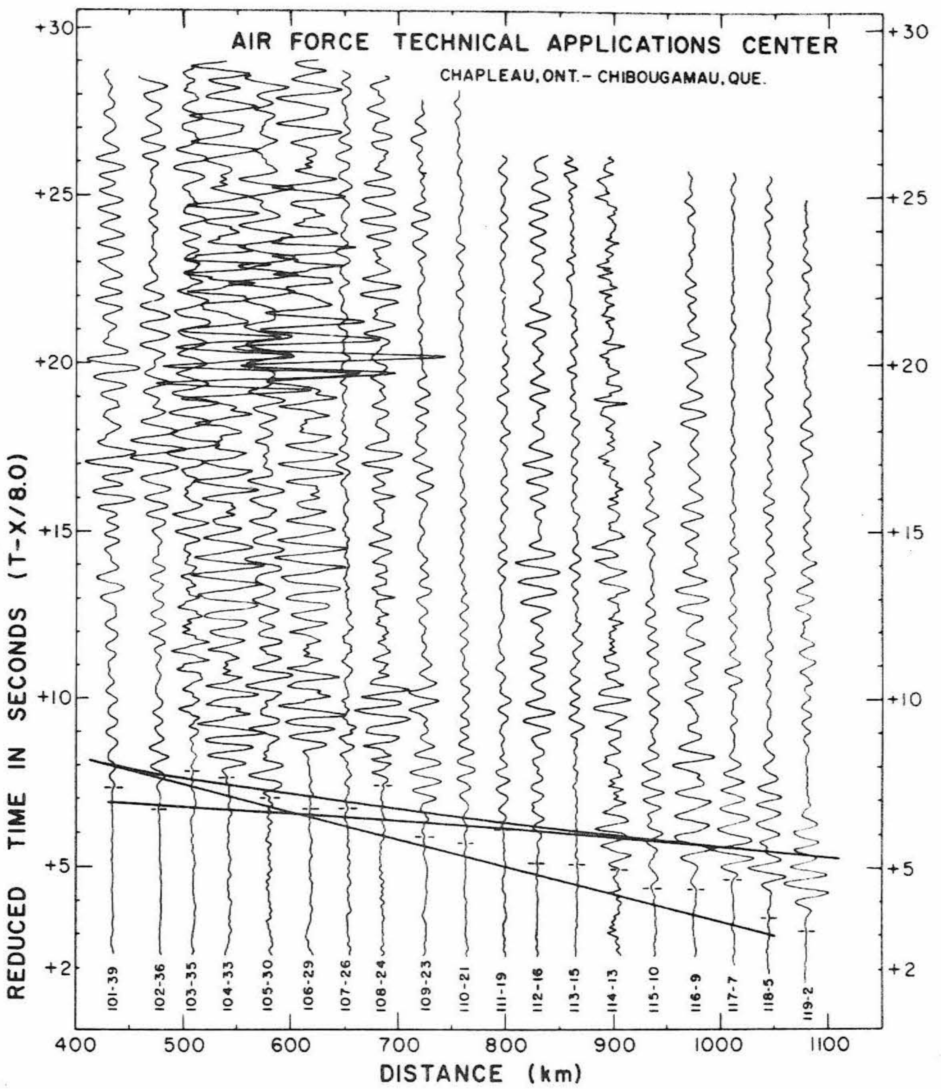

AIR FORCE TECHNICAL APPLICATIONS CENTER
CHAPLEAU, ONT. - CHIBOUGAMAU, QUE.
REDUCED TIME IN SECONDS (T-X/8.0)
DISTANCE (km)
+30
+25
+20
+15
+10
+5
+2
400
500
600
700
800
900
1000
1100
101-39
102-36
103-35
104-33
105-30
106-29
107-26
108-24
109-23
110-21
111-19
112-16
113-15
114-13
115-10
116-9
117-7
118-5
119-2

Figure 30

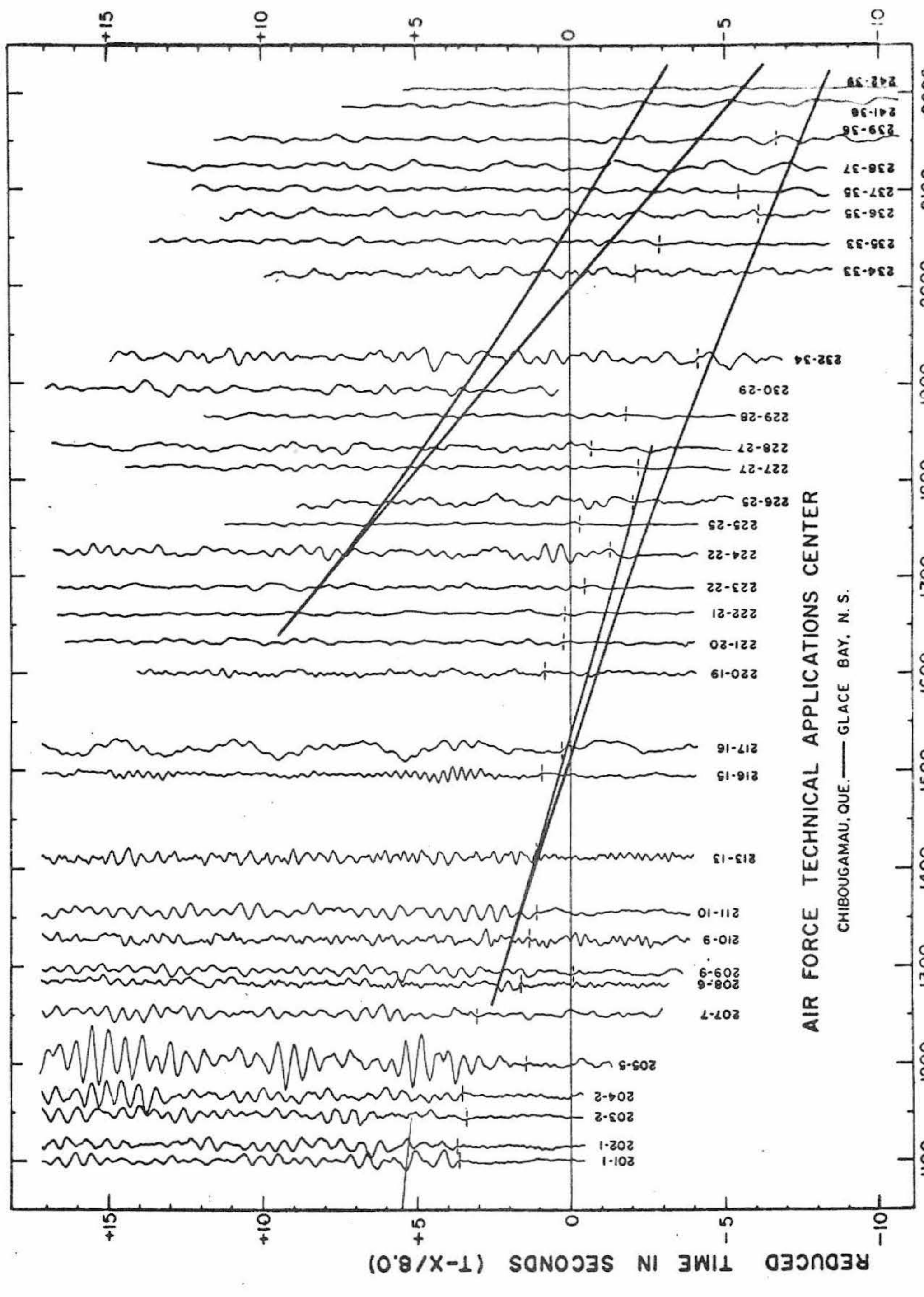
AIR FORCE TECHNICAL APPLICATIONS CENTER
CHIBOUGAMAU, QUE. —— GLACE BAY, N. S.
DISTANCE (km)
REDUCED TIME IN SECONDS (T-X/8.0)

Figure 31

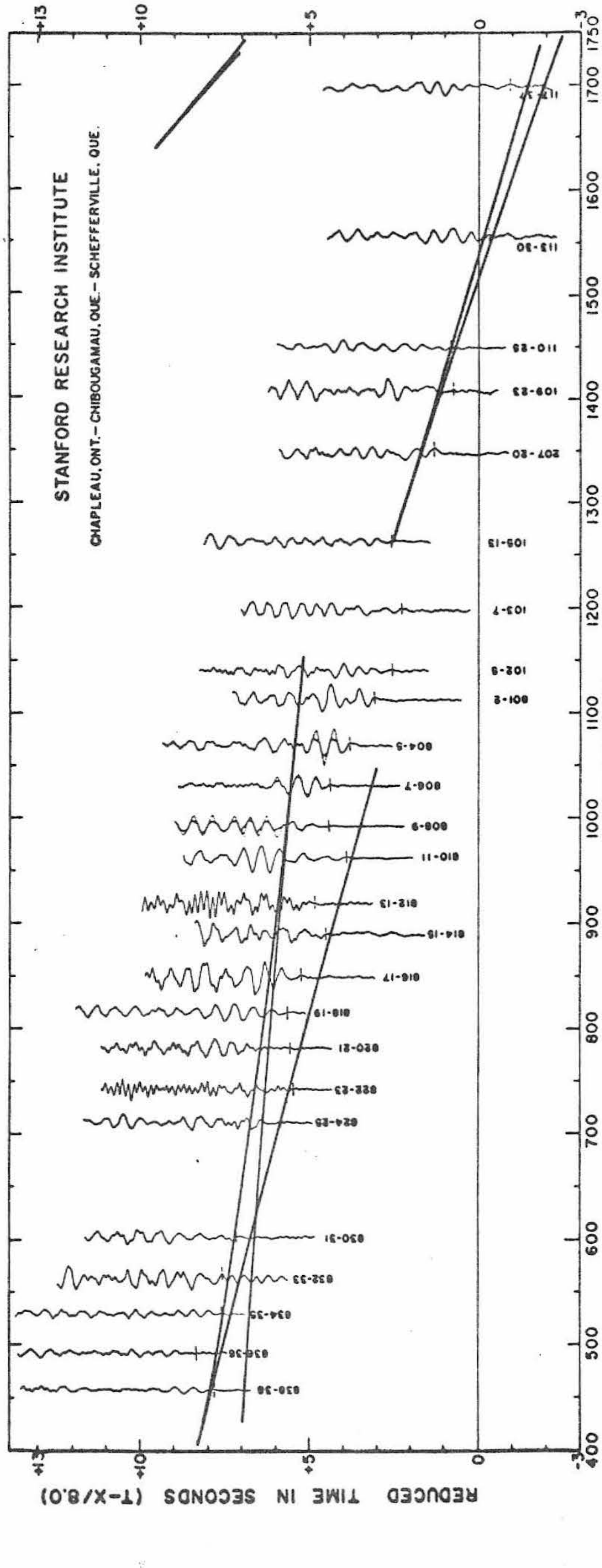
STANFORD RESEARCH INSTITUTE
CHAPLEAU, ONT.-CHIBOUGAMAU, QUE.-SCHEFFERVILLE, QUE.
DISTANCE (km)
REDUCED TIME IN SECONDS (T-X/8.0)

Figure 32

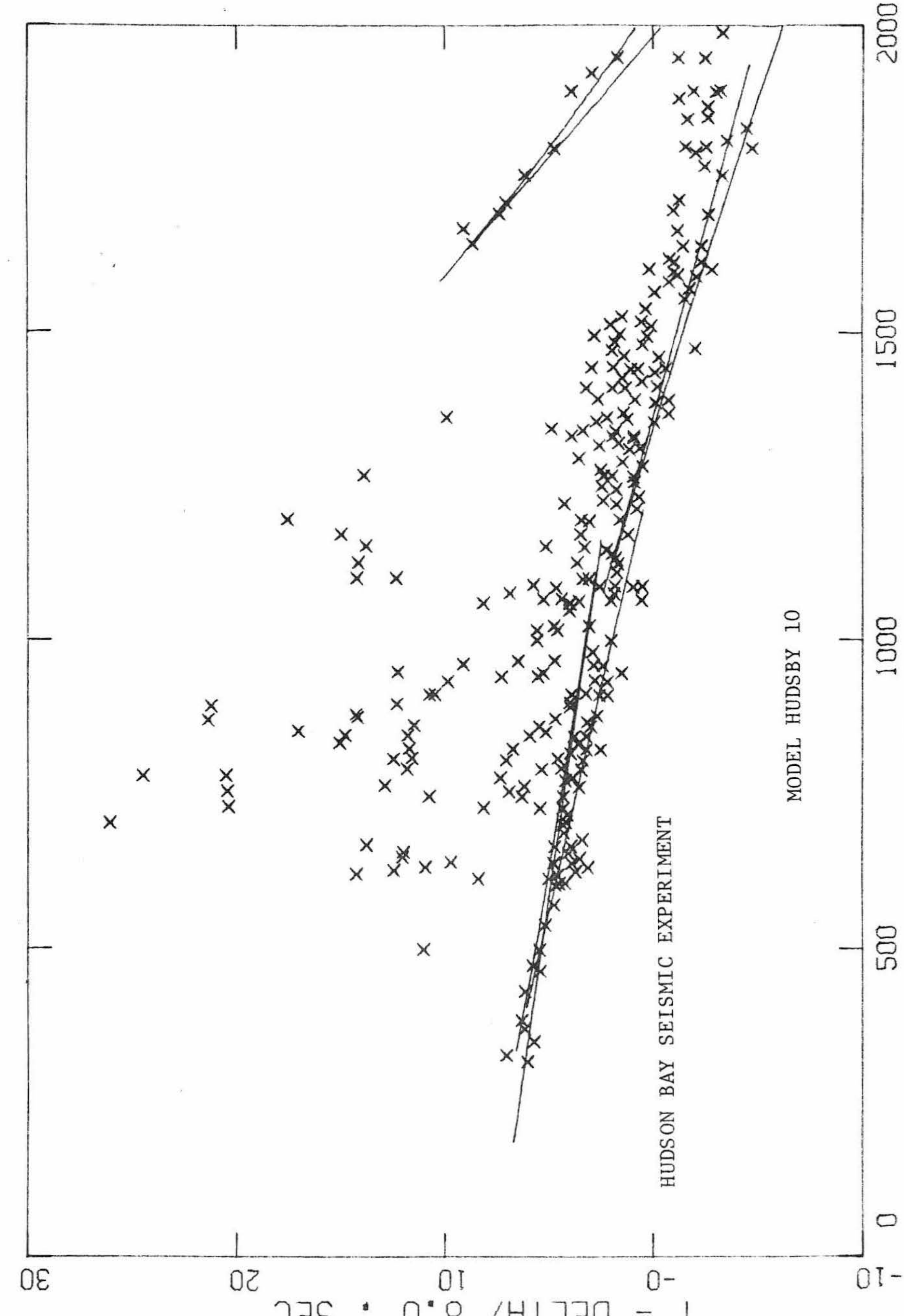
HUDSON BAY SEISMIC EXPERIMENT
MODEL HUDSBY 10
DELTA, KM
T - DELTA/ 8.0 , SEC
0
500
1000
1500
2000
30
20
10
-0
-10

Figure 33

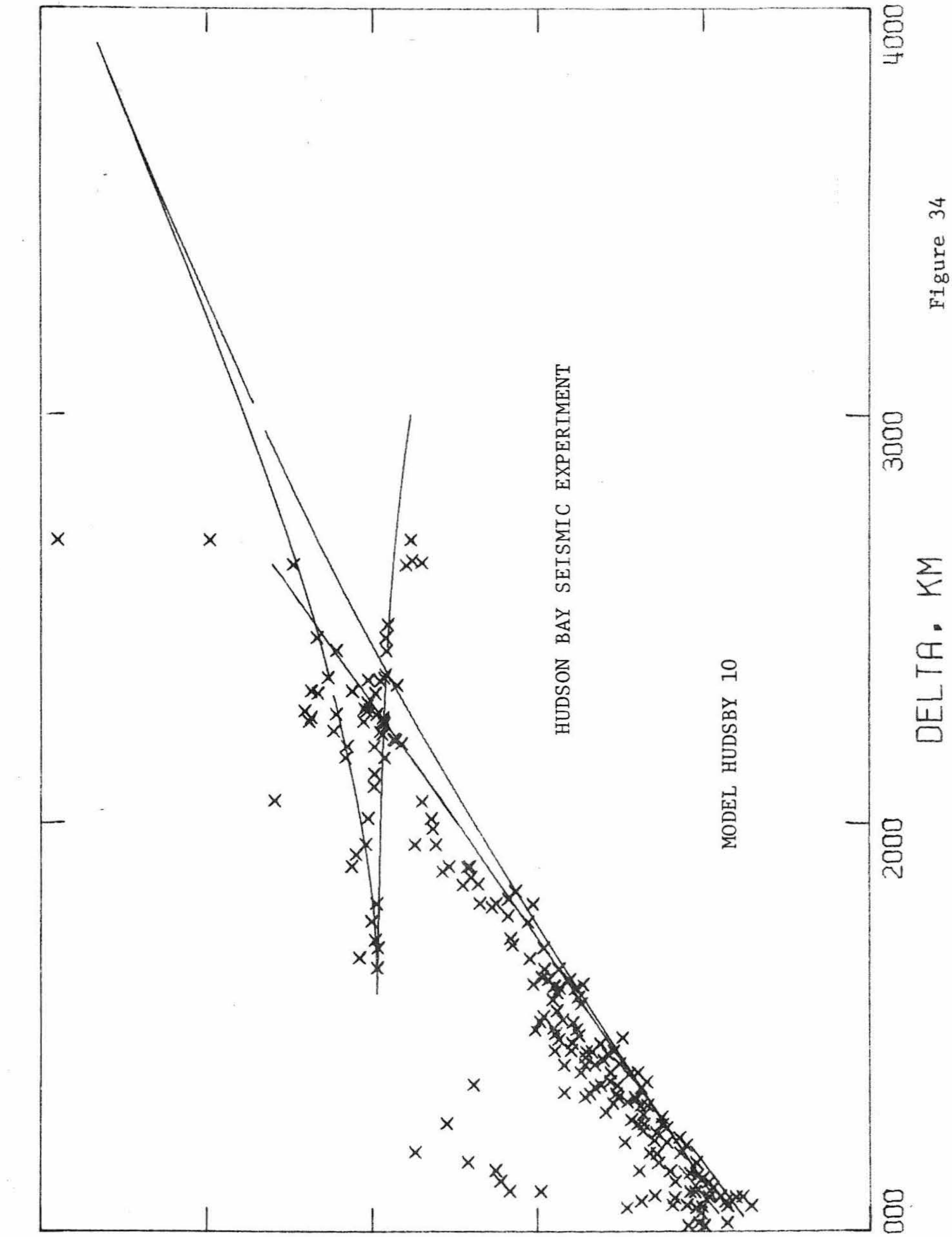
HUDSON BAY SEISMIC EXPERIMENT
MODEL HUDSBY 10
DELTA, KM
T - DELTA/10.0 , SEC
1000
2000
3000
4000
20
30
40
50
60
70

Figure 34

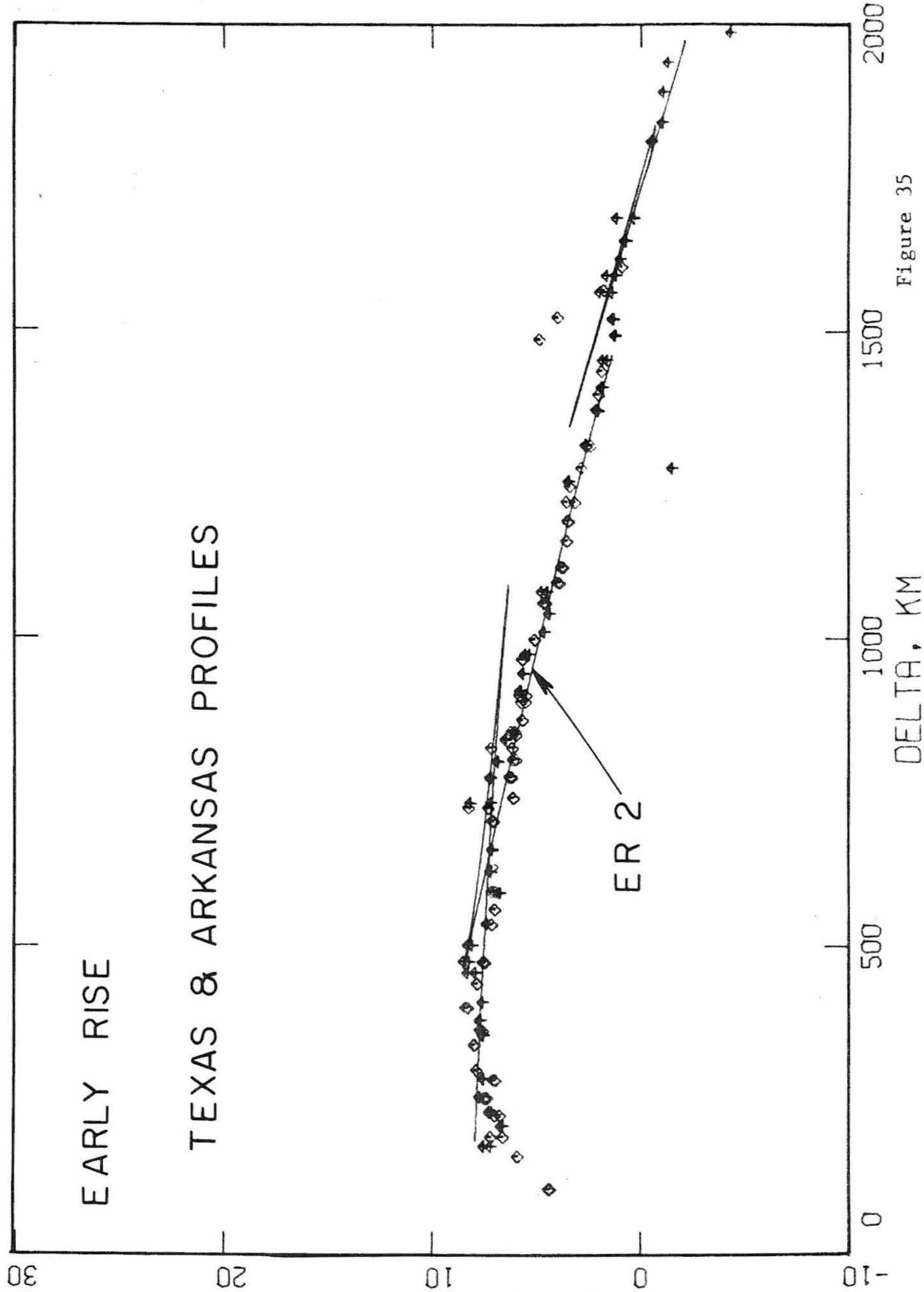
EARLY RISE
TEXAS & ARKANSAS PROFILES
ER 2
0
500
1000
1500
2000
DELTA, KM
-10
0
10
20
30
T - DELTA/ 8.0 , SEC

Figure 35

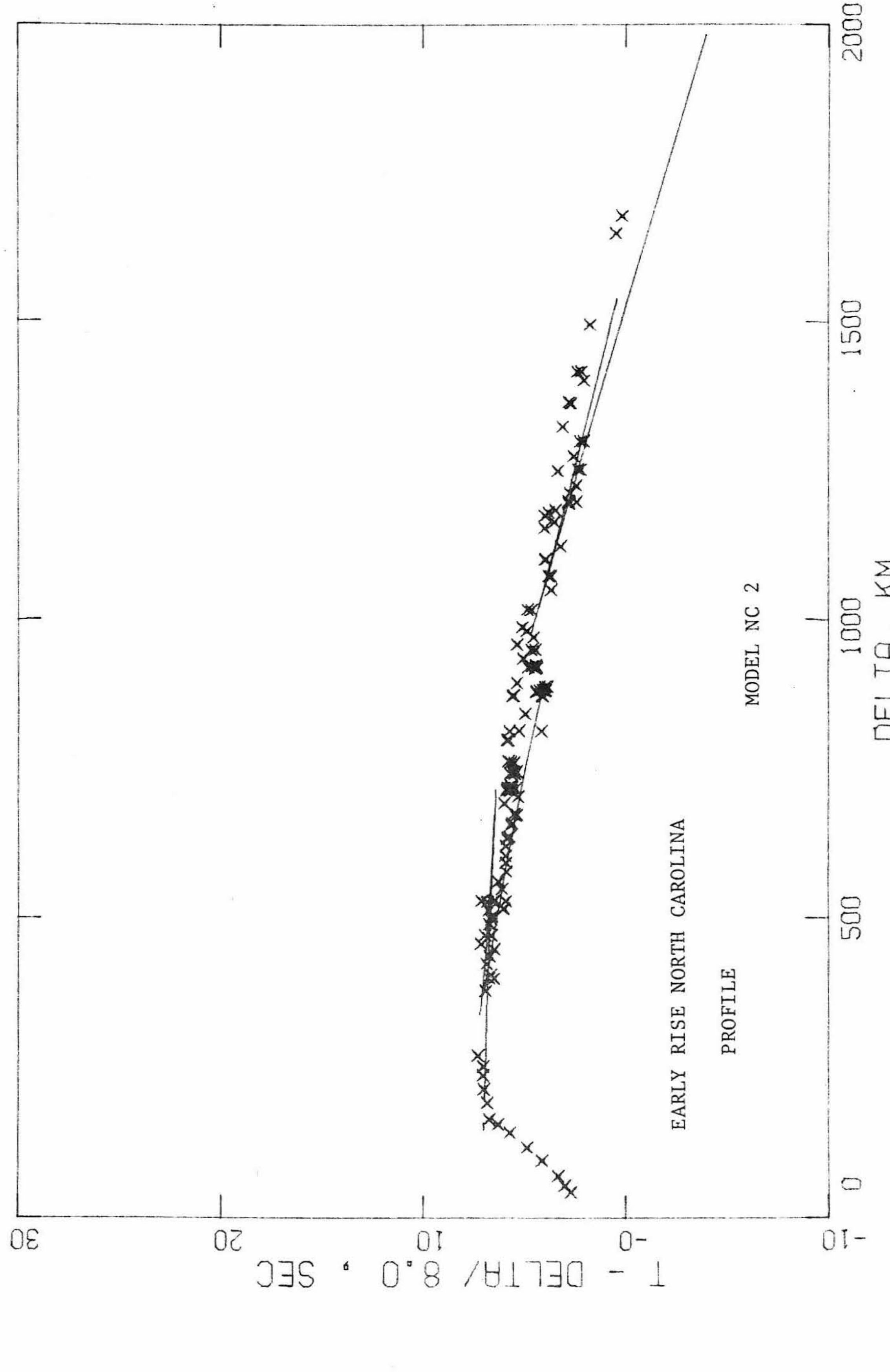
EARLY RISE NORTH CAROLINA
PROFILE
MODEL NC 2
DELTA, KM
T - DELTA/ 8.0 , SEC
0
500
1000
1500
2000
-10
-0
10
20
30

Figure 36

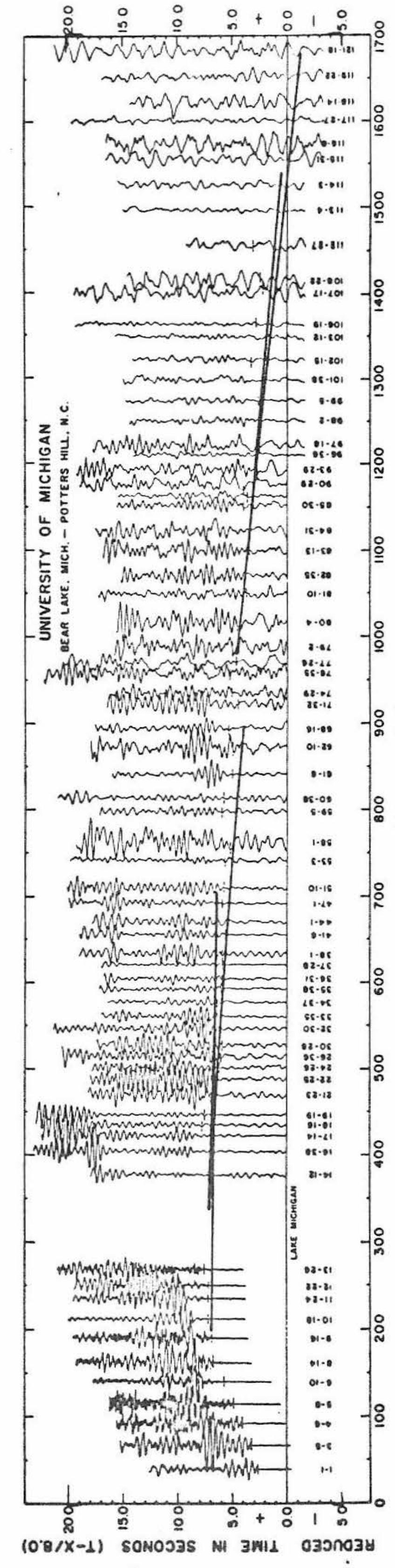
UNIVERSITY OF MICHIGAN
BEAR LAKE, MICH. – POTTERS HILL, N.C.
LAKE MICHIGAN
DISTANCE (km)
REDUCED TIME IN SECONDS (T-X/8.0)

Figure 37

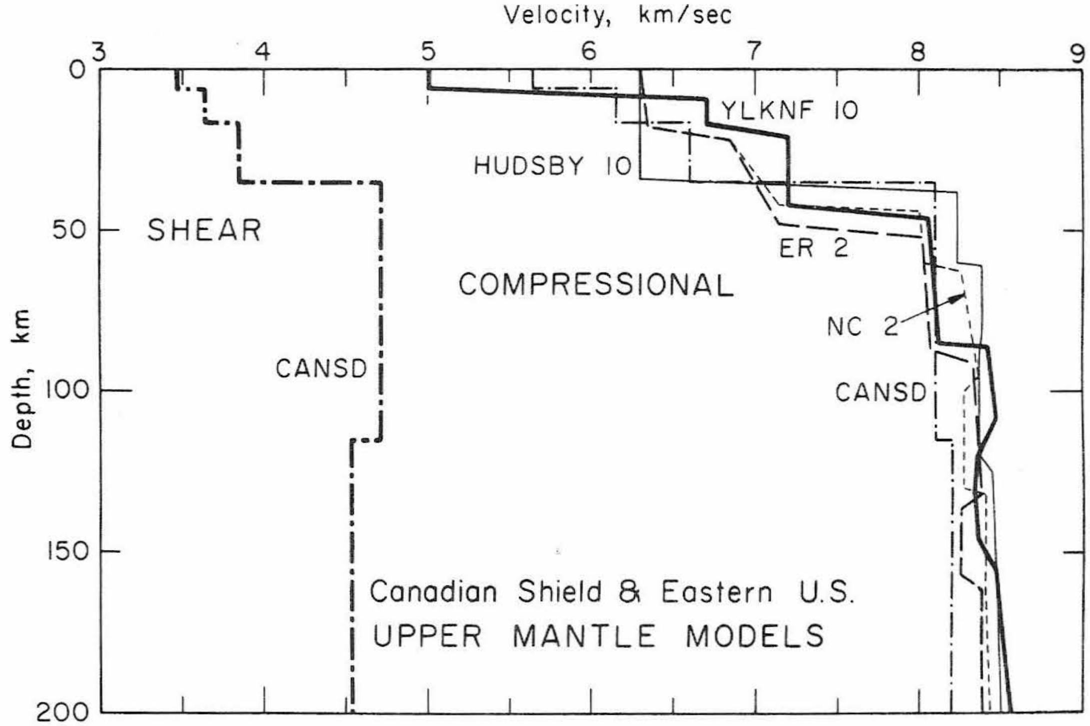

Velocity, km/sec
3
4
5
6
7
8
9
0
50
100
150
200
Depth, km
SHEAR
COMPRESSIONAL
YLKNF 10
HUDSBY 10
ER 2
NC 2
CANSD
CANSD
Canadian Shield & Eastern U.S.
UPPER MANTLE MODELS

Figure 38

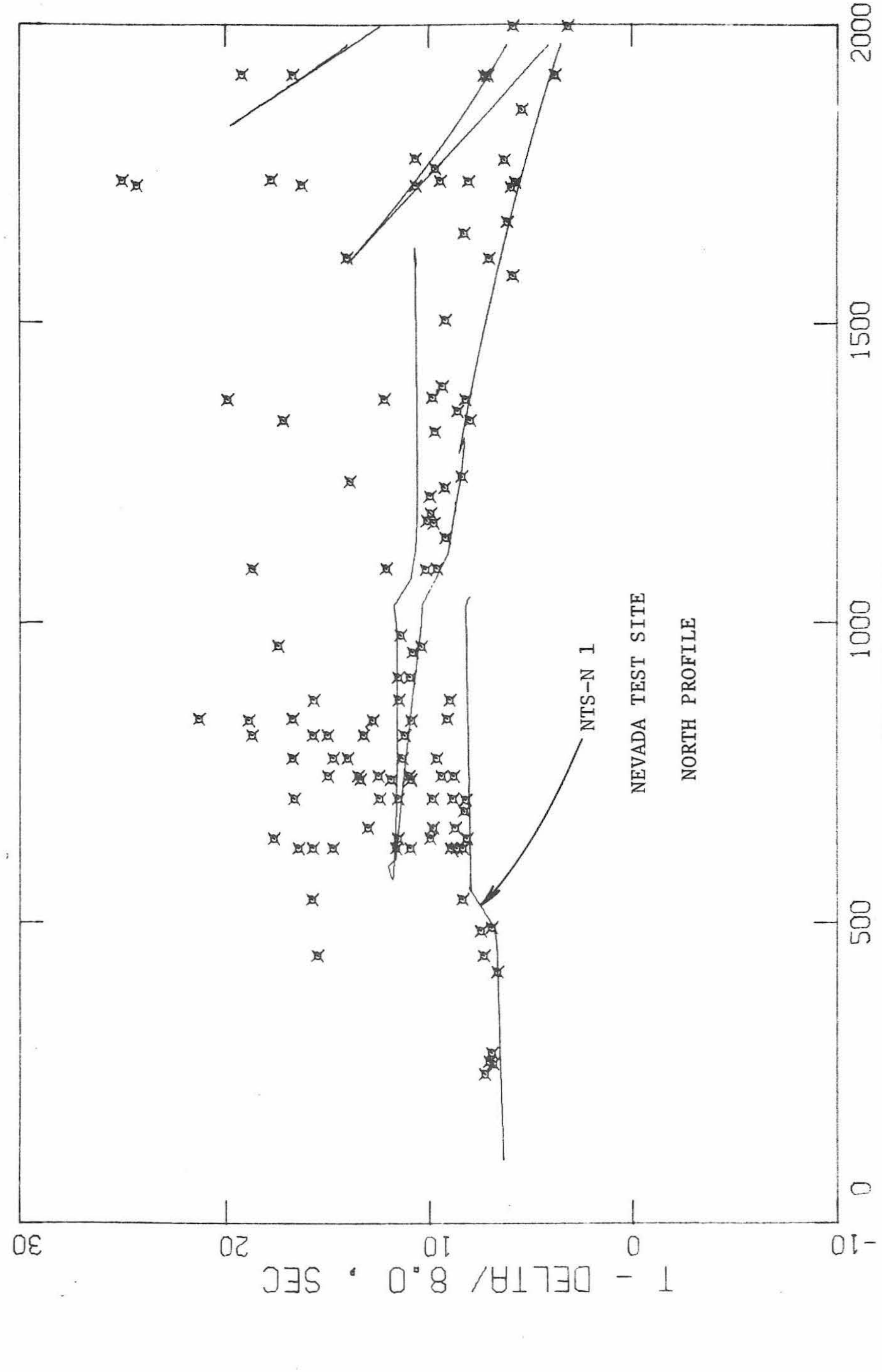
NTS-N 1
NEVADA TEST SITE
NORTH PROFILE
DELTA, KM
T - DELTA/ 8.0 , SEC
0
500
1000
1500
2000
-10
0
10
20
30

Figure 39

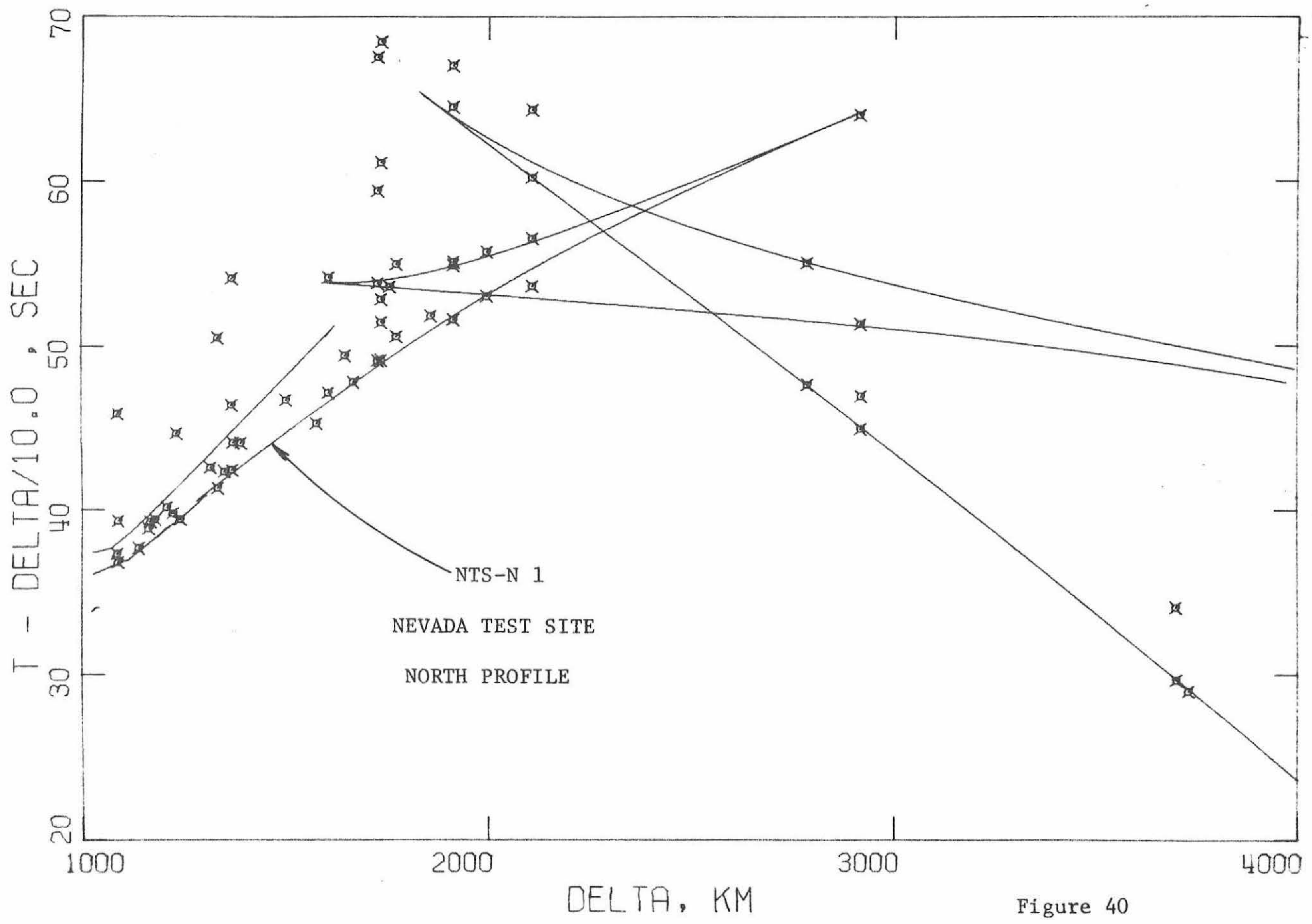

70
60
50
40
30
20
T - DELTA/10.0 , SEC
1000
2000
3000
4000
DELTA, KM
NTS-N 1
NEVADA TEST SITE
NORTH PROFILE

Figure 40

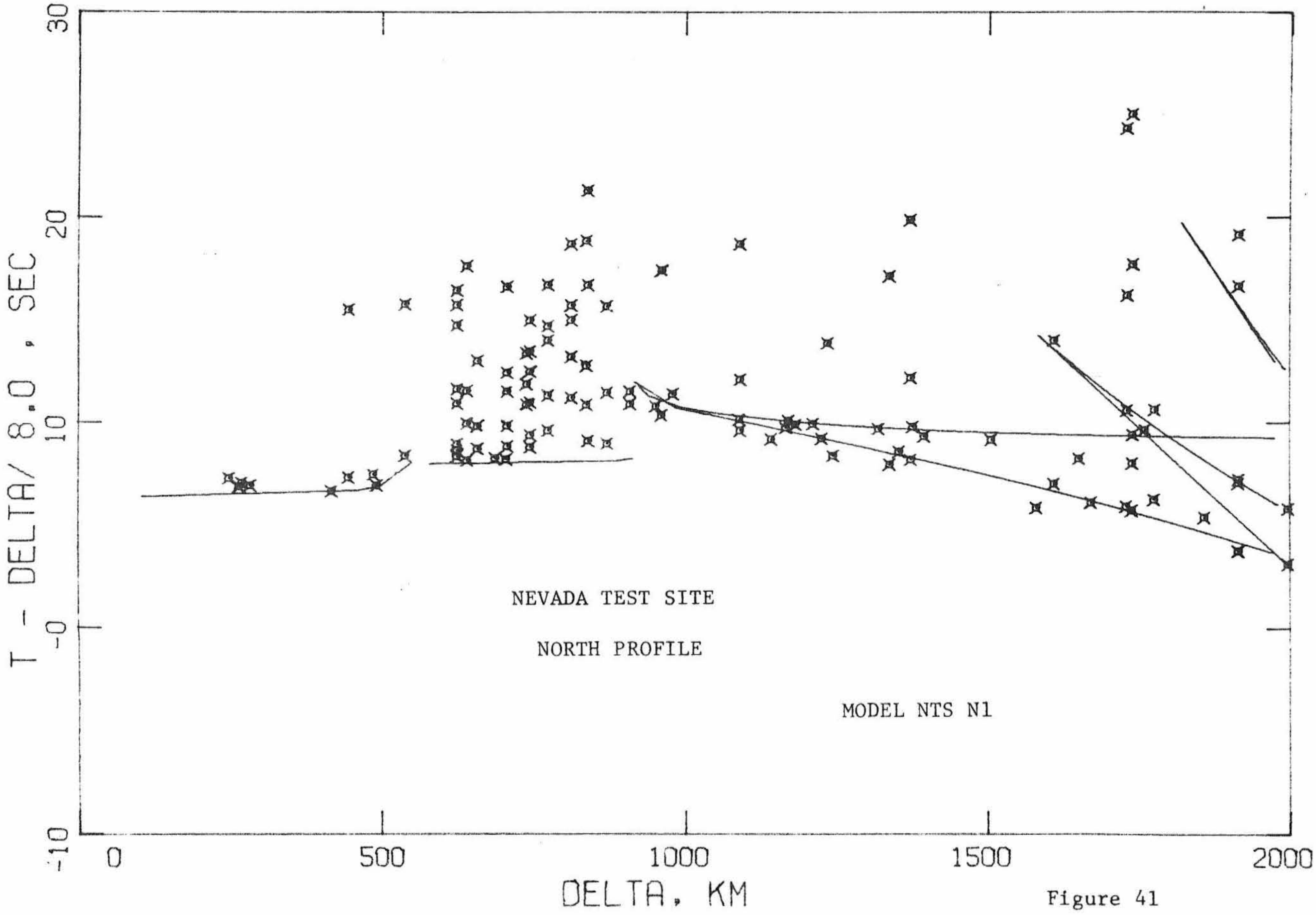

30
20
10
-0
-10
T - DELTA/ 8.0 , SEC
0
500
1000
1500
2000
DELTA, KM
NEVADA TEST SITE
NORTH PROFILE
MODEL NTS N1

Figure 41

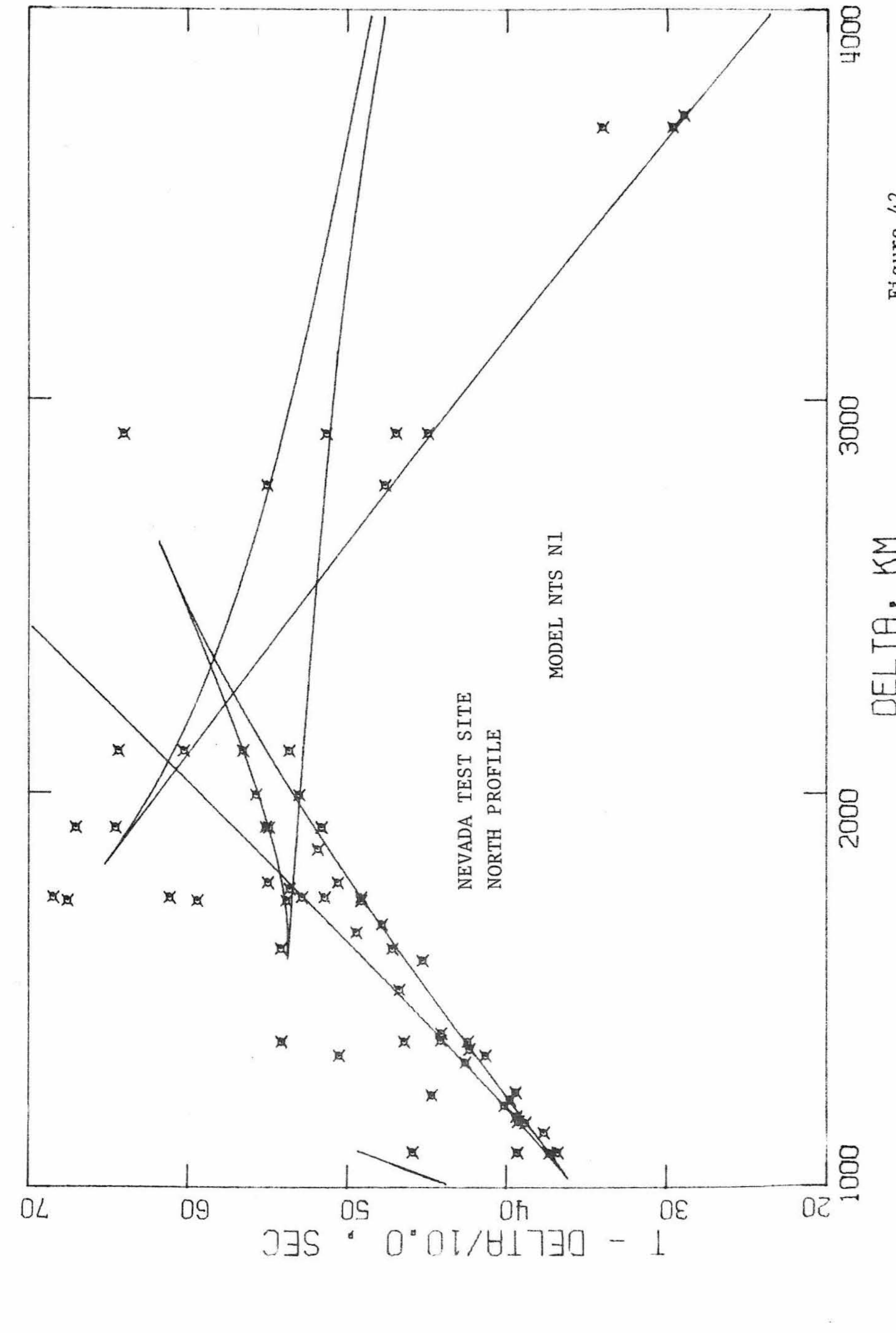

NEVADA TEST SITE
NORTH PROFILE
MODEL NTS N1
DELTA, KM
T - DELTA/10.0 , SEC
1000
2000
3000
4000
20
30
40
50
60
70

Figure 42

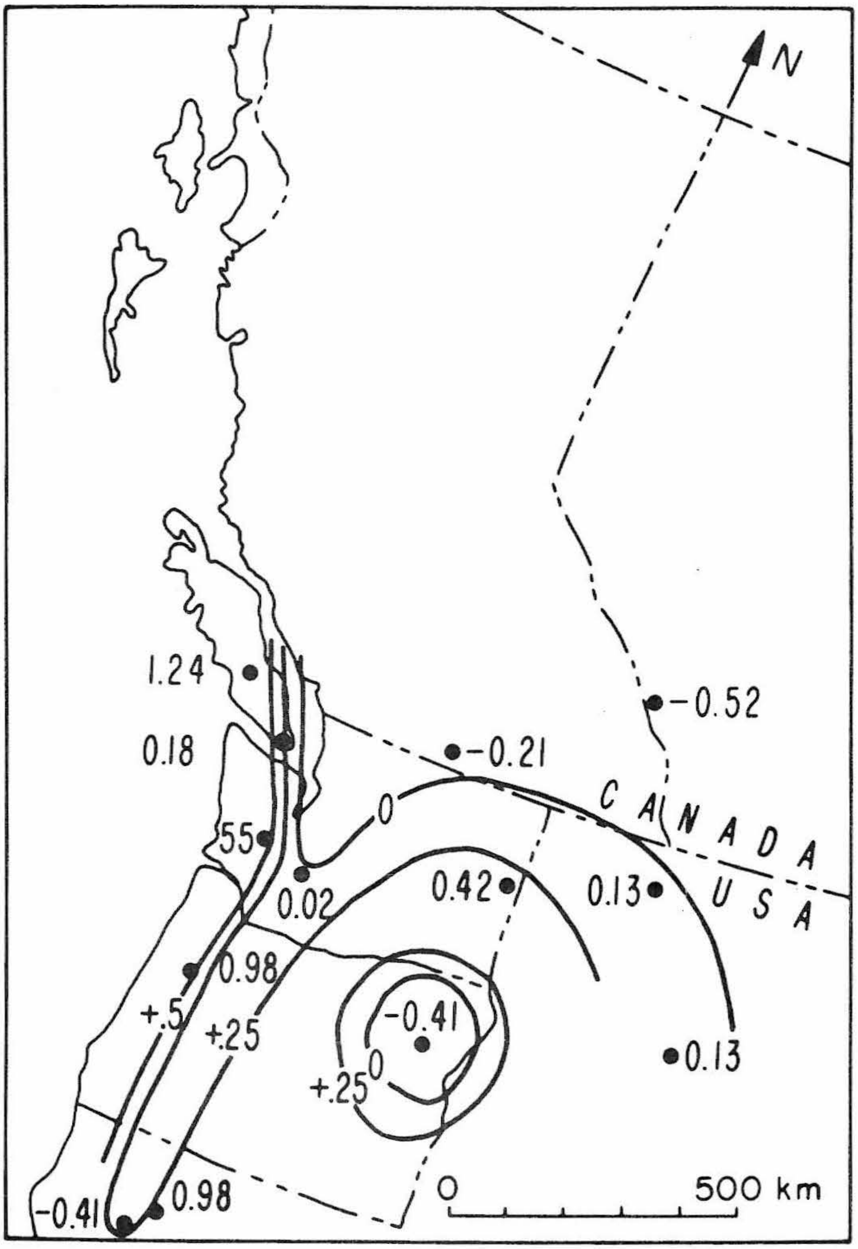
N
1.24
0.18
55
0.02
-0.21
-0.52
0
C A N A D A
U S A
0.42
0.13
0.98
+.5
+.25
-0.41
0
+.25
0.13
-0.41
0.98
0
500 km

Figure 43

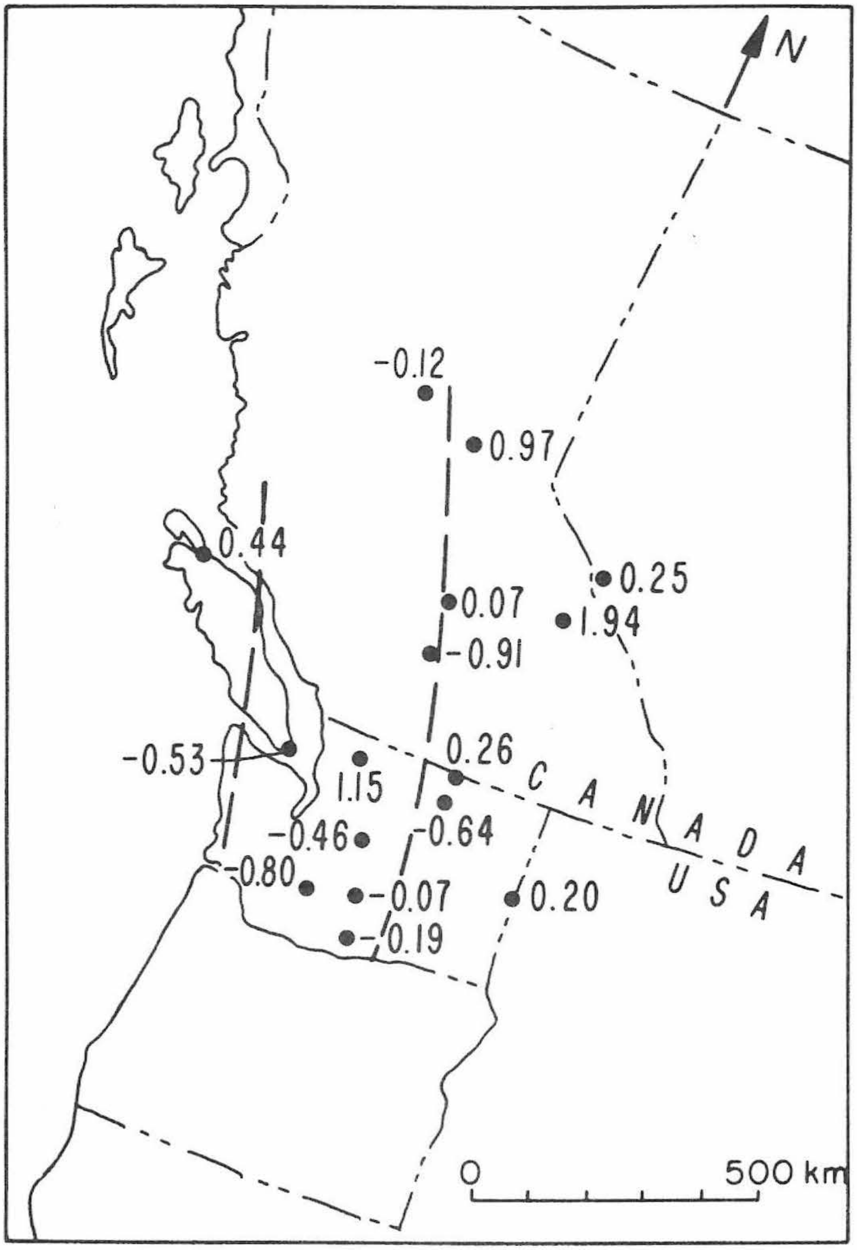
N
-0.12
0.97
0.44
0.25
0.07
1.94
-0.91
-0.53
0.26
1.15
C A N A D A
-0.46
-0.64
-0.80
-0.07
0.20
U S A
-0.19
0
500 km

Figure 44

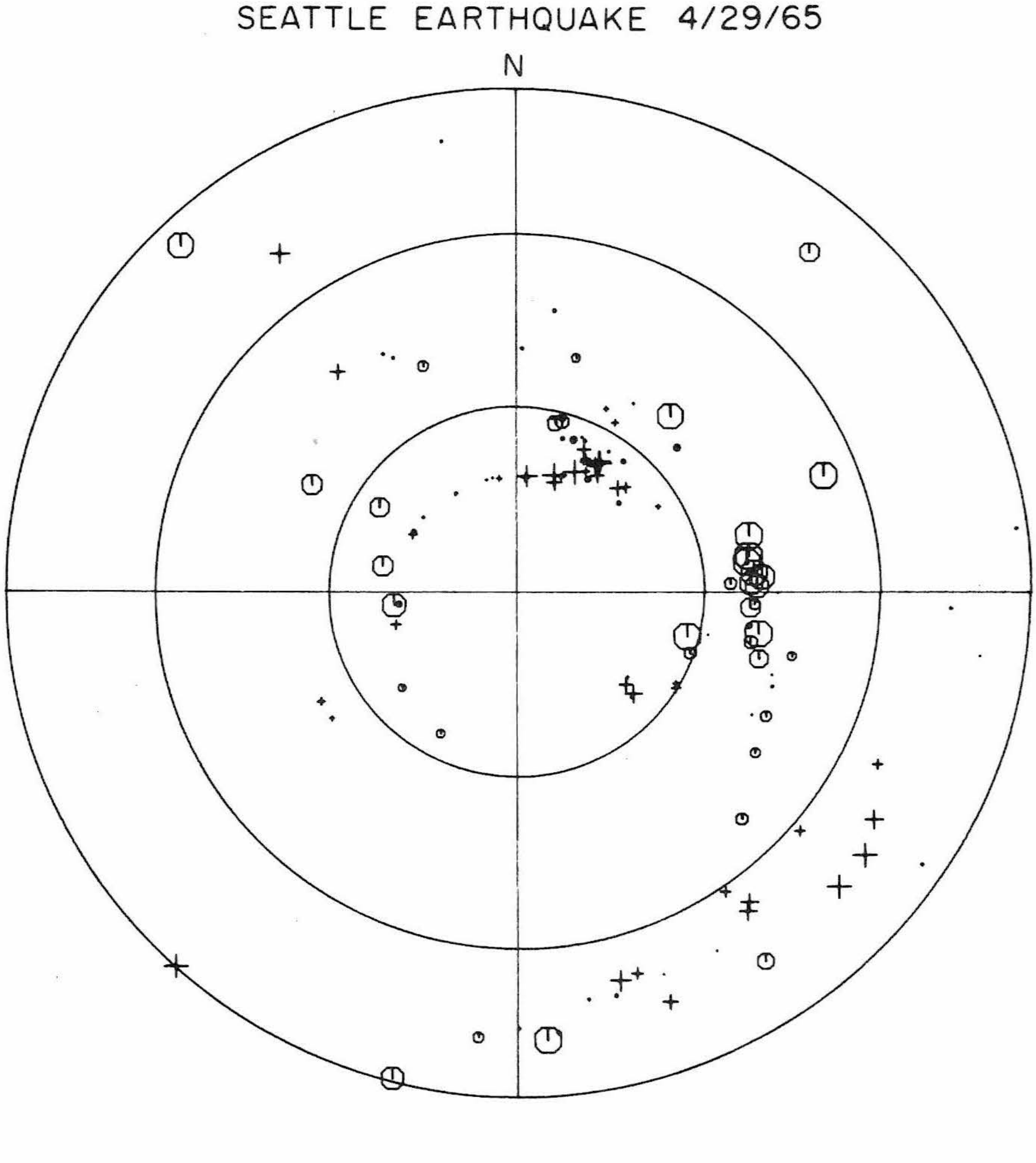

Figure 45

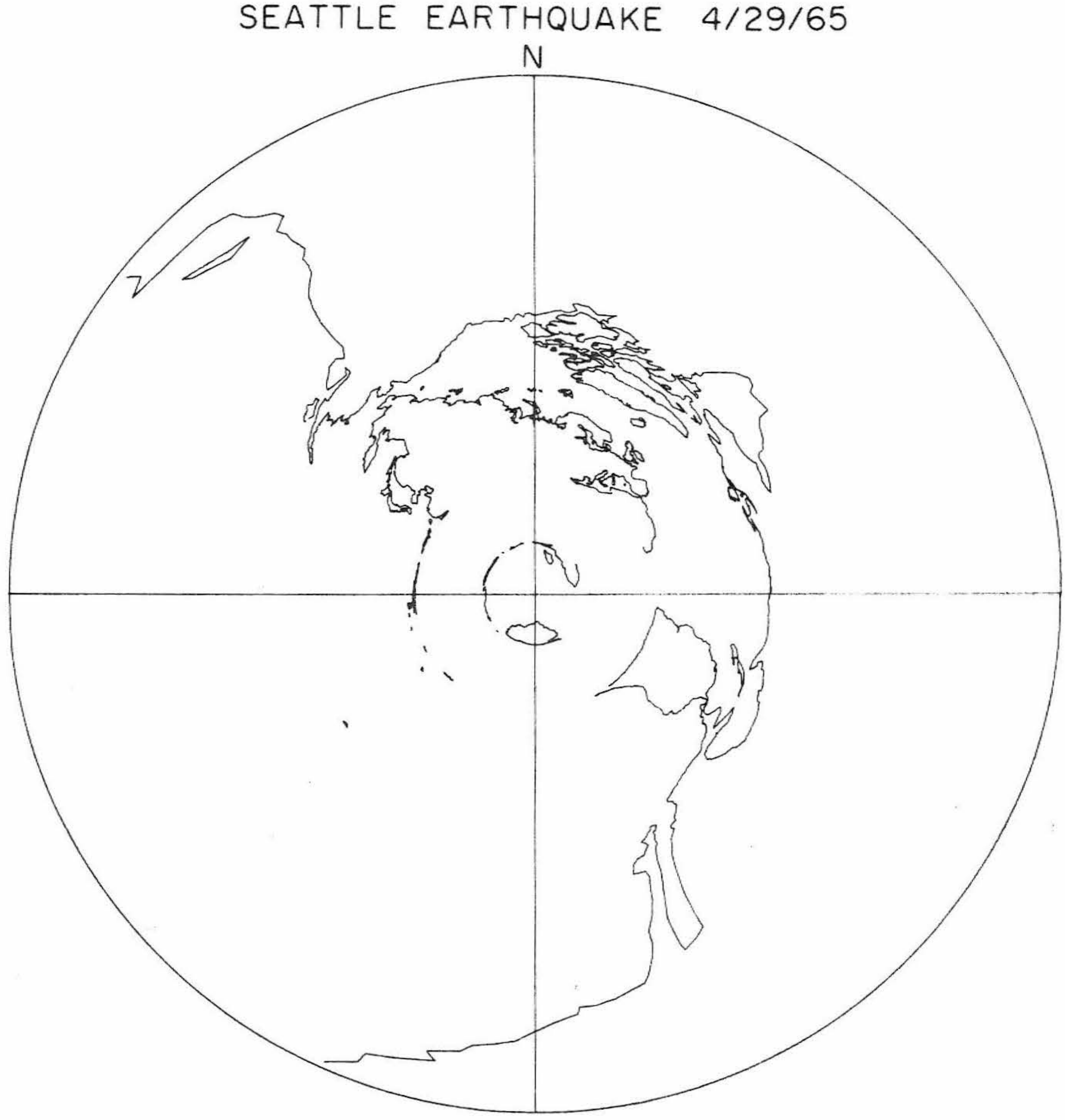

Figure 46

VANCOUVER IS. EARTHQUAKE 3/31/64

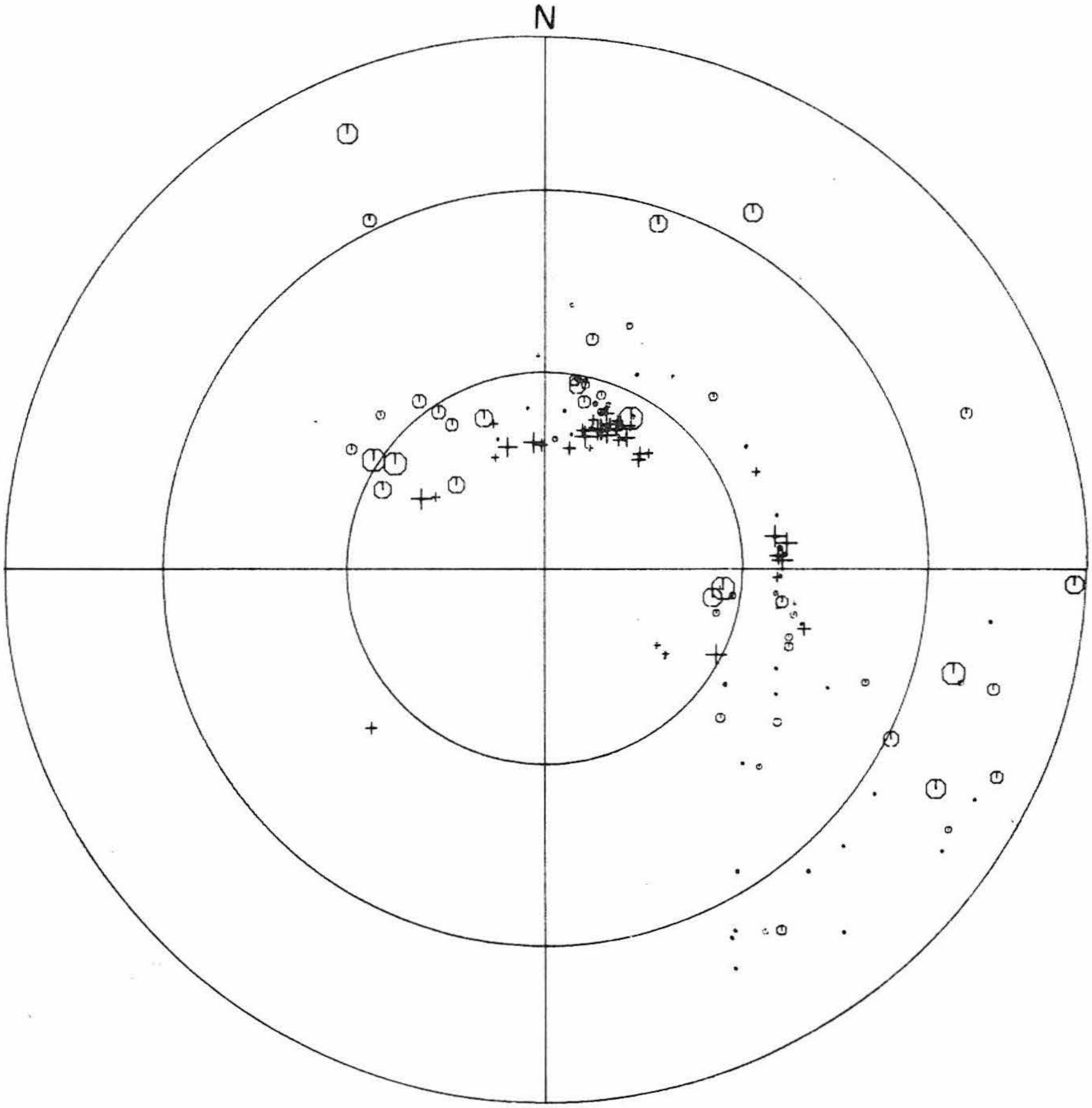

Figure 47

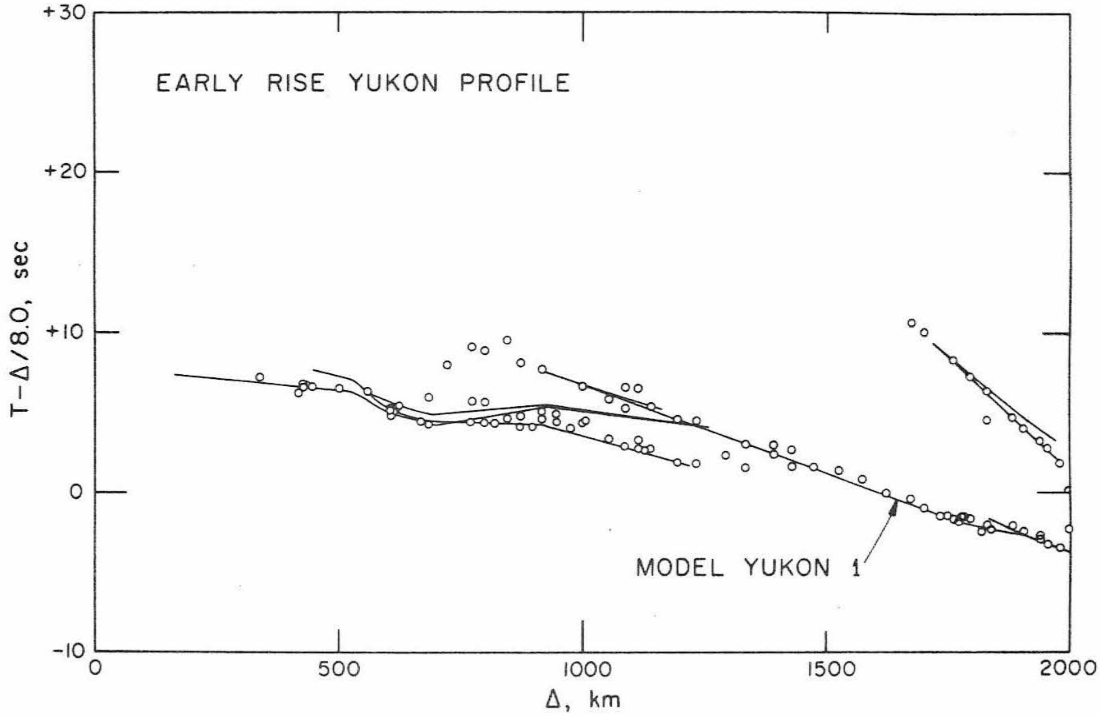
EARLY RISE YUKON PROFILE
+30
+20
+10
0
-10
T-Δ/8.0, sec
MODEL YUKON 1
0
500
1000
1500
2000
Δ, km

Figure 48

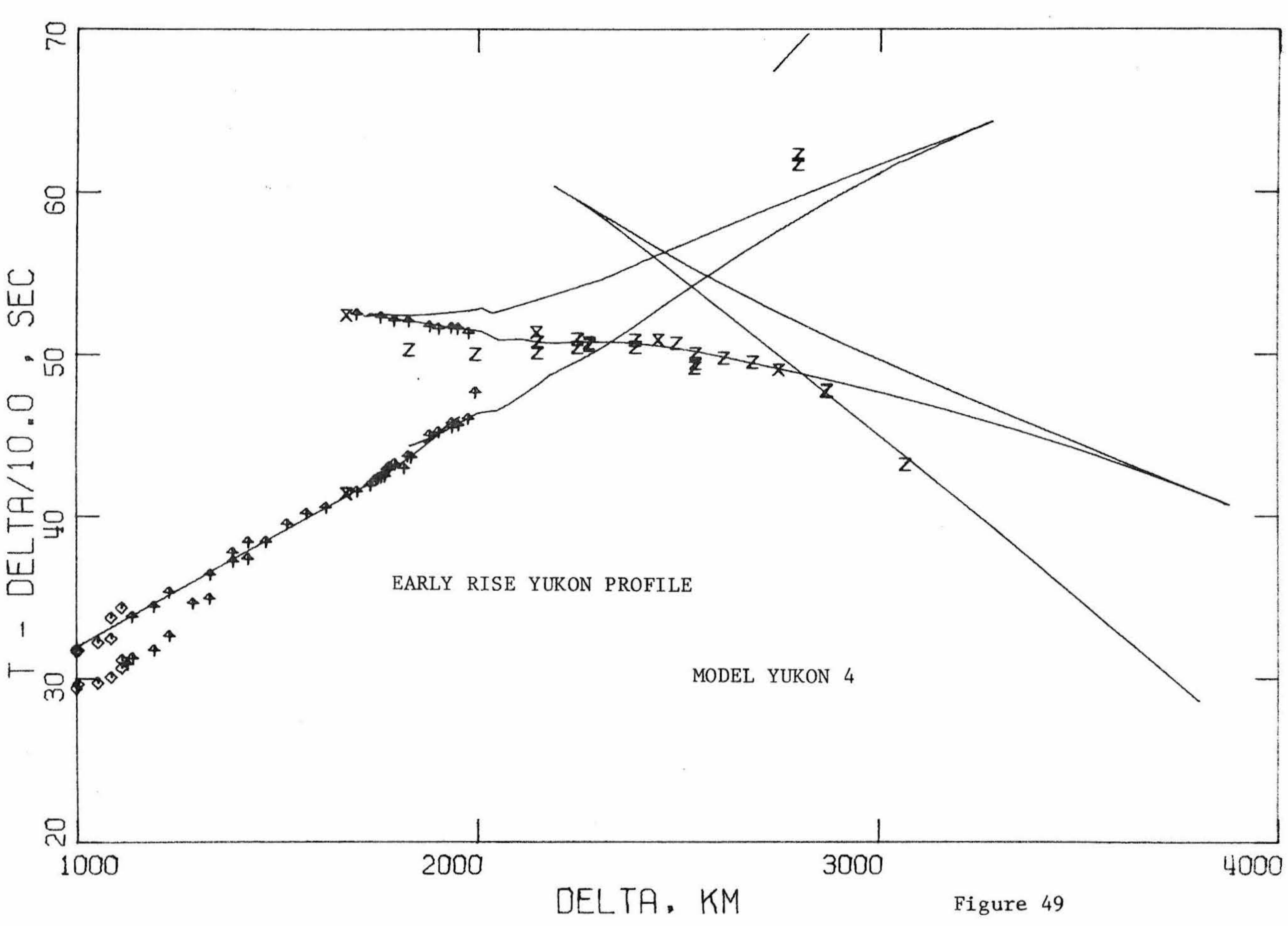
70
60
50
40
30
20
T - DELTA/10.0 , SEC
1000
2000
3000
4000
DELTA, KM
EARLY RISE YUKON PROFILE
MODEL YUKON 4

Figure 49

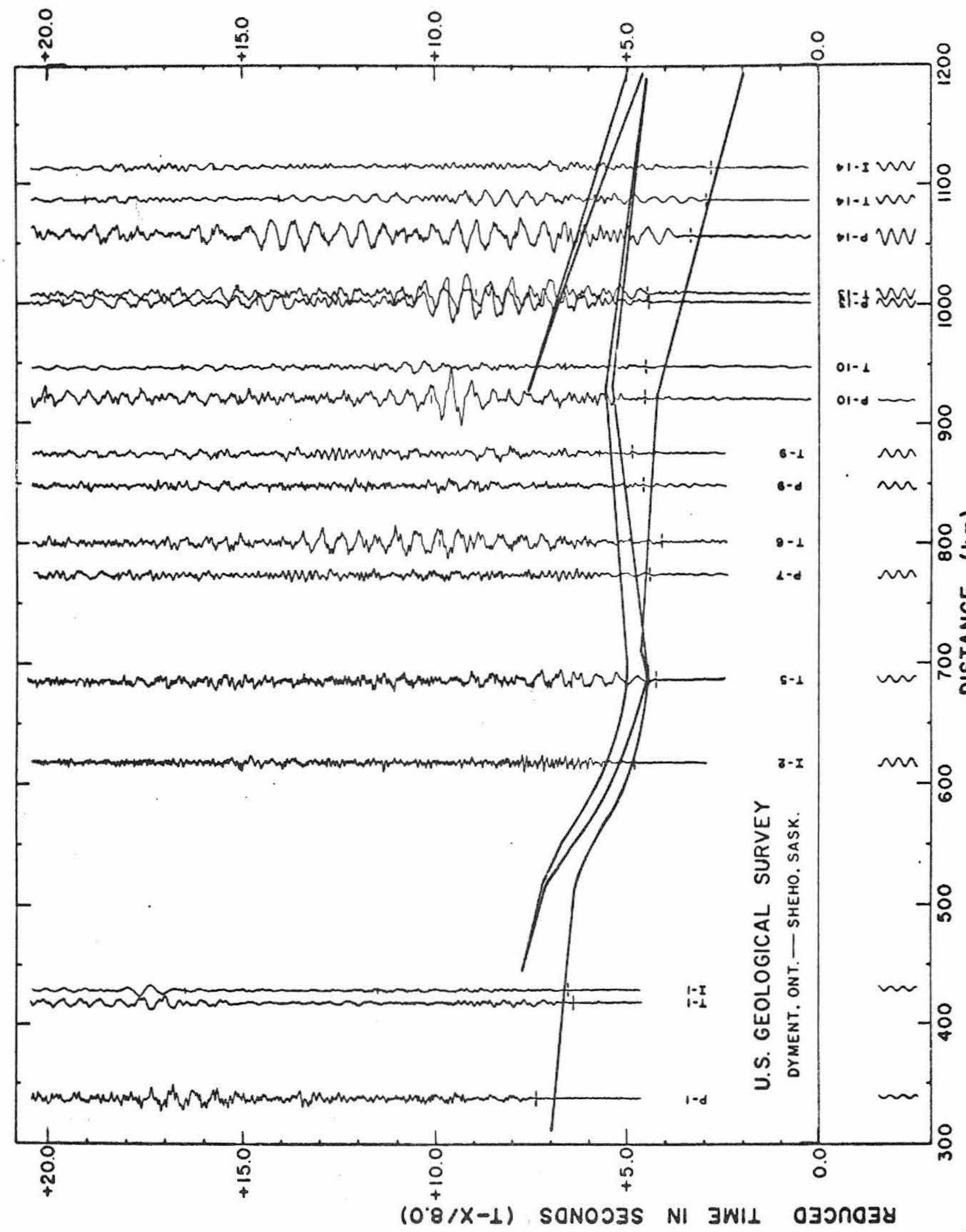
U.S. GEOLOGICAL SURVEY
DYMENT, ONT. — SHEHO, SASK.
REDUCED TIME IN SECONDS (T-X/8.0)
DISTANCE (km)
+20.0
+15.0
+10.0
+5.0
0.0
300
400
500
600
700
800
900
1000
1100
1200
P-1
T-1
T-8
T-5
P-7
T-6
P-9
T-9
P-10
T-10
P-14
T-14

Figure 50

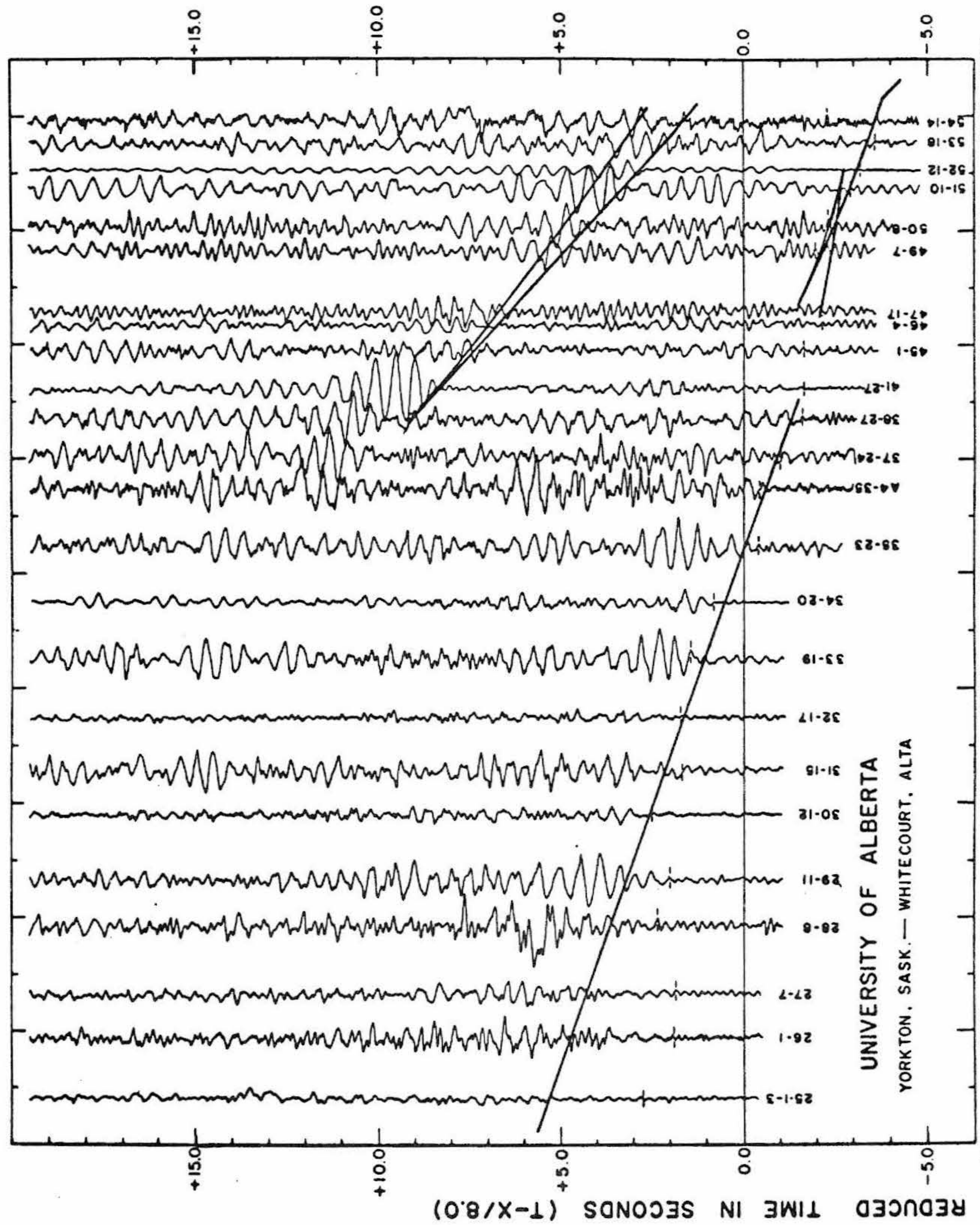
UNIVERSITY OF ALBERTA
YORKTON, SASK. — WHITECOURT, ALTA
DISTANCE (km)
REDUCED TIME IN SECONDS (T-X/8.0)

Figure 51

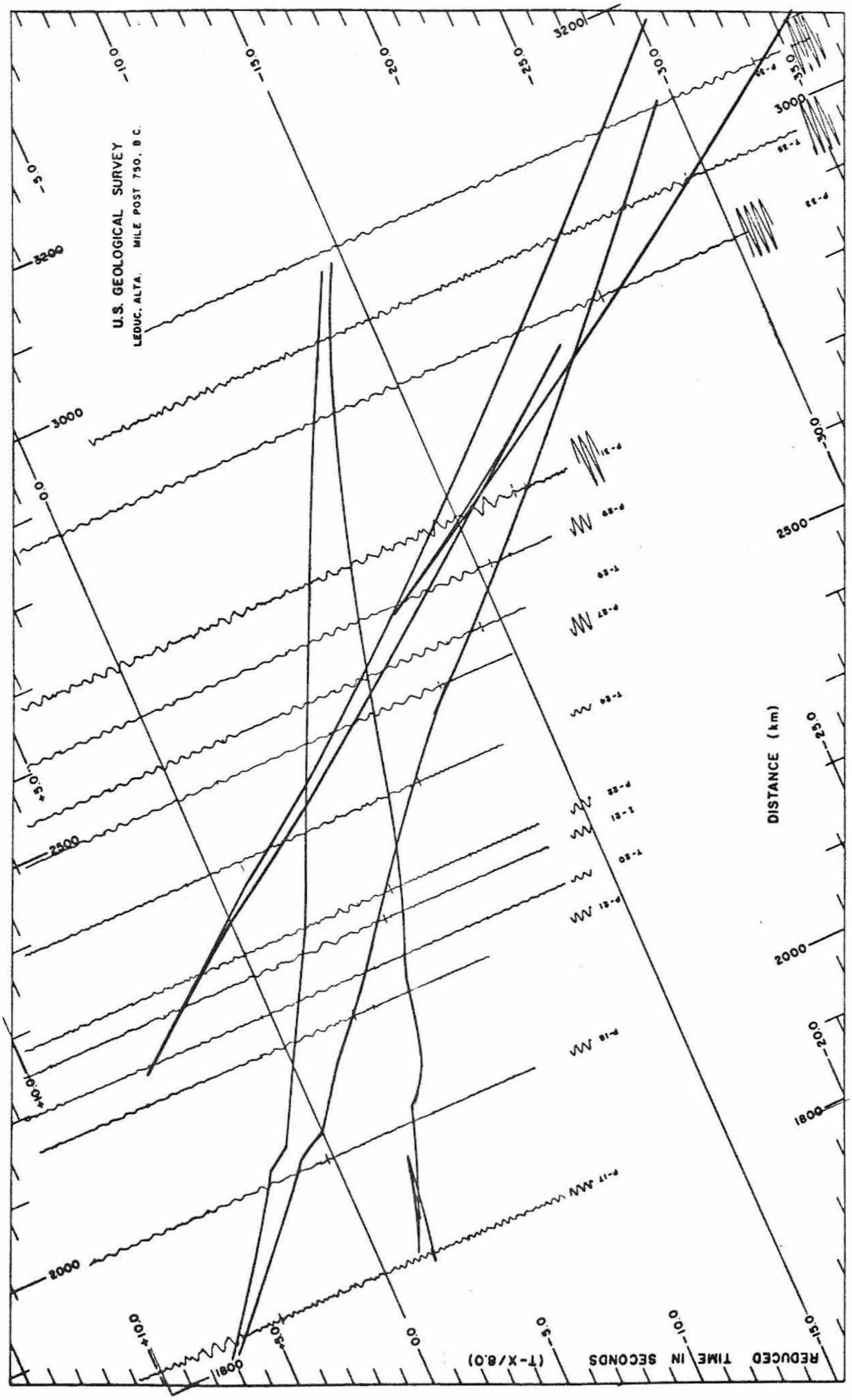
U.S. GEOLOGICAL SURVEY
LEDUC, ALTA. MILE POST 730, B.C.
DISTANCE (km)
REDUCED TIME IN SECONDS (T-X/8.0)

Figure 52

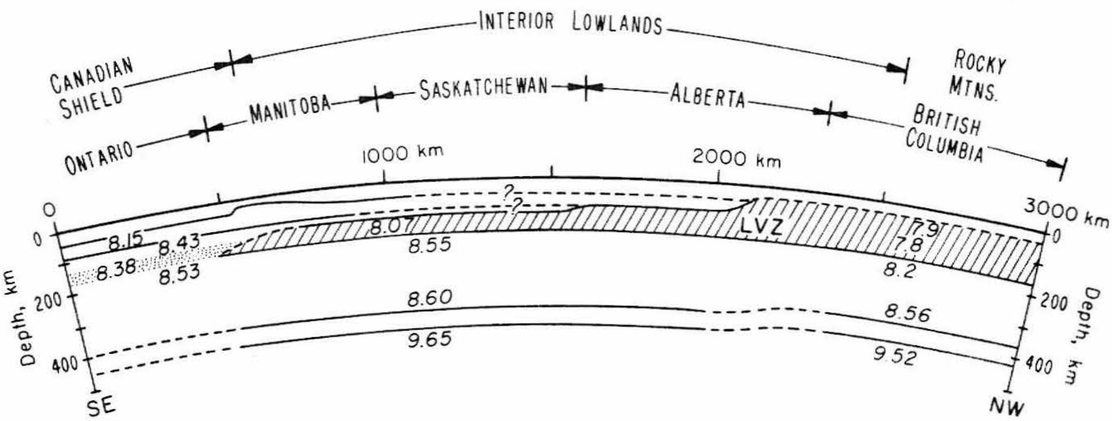
INTERIOR LOWLANDS
CANADIAN SHIELD
ROCKY MTNS.
ONTARIO
MANITOBA
SASKATCHEWAN
ALBERTA
BRITISH COLUMBIA
1000 km
2000 km
3000 km
0
8.15
8.43
8.38
8.53
8.07
8.55
LVZ
7.9
7.8
8.2
8.60
8.56
9.65
9.52
Depth, km
200
400
SE
NW

Figure 53

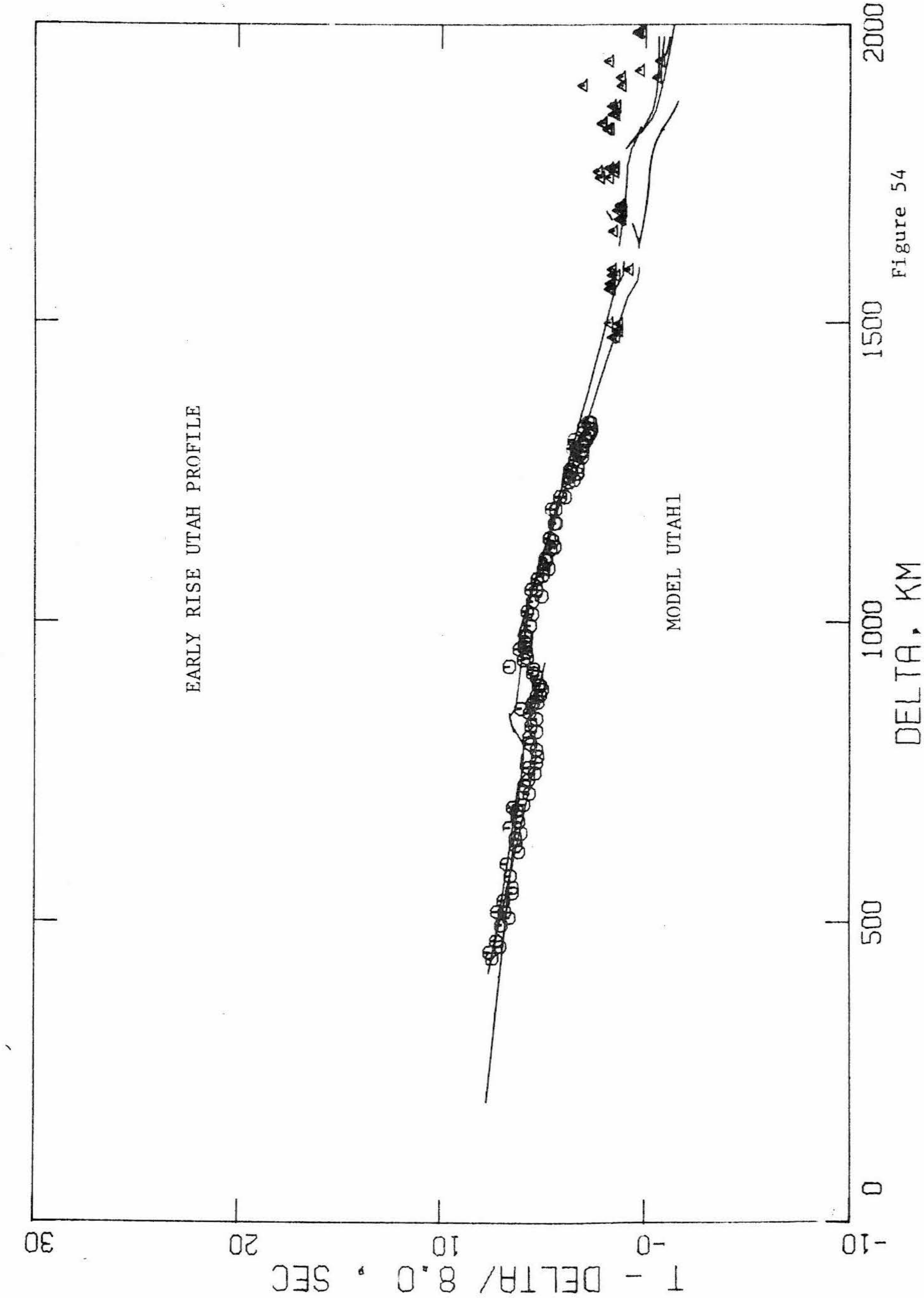
EARLY RISE UTAH PROFILE
MODEL UTAH1
DELTA, KM
T - DELTA/ 8.0 , SEC
0
500
1000
1500
2000
-10
-0
10
20
30

Figure 54

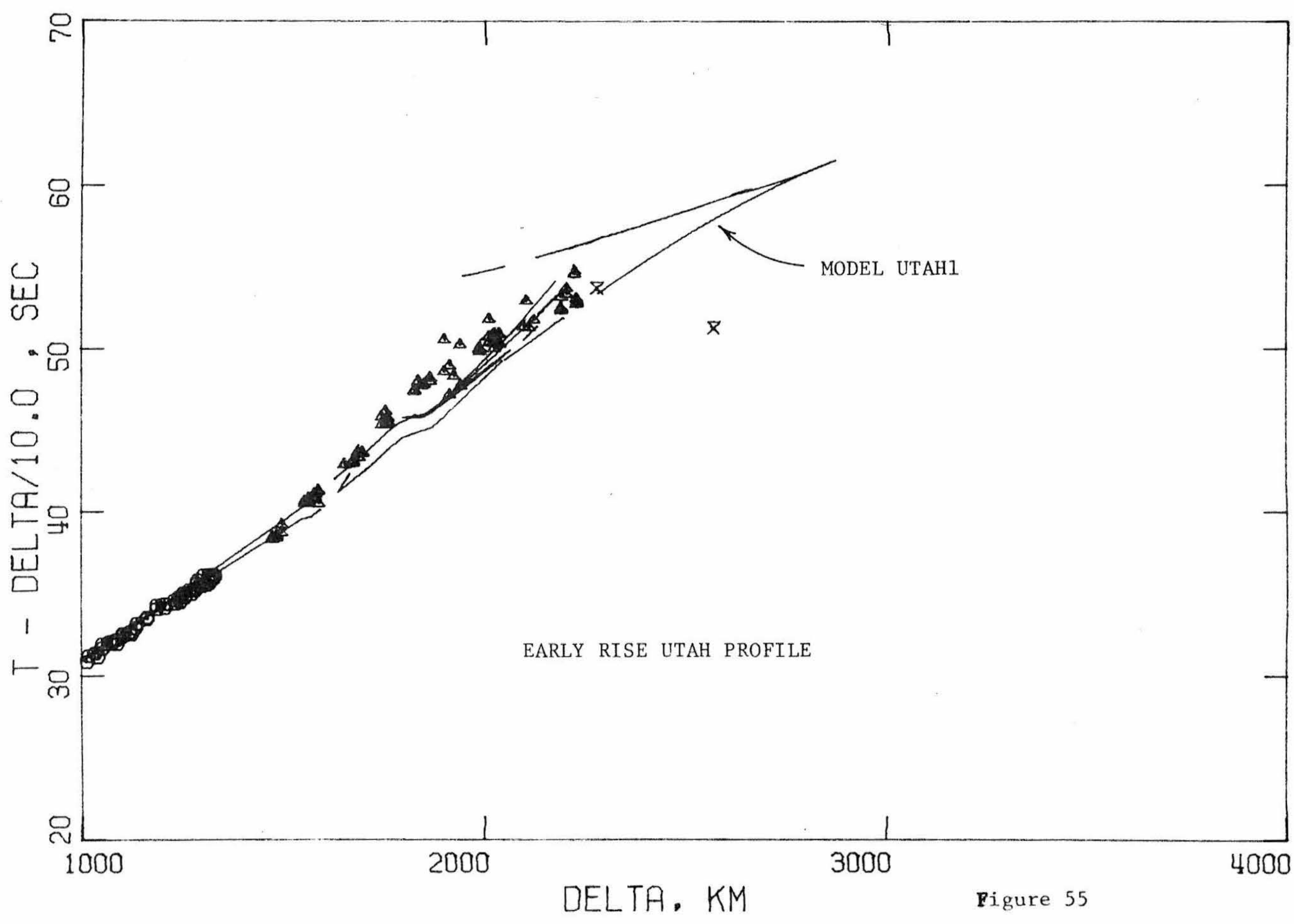
T - DELTA/10.0 , SEC
70
60
50
40
30
20
1000
2000
3000
4000
DELTA, KM
MODEL UTAH1
EARLY RISE UTAH PROFILE

Figure 55

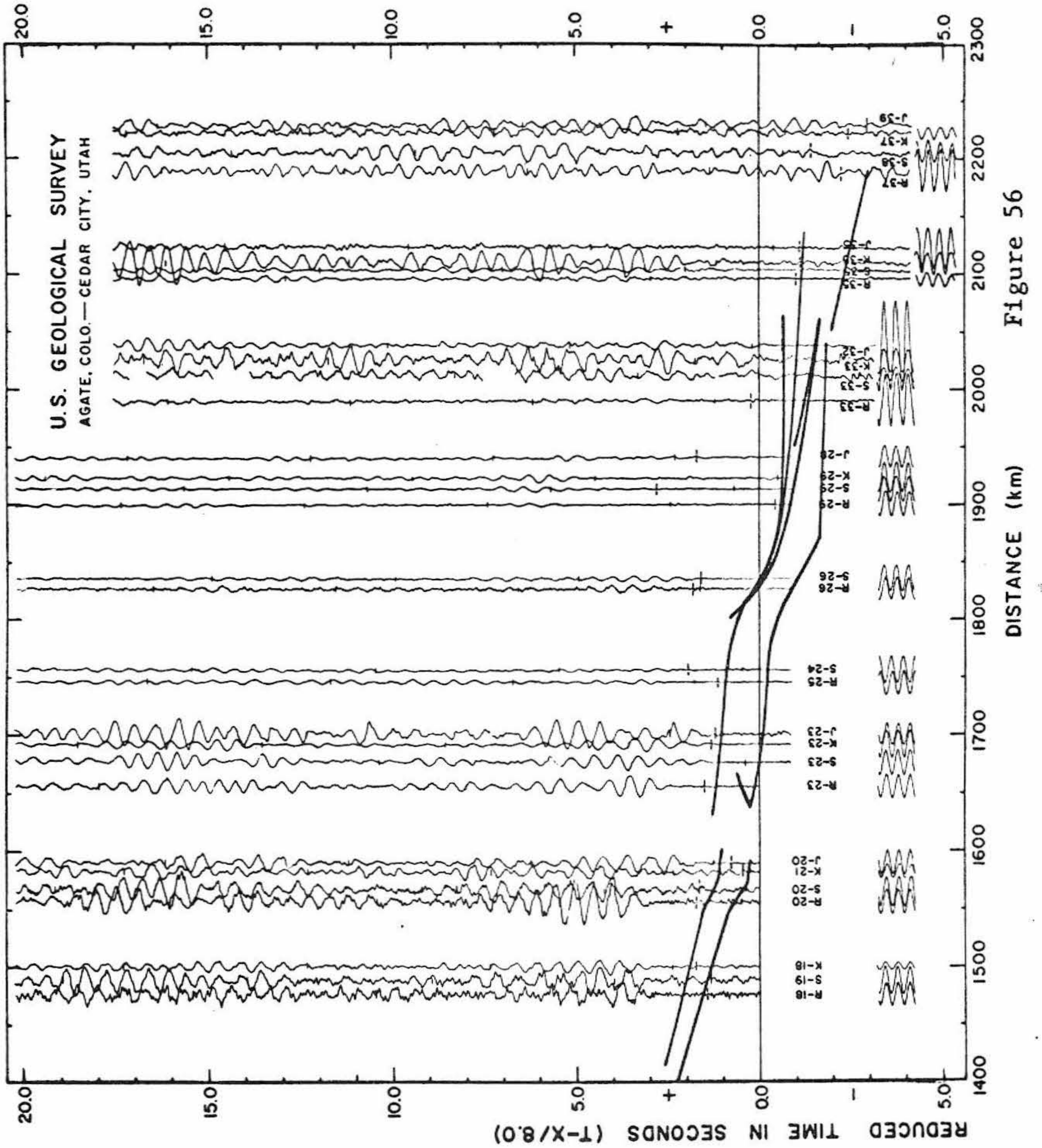
U.S. GEOLOGICAL SURVEY
AGATE, COLO.—CEDAR CITY, UTAH
DISTANCE (km)
REDUCED TIME IN SECONDS (T-X/8.0)

Figure 56

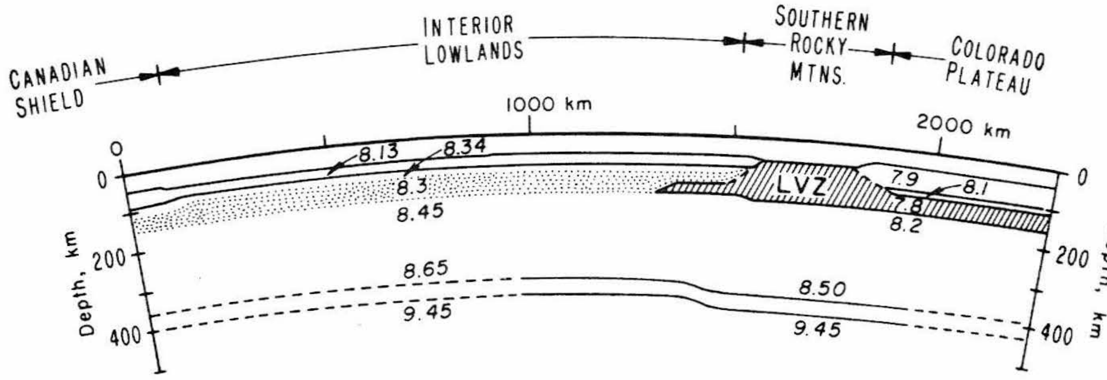
CANADIAN SHIELD
INTERIOR LOWLANDS
SOUTHERN ROCKY MTNS.
COLORADO PLATEAU
1000 km
2000 km
0
0
200
400
Depth, km
0
200
400
Depth, km
8.13
8.34
8.3
8.45
LVZ
7.9
8.1
7.8
8.2
8.65
9.45
8.50
9.45

Figure 57

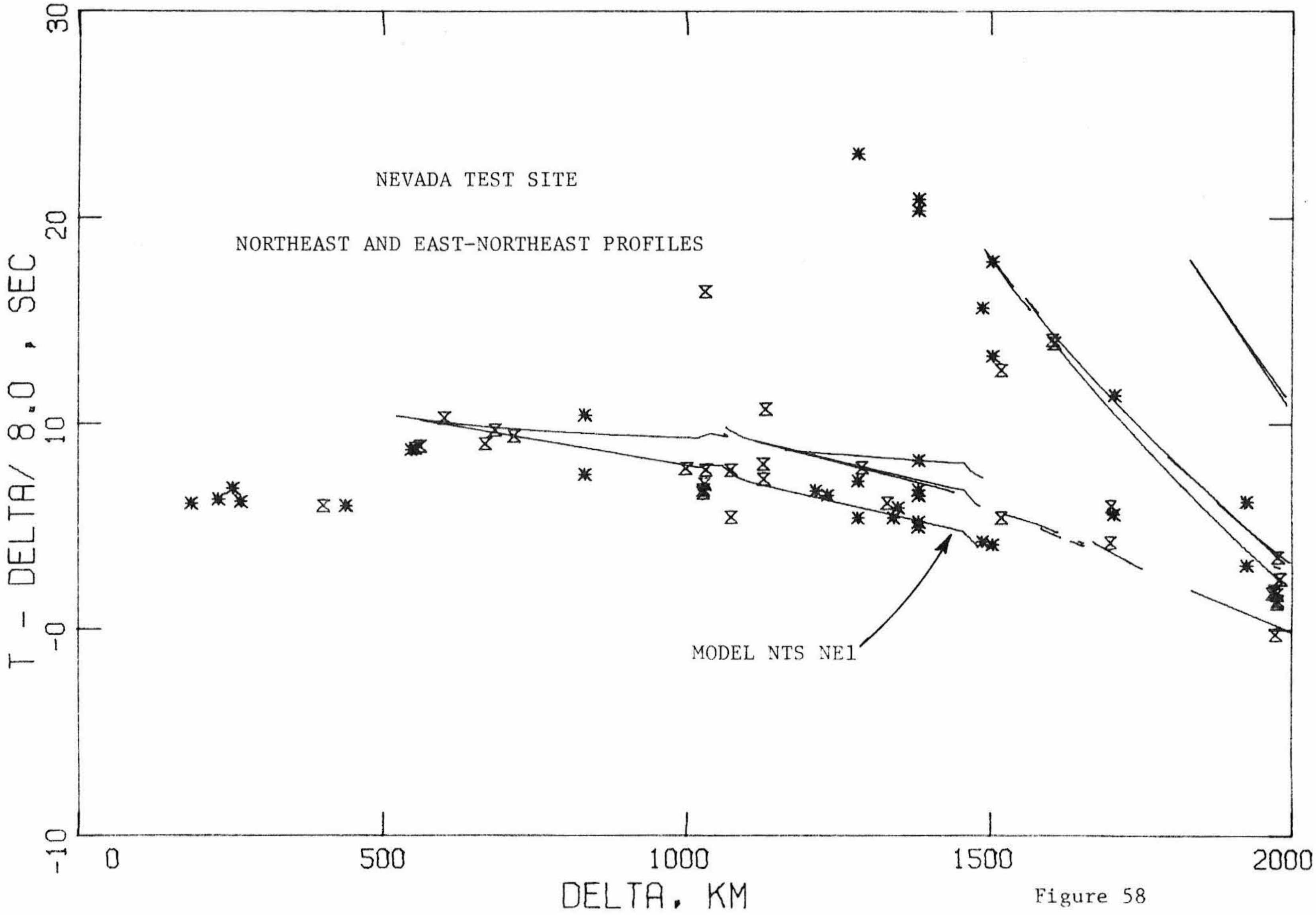
NEVADA TEST SITE
NORTHEAST AND EAST-NORTHEAST PROFILES
MODEL NTS NE1
T - DELTA/ 8.0 , SEC
30
20
10
-0
-10
0
500
1000
1500
2000
DELTA, KM

Figure 58

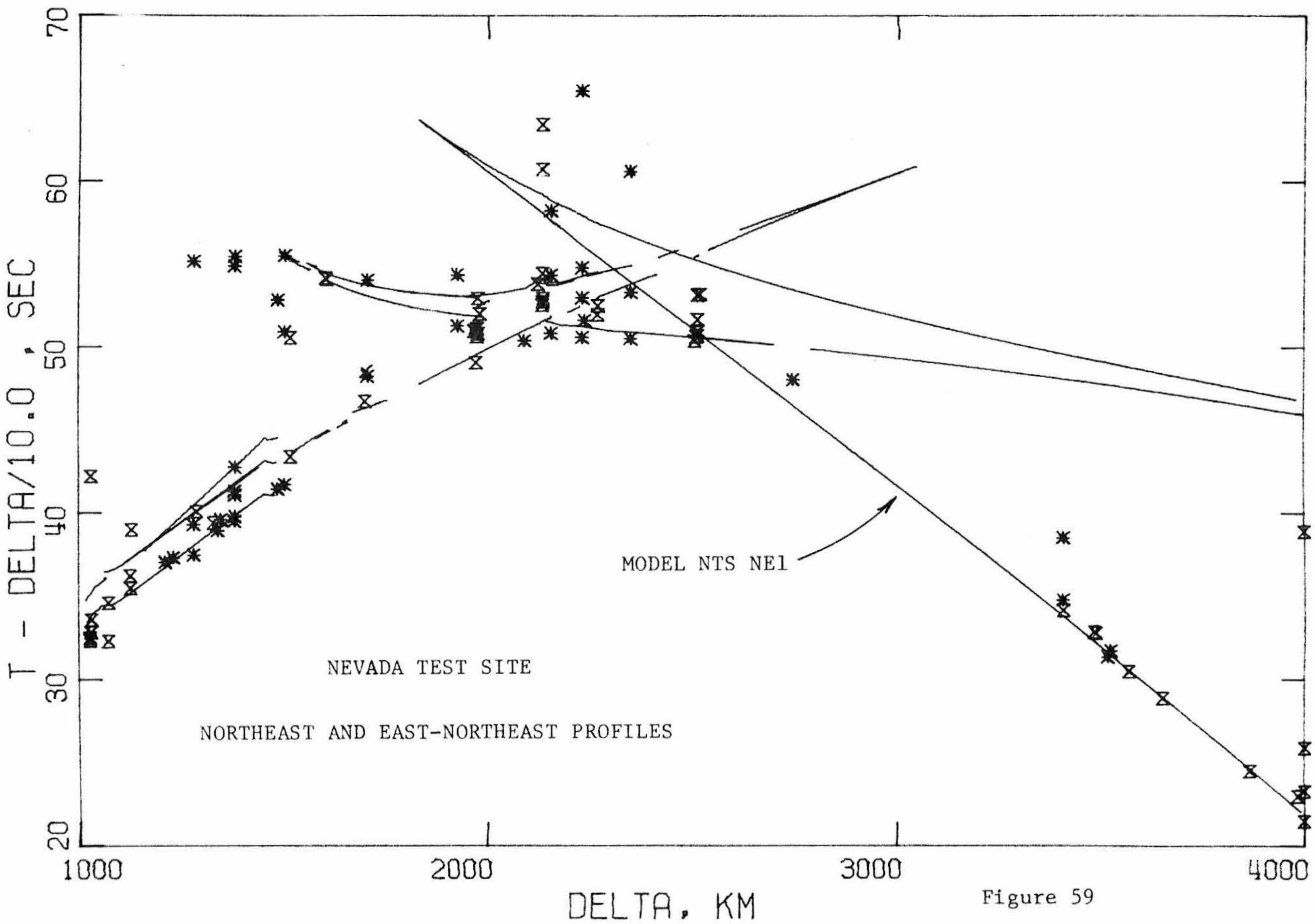
T - DELTA/10.0 , SEC
70
60
50
40
30
20
1000
2000
3000
4000
DELTA, KM
MODEL NTS NE1
NEVADA TEST SITE
NORTHEAST AND EAST-NORTHEAST PROFILES

Figure 59

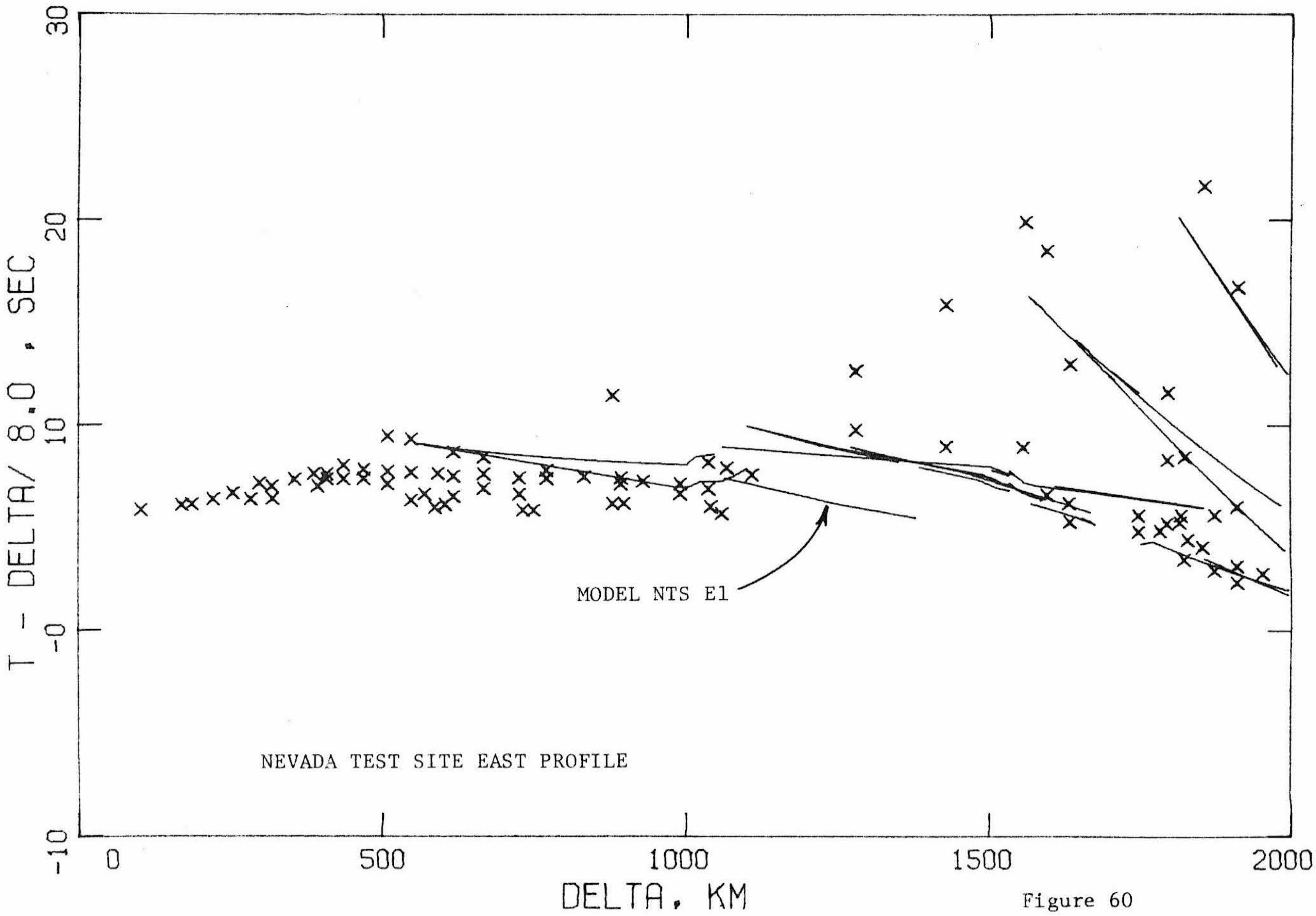
30
20
10
-0
-10
T - DELTA/ 8.0 , SEC
0
500
1000
1500
2000
DELTA, KM
MODEL NTS E1
NEVADA TEST SITE EAST PROFILE

Figure 60

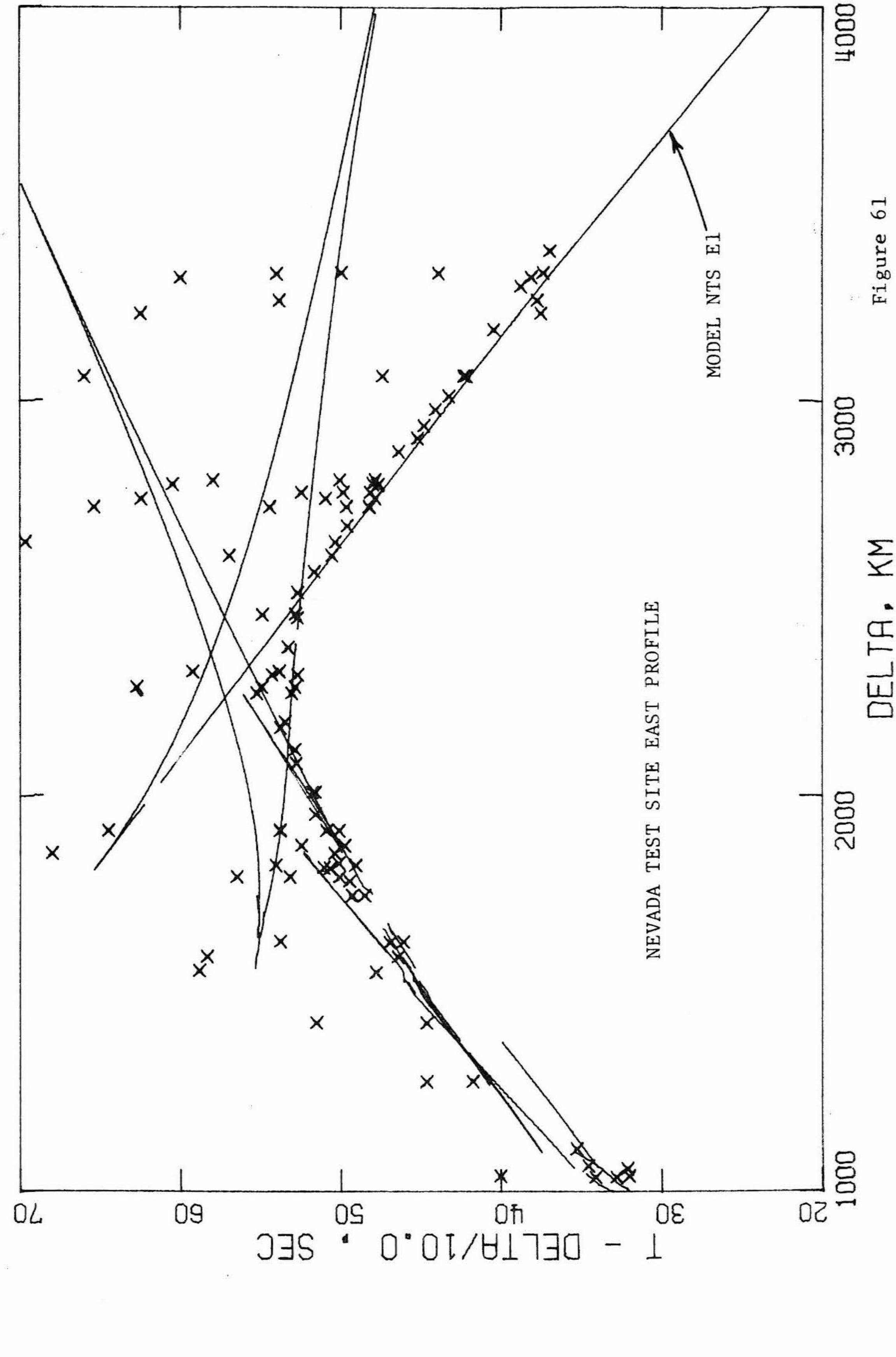
NEVADA TEST SITE EAST PROFILE
MODEL NTS E1
DELTA, KM
T - DELTA/10.0 , SEC
1000
2000
3000
4000
20
30
40
50
60
70

Figure 61

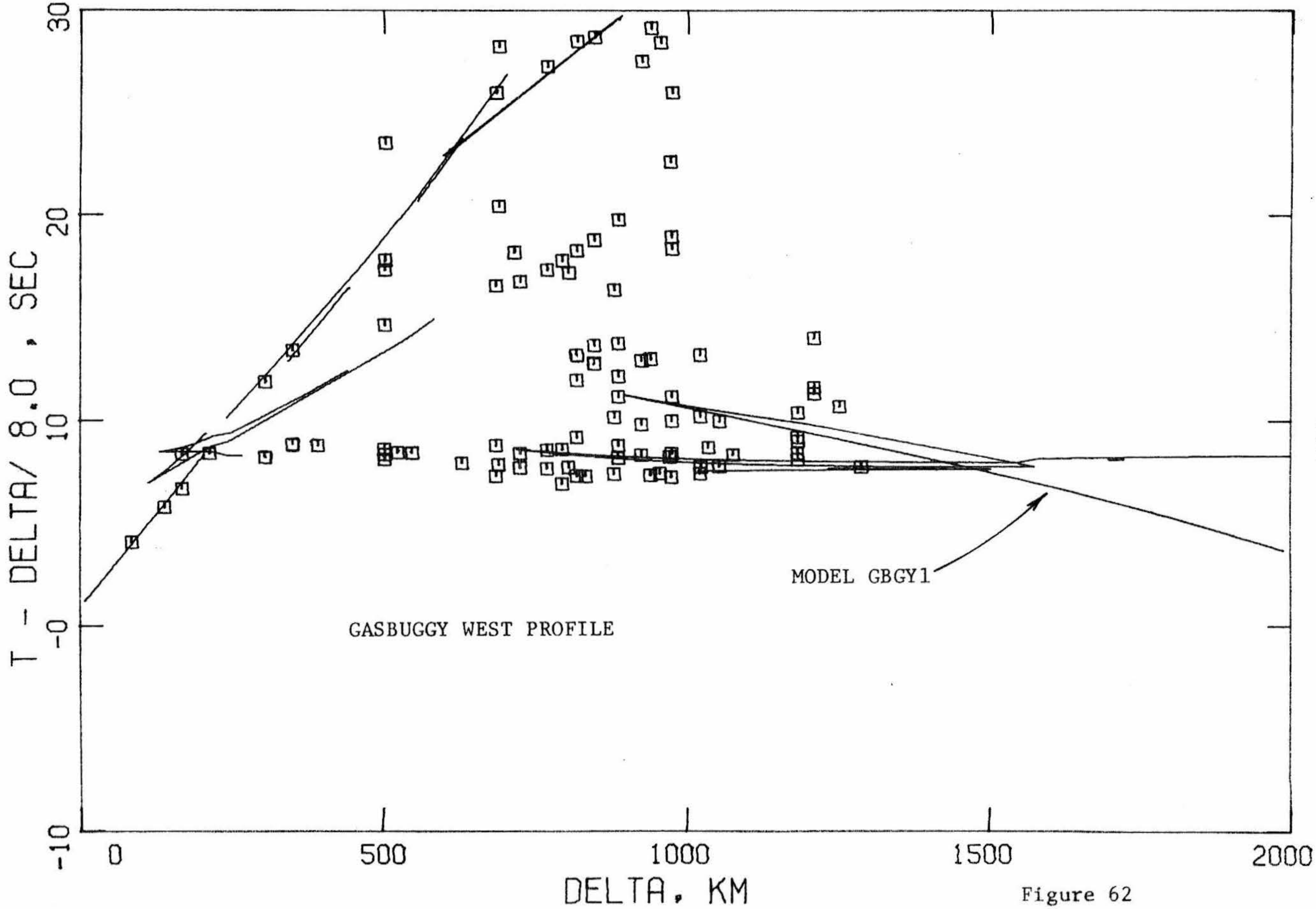
T - DELTA/ 8.0 , SEC
30
20
10
-0
-10
0
500
1000
1500
2000
DELTA, KM
GASBUGGY WEST PROFILE
MODEL GBGY1

Figure 62

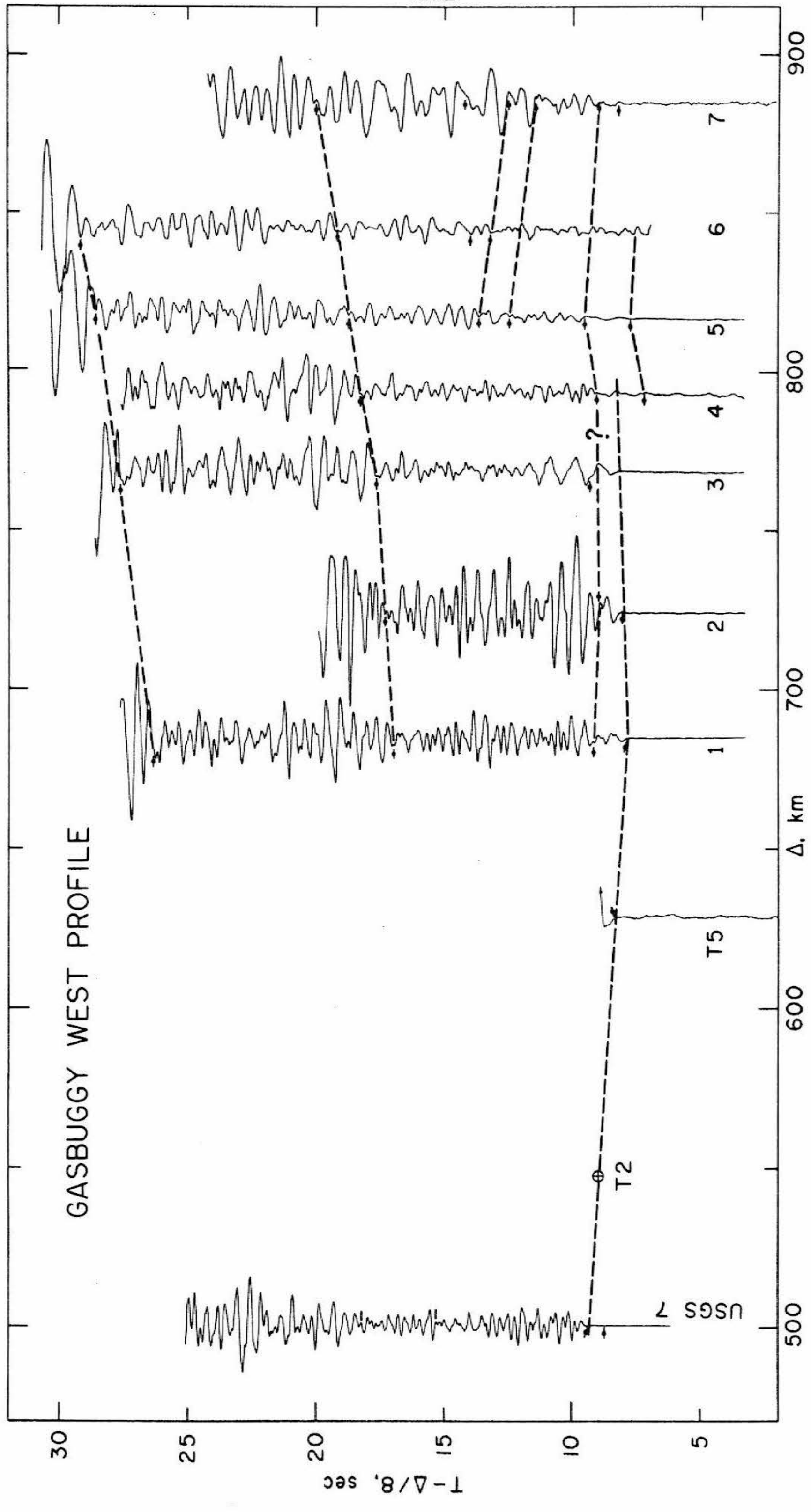

Figure 63

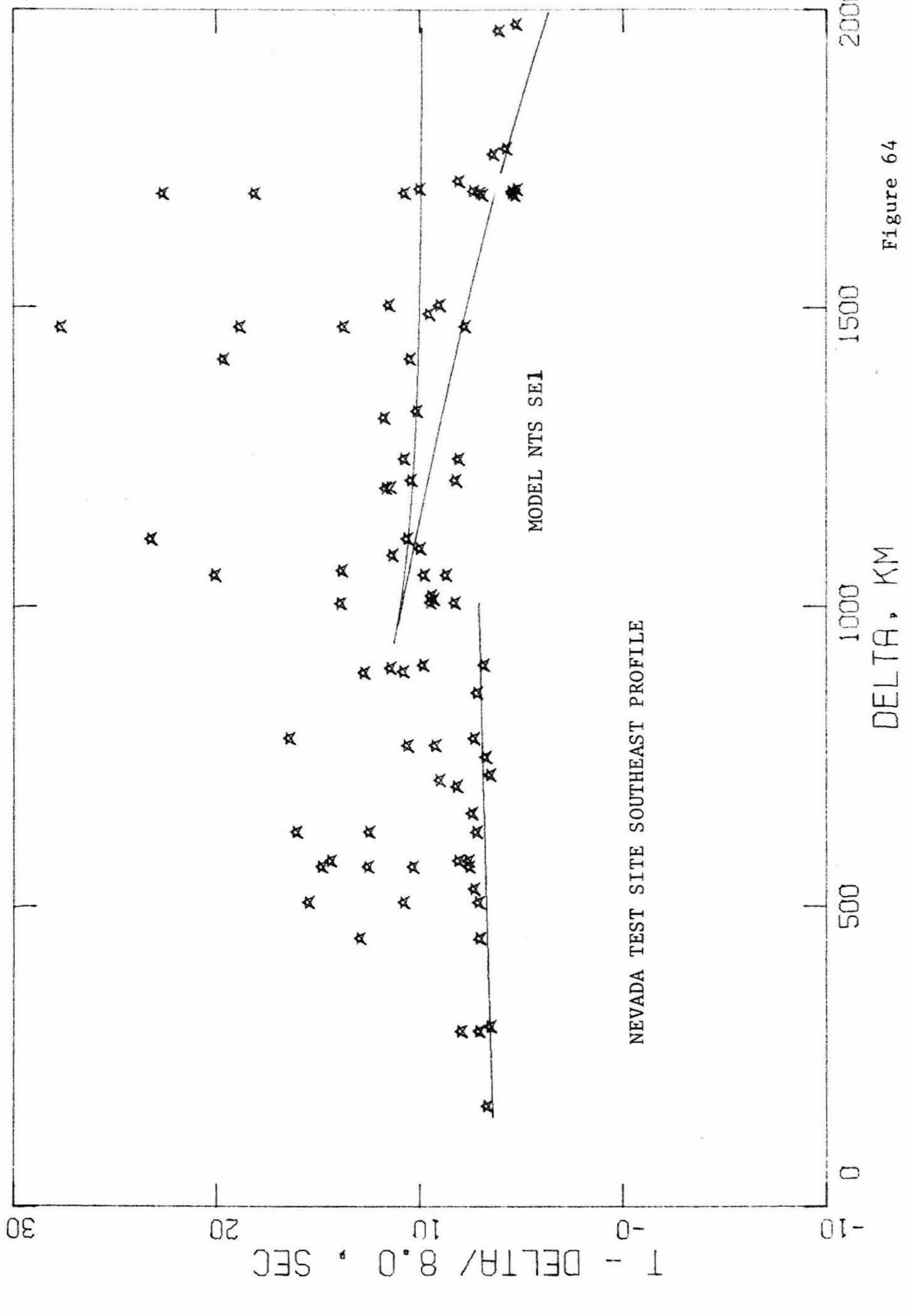
NEVADA TEST SITE SOUTHEAST PROFILE
MODEL NTS SE1
DELTA, KM
T - DELTA/ 8.0 , SEC
0
500
1000
1500
2000
30
20
10
-0
-10

Figure 64

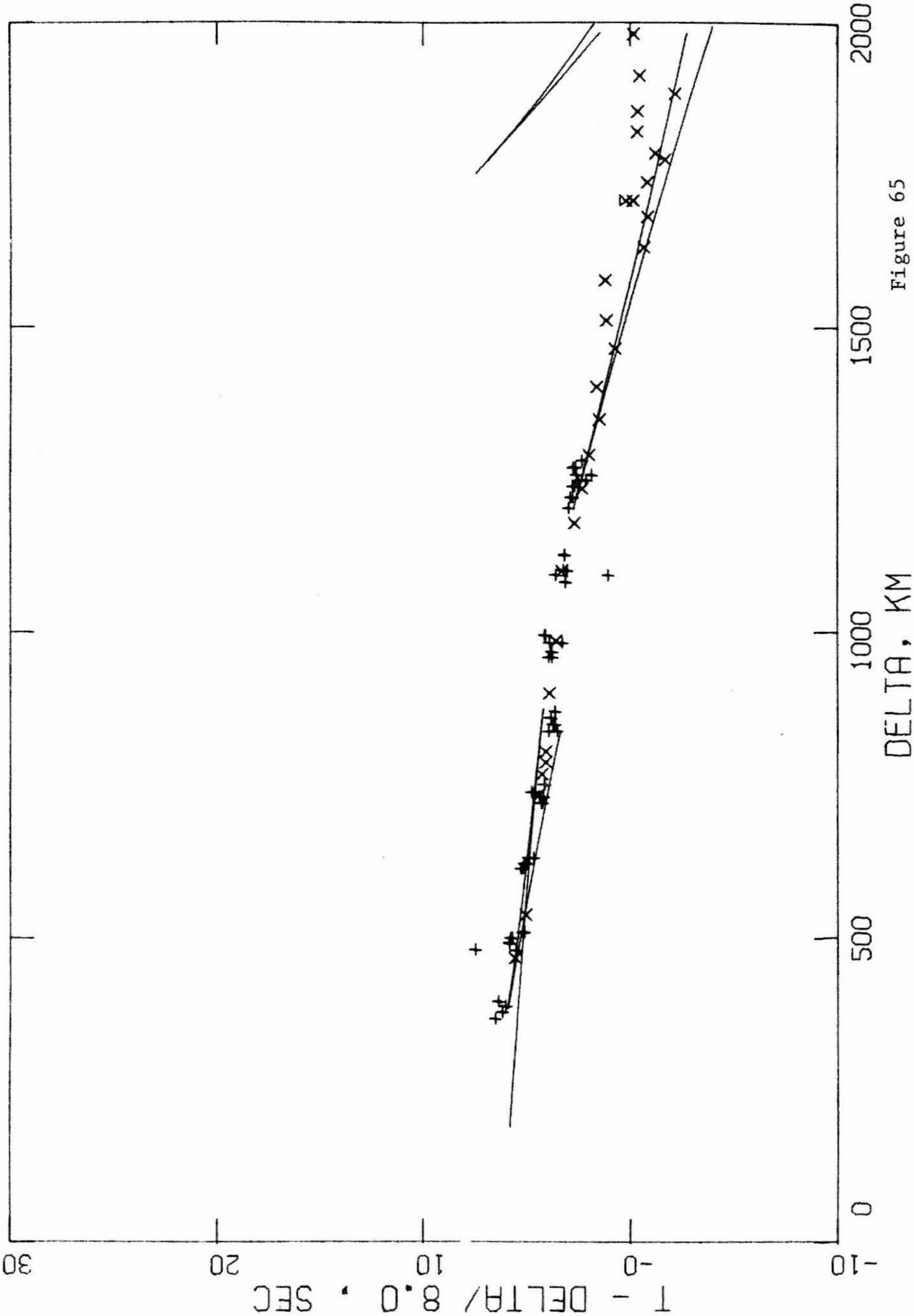

Figure 65

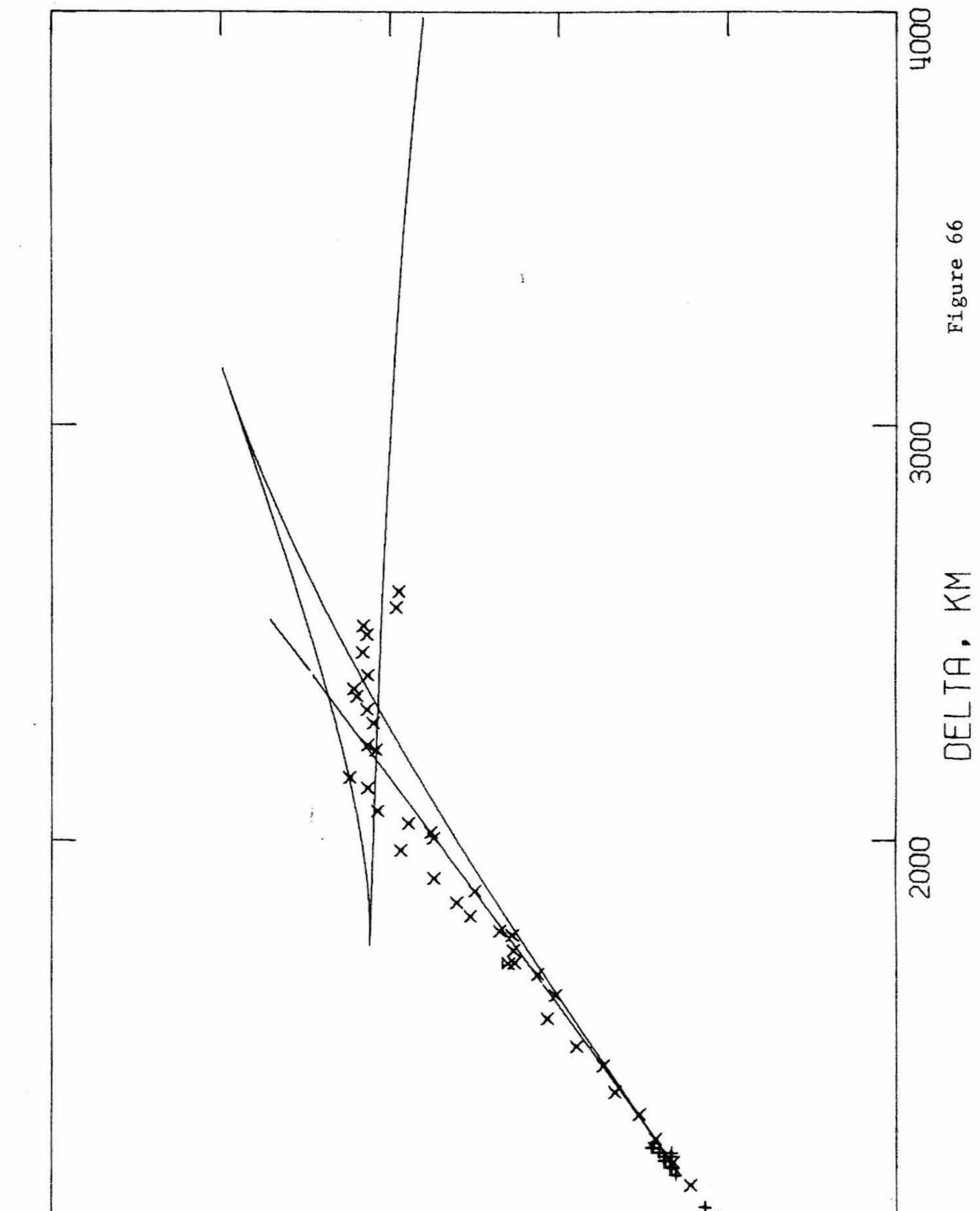

Figure 66

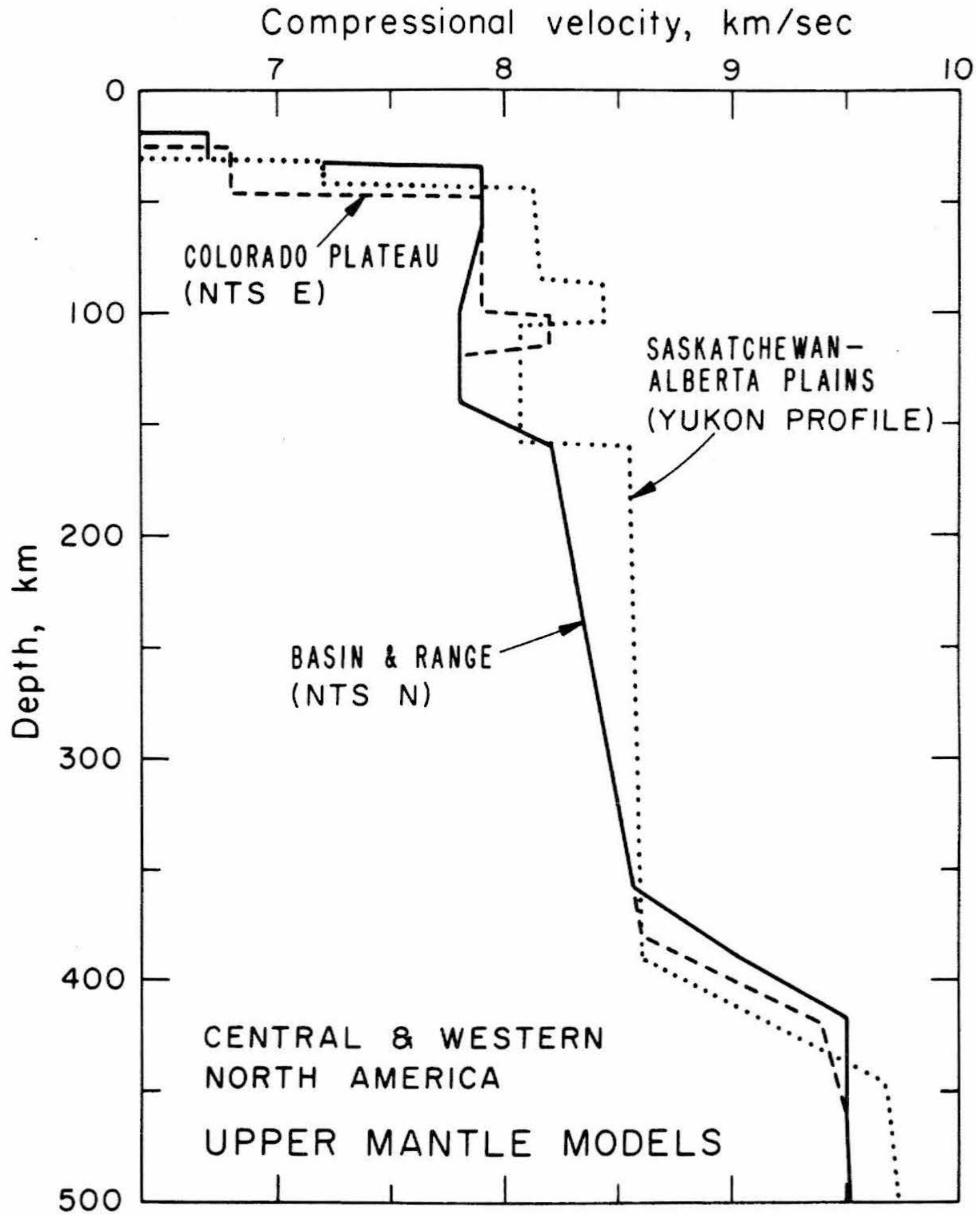

Compressional velocity, km/sec
7
8
9
10
0
100
200
300
400
500
Depth, km
COLORADO PLATEAU
(NTS E)
SASKATCHEWAN-
ALBERTA PLAINS
(YUKON PROFILE)
BASIN & RANGE
(NTS N)
CENTRAL & WESTERN
NORTH AMERICA
UPPER MANTLE MODELS

Figure 67

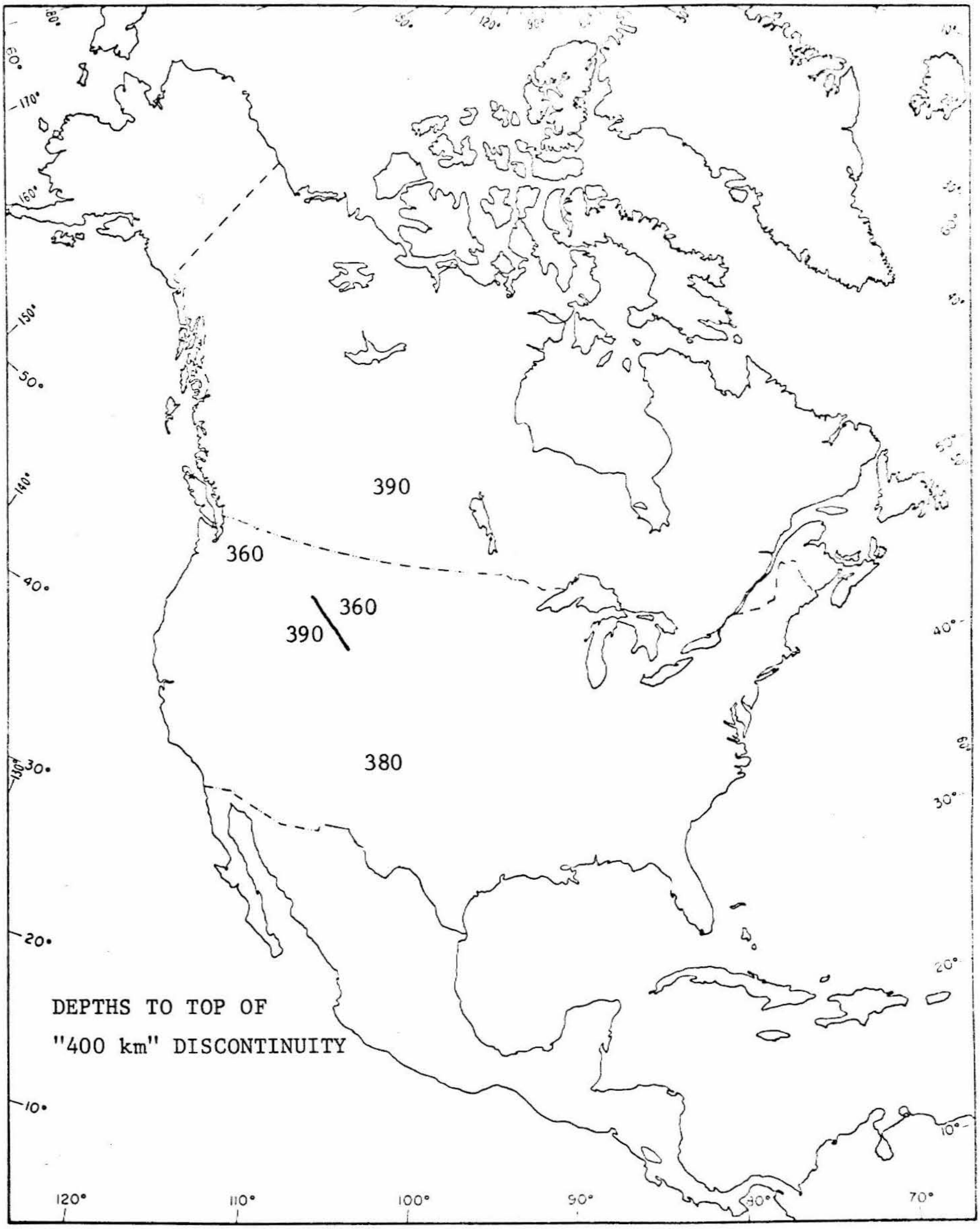
DEPTHS TO TOP OF
"400 km" DISCONTINUITY
390
360
360
390
380
120°
110°
100°
90°
80°
70°
40°
30°
20°
10°

Figure 68

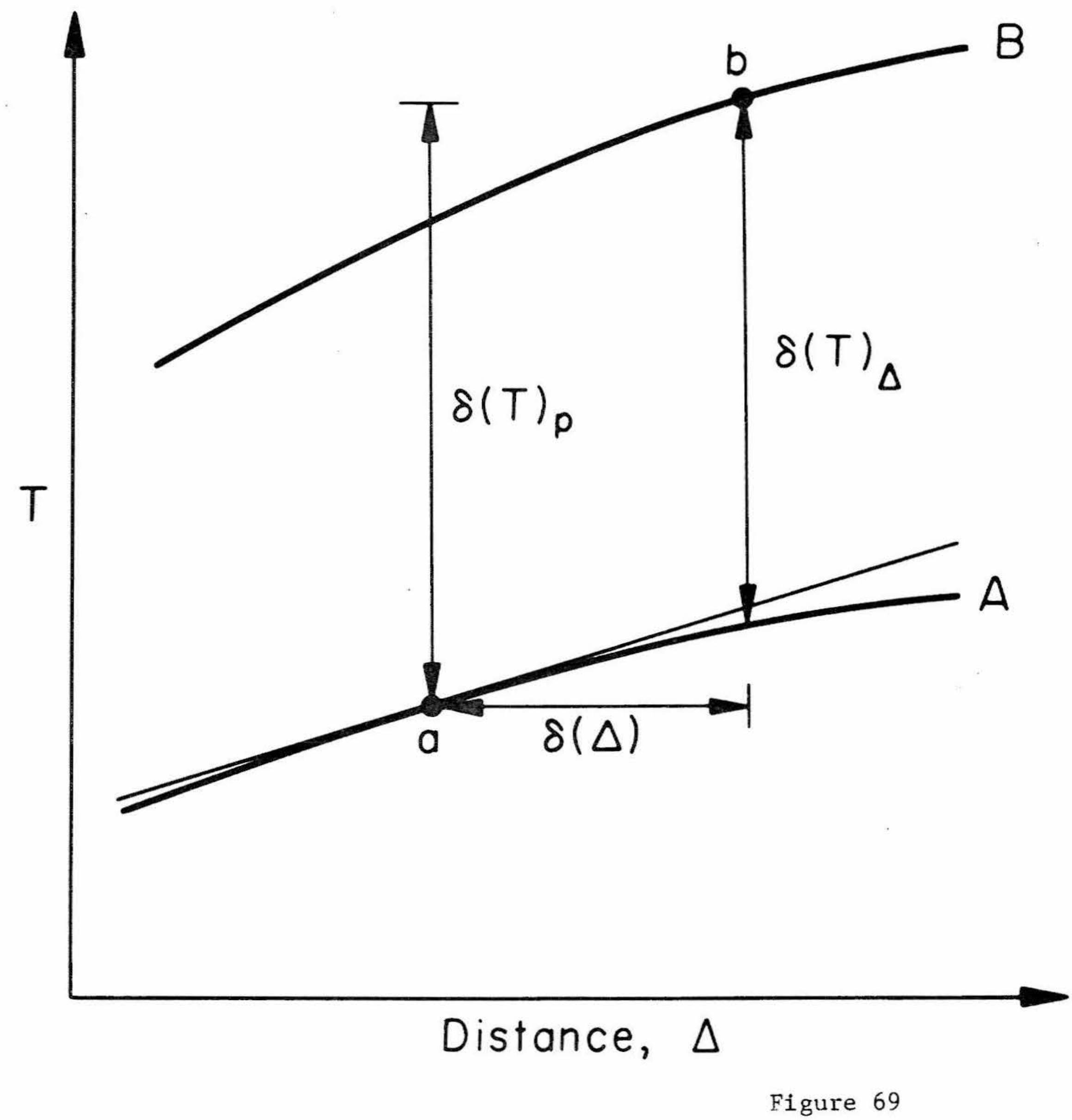

Figure 69